

Abstract

The investigation of the interaction and kinetics of hydride forming materials under high frequency electromagnetic fields was undertaken in a joint research project between the university of Birmingham and C-Tech Innovation Ltd. The work was initiated in order to identify and examine two specific areas of materials science, the effects of dielectric fields on the processing and reactions of materials for the solid state storage of hydrogen and the use of dielectric fields for the processing of materials using hydrogen.

The improvement in the reaction rate of materials with hydrogen is a key step in the development of cost effective hydrogen storage technologies to make an effective fuel cell system for energy storage applications. The use of microwaves and radio frequency fields has been widely reported to improve reaction kinetics in a number of reactions and the evidence for improved diffusion rates suggests that electromagnetic fields could impact on this.

C-Tech Innovation Ltd has a long track record in the development of microwave and radio frequency technologies and in the processing of materials using these technologies. The development of specific test and measurement equipment was a key objective of the project and has resulted in the development of a temperature controlled microwave /RF hybrid system to allow measurement of material sorption characteristics at controlled temperatures and pressures. Specifically the equipment allows the exposure of materials to high frequency electromagnetic fields at temperatures up to 800°C, under hydrogen or mixed gas atmospheres of 18 bar and with up to 2.5kW of applied electromagnetic radiation at 2 frequencies.

Magnesium hydride was selected for the basis of the work as well characterised and yet potentially useful material for hydrogen storage applications. The effects of a range of catalytic additions are then assessed for performance advantage under electromagnetic fields.

Other materials with potential applications for hydrogen processing were also investigated under electromagnetic fields and these include $\text{Nd}_2\text{Fe}_{14}\text{B}$ rare earth magnetic materials and palladium.

All materials are characterised using standard analytical techniques such as X-Ray diffraction and gravimetric analysis prior to processing under electromagnetic fields and there were no observable changes in material structure or behaviour following processing under either microwave or radio frequency fields.

Interestingly, it was observed that changes in reaction kinetics are observed both in the hydrogenation reactions and dehydrogenation reactions and could be associated with the application of electromagnetic fields at temperatures ranging from 470-630K.

The changes in the rates of reaction showed a strong correlation with field strength and showed reaction kinetics not observed under standard conditions. In the respect of desorption kinetics the reaction rates were increased substantially in all cases, but in most particularly in un-catalysed magnesium hydride where the desorption rate increased 10x under the same conditions.

Interestingly the reaction rate for the absorption of hydrogen by magnesium to form magnesium hydride was reduced significantly by the presence of an electromagnetic field.

In all cases control of the system by compensation of the radiant heating system to control the sample temperature throughout allowed this work to be undertaken with no observable change in temperature in the material.

Acknowledgments

The process of developing the technology and writing this thesis has been an interesting, challenging, and rewarding period, made all the more interesting by the people I have worked with along the way.

I would like to acknowledge the help of Dr David Book, Professor Rex Harris, Dr Allan Walton and Dr Andy Williams for their support, guidance and assistance throughout the last few years. This help has been practical in providing equipment, lab space and experimental direction, as well as creating a supportive and enjoyable atmosphere in which to spend time spend in the discussion of results.

I would also like to thank C-tech Innovation and John Collins in particular for his efforts in giving direction to the project and spending the time to help work through every equipment issue that arose.

Finally I would like to express my thanks to two people who have been a great loss to all those who have had the pleasure to know them.

Ruth Wroe for the time and effort she put in to this project and whose untimely loss has left a large and lasting impression on many including myself.

Dr Andy Williams with whom I shared a great deal of fun at several stages of the last few years; firstly as my lecturer, then as my colleague, and finally as a collaborator but always and most importantly as a friend.

Many thanks to all.

| | |
|--|----|
| Figures..... | 9 |
| 1. Microwave assisted treatments of solid state hydrogen storage materials | 1 |
| 1.1 Introduction..... | 1 |
| 1.2 Business Context of the Project..... | 1 |
| 1.2.1 The Problem of Energy Supply..... | 3 |
| 1.3 The Storage, Transportation and Use of Energy | 4 |
| Table 1: Targets set for system performance by US Department of energy and the EU under the 6 th framework program [4, 5] | 5 |
| 1.4 Energy Storage Options for Transport Applications | 6 |
| 1.4.1 Batteries and Chemical storage options | 7 |
| 1.4.2 Hydrogen Production and Storage..... | 9 |
| 1.5 Metal hydride Materials | 14 |
| 1.5.1 The formation of metal hydrides | 14 |
| 1.5.2 Reaction Steps and Kinetic Considerations | 17 |
| 1.6 Fundamental properties of Magnesium Hydride..... | 21 |
| 1.6.1 Structure | 21 |
| 1.6.2 Electronic and thermal properties of magnesium hydride | 23 |
| 1.7 Formation steps in absorption process for magnesium Hydride..... | 24 |
| 1.7.1 Surface interactions at Solid Gas Interface..... | 25 |
| 1.7.2 Diffusion mechanisms sub surface and in bulk | 28 |
| 1.7.3 Phase nucleation and growth of MgH ₂ | 29 |
| 1.8 Desorption Process | 31 |
| 1.9 Mechanical processing of MgH ₂ | 36 |
| 1.9.1 Milling effects | 38 |

| | |
|---|----|
| 1.9.2 Reduction of grain size | 38 |
| 1.9.3 Thermal stability and grain growth | 39 |
| 1. 10 Catalysis of Magnesium Hydride | 40 |
| 1.10.1 Surface Interactions with Transition metal Oxides | 41 |
| 1.10.2 Catalytic Effects of Transition Metal Additions | 43 |
| 1.10.3 Addition of complex hydrides | 44 |
| 1.10.4 Destabilisation of Magnesium Hydride | 44 |
| 1.11 Microwave assisted sorption processes | 46 |
| 1.12 Microwave technologies | 47 |
| 1.12.1 Microwave production | 49 |
| 1.12.2 Microwave applicators | 50 |
| 1.12.4 Dielectric heating mechanisms | 51 |
| 1.12.5 Temperature measurement in microwave fields | 57 |
| 1.12.6 Diffusion under microwave fields | 58 |
| 1.12.7 Microwave catalysis | 67 |
| 1.12.8 Non thermal microwave effects | 68 |
| 1.12.9 Non Faradaic Electrochemical Modification of Catalytic Surfaces | 69 |
| 2. Technology development | 71 |
| 2.1 Prior C-Tech Innovation technology | 72 |
| 2.1.1 Commercially Available Microwave Chemistry Apparatus | 76 |
| 2.2 Outcomes required | 77 |
| 2.2.1 Development Iterations in the technology | 78 |
| 2.2.2 Development rig based on a domestic microwave | 79 |

| | |
|--|-----|
| Table 2.1: power settings and electric field strength of the multimode microwave | 80 |
| 2.2.3 The development of a volumetric gas control system | 81 |
| 2.3 Development of the Mixed Gas Control System | 85 |
| 2.3.1 Variable power microwave with temperature control and MGCS | 93 |
| 2.3.2 C-tech rig development with high pressure gas control system | 95 |
| 2.3.3 The development of fibre optic temperature control system | 99 |
| 2.3.4 RF variations collar/ sample holder changes power input tuning | 101 |
| 2.3.5 The measurement of dielectric properties of magnesium and magnesium hydride | 102 |
| 3. Results of the reaction kinetics of metal hydrides under microwave fields.... | 104 |
| 3.1 Material Characterisation of Magnesium Hydride | 104 |
| Table 3.1: Calculated grain size from XRD patterns using the Sherrer equation and full width half maximum values for as received and ball milled material and error calculated as standard error + variation | 110 |
| 3.2 Calibration and development of the flowing gas measurement system... | 114 |
| 3.2 The development of the measurement system..... | 115 |
| 3.3 The measured dielectric properties of magnesium and magnesium hydride | 117 |
| 3.4 The desorption of hydrogen under microwave fields | 120 |
| 3.4.1 The effect 300W microwave field on the desorption of H from MgH ₂ | 120 |
| 3.4.2 Material Properties after cycling under microwave and radiant conditions..... | 124 |
| 3.4.3 The influence of increasing the microwave field strength | 125 |
| 3.5 The absorption of Hydrogen by Magnesium under microwave fields | 127 |

| | | |
|-------|---|-----|
| 3.5.1 | The effect of Microwave fields on the Absorption behaviour of magnesium | 128 |
| 3.5.2 | The effect of reducing the microwave field strength on absorption behaviour | 132 |
| 3.6 | Catalysed magnesium hydride | 135 |
| 3.6.1 | The effect of nickel addition on the desorption kinetics..... | 136 |
| 3.6.2 | Lower temperature desorption under microwave field | 140 |
| 3.6.3 | The absorption of hydrogen at lower temperature using Ni catalysed Mg | 143 |
| 3.6.4 | The sorption Kinetics of Mg catalysed with Fe | 145 |
| 3.6.5 | Comparison of rates of desorption under microwave fields | 148 |
| 3.6.6 | The appearance of activation energy change | 150 |
| 3.6.7 | The effect of microwaves on other hydride systems | 152 |
| 4 | Discussion of results, | 158 |
| 4.1 | Temperature measurement | 160 |
| 4.2 | The effects of the microwave field on the desorption of hydrogen..... | 162 |
| 4.2.2 | Changes in diffusion rates | 164 |
| 4.2.3 | Changes to the reaction equilibrium | 167 |
| 4.2.4 | Physical changes in the material structure..... | 168 |
| 4.3 | Absorption kinetics, | 169 |
| 4.3.1 | Microwave enhanced diffusion..... | 169 |
| 4.3.2 | Temperature effects..... | 169 |
| 4.3.3 | Changes in the surface gas interactions | 170 |
| 4.3.4 | Changes in the structure of the material | 171 |
| 4.4.4 | Other possibilities | 172 |

| | |
|---|-----|
| 4.5 The effect of microwave fields on the reaction of Palladium with hydrogen | 172 |
| 4.6 Conclusions..... | 173 |
| 4.7 Future work | 174 |
| 4.8 Future applications | 175 |
| 5. The Effect of Microwave Fields on the Hydrogen Decrepitation of NdFeB Type Materials | 177 |
| 5.1 Objectives and Business case..... | 177 |
| 5.2 Introduction to rare earth magnets | 177 |
| 5.3.2 Origins of Magnetism | 179 |
| Table 5.1, Examples of some hard magnetic materials [128]..... | 184 |
| 5.4.3 Decrepitation of Neodymium Iron Boron Compounds..... | 187 |
| 5.4.4 NdFeB Magnet Production..... | 189 |
| 5.4.5 The HDDR process..... | 190 |
| 5.4.6 Compaction and alignment | 191 |
| 5.4.7 Finishing | 191 |
| 5.4.8 Coating | 191 |
| 5.5.1 Equipment..... | 192 |
| 5.5.2 Materials | 193 |
| 5.5.3 Sample preparation | 194 |
| 5.5.4 Decrepitation of HDD samples..... | 195 |
| 5.6. Results and discussion..... | 195 |
| 5.7 Conclusion..... | 208 |

Figures

| Figure and caption | Page |
|---|------|
| Figure 1.1: Price fluctuations and key geo-political events in nominal cost of crude oil in US\$ per barrel 1983-2008[3] | 3 |
| Figure 1.2: Comparison of energy density for energy storage options when compared to gasoline showing US DoE targets for 2010 (Adapted from Fichtner [6]) | 6 |
| Figure 1.3: Current status of hydrogen storage showing system capacity and cost of delivery, excluding reprocessing, compared to performance targets for 2010 and 2015 [5] | 10 |
| Figure 1.4: Relative volume of 4 kg of hydrogen stored by compression, condensation and solid state storage, illustrating the volumetric storage relative to the size of a car[12]. | 11 |
| Figure 1.5 Volumetric and gravimetric hydrogen density of some selected hydrides and pressurised gas storage is shown for steel and a hypothetical composite material, with the 2010 DoE Target highlighted for reference (adapted from [16]) | 14 |
| Figure 1.6 :Pressure–concentration–temperature plot and a van't Hoff curve[12] (logarithm of the equilibrium or plateau pressure against the reciprocal temperature) | 17 |
| Figure 1.7 : Graphical illustration of the hydrogen uptake kinetics(above) and hydrogenation rate (below) for the two major classes of hydrogenation and dehydrogenation curves[25]. | 19 |
| Figure 1.8: Illustration of the pressure induced structural changes that can occur in MgH_2 , (a-Alpha b-Beta c-Gamma d- Delta) [36] | 22 |
| Figure 1.9: The change in cell volume of MgH_2 with increasing pressure showing the changes in structure with the pressures noted.[36] | 22 |
| Figure 1.10 a)Schematic represnetaion of the processes of hydrogen interaction and phase formation in metal hydrides adapted from Schlapbach and Zuttler [11] | 23 |
| Figure 1.10b Physisorption and chemisorption represenatations from Schlapbach& Zuttler [12] | 25 |
| Figure 1.10C: subsurface hydrogen from Schlapbach& Zuttler[12] | 26 |
| Figure 1.10D: formation of the α solid solution represenatation from Schlapbach& Zuttler[12] | 27 |
| Figure 1.10e:representationof the Formation of the hydride β phase from Schlapbach& Zuttler[12] | 29 |
| Figure 1.11: Absorption energy as a function of structure for the formation of H-Mg-H layers and MgH_2 rutile structure[45]. | 29 |
| Figure 1.12: Absorption kinetics of ball-milled MgH_2 . The absorption behaviour is best described by a three-dimensional controlled contracting volume $_L \rightarrow L_{\infty}$ model with decreasing interface velocity (adapted from [46]). | 32 |
| Figure 1.13: Micrograph showing the alpha and beta regions of partially decomposed magnesium hydride[24] | 33 |
| Figure 1.14.: Thermal decomposition traces showing the rate of desorption as a function of temperature for fully reacted MgH_2 [24](heating rates 1. 24 k/min 2. 12 k/min 3. 6 k/min 4. 3 k/min 5. 1.5 k/min) | 34 |

| | |
|---|----|
| Figure 1.15: Thermal decomposition traces showing the rate of desorption as a function of temperature for partially desorbed magnesium hydride with 75% alpha phase[24]. (heating rates 1. 24 k/min 2. 12 k/min 3. 6 k/min 4. 3 k/min 5. 1.5 k/min) | 35 |
| Figure 1.16: Schematic depiction of the ball motion inside a planetary ball mill. | 36 |
| Figure 1.17: The effect of milling time on the dehydrogenation kinetics of magnesium hydride at 300°C[56] | 39 |
| Figure 1.18: Comparison of transition-metal oxides and their catalytic effect on the hydrogen desorption reaction rate of magnesium hydride at 300°C. (calculated between 20% and 80% of the respective maximum capacity.)[72] | 42 |
| Figure 1.19: Hydrogen desorption and absorption curves of MgH + 5at% (Ti, V, Mn, Fe, Ni) composites at 300°C[75] | 43 |
| Figure 1.20: Electro catalysis of hydrogen absorption in Mg; hydrogen is dissociated and dissolved in the Pd-cap layer, before forming the hydride, with the reaction controlled by the potential between the two electrodes. | 46 |
| Figure 1.21 Components Of Electromagnetic Wave - Electric and magnetic fields vibrate perpendicular to each other[90] | 48 |
| Figure 1.22: Internal structure of a cavity magnetron[92] | 50 |
| Figure 1.23: Showing the variation in the magnitude of the dielectric constant and dielectric loss factor as a function of frequency and the loss mechanisms[44]. | 53 |
| Figure 1.24: Density versus sintering temperature for alumina sintered in a microwave and a conventional furnace[100] | 62 |
| Figure 1.25: Normalised linear shrinkage of zirconia plotted as a function of sintering temperature for conventional and microwave assisted sintering, showing the effect of switching off the microwaves during processing (1080°C)[102] | 63 |
| Figure 1.26: Comparison of conventional and microwave-assisted oxygenation of melt-processed YBCO; 20 hour hold at 400°C. | 65 |
| Figure 1.27: H ₂ S conversion vs. temperature showing the improvement of the reaction rate above the equilibrium for the same catalysts in microwave fields and thermally.[109] | 68 |
| Figure 1.28: Schematic representation of a metal electrode deposited on a O ₂ -conducting and on a Na ⁺ -conducting solid electrolyte, showing the metal-electrolyte double layer and the double layer created at the metal-gas interface[114]. | 70 |
| Chapter 2 | |
| Figure 2.1: Gas heated lab scale hybrid microwave furnace, using mixed mode microwave system from 3 microwave sources[101, 116] | 74 |
| Figure 2.2: Industrial tunnel kiln developed to process 1m ³ of product per hour[117, 118] | 75 |
| Figure 2.3: Example of commercially available Sineo microwave batch reactor showing 12 high pressure reactors with pressure and temperature monitoring[13]. | 77 |
| Figure 2.4: schematic representation of the fixed volume gas system. | 81 |
| Figure 2.5: Silica sample tube positioned in the multimode domestic microwave cavity | 83 |

| | |
|---|-----|
| Figure 2.6: Choke sleeve assembly, showing the retaining nut spaces and sleeve | 84 |
| Figure 2.7: Gas fittings and holder in position through the cavity wall of the microwave. | 85 |
| Figure 2.8: Schematic diagram of the gas control system | 86 |
| Figure 2.9: Image of the gas control system in position | 87 |
| Figure 2.10: Mode 1 operation with mass flow controllers in series | 88 |
| Figure 2.11: Mode 2 operation of the system with mass flow controllers used in parallel to provide mixed atmospheres | 89 |
| Figure 2.12: Wiring diagram for the mass flow control system using an RS 485 control system | 90 |
| Figure 2.13: Rack mounted control and power supply unit for the mass flow control system | 90 |
| Figure 2.14: The control interface for the MGCS built in Microsoft visual basic | 91 |
| Figure 2.15: Microwave system with gas control board at the University of Birmingham, with vacuum system control and logging computer and the adapted multimode microwave system. | 94 |
| Figure 2.16: Sample temperature increase during heating and microwave irradiation at low power, showing the uncontrolled heating of a magnesium hydride. | 95 |
| Figure 2.17a) External view of the hybrid furnace at C-Tech Innovation showing the glove box, 2.17b) internal view of the system showing the insulation silica muffle heating elements and control thermocouples | 96 |
| Figure 2.18 a) Top housing for the silica muffle incorporating pressure relief, gas exit, and water cooling channels to aid sealing. b) bottom muffle housing incorporating gas inlet, exhaust, and glove box coupling. | 98 |
| Figure 2.19: Schematic representation of an OpSens white light interferometer fibre optic tip | 100 |
| Figure 2.20: OpSens fibre optic probe before and after 2 hours at 350°C under 7 bar hydrogen atmosphere | 101 |
| Chapter 3 | |
| Figure 3.1: SEM micrograph of the as received Goldschmidt magnesium hydride and the material after 5 hour of ball milling, showing the reduction in the particle size and the increased surface roughness of the particles. | 105 |
| Figure 3.2: X-ray powder diffraction pattern for Goldschmidt magnesium hydride as received. | 106 |
| Figure 3.3: X-ray powder diffraction pattern for Goldschmidt magnesium hydride after 5 hours milling | 107 |
| Figure 3.4: showing the flat gradient of the Williamson-Hall plot which indicates the relatively insignificant contribution of microstrain to the line broadening. | 109 |
| Figure 3.5: TGA trace of desorption behaviour of as received and ball milled magnesium hydride. Heated at 2°C/min to 400°C under flowing argon atmosphere | 111 |
| Figure 3.6: TGA traces showing the consistency of ball milled magnesium hydride | 112 |

| | |
|--|-----|
| produced over a period of two years. | |
| Figure 3.7: Van't hoff plot of log of the plateau pressure plotted against the reciprocal of temperature, with data from the Hydpark database plotted for reference. | 113 |
| Figure 3.6: Cumulative desorption from the 1 st desorption cycle of 3 separate magnesium hydride samples at 330°C. (Samples taken from a single batch and measured over a 2 week period) | 116 |
| Figure 3.7: Figure showing frequency dependence of dielectric loss factor of Mg and MgH ₂ measured under Argon using a concentric surface probe applicator at 298K. | 117 |
| Figure 3.8: Sample temperature change under microwave heating at a field strength of 300W | 119 |
| Figure 3.9: 3 consecutive cycles showing the cumulative desorption traces of magnesium exposed to a microwave field of 300W, no microwave and then 300W microwave. (Temperature 330°C pressure of hydrogen 500mbar.) | 121 |
| Figure 3.10: Plot of desorption rate measured in cm ³ /second for 2 cycles at 330 °C with a pressure of 500mbar. This shows a 400% increase in the peak rate of desorption with 300W microwave field present. | 122 |
| Figure 3.11: Plot of measured sample temperature and cavity temperature during the desorption at 330°C | 123 |
| Figure 3.12: variation in desorption rate throughout the reaction with the microwave field cycled on and off for 600 second intervals and the total desorption in the period. | 124 |
| Figure 3.13: Desorption of hydrogen from MgH ₂ with varying microwave field strengths from 300W to 100W at 310°C | 126 |
| Figure 3.14: The absorption of hydrogen by magnesium at 7000mbar and 330°C absorption cycle 1 and 2 | 128 |
| Figure 3.15: Absorption behaviour of Mg at 330°C and 7 bar hydrogen pressure with and without a 300W microwave field | 129 |
| Figure 3.16: Sample temperature of Magnesium samples during absorption with and without 300W microwave field | 130 |
| Figure 3.17: Absorption rate of magnesium hydride at 330°C and 7000mbar, showing the displacement of the reaction under the 300W microwave field until the electromagnetic field is removed | 131 |
| Figure 3.18: The effect of alternating the microwave field on and off during the absorption process at 7000mbar and 330°C with a non-microwave absorption curve for comparison | 132 |
| Figure 3.19: Absorption rate for magnesium at 330°C at 7 bar with a range of applied microwave field strengths (300W, 200W 100W, and non-microwave for comparison). | 133 |
| Figure 3.20: Absorption of hydrogen by magnesium at 330°C and 7000 mbar with reducing microwave field strength from 300W to 50W showing an increasing absorption rate with power reduction. | 134 |
| Figure 3.21: Desorption from MgH ₂ catalysed with 2mol% Ni at 310°C 500mbar with non-catalysed MgH ₂ as a comparison | 137 |

| | |
|--|-----|
| Figure 3.22: Desorption from MgH_2 catalysed with 2 mol% Ni with and without a 300W microwave field at 310°C and 500mbar. | 138 |
| Figure 3.23: Desorption rate (cm^3S^{-1}) profile from MgH_2 catalysed with 2 mol% Ni with and without a 300W microwave field at 310°C and 500mbar | 139 |
| Figure 3.24: Desorption from MgH_2 Catalysed with 2 mol% Ni with 300W microwave field at 310°C and 500mbar with un-catalysed MgH_2 as a comparison | 140 |
| Figure 3.25: Desorption from magnesium hydride with 2mol% Ni, at 270°C with and without a 300W microwave field. Desorption only occurs with the microwave field present. | 142 |
| Figure 3.26: Temperature plot during the desorption in Figure 3.25 with a 300W microwave field. | 143 |
| Figure 3.27 Shows the absorption of a Ni catalysed sample held at 270°C and 7bar pressure of hydrogen under a 300W microwave field. The microwave is removed at 5100 seconds. | 144 |
| Figure 3.28: Desorption at 330°C and 500mbar showing the addition of 5mol% iron when compared to the pure milled magnesium with no microwave field applied | 146 |
| Figure 3.29: Desorption from MgH_2 with 5mol% Fe at 330°C and 500mbar hydrogen pressure showing the improvement in desorption rate with the microwave field | 147 |
| Figure 3.30: comparison of Microwave assisted desorption of milled Mg and Mg with 5mol% Fe | 148 |
| Figure 3.31 shows a comparison of the rate of desorption from Pure MgH_2 and material Catalysed with 5mol% Fe and 2mol% Ni throughout the decomposition from 100% MgH_2 to the metallic Mg at 330°C with 300W of microwave field | 149 |
| Figure 3.32: Comparison of $\ln K$ values for the calculation of activation energy from the onset temperature of desorption in at a range of ramp rates. | 152 |
| Figure 3.33: Hydrogen absorption rate of palladium at 200°C with increasing pressure with and without 300W microwave field. | 155 |
| Figure 3.34: Desorption of Pd at 200°C with pressure reducing from 8bar to 1bar at 100mbar/min | 156 |
| Figure 3.35: Desorption of Pd at 200°C with pressure reducing from 8bar to 1bar at 300mbar/min compared to a pressure reduction rate of 100mbar/min | 157 |
| Figure 3.36: a) Graphical illustration of the hydrogen uptake kinetics (above) and hydrogenation rate (below) for the a diffusion limited and b nucleation and growth limited hydrogenation and dehydrogenation curves[25] b) shows the measured desorption rate under a microwave field for milled magnesium at 330°C | 164 |
| Figure 3.37. Comparison of transition-metal oxides and their catalytic effect on the hydrogen desorption reaction rate of magnesium hydride at 300°C. (calculated between 20% and 80% of the respective maximum capacity.)[72] | 166 |
| Chapter 5 | |

| | |
|--|-----|
| Figure 5.1, Magnetic classification of elements within the periodic table [19] | 180 |
| Figure 5.2: Summary of magnetic behaviours in materials with respect to magnetic moments and field directions (from A.J Williams [19]). | 182 |
| Figure 5.3 Schematic illustration of the break-up of magnetisation into domains and the external field pattern for a (a) single domain, (b) two domains,(c) four domains and (d) closure domains[127]. | 183 |
| Figure 5.4: Vertical section through the NdFeB phase diagram passing through pure Fe and Nd ₂ Fe ₁₄ B (after Schneider et al 1987). | 185 |
| Figure 5.5. Crystal structure of Nd ₂ Fe ₁₄ B with hard magnetic c direction vertical after Herbst et al [129]. | 186 |
| Figure 5.6. Schematic representation of the Hydrogen Decrepitation process in NdFeB alloys | 189 |
| Figure 5.7: Schematic representation of a jet mill used to reduce the particle size with supersonic gas flow[142] | 190 |
| Figure 5.8 Photographs of the voice coil motor magnet samples (a) with the nickel coating and (b) with the coating removed. | 193 |
| Figure 5.9: SEM micrographs showing cross sections of the nickel coating on the samples that is removed prior to experiments. | 193 |
| Figure 5.10: Sample in 1 bar hydrogen, no microwave treatment, showing the activation of hydrogen decrepitation reaction and subsequent temperature rise and pressure drop associated with the exothermic reaction | 197 |
| Figure 5.11: Typical pressure change over time from 1 bar hydrogen starting pressure and surface temperature in a closed system at room temperature with no microwave treatment. | 198 |
| Figure 5.12: Showing the distribution of initiation times for the untreated samples and those exposed to 30 and 60 seconds of microwave power. | 201 |
| Figure 5.13: Temperature and pressure profile of the decrepitation process with no microwave exposure | 202 |
| Figure 5.14: Temperature and pressure profile of the decrepitation process of a sample with 30 second microwave treatment. | 203 |
| Figure 5.15: Temperature and pressure profile of the decrepitation process of a sample with 60 second microwave treatment. | 203 |
| Figure 5.16: Temperature of the surface 20 seconds prior to the initiation of the decrepitation process for samples with 3 levels of microwave exposure. | 204 |
| Figure 5.17: Cross section of the surface of the magnet after the removal of the nickel coating after exposure to laboratory air for 24 hours prior to mounting | 205 |
| Figure 5.18: Cross section of the surface after exposure to 1 bar hydrogen for 400seconds | 206 |
| Figure 5.19: Cross section of the surface of a sample exposed to 1 bar hydrogen atmosphere for 400 seconds with 60 seconds microwave treatment | 206 |
| Figure 5.20: Shows the effect of constant temperature exposure, provided by a water bath, throughout the experiment and the reduced activation time with increased temperature | 207 |

1. Microwave assisted treatments of solid state hydrogen storage materials

1.1 Introduction

This Eng D project was initiated in order to identify and examine the effects of dielectric fields on the processing and reactions of materials under hydrogen atmospheres.

C-Tech Innovation has a long history of scientific research and applying fundamental understanding to commercially promising technologies. The processing of materials under microwave and radio frequency fields has been a key technology for the company that has been applied to many industrial applications from ceramic sintering to the processing of food products.

Observed changes to the reaction rates and final properties of the products over the course of many experiments in materials processing has lead the researchers at C-Tech to investigate several applications of the microwave technology and some of these will be explored in this work.

1.2 Business Context of the Project

The project is undertaken as part of the Innovative Hydrogen Solutions development work which is a spin-off company from C-Tech Innovation, the project aims were to explore the possible applications of technology developed in other areas to the field of hydrogen storage. This would involve the application of intellectual property and expertise in the development of a system to assess the reactions of metal hydrides under high frequency electric fields.

The funding vehicle “Innovative Hydrogen Solutions” (IHS) aims to find applications within the field for the hybrid microwave, radiofrequency and radiant heating technology that has been developed and extensively exploited by C-Tech

innovation over the last 15 years. By setting up a subsidiary within the structure of C-Tech it was possible to raise additional capital from investors looking to benefit from the future income successful implementation of the project and related intellectual property.

This aim is to assess the viability of dielectric field assistance to enhance the charge / discharge kinetics and diffusion properties of existing solid-state hydrogen storage materials.

With over 60 million cars and other vehicles produced each year and with the vast majority currently running on petrol or diesel, the move to alternative fuels offers a huge market [1]. A development in the field of hydrogen storage that could result in a small share of this multi-billion pound industry would be highly lucrative. The area of energy storage is a key enabling technology in the drive towards an energy economy that is less reliant on oil, therefore it is anticipated that any significant improvement in this field will be likely to generate substantial business opportunities in the forthcoming period.

The limitations of the solid state, liquid and high pressure gas stores will be discussed later but there is significant scope to develop processing or treatment methodology to increase the practicality of some of these systems.

While the application of microwave and dielectric fields are not expected to alter the fundamental properties of materials there are high capacity solid state hydrogen stores that are kinetically limited, so there is increased effort in the field to improve these in order to find a viable solution.

Although there has been limited work in the field high frequency electric field effects on the sorption behaviour of hydrogen storage materials, these have been focused on just one aspect of the process.

The system of gas control along side RF and microwave applicators will be the first attempts to study the reaction of hydrogen with metals in a controlled system. In order to ascertain and quantify the effectiveness of the approach the project will concentrate on well characterised materials and compare the effects

of conventional heating with that of conventional heating combined with dielectric fields.

1.2.1 The Problem of Energy Supply

One of the major concerns for the world economy this century is the supply of, and demand for, energy around the world. This will centre on both the supply and utilization of energy, as decreasing fossil fuel reserves will increase the drive for the developments of more efficient use of the remaining stocks.

The Developing World wants a cheap, efficient energy source similar to that the western world has enjoyed for decades. Currently that source is oil.

Oil accounts for around 45% of total energy supply globally and the past decade has seen price fluctuations from lows of \$14 per barrel to peaks of \$135 as illustrated in figure 1.1 [2, 3].

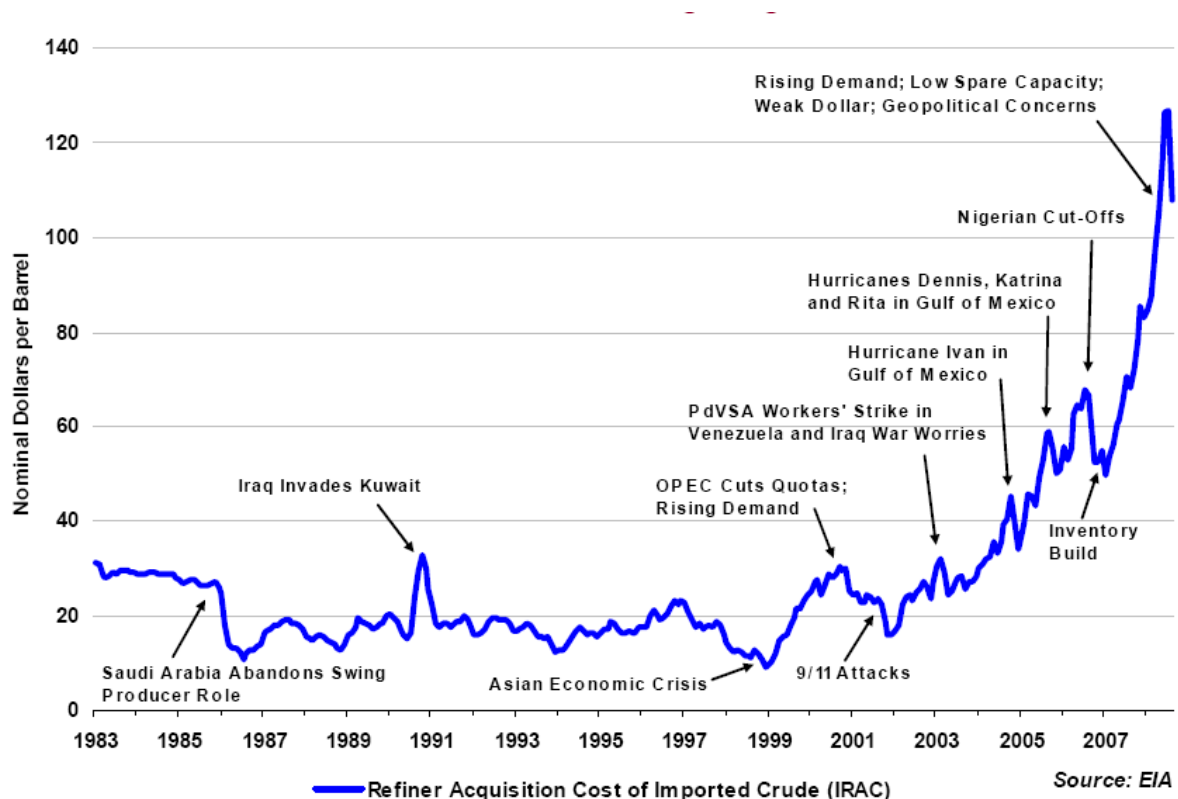


Figure 1.1: Price fluctuations and key geo-political events in nominal cost of crude oil in US\$ per barrel 1983-2008[3]

The effect of world events is clearly illustrated in the graph, showing the spikes at moments of conflict such as the start of the first gulf war in 1991. This is clearly not an ideal system to base the bulk of the worlds manufacturing, transport and domestic energy on such an unstable commodity. It is this variation in the cost of energy and the likelihood of future price increases that has hastened the search for alternative sources of energy and ways to reduce both the per capita consumption and the energy used per unit of GDP.

1.3 The Storage, Transportation and Use of Energy

To consider the solutions to future energy demand, it is important to understand that the use of energy falls into two main categories:

- Static; heating, lighting and powering equipment, used at home and industry
- Mobile; in the transport of goods and people

Energy for static applications can be supplied in two ways; firstly through local generation and secondly using centrally generated electricity distributed through a grid system. Energy for use in transport can be delivered in three ways:

- Tapping into a static source (e.g. electrified railways)
- On board transportation of the energy supply (e.g. petroleum)
- Collection of energy during transit (e.g. solar cells on spacecraft).

The problem with petroleum is that it is linked to a finite source (crude oil), and the pollutants produced in the energy conversion have a detrimental effect on the atmosphere.

To utilise the full range of renewable energy sources, that are not biomass derived, it will be essential that we use a common and efficient energy vector, where an energy vector is a means of converting storing and transporting one type of fuel into a form that can fulfil a variety of roles.

Electricity is currently the most common energy vector used in the developed world, and it is the flexibility in the output is essential to the way we live our lives. The reliability ease and efficiency of high voltage power transmission has allowed the centralisation of the energy generating equipment and the integration of a wide range of generation technologies from fossil fuels, nuclear and renewable systems.

The use of electricity does not create a panacea in the energy demand market as for mobile applications there continue to be very large challenges that we currently face. The problems are related to the storage and concentration of energy to a package that can be easily transported, efficiently accessed and readily refreshed.

For any emerging technology the benchmark is the current solution to the problem, in short there should always be a benefit in the adoption of the new technology. In the case of energy supply for transportation, oil based liquid fuels have many of the desirable properties allowing long range travel without refuelling, relatively low cost when tax is excluded, and simple to refill. The development of alternatives energy forms that meet many of the same performance criteria is a difficult task. Table 1 highlights the targets that have been set by the EU and US agencies

Table 1: Targets set for system performance by US Department of energy and the EU under the 6th framework program [4, 5]

| | US DoE 2010 | US DoE 2015 | EU StorHy 2010 |
|-----------------------------------|----------------|----------------|-------------------|
| Gravimetric Energy Density KWh/Kg | 2 | 3 | 2 |
| Volumetric Energy Density KWh/l | 1.5 | 2.7 | 1.5 |
| Cost Per KWh | \$4 | \$2 | |
| Refuelling time | 3min | 2.5min | 4min |

The US department of energy and the European Union have outlined the target requirements which an alternative system should meet if a new energy vector is to be viewed as a viable option for transport applications. These are based on a comparison with petrol and expect performance figures of: 300-500 km range between refuelling, cost of below 2\$ per KWh and production to have a very low environmental impact.

1.4 Energy Storage Options for Transport Applications

When the options for the viable alternatives are considered it is obvious there is not one stand out candidate to be considered. Figure 1.2 shows the challenges involved in matching the performance of petroleum based fuels; the most viable renewable options are more than an order of magnitude below current fuels both in energy density and specific energy measures.

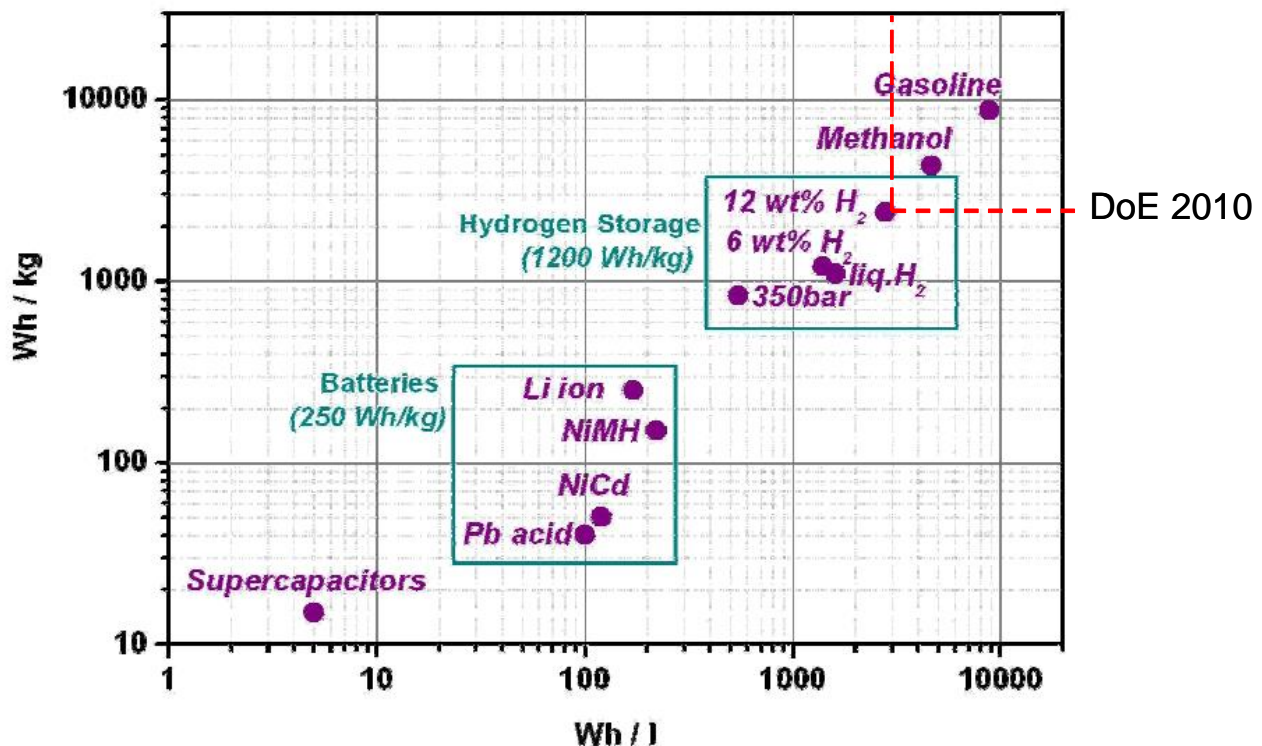


Figure 1.2: Comparison of energy density for energy storage options when compared to gasoline showing US DoE targets for 2010 (Adapted from Fichtner [6])

The problems in the materials range from volumetric or gravimetric energy density of the storage medium, requiring too large or too heavy a store to be viable for a transport application to systems that are unable to deliver the efficiency in the round cycle performance or slow charge and discharge performance. A solution to the weight and size of energy storage systems would enable a shift in the use of energy and is a key enabling technology if technology is to move away from the current energy vectors.

1.4.1 Batteries and Chemical storage options

The chemical storage of energy in the form of rechargeable batteries has been used for over 100 years, from the first lead acid systems to the development of new higher energy density cell chemistries such as lithium ion. The variation in the chemistry and structure of batteries is often tailored to suit specific applications.

The high power batteries that have been suggested and trailed for automotive and transportation applications are: lithium ion cells, high temperature molten sodium systems such as the Zebra battery and nickel metal hydride systems. These have shown some success and are the basis for many hybrid systems currently on sale in the UK. In the struggle for increased range there are also experimental chemistries under development that offer further advancement in energy storage which include lithium air and zinc air batteries.

The basic concept of the nickel-metal hydride negative electrode emanated from research on the storage of hydrogen for use as an alternative energy source in the 1970s. Certain metallic alloys were observed to form hydrides that could capture (and release) hydrogen in volumes up to nearly a thousand times their own volume. By careful selection of the alloy constituents and proportions, the thermodynamics could be balanced to permit the absorption and release process to proceed at room temperatures and pressures. Now that the technology is reasonably mature, NiMH batteries have begun to find use in high voltage

automotive applications as the energy density is more than double that of Lead acid and the cost is lower than the equivalent Li Ion cells.

Lithium Ion batteries are characterised by high specific energy, high efficiency and are reasonably resistant to cycling. These properties have made lithium Ion batteries the power sources of choice for a large part of the consumer electronics market with a production of the order of billions of units per year. These batteries can also be expected to find a prominent role in electrochemical storage systems for sustainable vehicles, such as hybrid and electric vehicles. However, scaling up the lithium battery technology for these applications is still problematic, as issues such as safety, costs, operational temperature and materials availability, are still to be resolved [7].

The high temperature cells are generally use molten anode of sodium or a sodium salt that is reacted through a solid alumina electrolyte. These systems have a relatively high power density of 150 Wh/kg and due to the molten state of the electrode materials these devices are able to withstand rapid charge/discharge cycles with large currents [8]. The major disadvantage with these technologies is the losses associated with the heating which can account for more than 15% of the stored energy when not in use.

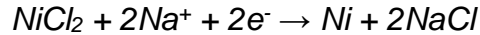
The sodium sulphur battery is one example where the liquid sodium is stored at over 300°C separated from the container of molten sulphur by a beta-alumina solid electrolyte[9]. The discharge process can be represented as follows:



The ZEBRA battery is a development of the molten sodium sulphur cell which operates at 250 °C (482 °F) and utilises molten sodium aluminium chloride (NaAlCl₄), which has a melting point of 157 °C (315 °F), as the electrolyte[10]. The negative electrode is molten sodium. The positive electrode is nickel in the discharged state and nickel chloride in the charged state. The ZEBRA battery has an attractive specific energy and power (90 Wh/kg and 150 W/kg).

The electrode reactions are[10];

Anode



Cathode



And therefore the total cell reaction is



1.4.2 Hydrogen Production and Storage

Hydrogen has the potential to be an attractive alternative energy carrier, particularly for the transportation sector. It can be clean, efficient, and derived from diverse range of energy sources, including renewable forms of energy such as: biomass, hydroelectric, wind, solar, geothermal as well as fossil fuels and nuclear energy.

The key advantages of hydrogen as a replacement for petroleum based fuels in the transport sector are:

- Flexible source not linked to any single finite resource.
- When reacted with oxygen it only produces water.
- Hydrogen has the highest known energy density per unit mass.

There are three primary barriers that must be overcome to enable industry commercialisation of hydrogen fuel cell vehicles:

- On-board hydrogen storage systems are needed that allow a vehicle driving range of greater than 300 miles while meeting vehicle packaging, cost and performance requirements;
- Fuel cell system cost must be lowered to \$30 per kilowatt by 2015 while meeting performance and durability requirements;
- The cost of safe and efficient hydrogen production and delivery must be lowered to be competitive with gasoline independent of production pathway and without adverse environmental impact.

The barriers associated with hydrogen production, delivery and fuel cells are essentially cost-driven. However as figure 1.3 shows, in the case of on-board vehicular hydrogen storage, no approach currently exists that can meet the technical requirements for greater than 300-mile range while meeting all performance metrics, regardless of cost.

The production of hydrogen is not currently a low CO₂ emission process with the majority of hydrogen produced from natural gas through a process of steam reforming.

The electrolysis of water is an energy intensive process requiring large amounts of electricity that will have to be generated from a separate source. If this electricity is generated in a fossil fuel fired power station, as is the case in much of the UK then there will still be the associated CO₂ emissions.

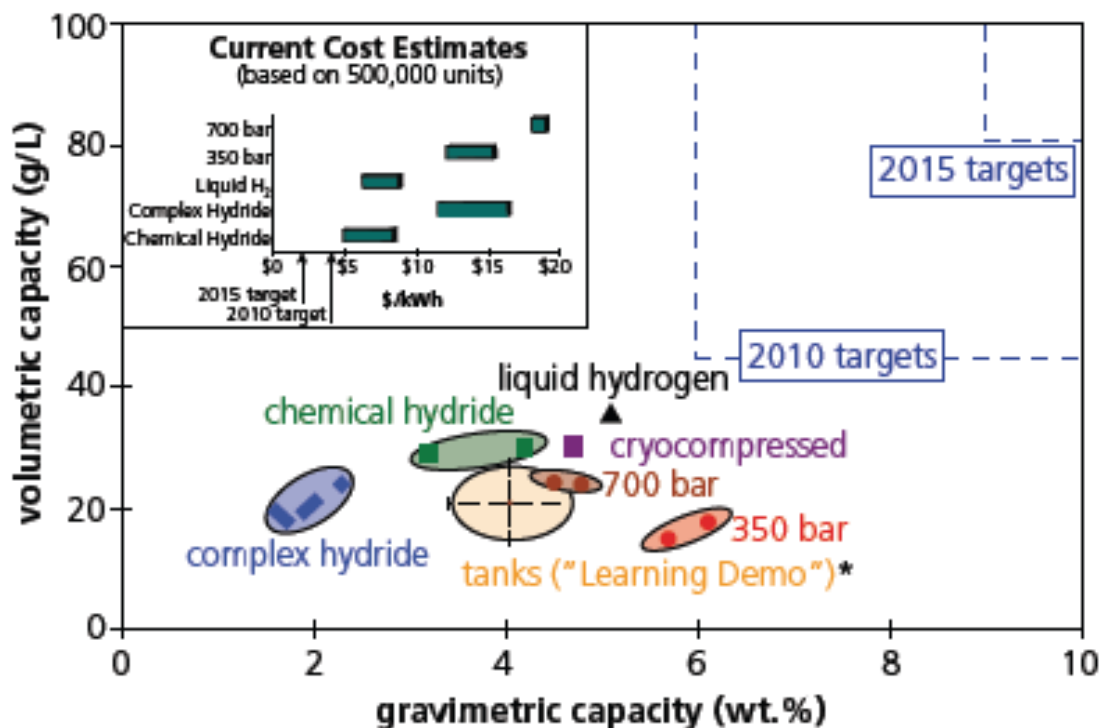


Figure 1.3: Current status of hydrogen storage showing system capacity and cost of delivery, excluding reprocessing, compared to performance targets for 2010 and 2015 [5]

In the case of fossil fuels, natural gas is likely to be used for the distributed production of hydrogen in the near term, before the infrastructure required for

centralised production and hydrogen delivery is developed. In the longer term, centralised hydrogen production may involve the use of clean coal with carbon sequestration or nuclear energy.

The most pressing problem in the path towards a hydrogen based transportation sector is the onboard storage of enough hydrogen to deliver the range required.

For both mobile and stationary applications, there are three possible ways to store hydrogen. These are in cylinders of compressed gas, in tanks of liquid hydrogen or in hydrogen storage materials Figure 1.4 [11, 12].

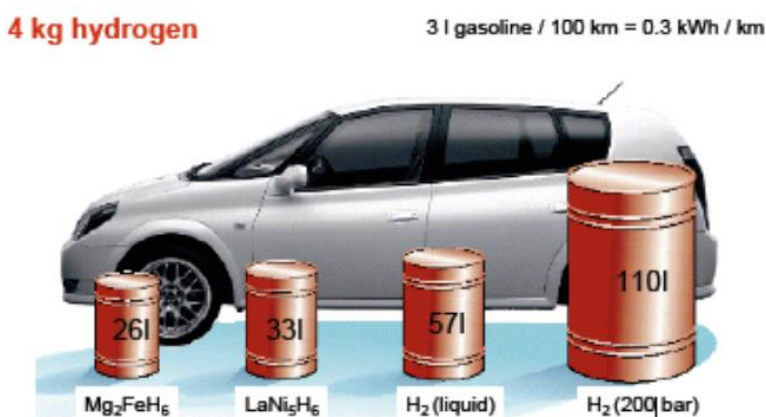


Figure 1.4: Relative volume of 4 kg of hydrogen stored by compression, condensation and solid state storage, illustrating the volumetric storage relative to the size of a car[12].

Pressurised hydrogen can be stored in light weight cylinders made from composite materials which can be designed to withstand pressures of up to 700 bars in order to provide enough fuel for a driving range of 400-500km. Significant disadvantages of this method are the energy expended every time the hydrogen is compressed (up to 18% of the available energy), the safety risks associated with the on board cylinder and the risk of failure at sub-zero temperatures.

Despite these issues the European Union launched in 2001 the Clean Urban Transport for Europe project to demonstrate the technical feasibility of using hydrogen to power vehicles. Within this project, 33 hydrogen fuel cell powered

buses are operated in 9 cities around the world - Amsterdam, Barcelona, Beijing, Hamburg, London, Luxembourg, Madrid, Perth, Reykjavik[13].

The systems use gaseous hydrogen, compressed in gas cylinders at a pressure of 350 bar, to generate electricity in a stack of fuel cells that powers a central electric motor. However, gas cylinders able to support such a high pressure are too heavy to be widely used in private cars.

Condensation into liquid or even solid hydrogen is, of course, particularly attractive from the point of view of increasing the mass per container volume. The density of liquid hydrogen is 70.8 kg m^{-3} . But the condensation temperature of hydrogen at 1 bar is -252.7°C and the vaporization enthalpy at the boiling point amounts to 452 kJ kg^{-1} . As the critical temperature of hydrogen is -241.7°C liquid hydrogen containers must be open systems to prevent strong overpressure[12]. Therefore, heat transfer through the container leads directly to the loss of hydrogen which can be up to 2% per day[14]. The option of storing cryogenic liquid hydrogen also has significant disadvantages such as boil-off, tank design and the large amount of energy associated with the refrigeration process; besides technical complexity, the process of hydrogen liquefaction consumes about 20% of the recoverable energy[14].

BMW have built an automated liquid-hydrogen filling station, and developed and tested several cars running with hydrogen in newly designed vessels to reduce losses by evaporation to below 1.5 mass% per day[15].

Because of these drawbacks with the competing technologies for hydrogen storage, solid state hydrogen storage materials are potentially the most attractive option.

The ideal storage material for mobile applications would have the following characteristics:

- High weight % and a high volumetric density of hydrogen.
- Ability to absorb (or adsorb) and desorb hydrogen at or close to room temperature and at pressures of around 1 bar.

- Rapid absorption (or adsorption) and desorption kinetics.
- Cheap and readily available materials.
- Straightforward and low energy method of preparation.
- Resistant to poisoning by trace impurities.
- Good thermal conductivity in charged and uncharged condition for ready heat management.
- Safe and reusable on exposure to air.
- Capable of being regenerated and readily recycled.

This is a formidable list of required properties and no such material exists at present[14]. In the USA the Department of Energy has set the technical targets for hydrogen storage materials for 2010 and 2015 of more than 6 wt% of hydrogen (including the tank and valves) and the filling time should not exceed 5 minutes[5]. Further the temperature necessary to release the hydrogen from the storage material should not exceed the temperature of the exhaust gas of the fuel cell. This temperature is around 80°C for a standard PEM fuel cell.

Figure 1.5 illustrates the gravimetric and volumetric storage properties of some solid state storage materials compared to high pressure and cryogenic stores, with the selection criteria system targets for 2010 from the Department of energy highlighted. For the solid state stores this highlights the small number of available compounds that meet this basic requirement without the further practical considerations of reversibility, reaction kinetics, resistance to degradation and system efficiency.

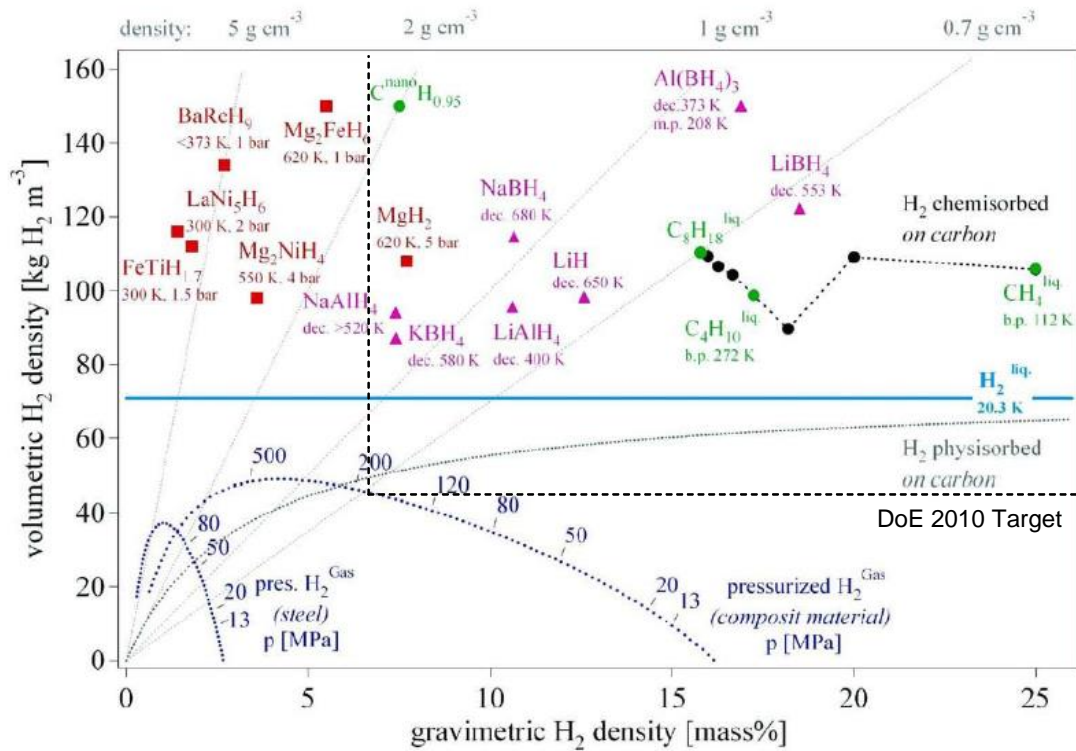


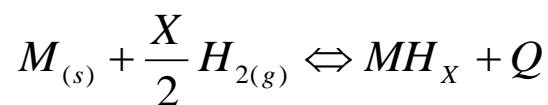
Figure 1.5 Volumetric and gravimetric hydrogen density of some selected hydrides and pressurized gas storage is shown for steel and a hypothetical composite material, with the 2010 DoE Target highlighted for reference (adapted from [16])

1.5 Metal hydride Materials

1.5.1 The formation of metal hydrides

The reaction of hydrogen with a metal is often seen as a relatively simple chemical reaction[17] without real consideration of the complex mechanisms involved. The formation of a stable metal hydride is an exothermic process with two reagents and one product usually found in the form:

Equation 1



Where Q is the released heat during reaction, as materials of practical interest for energy storage the reaction with hydrogen is exothermic[18].

That the formation of the metal hydride is the thermodynamically exothermic is important of the reversibility of the hydride materials due to temperature change. The negative value of the entropy allows the compounds to be destabilised by heating and driving the dehydrogenation reaction.

The Gibbs free energy equation shows the relationship between enthalpy and entropy:

Equation 2

$$\Delta G = \Delta H - T\Delta S$$

Where ΔG is the change in gibbs free energy, ΔH is the change in enthalpy, T is temperature in Kelvin and ΔS is the change in entropy.

Rearranging this equation at the point of equilibrium, where $\Delta G = 0$, shows that;

$$\Delta H = T\Delta S$$

As can be seen from this increasing the temperature will increase the entropy of the system and allow the decomposition to proceed spontaneously.

Metal hydrides are generally composed of metal atoms that constitute a host lattice with hydrogen atoms arranged geometrically in the crystal, where the metal and hydrogen reactions arrange to form two different kinds of hydride structures; the α phase at which hydrogen is absorbed into interstitial sites within the lattice forming a solid solution, and the β phase at which hydride is fully formed as a crystalline phase. When the hydrogen pressure at isothermal conditions is increased the adsorbed amount of hydrogen will increase only slightly corresponding to the formation of a solid solution of hydrogen, when the maximum solubility of hydrogen in the α phase is reached the hydride (β phase) will start forming. Increasing the hydrogen pressure further, results in a substantial increase in the absorbed amount of hydrogen as expected by the Gibbs phase rule[19].

Equation 3

$$F = 2 - \pi + N$$

Where F is the number of degrees of freedom, π is the number of phases and N is the number of chemical species.

The process, by which the material transforms, from a solid solution through a two phase region and to the final single β phase state, occurs on a region of constant pressure. This plateau pressure describes the stability of the hydride at a given temperature and is the key thermodynamic property. The formation and decomposition of the hydride occur on the plateau and is usually characterised by a hysteresis phenomenon. The hydrogen equilibrium pressure during absorption is higher than that of desorption. This is commonly attributed to the extra energy necessary to overcome the constraints related to the lattice expansion[18].

The relationship between the temperature and plateau pressure is determined by the physical structure of the material. The stability of the formed hydride is determined by its hydrogen equilibrium pressure at a given temperature. Thus, thermodynamic properties of hydrides are usually described in pressure-composition isothermal (PCI) curves. A typical set of PCI curves for an ideal intermetallic compound able to reversibly absorb hydrogen is represented in figure 1.6

As the reaction of hydrogen is reversible for metal hydrides the plateau pressure can be measured at a variety of temperatures. This data can be plotted on a graph with measured plateau pressure on the Y-axis and $1/T$ on the X-axis. The data should have a linear relationship, the equation for which can be found by fitting the data using the linear form of the Van 't Hoff equation.

Equation 4

$$\ln P_{(eqH)} = \frac{\Delta H}{RT} - \frac{\Delta S}{R}$$

Figure 1.6 shows the PCT behaviour for a material, with the variation in the plateau pressure dependant on temperature. Further information can be obtained by taking the midpoint of the plateau and plotting against the reciprocal of temperature. By increasing the temperature it is possible to change the equilibrium pressure at which the absorption and desorption reactions occur. This behaviour can generate a pressure composition isotherm for a material which can be plotted to give a PCT relationship.

This gives the Van't Hoff Plot where the gradient divided by the gas constant R corresponds to the heat of formation of the hydride, and the intercept relates to the entropy.

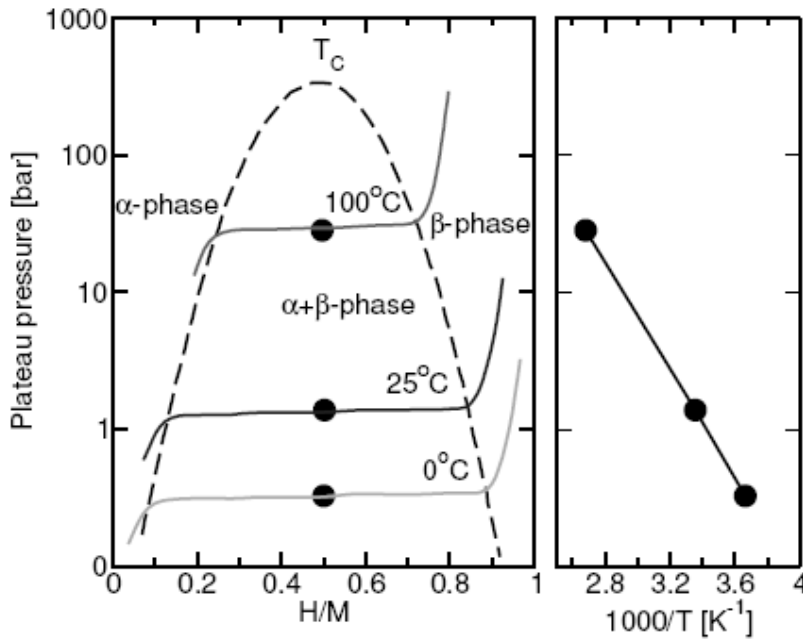


*Figure 1.6 :Pressure–concentration–temperature plot and a van't Hoff curve[12]
(logarithm of the equilibrium or plateau pressure against the reciprocal temperature)*

1.5.2 Reaction Steps and Kinetic Considerations

While the Gibbs Phase Rule can be sufficient for thermodynamic considerations, it is probably misleading, from a kinetic point of view to think of the formation of a metal hydride as a single reaction as there are several steps involved in the

reaction, relating to surface interactions, diffusion processes. Additionally second phase nucleation and growth that play an important role in the rate of reaction and the temperature at which a reaction will proceed.

When considering the reaction of a gas phase reactant with a metal surface it is important to understand the relevant steps in the formation of the hydride, namely the adsorption, dissociation, subsurface penetration, bulk diffusion and hydride formation[20].

For the reaction between the gas phase hydrogen molecule and a metal surface to proceed requires the two species to come into contact. As the molecule is moved closer to the surface the potential energy will increase due to repulsion. At some point in the process the potential energy of the H_2 molecule will become equal to the hydrogen dissociation energy after this point, it is more favourable for the two hydrogen atoms to be separated and chemisorbed on to the metal surface rather than bonded in a molecule. An H_2 molecule moving towards the surface will, at some point, feel a weak attractive force in the range of approx. 0-20 kJ/mol H (van der Waals forces) corresponding to molecular physisorption.

If the dissociated form is at a potential energy larger than the gas phase H_2 dissociation energy the reaction is said to be activated and the difference determines the activation barrier for dissociation[21]. In this case where activation energy is required, only a percentage of the molecules with sufficient energy above that of the activation barrier will be able to dissociate relating to the Boltzman distribution of energies within the population.

If the hydrogen-metal bond is stronger than the H-H bond, chemisorption is said to be exothermic. Beyond the point of chemisorption the hydrogen atoms can penetrate the first metal atomic layer into the subsurface through an activated process from which it can diffuse into the bulk (as a solid solution) of the metal[21].

By developing equations for the material transformations and applying a simplified choice of geometry along with appropriate initial and boundary conditions it is possible to solve the hydrogen concentration profile as a function

of space and time. However with the multiple reaction steps involved, coupled to the numerical complexity, often leads to the adoption of the assumption of a rate limiting step being used to describe the macroscopic system. This effectively results in a significant reduction of the complexity[22].

When experimental kinetic data is fitted with a rate equation, limitations due to either hydride nucleation and growth, or diffusion, are often regarded as the most likely candidates for the rate limiting step[23, 24].

When reviewing the shape of reported hydrogenation/dehydrogenation curves, i.e. macroscopic hydrogen uptake/release as a function of time, they can roughly be divided into two major classes, one with a monotonically decreasing uptake rate and one with a sigmoidal shape.

The two types are illustrated in figure 1.7; curve A highlights the monotonically decreasing uptake and is usually rationalised in terms of either a surface process such as dissociation or bulk diffusion is rate limiting the overall kinetics.

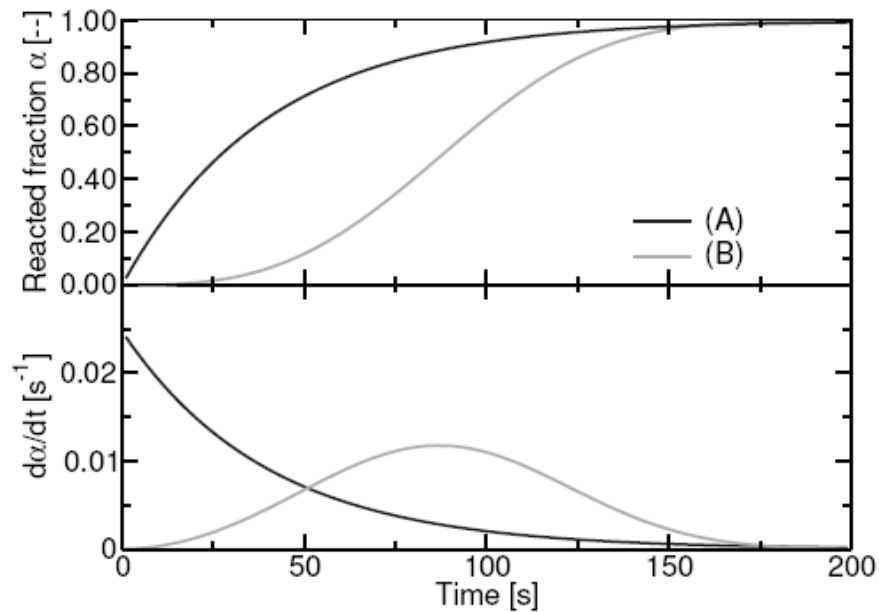


Figure 1.7 : Graphical illustration of the hydrogen uptake kinetics(above) and hydrogenation rate (below) for the two major classes of hydrogenation and dehydrogenation curves[25].

The sigmoidal shape of curve B is usually rationalised in terms of a nucleation and growth mechanism limiting the overall kinetics. Kinetic descriptions of the nucleation and growth process is usually explained by a Johnson-Mehl-Avrami (JMA) rate equation

The Johnson Mehl Avrami equation is usually expressed in the form

Equation 5

$$\alpha(t) = 1 - \exp(-(kt)^n)$$

where n , is the Avrami exponent and the parameters describing nucleation and growth rates are contained within the effective kinetic parameter or rate constant, k

The temperature dependency of the rate constant k is usually described by an Arrhenius relation

Equation 6

$$k = A \exp\left(-\frac{E_A}{RT}\right)$$

where A is a pre-exponential factor, E_A is the apparent activation energy and R is the universal gas constant

The JMA equation is useful as it describes not only curves with a sigmoidal shape, where the value of n is between 1.5 and 2, but also the monotonic curves in figure 1.7, describing situations where diffusion may be rate limiting or where nucleation and growth represent the most significant restriction.

This is probably why the JMA model is often successfully invoked when dealing with the kinetics of hydrogenation/dehydrogenation of metal hydrides and its use sometimes results in conclusions about a diffusion process being rate limiting. In situations where diffusion limits reaction kinetics the value of the n given is less than 1.

It is also interesting to note that a sigmoidal uptake curve can be a result of a hydride with a protective surface oxide layer as observed for magnesium. During

the first hydrogenation, cracks are developed in the oxide layer due to the volume expansion of the hydride formed underneath. Even though the JMA equation may provide a good fit, any conclusions about nucleation and growth being rate limiting in such a process should of course be taken with care.

1.6 Fundamental properties of Magnesium Hydride

Magnesium hydride is an attractive proposition for a hydrogen storage material, with a theoretical maximum hydrogen storage capacity of 7.6 wt% giving the highest energy density (9 MJ/kg Mg) of all reversible hydrides. Allied to this the low cost of the relative abundance of magnesium adds to the case for application a wide scale hydrogen storage material[26]. However, a major disadvantage is its extremely slow absorption and desorption kinetics, arising both from diffusion limitations and high oxidation sensitivity of the Mg surface, hindering the dissociation of hydrogen molecules.

Besides kinetic limitations, MgH_2 is also very stable, reaching an equilibrium pressure of 1 bar only at around 300°C[27]. Numerous studies [25, 28-35] have aimed to overcome the kinetic limitations by the addition of a wide range of catalysts to enhance the dissociation rate of hydrogen at the Mg surface and by reducing the particle size to shorten the diffusion length, which will be covered in more detail subsequently. Despite the great experimental efforts to overcome its limitations, practical application of Mg remains problematic and there is still much discussion of the rate limiting step in the process.

1.6.1 Structure

As a metal, magnesium will crystallise into the close packed hexagonal phase like the other alkali metals. Hydriding the material forms one of several polymorph phases which may be present depending on the pressure. Vajeeston et al[36] found have been able to accurately predict and confirm the structure of the alpha (α), beta (β), gamma (γ), and delta prime (δ') phases of MgH shown in Figure 1.9. During compression γ MgH_2 starts to form at 5.5 GPa and coexists

along with α MgH_2 up to around 9.5 GPa and In a narrow pressure window between 9.35 and 10.36 GPa the β MgH_2 polymorph also exists in a three-phase mixture.

Although these phase changes are stable at high pressure, due to hysteresis the reordering there is the possibility to retain a small meta stable regions within the material due to the close structural relationship between the alpha and gamma phases. Figure 1.8 illustrates the changes in structure from the rutile structure of the α phase (a) to the distorted cubic stricture of the gamma phase (C) and the very high pressure CaF_2 and AuSn structures of the beta and delta phases.

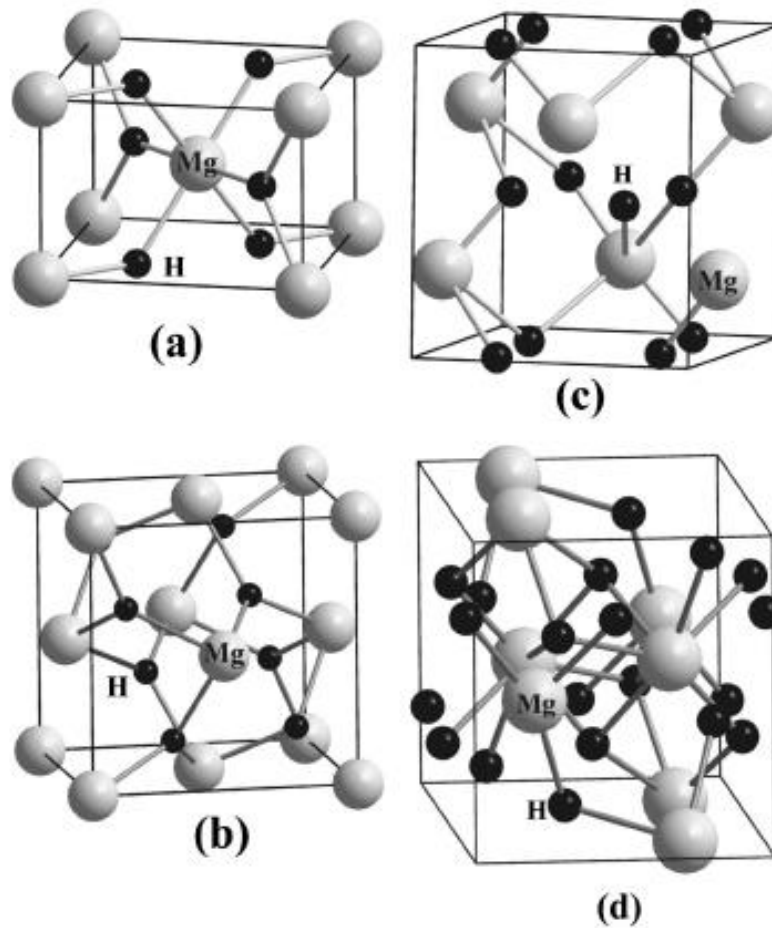


Figure 1.8: Illustration of the pressure induced structural changes that can occur in MgH_2 , (a-Alpha b-Beta c-Gamma d- Delta) [36]

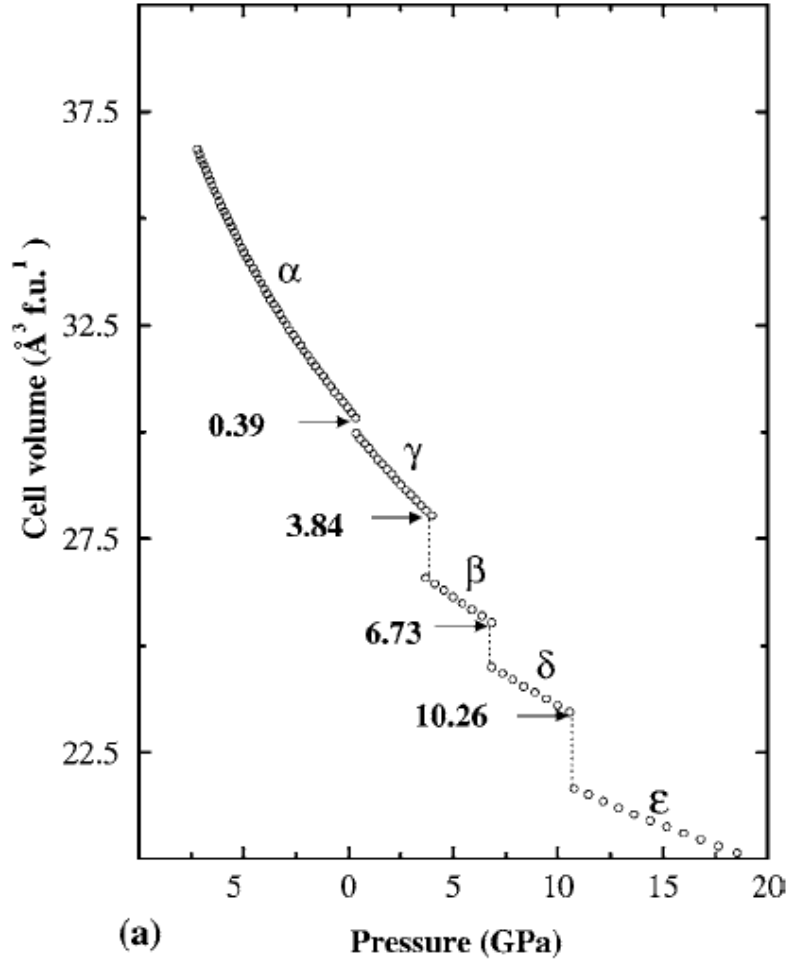


Figure 1.9: The change in cell volume of MgH_2 with increasing pressure showing the changes in structure with the pressures noted.[36]

1.6.2 Electronic and thermal properties of magnesium hydride

This work will consider the effects of electric and magnetic fields upon the reactions of magnesium and hydrogen, it is therefore important to understand the nature of the interaction with the fields.

At standard temperature and pressure magnesium hydride is an insulating material with low electrical conductivity and low dielectric losses. The work by Aroujo et al and Isidorsson et al, both compared calculated and measured values for both the band gap energies and dielectric properties of magnesium hydride in the alpha, gamma and beta phases[37, 38]. For the alpha phase the direct band

gap to the conduction band is 6.52 eV which is far higher than the photonic energy of a microwave photon which is 1×10^{-6} eV. For the gamma and beta phases the calculated direct band gaps were 5.33 eV and 4.72 eV, respectively, with the narrower band gap obtained for high pressure beta phase as a consequence of weaker ionic bonding between the magnesium and hydrogen ions in the CaF_2 structure[38].

For the dielectric properties of magnesium hydride the optical studies in the work have little relevance for the microwave and RF frequency fields examined in this work. There is little published data on the dielectric properties of magnesium hydride at lower frequencies and very little specifically at 2.45 GHz, additionally the temperature regime during processing may significantly affect the dielectric properties of the magnesium hydride. At high temperature there is no published data as these measurements are extremely difficult to perform and the relevant measurements have not been carried out. Therefore the accurate measurement of the dielectric properties of the magnesium hydride is undertaken in this study.

1.7 Formation steps in absorption process for magnesium Hydride

As discussed previously the kinetic involved in the absorption of hydrogen can be broken down into several key steps. These being the surface interaction, dissociation of the H_2 molecule, diffusion through the magnesium and magnesium hydride, and formation and growth of the magnesium hydride phase. Magnesium is known to be kinetically slow when reacting with hydrogen. It is, however, still unclear if this is primarily due to a poor ability to dissociate H_2 or to the creation of a stable surface hydride structure limiting the diffusion of atomic hydrogen into the magnesium matrix.

It is important to understand both the process and the influence of each aspect in order to gain a better understanding of the effects of processing techniques. The outline schematic in Figure 1.10 below shows the 5 steps involved in the formation of the final hydride phase. Points 1 & 2 are the gas surface interactions

associated with absorption and desorption. Point 3 & 4 are the surface penetration and transition into the subsurface region. Points 5 and 6 illustrate the formation and growth stages in the second phase hydride.

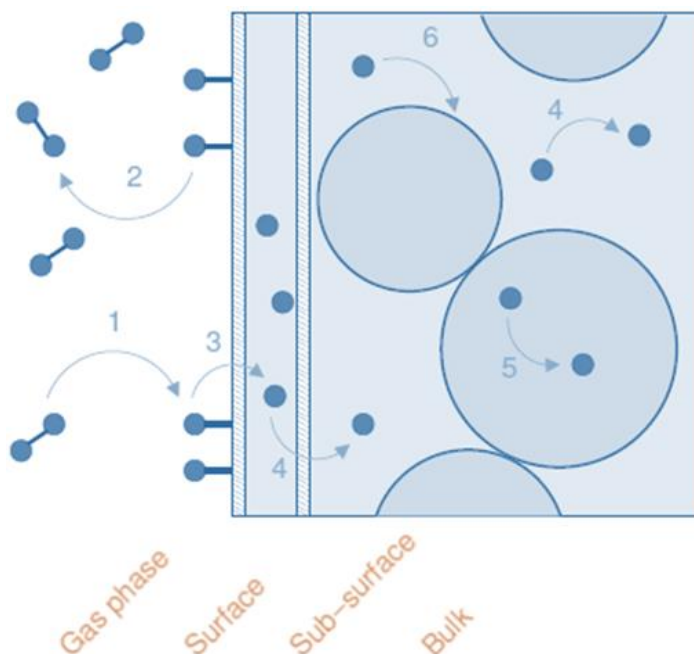


Figure 1.10 a) Schematic representation of the processes of hydrogen interaction and phase formation in metal hydrides adapted from Schlappbach and Zuttel [11]

The following sections detail the processes being undertaken and the mechanistic steps during the absorption of the hydrogen and the formation of MgH_2 .

1.7.1 Surface interactions at Solid Gas Interface

An understanding of the reactions taking place at the gas solid interface is a key aspect of the absorption and desorption process. There is a large body of work looking at the various aspects of the solid gas interface reactions covering a variety of situations from heterogeneous catalysis to models of hydrogen interaction with metal surfaces[39].

Hydrogen, being the simplest element to model theoretically, has been the subject of a large amount of research in order to test the understanding and

accuracy of simulations. However the understanding of the process still limited by the complexity of dealing with real materials where small changes in the crystallographic orientation lattice strain and defect structures can lead to changes in the observed results[40].

The primary step in moving from the hydrogen gas is the physisorption of the hydrogen onto the surface. At the point of interaction with the surface a molecule of hydrogen (H_2) will close enough to the surface of the metal to interact with it. At this point there are 2 possible options, either the molecule will move away from the surface and remain in the gas phase, or the specific site is suitable for the molecule to become weakly bonded to the surface. The next step of chemical adsorption or chemisorption is the dissociation of the hydrogen molecule in to hydrogen atoms. The reaction outcome is governed by statistical

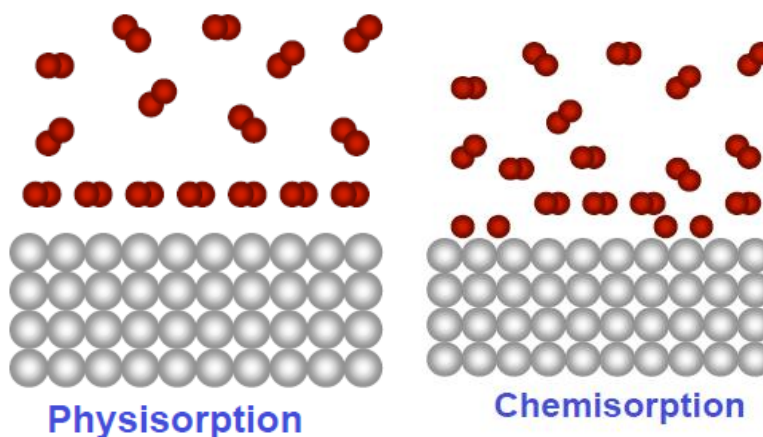


Figure 1.10b Physisorption and chemisorption representations from Schlappbach & Zuttel [12]

For physisorption on to the [0001] plane Vegge et al[41] modelled an array of magnesium atoms and found that the lowest energy barrier for the dissociation of hydrogen molecules and the subsequent chemisorptions was found at the bridge site between surface atoms. However, due to the relatively high activation energy of 1.06 eV it was found that only 1.6×10^{-11} molecules per site would be dissociated.

Further to this the absorption into the subsurface region was found to have an additional activation energy of 0.53 eV, from this it was concluded that the dissociation and penetration of hydrogen are the rate limiting steps in the absorption reaction. This work was looking at low surface coverage ratios of less than 25% mono layer coverage. The work by Jiang et al [21] on modelling larger coverage showed a decrease in the energy of absorption as the coverage increased. This was rationalised as an effect of increased hybridisation between the adsorbed hydrogen and the magnesium surface.

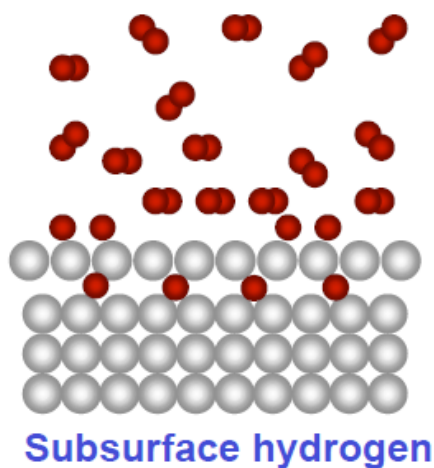


Figure 1.10C: subsurface hydrogen from Schlappbach & Zuttel [12]

In order to explain this relationship the work by Sprunger et al [42] has observed a relationship between the electron density of the metal atoms and the absorption behaviour. Materials with a high electron density, such as aluminium and beryllium, will adsorb hydrogen on to the surface but due to a high activation energy barrier to inward diffusion, absorption will not occur. For lower electron density materials such as magnesium hydrogen is localised at the surface at low temperatures. However, at higher temperatures the local charge density at the surface is not large enough to screen out the highly electronegative hydrogen ion, consequently, a hydride phase is the lower energy configuration.

1.7.2 Diffusion mechanisms sub surface and in bulk

The understanding of the true order of events in the process of absorption of hydrogen into magnesium is complicated by the nature of the structures that are formed. It has been suggested that the diffusion of hydrogen may be the rate limiting step in the process.

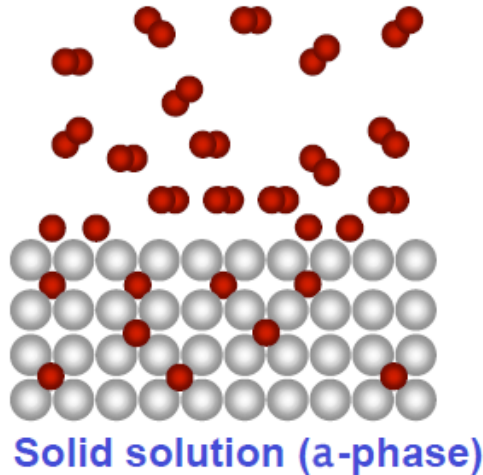


Figure 1.10D: formation of the α solid solution representation from Schlappbach & Zuttel[12]

However measurement and calculation of the diffusion coefficients would suggest that hydrogen diffusion through the beta hydride phase is up to three orders of magnitude lower than in magnesium[43], highlighting the importance of the structure. The calculations of the diffusion paths are consistent with experimental evidence in that the activation energy for an interstitial to diffuse in the Mg metal is small, only 0.22 eV, but the activation energy for diffusion through the hydride is very large, over 2 eV. This, together with the fact that the hydrogen atom has to climb uphill in energy by 0.42 eV in going from the hydride to the metal explains how the formation of a hydride film at the surface of a Mg crystal can effectively stop the absorption of hydrogen when the temperature is below 400 K[44].

1.7.3 Phase nucleation and growth of MgH_2

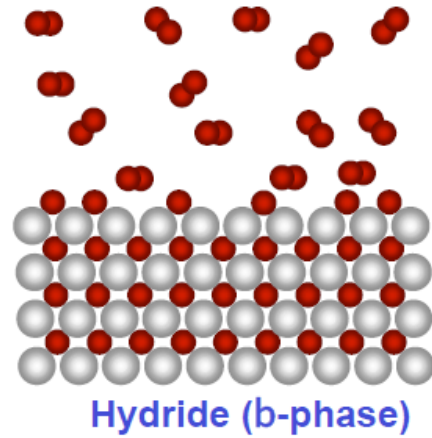


Figure 1.10e: representation of the Formation of the hydride β phase from Schlappbach & Zuttel [12]

For the nucleation and growth of the hydride phase, the dissociated hydrogen at the surface must find a route into the bulk material. At the surface the formation of a hydride was found by Jiang et al to be unlikely due to the high energy barrier, with calculations showing that the lower energy structure was to generate hydrogen–magnesium–hydrogen multilayers below the surface [45]. After the formation of three tri-layers it becomes favourable to form the rutile structure of magnesium hydride as highlighted in figure 1.11

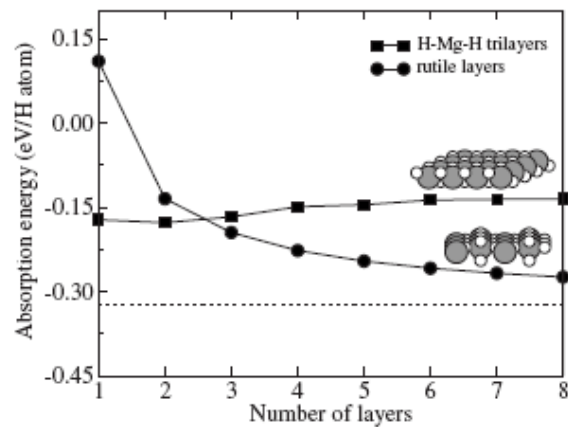


Figure 1.11: Absorption energy as a function of structure for the formation of H-Mg-H layers and MgH_2 rutile structure [45].

As the formation of the second phase with a much lower diffusion coefficient is likely to occur around the edge of particles this can lead to a drop in the uptake rate throughout the reaction. In this case the situation is described as forming a shell of magnesium hydride that influences the kinetics of the reaction. This time dependent relationship can be mathematically described using a contracting volume model. Borgschulte et al[46] found that absorption behaviour is best described by the three-dimensional diffusion controlled contracting volume model with decreasing interface velocity, where after an initial nucleation state, a dense MgH_2 layer is formed at the surface of a Mg grain. As hydrogen uptake in magnesium corresponds to the growth of the hydride layer, this corresponds to an increase in the diffusion path length (Figure 1.12).

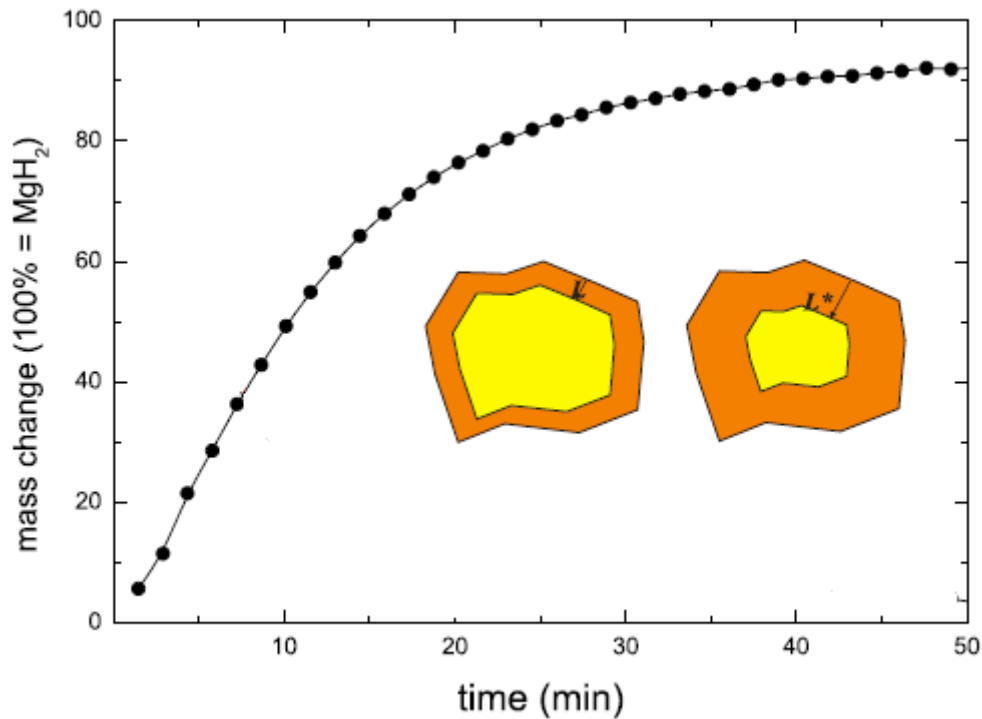


Figure 1.12: Absorption kinetics of ball-milled MgH_2 . The absorption behaviour is best described by a three-dimensional controlled contracting volume $L \rightarrow L^*$ model with decreasing interface velocity (adapted from [46]).

1.8 Desorption Process

As with the formation of magnesium hydride, there is continued discussion over the rate limiting steps in the desorption process and the factors which contribute to this. The overwhelming majority of researchers use the Avrami equation to estimate of the kinetic parameters of the reaction. Such an approach is only justified if a single rate limiting step is the dominant factor throughout the reaction.

From work by Fernandez et al[23], analysing the desorption curves, and in situ X ray diffraction by Jenson et al[25], the magnitude of the Avrami exponent ($n=2$) for the nucleation and growth parameters has been determined. However in these studies it was not possible to distinguish between the possible mechanistic factors. The results of curve fitting could equally be consistent with constant nucleation and a growth control by diffusion rates or fast initial nucleation with a process that is dominated by the two dimensional interface growth.

Alternatively attempts to describe hydrogen desorption process as a contracting volume of the hydride β phase have shown some interest but have not been widely studied.

Models working on the premise that the reacted fraction of the hydride was a key variable, suggested that the rate-controlling step for the desorption of magnesium hydride is the interface chemical reaction at the β magnesium hydride to α magnesium solid solution phase boundary[47, 48]. If the rate controlling step is the diffusion of hydrogen through the α phase the desorption rate should be fastest from a sample with a high reacted fraction and a large proportion of surface hydride and consequently reduced diffusion through the alpha phase. However experimental results obtained by desorbing hydrogen from varying levels of reacted states show the reverse that diffusion of hydrogen through the alpha phase is not the rate-controlling step, Han et al[48].

If the alpha Mg – beta MgH_2 reaction is the rate controlling step then it would be presumed that at the initial stage of desorption, with a sample with a low reacted fraction of alpha Mg, there will be a significant volume of hydrogen in the alpha

magnesium solid solution phase, this should therefore show the highest rate of the desorption at the initial stage.

This is not result of desorption from the hydride phase as modelling of the recombination of the hydrogen molecule on a magnesium hydride surface by Vegge [41] determined that desorption from the surface of the hydride can be a slow process due to the high activation energy for the desorption processes.

Hydrogen recombination is the rate-limiting step as the last barrier for out-wards diffusion to the surface is low and the diffusion rate was significantly higher than the rate of recombination on the surface.

Evard et al[24] have subsequently extended the work Han and looked at the formation of magnesium islands on the surface of the particles and the relationship with the rate of desorption.

It was observed that the desorption kinetics can be explained by the fact that not completely hydrogenated magnesium has metallic islands reaching the surface of each powder particle. These serve as an easier channel of desorption than the surface of the hydride phase (Figure 1.13).

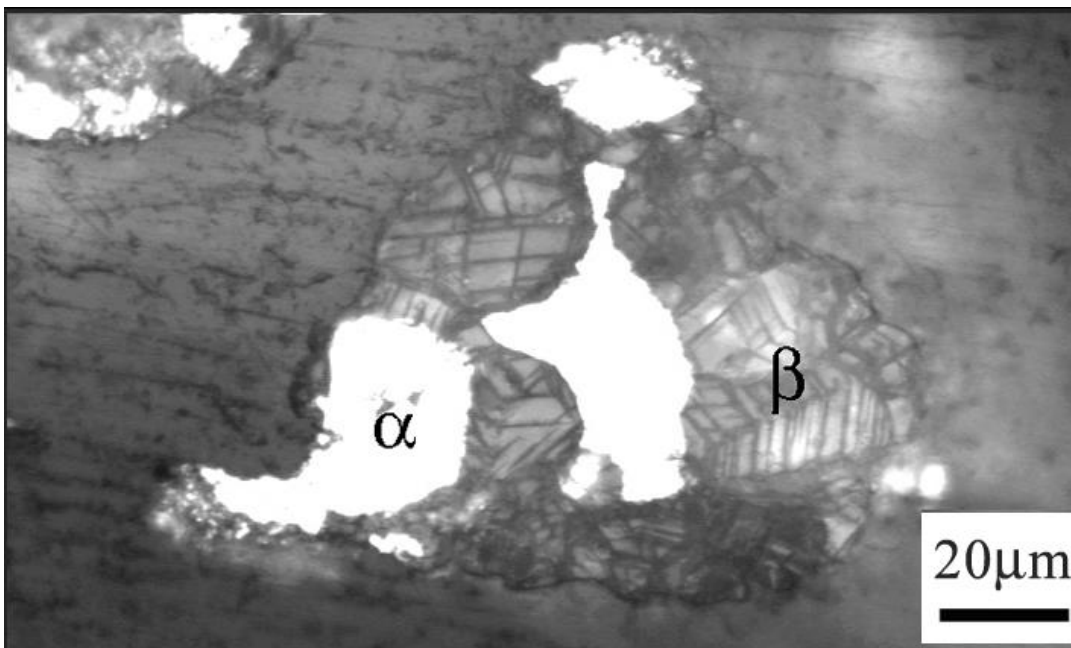


Figure 1.13: Micrograph showing the alpha and beta regions of partially decomposed magnesium hydride[24]

Magnesium hydride by its nature is an ionic-covalent compound, whose catalytic properties with respect to adsorption- desorption processes are much lower than the metal as shown by Vegge[41]. Desorption from the magnesium particles was found not to occur until a nucleus of the metal phase appears on the surface of each particle of the hydride powder.

Experimental evidence of this was found if the sample was heated rapidly, the temperature could reach 180°C above thermodynamic equilibrium temperature before the metallic island has a chance to form.

Hydrogen is then desorbed quickly through this channel, and widens permanently with hydrogen liberation and the growth of the alpha phase surface. This is shown clearly in figure 1.14 where there is a strong relationship between the heating and the initiation of the hydrogen desorption.

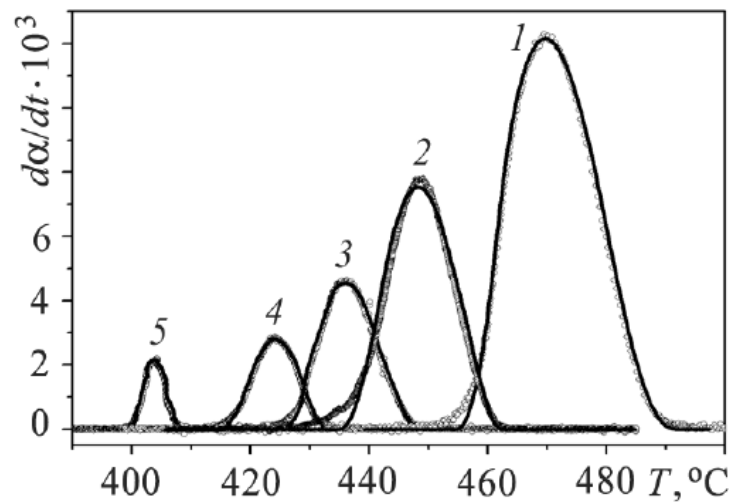


Figure 1.14.: Thermal decomposition traces showing the rate of desorption as a function of temperature for fully reacted MgH_2 [24](heating rates 1. 24 k/min 2. 12 k/min 3. 6 k/min 4. 3 k/min 5. 1.5 k/min)

The formation of nuclei of the metal phase on the surface of an ionic-covalent compound is complex process. Metallic clusters can be formed on the surface due to the coalescence of several hydrogen vacancies or possibly, oxygen and other contaminants on the surface[24]. This effect leads to the observed incubation period at the start of the desorption where the period before the

formation of metallised islands restricts the hydrogen desorption reaction. Further support is given to this model when samples with low reacted fraction, and therefore a high surface area of alpha phase are heated at increasing rates but the onset of desorption occurred at similar temperatures. (Figure 1.15).

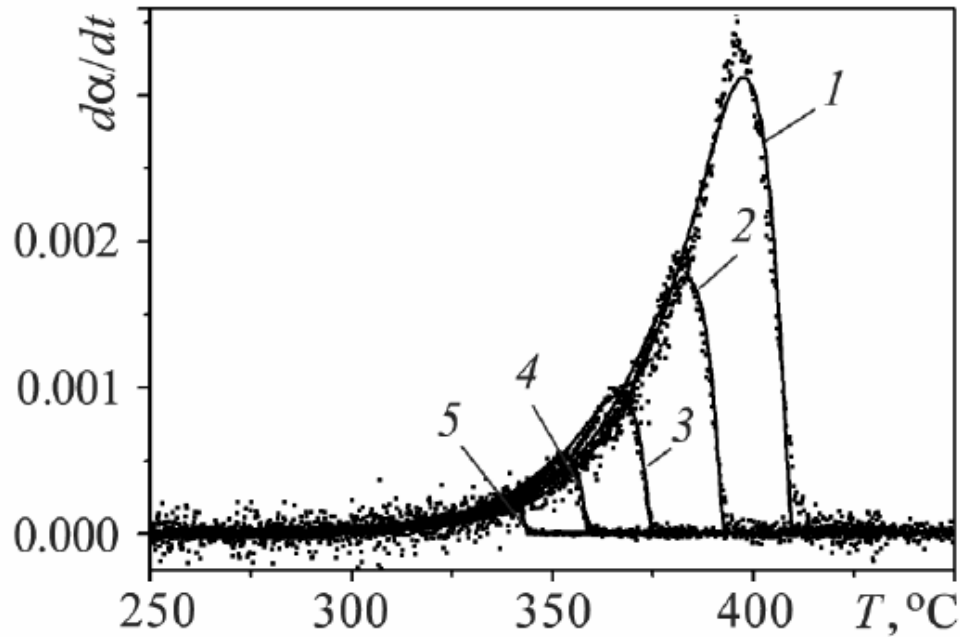


Figure 1.15: Thermal decomposition traces showing the rate of desorption as a function of temperature for partially desorbed magnesium hydride with 75% alpha phase[24]. (heating rates 1. 24 k/min 2. 12 k/min 3. 6 k/min 4. 3 k/min 5. 1.5 k/min)

The desorption rate depends on the hydrogen concentration in metallic magnesium. This concentration, irrespective of the heating rate, is determined only by the temperature. This means that, at least, in the domain of coincidence of the fronts of curves, hydrogen liberation is strictly limited by the desorption rate from the surface, and the hydrogen concentration in the metal. The concentration of hydrogen in solid solution is function of temperature and will be in equilibrium with the hydride phase.

This has been applied to model the rate of desorption from a sample once the metallic islands have formed. The rate of hydrogen desorption d is given by:

Equation 6

$$d \frac{d}{dt} (C_s V_s(t) + C_h V_h(t)) = -b(t) C_s^2 S_s$$

where $V_h(t)$ and $V_s(t)$ are the volumes of the hydride and solution phases, C_s and C_h are the concentration of hydrogen in the alpha and beta phases, S_s is the external surface of solution, and $b(t)$ is the rate constant of desorption from the solution surface.

The rate constant of the surface desorption $b(t)$ is given by:

Equation 7

$$b(t) = b_0 \exp\left(\frac{-E_d}{RT(t)}\right)$$

as the reacted fraction (α) is V_s/V_s+V_h this can then be expressed in the form:

Equation 8

$$\alpha = A \exp\left(\frac{-E_d}{RT}\right)$$

where A is given by:

Equation 9

$$A = \frac{b_0 C_s^2 S_s}{V_0 (C_h - C_s)}$$

This relationship links the increased kinetics observed in the dehydrogenation kinetics to the increase in surface area of the particles and the increase in number of nucleation sites for the metallic alpha phase to form.

1.9 Mechanical processing of MgH_2

While there is some debate about the nature of the rate determining step in the absorption and desorption processes, experimental results have shown the clear benefits of reducing the particle size for magnesium hydride[49-51] either through the use of nanoparticles or the use of mechanical processing.

Mechanical milling is a process for reducing particle size and/or grain size, inducing phase changes and creating an increased density of defect structures with in the material.

The process involves placing the MgH_2 materials into a mill, along with a grinding medium (typically stainless steel balls). This is then rotated for the desired length of time until the desired particle size is achieved.

For planetary milling the action of the rotating main plate and counter rotating milling pots produces a situation where, the centripetal force moves the balls towards the outside edge impacting the powder against the wall of the milling pot figure 1.16. This is a high energy process where the forces at the point of contact can be high enough to trigger chemical reactions, and induce meta-stable phase changes[52].

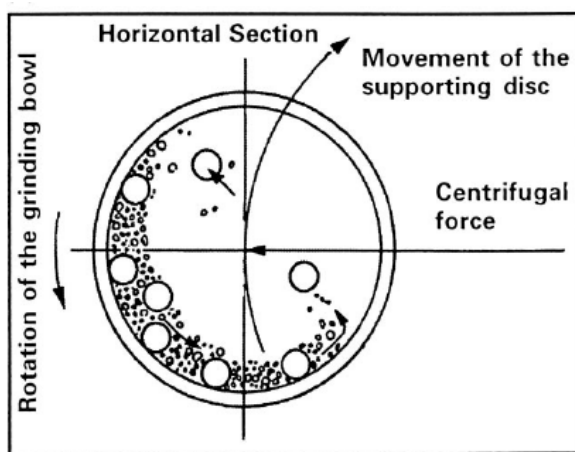


Figure 1.16: Schematic depiction of the ball motion inside a planetary ball mill.

Mechanical milling is a complex process; therefore, there are a number of variables that can be manipulated and optimised to achieve the desired microstructure and particle size. Some of the important parameters that can be changed to affect the final powder are:

- Milling action
 - milling speed / time / and program
 - ball to powder weight ratio
 - the milling atmosphere
- The equipment choices
 - milling container material
 - milling ball material

All these variables are not totally independent of each other. For example, the time of milling is dependent upon the type of milling action used, the weight of the balls and the ball to powder ratio.

In general it is the energy of the collision and the properties of the material that will affect the time required to reach a specific structure, with this relating to the work done upon the material. The energy of the collision is dominated by two factors: the speed of the mill and the size of the milling ball[21, 52]. The faster the mill rotates the higher the energy input into the powder. However, there are limitations to the maximum speed that can be employed. Increasing the speed of rotation will increase the speed with which the balls move, above a critical speed, the balls will be pinned to the inner walls of the milling pot and not exert any impact force. Another limitation to the maximum speed is that at high speeds, or intensity of milling, the temperature of the material may increase. This may cause decomposition of phases formed during milling of some decompositions hydride due to the increased temperature.

The choice of materials is also an important factor in the milling process as contamination from the milling pot or ball can affect the material being milled. For example materials such as stainless steel have been shown to contaminate samples with small quantities of elements such as chromium nickel and iron.

Depending on the milling time and sensitivity of the sample this can have a significant bearing on results[53].

1.9.1 Milling effects

For magnesium hydride mechanical milling has been shown to improve both the absorption process and the dehydrogenation kinetics.

The reduction in the particle size has been shown to improve the kinetics by substantially reducing the diffusion path for hydrogen, increasing the surface area of the particles and introducing a far greater number of defects into the crystal structure.

All three of these actions contribute to increasing the reaction kinetics.

1.9.2 Reduction of grain size

The reduction in the grain size reduces the diffusion length for the hydrogen in both the formation and desorption processes. The production of nano particles has been demonstrated with varying processes, including mechanical milling for extended periods[54], hydrogen combustion synthesis and gas phase plasma reactions.

The kinetics improvements over the polycrystalline starting material is clearly demonstrated in figure 1.17, where the rate of desorption at 300°C is clearly enhanced by milling for just 5 hours. X-ray diffraction measurements performed after ball milling magnesium hydride for 20 hours, show that crystallite size is reduced from the order of microns to about 20 nm[55]. Milling times of up to 200 hours have been trailed and have been shown to reduce the particle size and increase the strain in the crystal but have little impact on reducing the mean crystallite size[28].

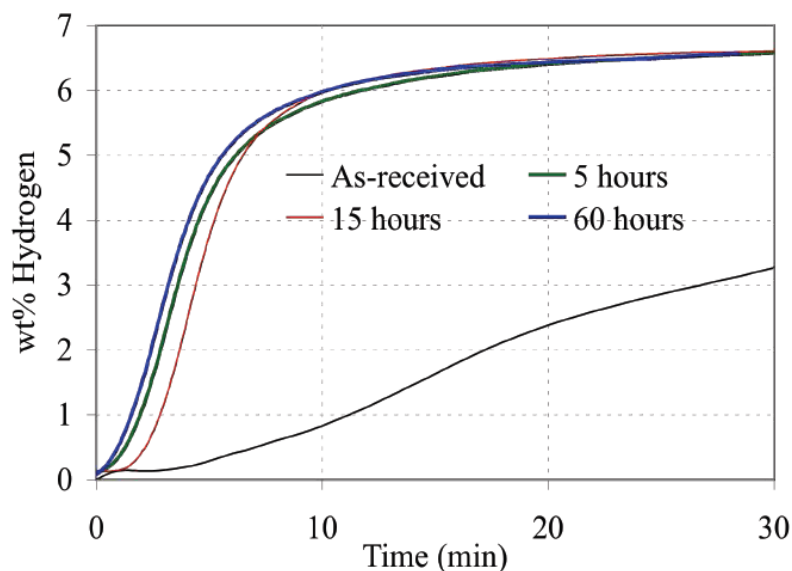


Figure 1.17: The effect of milling time on the dehydrogenation kinetics of magnesium hydride at 300°C[56]

1.9.3 Thermal stability and grain growth

The effect of the grain size on sorption kinetics was demonstrated by annealing experiments,[57] where after annealing at 300C major changes were observed in the crystallite size. Grain growth/grain coarsening increased the grain size to larger than 200 nm, this corresponded with a significant decrease in absorption kinetics.

The growth of the crystallite size is not the only change that can occur upon heating that can impact on the structure, as the loss of the defect structures developed during the milling process can have a significant effect.

Novakovic et al studied the effect of ion bombardment and the subsequent defect structures they produced on the desorption kinetics of MgH₂. They found that an increase in the rate of desorption under DSC studies and attributed to a higher concentration of defects in the sub surface region[58].

Further Dinaie et al observed the formation of deformation twins in TEM analysis of milled magnesium hydride[59]. It is suggested that these could be a significant contributor to the milling-induced kinetic enhancement due to the higher diffusivity of the hydrogen ions through the twin boundaries.

These physical changes to the structure of the magnesium hydride should be considered as temporary features, as the increase in defect density and the very fine grain sizes achieved through the high energy mechanical processing are meta-stable.

The desirable features may very easily be lost upon cycling due to the phase changes associated with the hydrogenation reactions and the likelihood of grain growth at the temperatures above 300°C required in most hydrogen storage situations. The benefits mechanical processing offers in terms of kinetic improvement are a real advantage but the high energy intensity involved in mechanical processing for such extended periods of time may make this processing route uneconomic.

1. 10 Catalysis of Magnesium Hydride

The aim to improve the kinetic response of magnesium hydride has moved towards the efforts based on additives to catalyse the system. A catalyst is material that reduces the energy barrier required in order for the activation of a chemical reaction. The general mechanism of catalysis implies that the catalyst and reactant form an intermediate state, whose binding energy is smaller and the formation rate is faster compared with the non-catalysed reaction.

In the area of hydrogen storage catalysts have been added to improve the surface reactivity for the dissociation and recombination of the hydrogen molecule. However in contrast to the enormous body of empirical knowledge and fundamental principles of catalysis and catalysts frequently used in chemistry, relatively little attention has been given to catalysis for the absorption of hydrogen[60].

Several attempts have been made to enhance surface kinetics using different additives. Among the additives with positive effect on sorption kinetics of Mg-based hydrides are platinum group metals like Ni[25, 61], hydride-forming elements such as Ce, Nb and Ti [62] low-temperature metal hydrides such as LaNi₅[63] and FeTi, non-hydride-forming elements such as Fe, Co and Cr[64,

65], and transition-metal compounds, for example, metal oxides. Transition metals and transition metal oxides in particular have been proven to enhance sorption kinetics significantly[66-68].

It has been experimental research looking at the effect of the addition on the kinetic response of magnesium that has dominated the literature in this area, without too much attention to the mechanisms involved. The mechanics of the hydrogen-catalyst interaction can be highly complex dependent on both the electronic structure of the catalyst surface and the influence of the magnesium or magnesium structure the catalyst is supported by[69, 70]. This effect can make the understanding of the interactions difficult due to the changing nature of the support structure, due to phase changes, the changes in the rate determining steps affecting the kinetic response and the effects of oxygen all playing a significant role.

1.10.1 Surface Interactions with Transition metal Oxides

The role of oxides in the dissociation and recombination of hydrogen has been shown to have a significant effect. The exposure to oxygen of the surface of the powder prior to milling and the addition of magnesium oxide[71] has been shown to produce a response similar to the addition of many catalysts.

There is a clear link in the stability of the transition metal oxide catalyst in relation to magnesium oxide and the effectiveness, illustrated in a review of the subject by Barkhordarian et al [72]. It was found that in all cases the effective oxides had a lower stability than MgO and that the valence of the oxide also played an important role[72, 73].

It was assumed that this effect was related to the partial reduction of the oxide catalyst during the milling process leaving a structure with oxygen vacancies at the surface. It was also observed that the effectiveness of transition metals such as vanadium could be improved through exposure to oxygen for a limited time, further highlighting the important interactions of oxygen in the dissociation and recombination reactions.

All effective oxide catalysts are less stable than magnesium oxide and on the basis of thermodynamics, a reduction of the transition-metal oxide by Mg is expected, forming a transition metal and MgO. However, this is generally not observed, which may be due to mechanical processing at low temperatures constraining the kinetics, or the decomposition of MgH_2 may form an additional barrier for magnesium-oxide formation. Cycling of Nb_2O_5 catalysed material has been shown to have a reduced effect after higher temperature annealing suggesting that reduction of the oxide limits the reactivity[57]. In cases such as Re_2O_7 the relatively unstable compound reacts immediately with magnesium during hydrogen desorption at 300°C , and no significant catalytic effect is observed[72].

The performance of oxide catalysts has shown some remarkable improvements in the kinetic performance of magnesium hydride materials. Figure 1.18 outline the performance of the catalyst in the desorption reaction, where the two clearly outstanding performers are vanadium and niobium oxides.

Both of these materials are notable for their valence of 5 and relative stability to magnesium oxide that give the optimum surface for the recombination and dissociation reactions to take place upon.

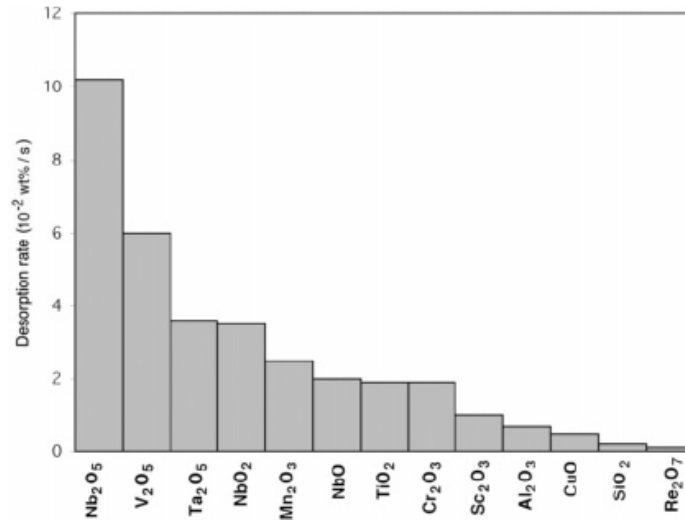


Figure 1.18: Comparison of transition-metal oxides and their catalytic effect on the hydrogen desorption reaction rate of magnesium hydride at 300°C . (calculated between 20% and 80% of the respective maximum capacity.)[72]

The kinetics of magnesium hydride doped with 1 mol% Nb_2O_5 has been shown by Hanada et al to be much improved. The ball milled composite rapidly absorb hydrogen of 4.5 mass% at room temperature and has been shown to desorbs hydrogen at 160°C under a zero partial pressure of hydrogen.[74]. This is currently the best performing catalyst that has been observed and has lead to a surge in interest in this material.

1.10.2 Catalytic Effects of Transition Metal Additions

The addition of transition metals to magnesium hydride has shown a considerable improvement in the hydrogen sorption kinetics. The addition of materials with an active surface allows the dissociation to occur with much lower activation energy. The reduction in the activation barrier for dissociation with the addition of transition metals can be more than 90%.

Calculated values for the activation energy for the dissociation of hydrogen are of the order of 0.06 eV for nickel, and for iron 0.003eV. Figure 1.19 shows the effect on the sorption kinetics at 300°C for a selection of transition metal additions. The addition of nickel has been one of the most common and successful addition to magnesium and the low cost and abundance of the material suggests that it will remain a cost effective option.

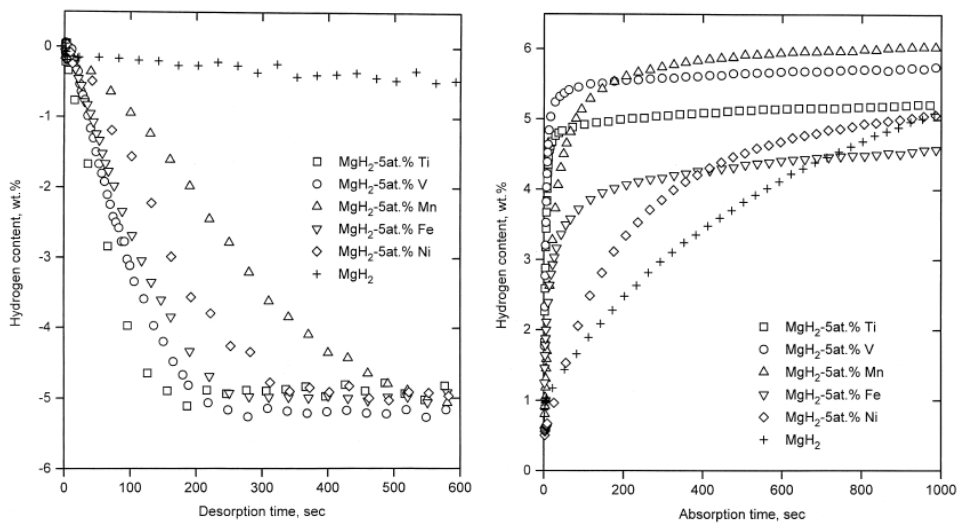


Figure 1.19: Hydrogen desorption and absorption curves of $\text{MgH} + 5\text{at}\%$ (Ti, V, Mn, Fe, Ni) composites at 300°C [75]

1.10.3 Addition of complex hydrides

In addition to much of the work carried out using metallic catalytic additions for the improvement in the sorption kinetics of magnesium hydride, work has been undertaken to investigate the addition of complex hydrides such as lithium borohydride.

The addition of LiBH_4 was initially investigated by Johnson et al [76] who found an increased rate of hydrogen desorption at 300°C using a 10:1 molar ratio of magnesium hydride to lithium borohydride. The rate of desorption was increased by over 100% when compared to magnesium hydride milled for in a planetary mill for 15 hours.

The main cause of the increased rate of desorption was unclear in the initial work but an increase in the diffusion rate of the hydrogen could account for the improvement.

It was observed that an increase in the unit cell of the material of around 0.8% could occurred after cycling and this could allow increased hydrogen diffusion through the material. The increase in cell volume was speculated to be the result of Li and B doping of the system expanding the unit cell but as there was no shift in the plateaux pressure the changes did not impact the thermodynamics of the system to destabilise the magnesium hydride.

This work was subsequently extended by Mao et al and rapid absorption of hydrogen at 200°C was observed using a similar preparation method [77]. It was also observed that the morphology of the material was altered through cycling with a significantly more deformation of the surface leading to improved kinetics over a number of cycles.

1.10.4 Destabilisation of Magnesium Hydride

In addition to improving the kinetics through the addition of catalysts efforts have been made to destabilise the magnesium–hydrogen bond, in order to lower the temperature of decomposition.

The addition of materials that will have a positive enthalpy of reaction with magnesium should provide an extra driving force for the reaction and reduce the energy required.

The addition of silicon will form the Mg_2Si intermetallic phase when in contact with the metallic magnesium. Therefore, formation of Mg_2Si reduces the standard enthalpy of hydrogenation from 75.3 kJ/mol for pure MgH_2 to 36.4 kJ/mol for $\text{MgH}_2 + \frac{1}{2} \text{Si}$ [35]. This reduction in the stability would result in a plateau pressure of 1 bar occurring at 20°C, and 100 bar at 150°C. These types of reactions have also been considered for germanium and tin additions, but in all cases the kinetics of recombination are too slow for practical applications[18, 78].

Theoretical work on the nature of the catalytic effect of transition metals by Tsuda et al [79] found that the charge on the hydrogen atom changes from minus to neutral on Mg-H bond cleavage. In respect of this finding, the proximity of an ionised molecule, from which one electron has been extracted, was found to considerably lower the stability of the neighbouring MgH_2 . This suggests that it is possible to reduce the H_2 desorption temperatures from MgH_2 without any catalyst, just by ionizing the MgH_2 causing the spin polarization of Mg-H bonding. If the calculations of the destabilization effect are correct the hydrogen desorption temperatures could be lowered to below room temperature, and even as low as 240K.

Looking for alternative methods to control the absorption of hydrogen steered Borgschulte et al to use an electric current to initiate the absorption process at room temperature in thin film samples[80].

In this method the electric field between the two electrodes required to initiate the reaction was 200 Vm^{-1} (figure 1.20). The polarity of the current had a strong effect on the location of the formation of the hydride phase, with all the growth occurring in the direction of the current flow.

Reversal of the current direction caused the growth direction to be inverted, suggesting that the field direction determines the diffusion characteristic of hydrogen at these low temperatures. It was concluded that the enhanced

diffusion characteristics could be associated with the electro migration of the negatively charged hydrogen ions through the structure, however due to the uncertainty of the nature of the hydrogen species in the α phase there must be some reservation over this.

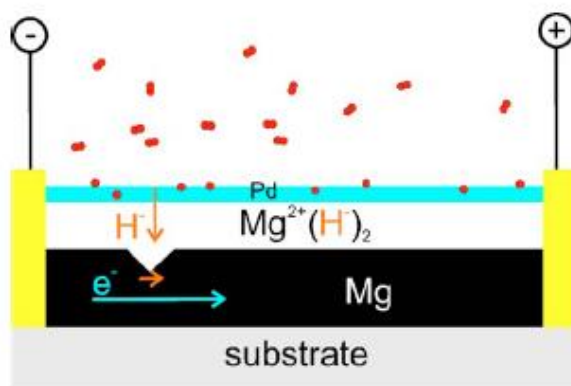


Figure 1.20: Electro catalysis of hydrogen absorption in Mg; hydrogen is dissociated and dissolved in the Pd-cap layer, before forming the hydride, with the reaction controlled by the potential between the two electrodes.

1.11 Microwave assisted sorption processes

After the exploration of a wide variety of chemical methods for the improvement of the kinetic properties of metal hydrides, and magnesium in particular, attention has been drawn to other methods of achieving the desired results.

Microwave processing is a complex and not well understood area of research; however, it has been shown to provide some interesting results when applied to both chemical catalysis reactions and diffusion based sintering[81, 82].

The first published example of the use of microwave fields to initiate the desorption reaction in magnesium hydride were two patents filed by Zaluska et al in 1999 and 2000[83, 84]. These patents covered a wide range of possible energy sources that could be used to cause the desorption reaction in magnesium hydride, including examples of possible systems based upon microwave fields, electric currents, ultrasonic waves and ionising radiation.

They presented general descriptions of experiments where magnesium hydride samples were treated with microwave radiation (2.45 GHz) repeatedly for a

period of 1 minute and XRD analysis used to infer the amount of gas desorbed. They claim that after a number of exposures the relative quantities of hydride and metallic phases were altered suggesting that some desorption of hydrogen had occurred. This study gave no indication of the temperatures reached or the rate at which the hydrogen had been desorbed, however it was suggested that the mechanism for initiating the reaction was direct excitation of the magnesium hydrogen bond.

Work by Nakamori et al lead to a series of papers looking at the heating a rate and desorption kinetics of a series of hydrogen storage materials using a range of microwave applicators and experimental apparatus[85-87].

The initial results were obtained using a domestic 2.45 GHz microwave oven with a sealed unit placed inside, fitted with temperature and pressure logging equipment. They found that it was not possible to heat the magnesium hydride due to the low loss nature of the material, and therefore observed no increase in pressure or desorption. However it was found that LiBH_4 could be heated and showed significant increase in the desorption kinetics when compared to radiant heating methods. Rapid heating behaviour was observed in LiBH_4 above the phase transition temperature of 390K caused by an increase in the energy absorption. Further investigation of this effect revealed superionic conductivity of the lithium ions was possible due to the change in structure which, greatly increased the energy absorption of the material[88]. The addition of more susceptible materials such as TiH_2 and carbon increased the heating rate of the LiBH_4 at lower temperatures and enabled the full desorption of the material, including heating from room temperature, in less than 5 minutes.

1.12 Microwave technologies

Microwaves belong to the portion of the electromagnetic spectrum with wavelengths from 1 mm to 1 m with corresponding frequencies between 300 MHz and 300 GHz. Within this portion of the electromagnetic spectrum there are a limited number of frequencies reserved for industrial processing and others reserved for communications technology, including mobile phones and satellite

television and military applications such as radar. Two frequencies are commonly used for microwave processing of materials 0.915 and 2.45 GHz[89]. The wide availability of microwave power sources of 2.45 GHz frequency and good microwave absorption properties of many materials in this range, coupled with improvements in efficiency have led to the emergence of industrial facilities for various applications, with currently hundreds of megawatts in total of installed microwave power worldwide[82].

The microwave, like all electromagnetic waves, consists of two components, the magnetic field and the electric field (Figure 1.21). These follow a sine wave function in parallel but with the magnetic field oscillating perpendicularly to the electric field.

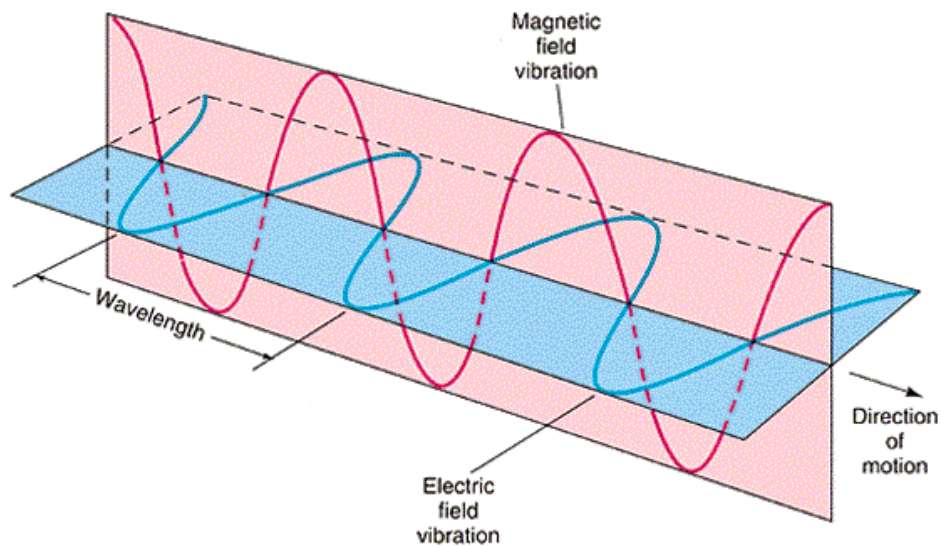


Figure 1.21 Components Of Electromagnetic Wave - Electric and magnetic fields vibrate perpendicular to each other[90]

Interest has grown rapidly in extending the application of microwave energy to the processing of a wide variety of new and engineered materials, including ceramics, polymers, composites, and chemicals. The growing interest is partly the result of increased awareness among materials scientists, processing engineers, and potential users of the many benefits of microwave processing. The use of microwave energy provides clean, rapid, and efficient heating over a wide range of temperatures, as well as new degrees of freedom and flexibility

over conventional processing methods. In some cases, microwave processing can synthesise new materials and microstructures that cannot be produced by other techniques[91].

1.12.1 Microwave production

For most microwave applications, which require high power and frequencies, the electromagnetic radiation is generated using a magnetron (Figure 1.22). Magnetrons are mass produced and widely available so are at the lowest cost source available. The electromagnetic radiation is generated within a vacuum tube by the acceleration of charge resulting in the generation of electromagnetic radiation. The anode is at a high potential compared to the cathode, and the potential difference produces a strong electric field. The cathode is heated to remove the loosely bound valence electrons. Once the electrons are removed from the cathode, they are accelerated toward the anode by the electric field. In a magnetron, an external permanent magnet (usually ferrite materials) is used to create a magnetic field orthogonal to the electric field, and the applied magnetic field creates a circumferential force on the electron as it is accelerated to the anode. As electrons pass the resonant cavities, the cavities set up oscillations in the electron cloud, and the frequency of the oscillations is fixed and dependent on the size of the cavities. The magnetron tubes use resonant structures to generate the electromagnetic field, and, therefore, are only capable of generating a fixed frequency electromagnetic field.

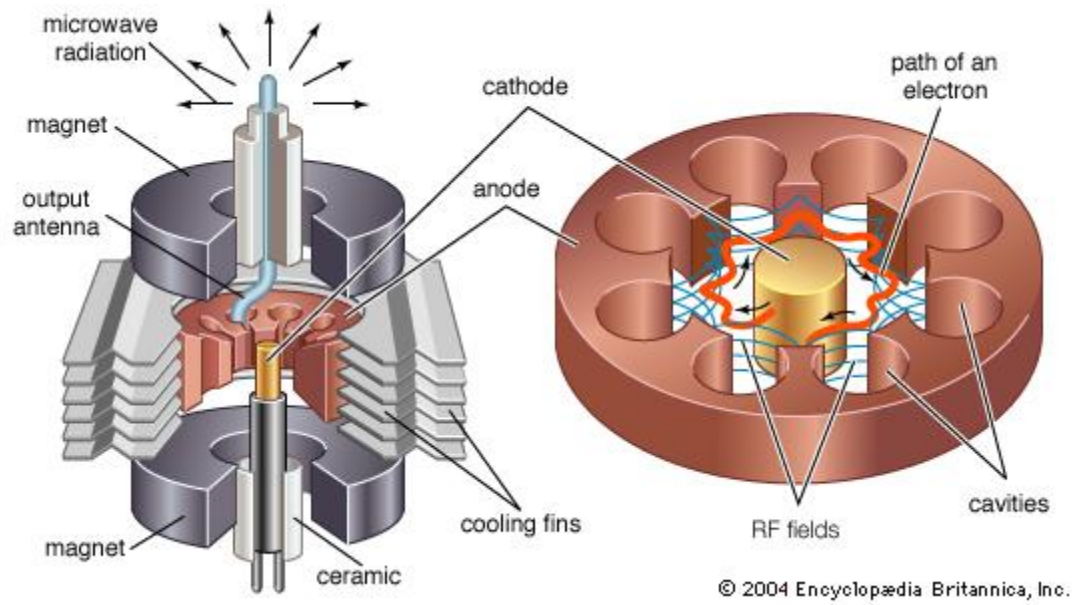


Figure 1.22: Internal structure of a cavity magnetron[92]

Two methods are commonly used to control the average power output of magnetron tubes, either by adjusting the period of operation or by lowering the output by adjusting the cathode current or by varying the applied magnetic field.

Changing the operation period is the easiest way to control average power, lowering the duty cycle will reduce the power but the field strength generated will be a constant.

In order to change the current on the cathode a robust and sophisticated control electronics that give a stable and variable high voltage DC supply

1.12.2 Microwave applicators

The design of single mode applicators is based on solution of the Maxwell equations to support one resonant mode. Consequently, the size of single mode applicators is of the order of approximately one wavelength, and to maintain the resonant mode, these cavities require a microwave source that has little variation in the frequency output. Because the electromagnetic field can be determined using analytical or numerical techniques, the areas of high and low electromagnetic field are known, and single mode applicators have non-uniform,

but predictable, electromagnetic field distributions. In general, single mode cavities have one “hot spot” where the microwave field strength is high[89] but can also be designed such that the maximum magnetic and electric components of the field can be separated. Single mode cavities are difficult to scale-up for many industrial applications due to the geometric limitations and non-uniformity of the fields. Therefore, single mode cavities are generally designed for specific purposes in research.

Multi-mode applicators are capable of sustaining a number of modes at the same time. This type of applicator is used in home microwave ovens. Unlike the design of single mode applicators, which are designed based on solutions of the electromagnetic field equations for a given applicator geometry, the design of multi-mode applicators are often based on trial and error, experience, and intuition. The presence of different modes results in multiple high field points within the microwave cavity. Like single mode cavities, local fluctuations in the electromagnetic field can result in localised overheating. To reduce the effect of hot spots, several techniques are used to improve the field uniformity. The uniformity of the microwave field can be improved by: increasing the size of the cavity (increasing the number of modes within the cavity improving the uniformity of field distribution), or introducing rotating mode stirrers to even out field distribution over time.

1.12.4 Dielectric heating mechanisms

The interaction of electromagnetic waves with matter is a complex relationship that is dependent on the frequency of the wave and the dielectric properties of the material. The dielectric properties of a material are strongly dependant on both the electronic structure of the material and the macroscopic interface geometry of the system.

The two key mechanisms for energy transfer are polarisation of charge distributions, either of electrons or molecules, and build up of charge at an interface in heterogeneous systems, named Maxwell-Wagner polarisation.

In polarisation, when microwaves penetrate and propagate through a material, the internal electric fields generated within the volume of the material induce translational motion to ionic or molecular dipoles. This motion is associated with the dipoles trying to align themselves with the field, and is applicable to both charge distribution around an atomic nuclei or due to the relative displacement of atomic nuclei because of the unequal distribution of charge in molecule formation.

In an ideal material, the dipoles of molecules will align themselves corresponding to the oscillating electric field instantaneously, in this situation there will be no energy loss and no heating. If dipole moments cannot follow the high frequency rotations of the electric field, a localised phase shift will occur, leading to energy dissipation. The resistance of these field induced motions causes losses, attenuating the electric field and volumetrically heating the material. The degree of absorption can be quantified by the electromagnetic properties of the material, such as electrical conductivity and permittivity and microwave frequency.

Where an energy transfer (heating) is occurring angle δ is the phase difference between the electric field and the polarisation of the material. This value is related to the efficiency of conversion between electromagnetic and thermal energy. The loss angle, δ , is also commonly quoted, although usually expressed in the form of its tangent. It is defined[44]:

Equation 10

$$\tan \delta = \frac{\epsilon''_r}{\epsilon'_r}$$

The absolute dielectric constant ϵ (permittivity) is the product of the complex relative dielectric constant (ϵ^*_r) and the electric field constant ϵ_0 . The complex relative dielectric constant (ϵ^*_r) completely describes the dielectric properties of a homogeneous material. It can be expressed as the sum of two parts, the real (ϵ'_r) and imaginary (ϵ''_r) dielectric constants[93]:

Equation 11

$$\epsilon^*_r = \epsilon'_r + i\epsilon''_r$$

The real part ϵ'_r is called the dielectric constant and is a measure of a materials ability to polarise, giving the ability to store energy. The imaginary part ϵ''_r is also called the dielectric loss factor and describes the dissipation of energy in the form of heat. The dielectric loss factor is both frequency and temperature dependent (figure 1.23; it is composed of elements relating to dissipation mechanisms resulting from electron polarisation, atomic polarisation and space polarisation[44].

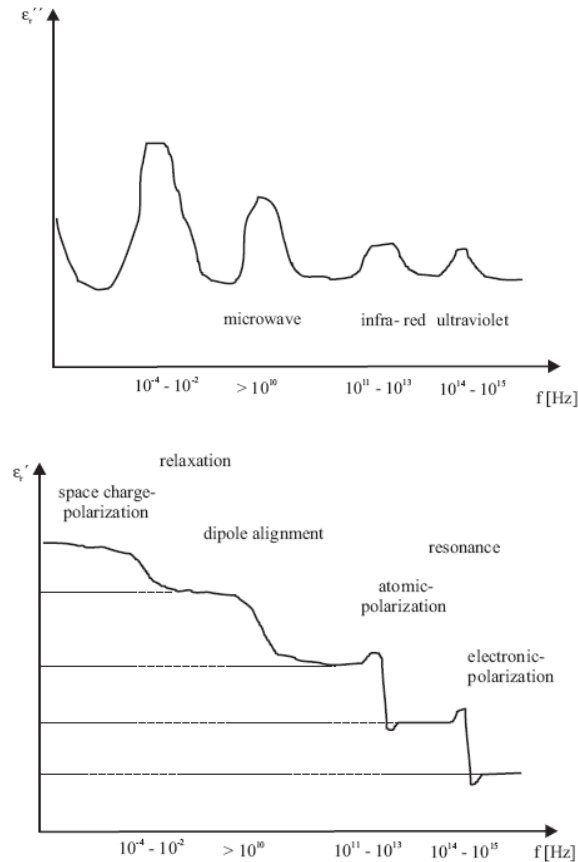


Figure 1.23: Showing the variation in the magnitude of the dielectric constant and dielectric loss factor as a function of frequency and the loss mechanisms[44].

The penetration depth, D_p is the depth at which the electric field falls to $1/e$ of the field at the surface. In the microwave frequency range, the penetration depth varies from metres to millimetres depending on the frequency, temperature, chemical composition and microstructure.[82] The value of the penetration depth (D_p) is inversely proportional to the frequency of the wave D_p is given by:

Equation 12

$$D_p = \frac{C}{2\pi f \sqrt{2\varepsilon'} \left[\sqrt{1 + \tan^2 \delta} - 1 \right]^{1/2}}$$

where: D_p - penetration depth, ε'_r - dielectric constant, δ - phase difference, f - frequency, (Hz); and C - speed of light, (m/s).

In conventional furnaces, heat is transferred to the material by thermal electromagnetic radiation. The penetration depth at infrared radiation is very small in the majority of solids ($D_p < 10^{-4}$ m) and this corresponds to direct heating of a very thin outer layer of the material and the rest of the material will be heated by conduction. The gradients of temperature variation will depend on the heat transfer properties of the specific material. Minimization of temperature gradient across a material as a result of microwave heating can therefore give more uniform heating[94].

The average power density P (volumetric absorption of microwave energy W/m^3) produced in a material when it is exposed to microwave energy is defined:

Equation 13

$$P = 2\pi f \varepsilon_0 \varepsilon''_{eff} E^2$$

Where: ε_0 -permittivity of free space (F/m); ε''_{eff} effective relative loss factor; and E -electric field strength inside material (V/m)

If the material exhibits magnetic losses the effect of the magnetic field must be considered, especially for materials exhibiting high magnetic susceptibility. The relevant equation can be rewritten as:

Equation 14

$$P = 2\pi f \epsilon_0 \epsilon_{eff}'' E^2 + 2\pi f \mu_0 \mu_{eff}'' H^2$$

where: μ_0 -permeability of free space, (H/m); μ_{eff} -effective magnetic loss factor; H-magnetic field strength, (A/m).

For materials that do not contain dipolar molecules, such as metals, there would be very little polar rotation therefore limited dielectric losses if only the electric field is considered. For this reason metals act as good reflectors for microwaves due to the very high electrical conductivity. Work by Cheng et al [95] identified the effect of the magnetic field could have on metallic materials. The magnetic field was used to account for the ability to sinter powdered metal samples including large size (100 mm diameter/1kg) that could be fully sintered in 30 min in a 2.45 GHz multi-mode microwave cavity. It was shown that sintering of such dense objects, with limited penetration depth, could not be explained by the skin depth absorption model. It was suggested that the heating in this situation was likely to be the result of eddy currents in the surface induced by the magnetic field. This conclusion was drawn from results showing the variation in heating rates when materials were exposed to either purely electric or magnetic components of the microwave field in a specially designed single mode cavity. The role of the magnetic field was also used to describe the change in heating rate for an iron sample around the Curie point, demonstrating that ferromagnetism is clearly an important variable.

The heating of metal powders is a complex process; the low penetration depth of the field into a bulk metal object would preclude it from heating. However the field percolation effect observed in powdered samples allows the penetration of the field much deeper into a powder sample. When the sample to be heated is

powder of an electrically conductive material, its effective conductivity can differ substantially from the conductivity of the homogeneous solid material[96].

The dielectric properties of such a compact can be expressed via the properties of its constituents via the effective medium equation, taking into account the density of the solid phase in the compact and assuming that each individual powder particle is spherical.

This gives the following equation for the effective complex dielectric permittivity ϵ_{eff} of the compacted material:

Equation 15

$$4\beta\epsilon_{eff}^2 + 2[\beta(3C - 2) + \epsilon_i(\gamma - 3\alpha C)]\epsilon_{eff} + \epsilon_c[\gamma(3C - 2) - 3\alpha C] = 0$$

where C is the relative volumetric concentration of solid in the compact, ϵ_i is the complex dielectric permittivity of the material separating the spheres of radius r, ϵ_c is the complex dielectric permittivity of the conductive material T is the thickness of the separating materials and α , β and γ are temperature dependent constants derived from:

Equation 16

$$\alpha = \left[1 - \left(\frac{1}{\xi^3} \right) \right] \left[\frac{2\epsilon_i + \epsilon_c - 6}{(1 - \xi^3)(\epsilon_0 - \epsilon_i) \ln \xi} \right] + \frac{3\xi_c}{\xi^3}$$

Equation 17

$$\beta = \frac{2\epsilon_i + \epsilon_c + (\epsilon_i - \epsilon_c)}{\xi^3}$$

Equation 18

$$\gamma = \frac{2\epsilon_i + \epsilon_c + 2(\epsilon_c - \epsilon_i)}{\xi^3}$$

where

Equation 19

$$\xi = 1 + \frac{T}{r}$$

1.12.5 Temperature measurement in microwave fields

Temperature measurement in a microwave cavity is not a trivial process. Whilst conventional heating may be assumed to give rise to uniform temperatures throughout a small sample, microwave heating imparts energy directly to the sample. Within the sample, inhomogeneous heating may occur at the millimetre or even sub-millimetre scale as the rate of conversion from microwave energy to heat is heavily dependent upon the dielectric properties of the sample. As the dielectric properties themselves are often heavily dependent upon the temperature, minor local temperature variations may become amplified through a positive feedback mechanism.

It is therefore unreasonable to make the assumption that accurate temperatures in a microwave-heated system may be measured in a conventional manner. The two basic methods for temperature measurement, contact probes (e.g. thermocouples) and thermography (e.g. pyrometers) are unreliable, as the former may cause perturbation of the microwave field precisely at the point of interest, and the latter only register surface temperatures in an environment where surface cooling is highly significant.

The operation of a pyrometer is based on the wavelength of infra-red photo emissions from the material being measured, this is a non-contact approach that can be very useful however the technique is limited to direct line of sight and infrared absorption from surrounding materials can be problematic.

In the absence of clear, critically assessed information on sample temperatures, many authors have alleged that microwave heating enhancement is due to non-

thermal effects resulting from the microwave electric or magnetic field. Whether effects can be classified as non-thermal or are related to errors in temperature measurement is of some debate.

1.12.6 Diffusion under microwave fields

There is a large and growing volume of empirical work that has looked at solid state diffusion of materials under microwave fields. This has shown a variety of effects such as reduced sintering times, increased diffusion coefficients and changes in the structure of materials. One of the key findings of these studies was a reduced time and temperature needed for a given degree of solid state reaction, and it was calculated that an increase in diffusion was the key parameter.

Many of these studies have looked at second order effects such as sintering rate or grain growth and therefore have often used a reduction in temperature for a specific reaction to justify the enhancement. One of the first studies to show a confirmed change in diffusion coefficients of single crystals was Janney et al [104]. In this study it was demonstrated that the Volume diffusion of oxygen in sapphire was enhanced by heating in a 28 GHz microwave furnace. The apparent activation energy for volume diffusion was reduced by 40% from 650 to 390 kJ mol⁻¹ and the pre-exponential factor was reduced by five orders of magnitude from 9.7×10^{-2} to 3.8×10^{-7} (m²s⁻¹).

The process of sintering is the densification of compacted powder bodies that occurs below the melting temperatures via shape accommodation of the powder particles. The main driving force for sintering is capillary stress, which acts to minimise the free energy associated with the surface area.

The thermal sintering of a ceramic is a complex process, with a number of diffusion mechanisms taking place which together produce the required increase in density, and changes in mechanical (and other) properties of the material. Through this diffusion, ions move into vacancies within the crystal lattice, resulting in a net transport of empty space from the bulk of the sample to the

surface, causing an eventual reduction in volume. It should be noted that the sintering and grain growth processes, being of diffusion nature, have an Arrhenius-type dependence upon the temperature and are often characterised by corresponding activation energies[97].

Several studies into the use of microwaves in the sintering process have suggested phenomena that are not observed when materials are heated conventionally. The reasons associated with these changes are linked to the heating rate and temperature profile associated with microwave processing. The high dielectric losses of many ceramic materials, coupled with the volumetric nature of the heating, allows the heating rate of microwave heated samples to be higher than that of conventional systems, without increasing internal stresses. In many cases, microwave processing is capable of improving the product quality or leads to results that cannot be achieved conventionally[44]

At different steps of sintering the diffusion processes vary with the particular mechanism: i.e. surface, grain boundary, and bulk diffusion, the mechanism and temperature determine the mass transport and thus the final microstructure. Inhibition of surface diffusion in the initial stage of densification is favourable for sintering as the formation of a rigid neck structure between grains, which occurs primarily by surface diffusion[97]. An increase in the rate of heating at the onset of densification inhibits this process, thus retaining high enough Laplace driving forces for densification[82].

Volumetric heating is another difference in the behaviour of microwave assisted sintering and conventionally processed materials. The volumetric nature of the energy deposition accelerates heating, which reduces the time needed to complete a process. The reduction in process time under microwave heating is especially significant when the process involves endothermic chemical reactions and/or phase transformations. In this case a sufficient energy supply is essential for a high process rate, which is determined at each point by the local temperature (the energy supply being the rate determining factor). Conventionally, the energy supply rate is always limited by slow heat transfer

processes. Due to volumetric energy deposition, microwave heating is, in principle, capable of providing any desired rate of an endothermic process, limited only by the power of the microwave source.

Selective heating is an advantage of microwave heating that can be applied to sintering of materials. Differential heating is achieved by the mixing of two materials with varying dielectric properties that will therefore have dissimilar heating rates. When a composite material is heated with microwave radiation, the temperature distribution lies in accordance with the absorption properties of the composite's components.

This process has been used successfully in the processing of composite materials consisting of a ceramic matrix impregnated with a metal–organic precursor and is one of the successful applications in this field[98]. Selective heating of a precursor and its subsequent pyrolysis makes it possible to obtain composite materials with microstructures quite different from those of conventionally produced materials. What is more, the selectivity of microwave heating allows efficient control over the microstructure and properties of the synthesised materials by choosing proper microwave absorption coefficients of the matrix material and precursor.[82]

The activation energy for mass transport is a key factor in the sintering process for a given material and the activation energy, and hence the diffusion coefficient will be different for each diffusion mechanism - surface and grain-boundary diffusion normally have significantly lower activation energies than volume diffusion. D is the diffusion coefficient, given by[99]

Equation 20

$$D = \nu_o a^2 e^{-\frac{\Delta g_m}{kT}}$$

where ν_0 is the characteristic lattice vibration frequency, a is the lattice constant, k is Boltzmann's constant, T is the absolute temperature, and Δg_m is the Gibbs free energy for motion through the lattice (the activation energy).

The use of microwaves during the sintering process has been observed, in several instances, to alter the rate and temperature at which densification processes are undertaken. There is a growing amount of experimental evidence to support the fact that microwave heating of ionic crystalline solids leads to an enhancement of the diffusion processes which occur during the sintering process. Samples processed within a microwave furnace are observed to sinter at a faster rate or at a lower temperature than those processed in a conventional system.

Janney and Kimrey [100] conducted research on the microwave sintering of alumina and have shown that, at 28 GHz, the microwave enhanced densification of high-purity alumina proceeds as if the activation energy is reduced from 575 kJ mol⁻¹ to 160 kJ mol⁻¹.

Figure 1.24 shows the significant changes that are produced during the microwave sintering process on the densification of alumina when compared to those of the conventionally processed material. The density of microwave sintered alumina rapidly increases with temperature compared with the thermally processed alumina.

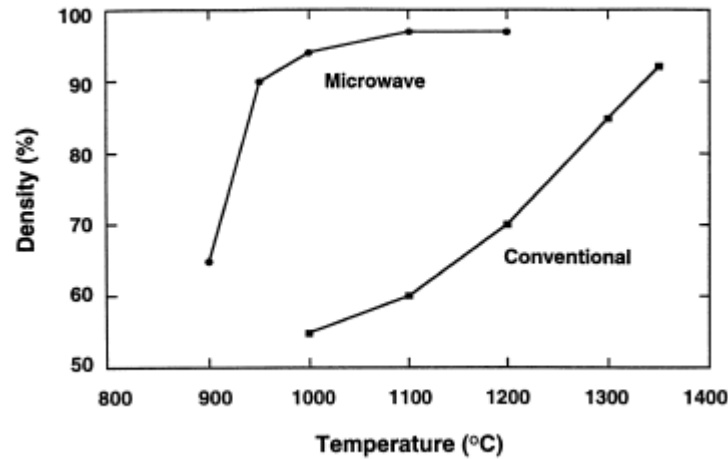


Figure 1.24: Density versus sintering temperature for alumina sintered in a microwave and a conventional furnace[100]

An observed enhancement of the densification during microwave solid-phase sintering of zirconia was reported by Wroe et al [101]. A study of microwave sintering of ZrO_2 revealed a non-thermal nature of this enhancement, during combined radiant and microwave heating.

The densification rate at each temperature was found to be sensitive to the proportion of microwave power. With full microwave power, the densification curve was shifted towards lower temperatures by approximately 100°C , as compared to conventional heating. It was also observed that the removal of the microwave field during the densification process produced a slowing in the rate of densification until the temperature had increased sufficiently for densification to continue without microwave assistance (Figure 1.25).

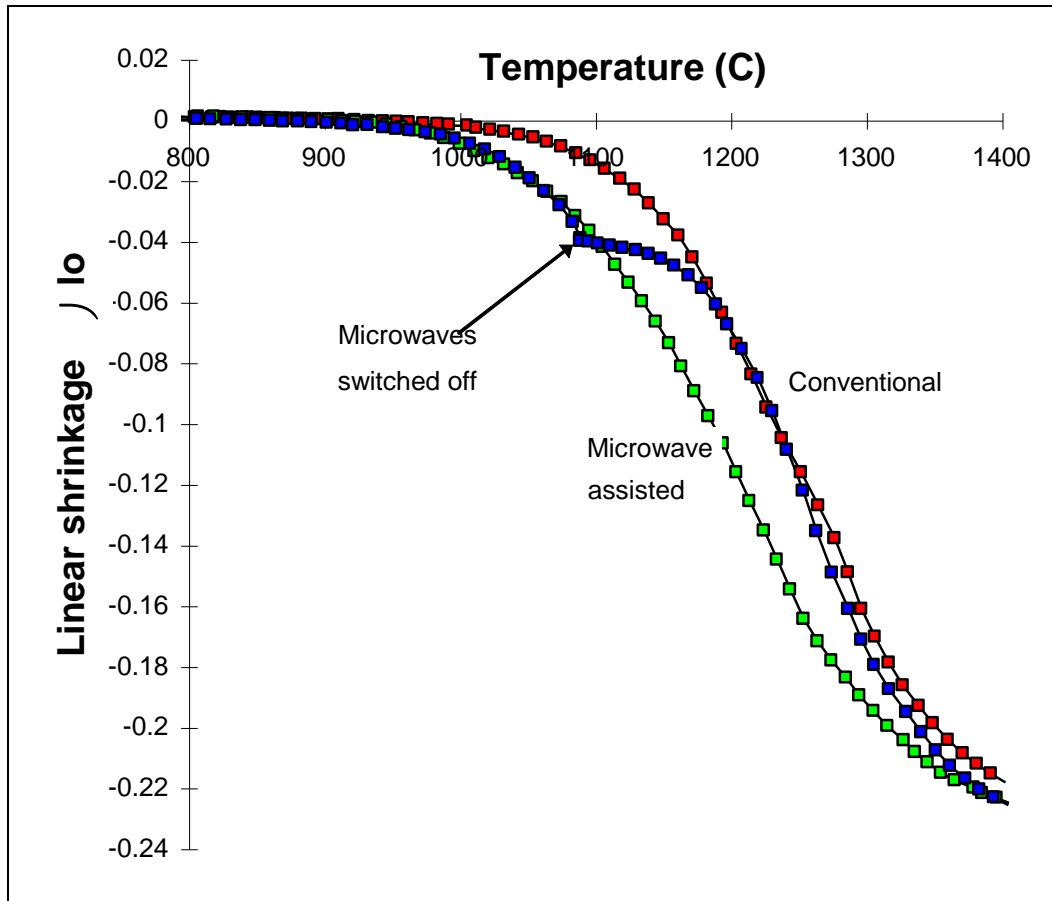


Figure 1.25: Normalised linear shrinkage of zirconia plotted as a function of sintering temperature for conventional and microwave assisted sintering, showing the effect of switching off the microwaves during processing (1080°C)[102]

Additionally the sintering of NiCuZn ferrites was studied by Saita et al [103] in a microwave field of 2.45 GHz. It was established that densification of NiCuZn ferrites was significantly promoted by microwave processing and the effective activation energy for diffusion during microwave sintering was half the value of the conventional sintering case. On the other hand, the microwave sintering showed little effect on the activation energy for isothermal grain growth in NiCuZn ferrite. The reduction in activation energy associated with a microwave processing is a controversial topic in the current literature with observations which cannot be explained in full on the basis of current knowledge in the field[82].

One explanation that has been put forward for the apparent increase in diffusion is an inaccurate measurement of temperature. In practice, inaccurate or incomplete temperature measurements pose a problem due to the nature of the temperature distributions. Thermocouple sensors generally measure the temperature of the thermocouple head, which may be close to the temperature of the material at the point at which the head touches, but it can still differ substantially from the temperature at other points of the material. The reasons are heat losses via the thermocouple, microwave absorption in the thermocouple, etc. Pyrometers measure temperatures on the surface of the material but these are different from those in the bulk so will not give a complete picture of the internal temperature profiles.

The inaccuracy of temperature measurement would be countered by the findings of Janney et al [104], in a study of oxygen diffusion in sapphire, and also Rowley et al in a study of oxygen diffusion in YBCO superconducting material[101].

Janney et al [104] found that the enhancement of oxygen diffusion in sapphire crystals heated in a 28 GHz mm-wave furnace equated with a 40% decrease in the apparent activation energy for bulk diffusion when compared to that of conventional heating. The suggested mechanism for the phenomenon of microwave-enhanced oxygen diffusion in sapphire was suggested to be the direct interaction of the microwave field with the defects responsible for diffusion, (vacancies and interstitials) elevating the energy state without affecting the overall temperature of the material.

Rowley et al[101] found a 30% increase in the effective diffusion coefficient with the use of microwaves in the oxygenation of melt processed bulk YBCO ceramics (Figure 1.26). In this case the temperature measurement can be determined by the equilibrium oxygen content after the processing, due to the strong inverse function of processing temperature and oxygen content; as the oxygen content is not affected by the application of microwave field, the sample temperature must be the same whatever the processing route.

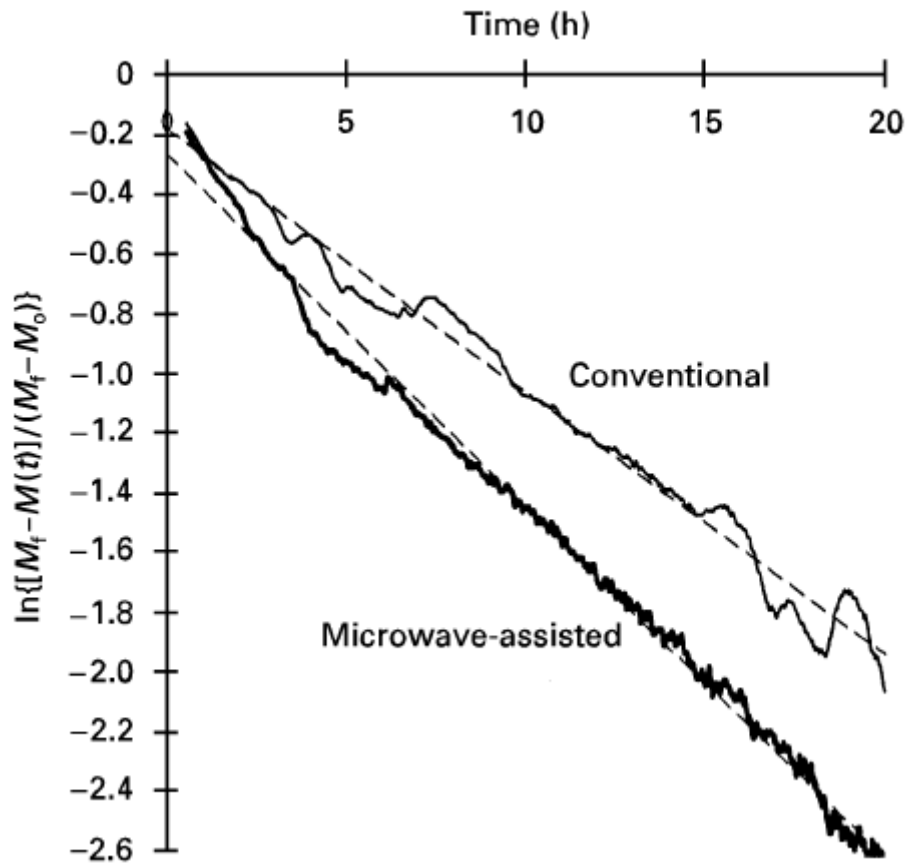


Figure 1.26: Comparison of conventional and microwave-assisted oxygenation of melt-processed YBCO; 20 hour hold at 400°C.

Further work on the oxygen diffusion kinetics in YBCO was performed by Wittiker et al[105], who analysed the relative diffusion of ions as a function of the angle to the microwave field. A significant difference was observed in the oxygen diffusion coefficient when the material was subjected to polarised microwave irradiation, showing an angular dependence for the diffusion rate that is not observed in conventionally processed samples. The preferred diffusion direction was consistently found to occur parallel with the polarised microwave electric field vector of the with the apparent diffusion coefficient parallel with the field observed to be up to 10 times greater than that perpendicular to it.

One model that has been suggested to account for these phenomena is the solid state ponderomotive effect, which is analogous to the ponderomotive effect seen in plasma physics.

In plasma an electromagnetic field can alter the motion of charged particles and influence reactions. For the solid state situation the nonlinear effect could exist near physical surfaces or interfaces, where there is an increase in vacancy diffusion induced by the alternating electric field[106, 107]. The volume affected and the size of the effect is calculated to be a function of both the sample permittivity, and the strengths of the high frequency fluctuating electric field.

The high-frequency electric field drives a high-frequency flux of charged mobile species within the material, which can lead to changes in the local vacancy concentration at a surface or interface. In the bulk of the material, the fluxes are spatially uniform so that the observed effect is not as large, however near the surface the high frequency field can result in harmonic oscillation of the ionic concentrations.

These oscillations cause the vacancies or charged species alternately to accumulate and deplete during a cycle and are in phase with the high frequency electric field oscillations. Any such in-phase oscillations of electric field and mobile charge concentration multiply to produce a rectified, quasi stationary flux of vacancies towards the surface. This process, given time, will affect the concentration gradient or electrochemical potential of the material and will therefore propagate into the bulk of the material.

This effort established that the magnitude of the ponderomotive force (PMF) for microwave field intensities typical of materials processing conditions can equal or exceed the magnitudes of other competitive transport driving forces that would be present in the absence of the microwave field[107].

Thus it was established that the microwave PMF is capable of explaining enhanced solid-state reactions by significantly enhancing reactant transport in ionic solids. It may seem remarkable that these solid-state ponderomotive forces can have such a significant phenomenological effect for relatively low radiation pressures in comparison, say, with mechanical stresses that may be present or can be applied.

1.12.7 Microwave catalysis

A catalyst is classically defined as a material which changes the rate of a chemical reaction, without itself appearing in the overall chemical equation. Catalysts work by providing an alternative mechanism or 'reaction pathway', which allows the reaction to occur via a lower energy intermediate state. The effect of this is that more molecular collisions have the energy needed to reach the transition state. Having a lower energy intermediate state allows a greater proportion of the reacting species to have the necessary energy to overcome the activation energy for that reaction. Hence, catalysts can enable reactions that, albeit thermodynamically feasible, would not run without the presence of a catalyst, allowing reactions to progress faster, with more specific products, or at lower temperatures.

Since the use of microwaves in catalytic reactions it has been frequently found that faster reaction rates greater selectivity and higher yields, all have been obtained. These advantages are often associated with the changes in the thermal gradient that can be achieved with microwave heating[108]. Heterogeneous catalysis has been a successful method for utilising the advantages of the thermal distributions that can be achieved with microwave heating. In heterogeneous catalysis the catalyst is of a separate phase from the reactants as in the case of a gas flowing over a solid catalyst. This can create situations where the catalyst will have a much higher heating rate in the microwave field and therefore can create hot spots on the catalyst surface. An example of this approach, taken by Zhang et al, is the decomposition of H_2S over a catalyst based on molybdenum oxide on a γ -alumina support[109]. It was found that under microwave fields there was an 'apparent' equilibrium shift in the reaction and that the conversion efficiency for the reaction which takes place in the microwave cavity is higher than that predicted on thermodynamic grounds (Figure 1.27). In this work the calculated temperature of the hot spots on the catalyst was found to be over 100°C higher than the probe temperature, thus showing the benefit of microwave heating.

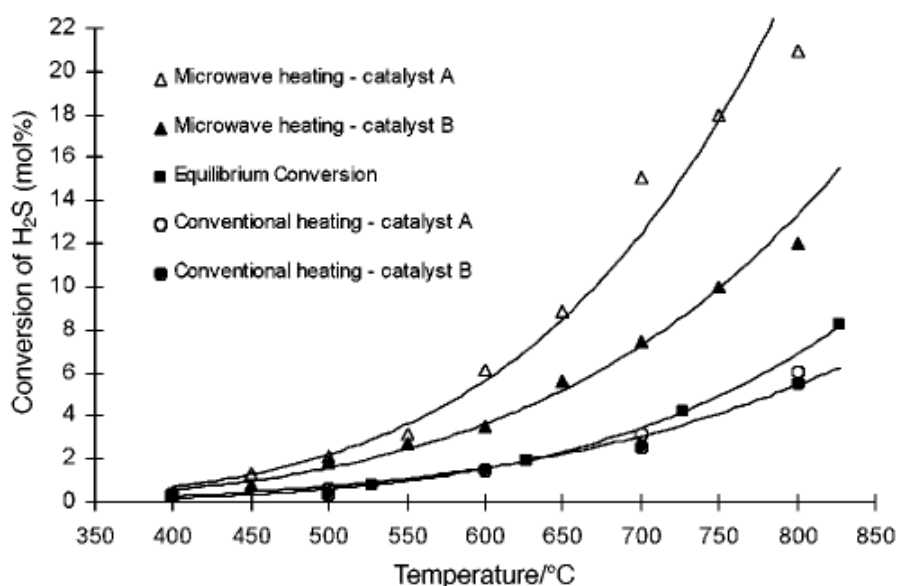


Figure 1.27: H_2S conversion vs. temperature showing the improvement of the reaction rate above the equilibrium for the same catalysts in microwave fields and thermally.[109]

1.12.8 Non thermal microwave effects

The foundation for the increased mass transport outlined above, is currently a topic for debate and this is due to both the limited number of claims of an observed non thermal effect and difficulties in the experimental identification of a particular mechanism involved. Freeman et al[110] found strong evidence for increase in the driving force for charge transport in NaCl crystals, which was not associated with an increase in mobility of defect species. This was claimed to fit with the model of Rybakov and Semenov [107, 111] which included interactions between high frequency electric fields and vacancies modelled as charged point defects.

In effect this theory suggested that the high frequency electric field could either create or remove point defects in the crystal at or near a surface. The removal or creation of defects would produce either a net depletion or an accumulation of defects that could constitute a driving force for diffusional flows of defects. This flow of defects is termed a ponderomotive force.

1.12.9 Non Faradaic Electrochemical Modification of Catalytic Surfaces

NEMCA (non-Faradaic-modification-of-catalytic-activity), discovered in the early 80s by Stoukides and Vayenas, is a special type of catalysis in which catalyst properties are modified by applying an electrical field[112]. The electrode of an electrochemical cell is thereby used as catalyst for two simultaneously occurring processes, a chemical and an electrochemical one. Although this effect has not been observed under microwave fields the use of alternating electric fields is not uncommon and the frequency of the bond vibrations is an order of magnitude higher than the frequency of the microwave electric field suggesting that direct interactions and coupling should be minimal.

The major part of the yield is achieved by the chemical reaction pathway, which can include a heterogeneous catalytic reaction. This is the non-Faradaic part of the yield. The superimposed electrochemical reaction is actually used to control and improve the catalytic properties of the catalyst (electrode) surface. The by-product of this electrochemical reaction pathway is the Faradaic part of the overall yield. Only a minor part of the yield is generated through that electrochemical pathway (Faradaic mode).

This combines different features common to heterogeneous catalysis and technologies based on electrochemical polarization and can have some very strong effects. Electrochemical O_2 diffusion to the catalyst electrode was found to cause a 6000% steady-state reversible enhancement in the rate of C_2H_2 oxidation[113].

It is thought that the electrochemical promotion is due to the current controlled electro-catalytic Faradaic introduction of ions to the catalyst/gas interface, where a double layer is formed that has overall neutral charge (Figure 1.28). The density of this double layer, and the field strength in it, varies with the applied potential, affecting both the work function of the surface and the chemisorptive bond strength of reactants and intermediates, causing the alterations in catalytic rate[114].

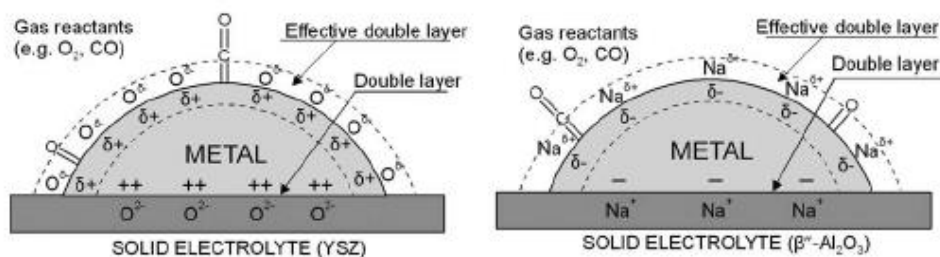


Figure 1.28: Schematic representation of a metal electrode deposited on a O₂-conducting and on a Na⁺-conducting solid electrolyte, showing the metal-electrolyte double layer and the double layer created at the metal-gas interface[114].

This effect has been demonstrated in a wide variety of heterogeneous reactions with both cations and anions showing similar responses, and the effect for both Na⁺ and O⁻ has been modelled with some accuracy. However there is still an open question of the mechanisms involved in H⁺ promotion and the nature of the species formed on the catalyst surface under electrical polarization [114].

A detailed discussion and investigation into the possible physical processes at work is beyond to scope of this work; however it is not beyond the realms of possibility that non Faradaic electrochemical promotional effects could influence the reactivities under microwave frequency electric fields.

2. Technology development

This project has technology development as a key aspect of the research, which has posed problems and required creative engineering solutions throughout. Although some of the technologies and measurement concepts had been developed previously there is no known system anywhere prior to this project that allows the study of the effects observed.

For most studies of the effects microwave fields have on chemical reactions the control of temperature is a difficult challenge. For most apparatus the only heat source is the microwave field which is used to heat the samples being studied in addition to any effect the field may have. In order to increase the temperature significantly it is therefore usual to apply a significant field to the material at which point it becomes difficult to separate the effects of heating mechanism from any more subtle influence that the oscillating electromagnetic field may have on any reaction. Additionally if the reaction affects the dielectric properties of the material, a change in heating rate would be impossible to avoid which would cause a significant obstacle to drawing firm conclusions. By using a hybrid microwave / radiant system it was possible to control the temperature of the sample throughout the reaction and reduce the error that can be associated with other systems.

The development of the technology and systems to monitor reaction rates in gas phase reactions, at high temperature, and under microwave fields was a key innovative aspect of this project. The developments have culminated in a system which gives C-Tech Innovation a unique technology that is already being directly exploited commercially as both a research tool and as the basis for several commercial systems that have been built for outside agencies.

Additionally some of the concepts developed for the systems have been replicated in other applications using the sealing and temperature sensing technologies developed in this work.

2.1 *Prior C-Tech Innovation technology*

The basis for the technology in this project is the prior development work by C-Tech Innovation in the field of microwave and RF assisted processing of materials, which has been a core part of the C-Tech Innovation technology offering for over 20 years[115, 116]. The technology developed has found commercial applications in the processing of materials, microwave chemistry and drying operations. The previous research on the benefits of microwave processing found that the rate of gas and liquid phase reactions and sintering rates of ceramic of materials can be enhanced by the controlled application of microwave and radio frequency fields during thermal processing[101, 102].

The hybrid microwave and radiant furnace development has been ongoing within C-Tech for the last two decades, and has enveloped a range of technologies from electric and gas powered laboratory furnaces to the development of larger continuous production tunnel kilns with varying temperature regimes. The development of hybrid microwave systems where both conventional and microwave power sources are used to solve many of the problems of process control that had limited the use of microwave systems for industrial applications. The initial work on microwave heating showed the promise of the technology but highlighted the technical challenges that need to be overcome relating to process control and reproducibility. The key early advance is the application of hybrid technology, where the conventional heating system of either radiant elements or gas burners is used to provide the majority of the thermal input and control the temperature. The microwave field is then used to assist processing of the materials either providing the volumetric heating or electric fields that may influence reaction kinetics. The hybrid approach has several key benefits:

- Providing 70-90% of the energy from conventional heating sources the capital equipment cost for industrial processes is significantly reduced. Microwave generator and magnetron units currently cost around £1000 per kW of installed capacity, which is an order of magnitude greater than conventional sources.

- Temperature control is much more straightforward when the cavity around a sample is heated to the same temperature as the sample and additionally there is a far greater opportunity to vary the amount of microwave power used to heat the sample which is not possible if the microwave field is the major heat source.

Rather than the classical temperature profiles observed in radiant heating processes, the electromagnetic interactions can generate heat volumetrically within the sample either uniformly or at specific locations. The change in the temperature distribution can make the accurate control of sample temperature a challenge, leading to effects such as local overheating or thermal runaway. Thermal run away is an effect that occurs where the energy absorbed by the material increases with an increase in temperature leading to a positive feedback loop.

Other issues relate to the temperature measurement, either in direct heating of the sensor, or through pick up of the electromagnetic radiation by electrical control system. Direct heating of the sensor can be reduced through the selection of low dielectric loss materials for the construction of the sensor or through the use of shielding materials and the careful positioning of the sensors.

By surrounding the thermocouple in an earthed metallic sheath the direct heating of the thermocouple can be reduced as more energy is reflected from the surface. For the thermocouples used in this work a platinum or inconel sheath provided sufficient protection to allow accurate temperature measurements.

It has been observed that the optimum way to ascertain if the temperature measurement is affected by the microwave field is to monitor rapid changes in the measured temperature when the sample is not in contact with the thermocouple. Due to the low thermal mass any localised heating caused by heating above the cavity temperature will quickly dissipate on removal of the field and give a clear indication of inaccuracies in the temperature measurement.

Examples of non contact sensors that are less prone to direct heating include IR thermometers which use the IR spectrum emitted from a surface to infer the

surface temperatures; however changes in surface emissivity can significantly affect the accuracy of the measurement. Additionally there are considerable challenges in engineering a solution to allow a clear view of the sample surface while keeping the sensor cool.

To prevent the interruption of the electronic circuitry in any of the control system it is essential to include filters in to the system to remove the high frequency AC components generated by pick up of the RF or microwave fields. These generally consist of capacitance added into the line to absorb and flatten out the high frequency components.

Figure 2.1 shows the 1st generation of the basic lab scale microwave assisted gas hybrid furnace (MAGF1) developed for trial applications and process development[116]. The system uses two gas burners and three 1.5kW magnetrons. This system is capable of operating at temperature up to 1600°C and was used to develop the control systems that would be used on larger furnace systems.



Figure 2.1: Gas heated lab scale hybrid microwave furnace, using mixed mode microwave system from 3 microwave sources[101, 116].

Once the technical hurdles of process and temperature control had been understood the development of larger industrial installations was the next step[117]. The type of tunnel kiln, shown in figure 2.2, enables the production of larger quantities of product while still demonstrating the cost reduction benefits that microwave processing allows.



Figure 2.2: Industrial tunnel kiln developed to process 1m³ of product per hour[117, 118]

Microwave safety is an important factor to consider in the design of the industrial and research systems and there have been several reports that have tried determine the safe exposure limits for microwave radiation[119]:

1. In 1960 the Post Office published a guide relating to "Safety Precautions relating to Intense Radio-Frequency Radiation". This recommended a maximum safe working level of 10 mW/cm², thereby setting a multiple of 10 safety factor

- 2 A committee of the Medical Research Council carried out a review in the late 1960s and their report in 1970 confirmed that the 10 mW/cm² limit for continuous exposure of personnel was acceptable. It also laid down parameters for short periods of exposure at higher levels.

- 3 An EEC draft proposal for a Directive on microwave and RF occupational exposure standards is at an early stage of negotiation. The proposal aims to safeguard workers by setting a limit on the specific absorption rate (SAR) but this

has not as yet been translated into exposure limits. In addition, limits are proposed for exposure based on the strength of associated electric and magnetic fields.

4 Proposals by the National Radiological Protection Board for "The Health Protection of Workers and Members of the Public against the Dangers of Extra Low Frequency, RF and Microwave Radiations" recommend the retention of the $10\text{mW}/\text{cm}^2$ level for the microwave frequency band for the continuous exposure of adults. A lower figure of $5\text{mW}/\text{cm}^2$ is proposed for the general public. Again limits are placed on the strengths of the associated electric and magnetic fields.

5 British Standard BS 5175: 1976 and International Electrotechnical Commission Standard IEC 335:25, specify maximum leakage rates from a microwave oven in service, of not more than $5\text{mW}/\text{cm}^2$ at 5 cm from any surface of the oven.

2.1.1 Commercially Available Microwave Chemistry Apparatus

The application of microwave fields at lower temperatures is used regularly in the processing of samples for small scale chemical and pharmaceutical experiments. The properties of volumetric heating and the possibility of high heating rates are seen as beneficial and can be used in the development of a range of chemical synthesis reactions.

In many of the published works looking at the reaction kinetics there are two common methods used: for basic experiments often for low temperature reactions such as curing, sealed vessels are placed in a microwave oven for a period of time before samples were taken in order to characterise the reaction rate.

Alternatively basic monitoring of the reaction was undertaken by recording the pressure in the vessel through a link to a pressure sensor mounted outside of the microwave cavity.

Systems are commercially available that will monitor pressure and temperature of a sample in a sealed vessel within a microwave cavity as in Figure 2.3[13].



Figure 2.3: Example of commercially available Sineo microwave batch reactor showing 12 high pressure reactors with pressure and temperature monitoring[13].

These systems use a carousel of sample containers, designed to take a liquid sample. The pressure monitoring is passive with pressure release valve allowing little control over the process conditions and the temperature is monitored but not easily controlled.

These systems were considered as a possible starting point for the development of the system; however, the problems of inertly loading, evacuating, controlling hydrogen pressure and sealing the containers would be large obstacles.

By moving to a bespoke gas control and measurement system several key barriers had to be overcome in order to operate the system both safely and effectively. In order to allow a flow of gas through a microwave cavity it is necessary to create holes in the skin of the cavity, which for safety must not allow the microwave field to escape.

2.2 Outcomes required

During the design and build of the system it was essential to understand the required operating conditions and the type and performance of the data acquisition system. The design process for the gas control systems depended on

the physical characteristics of the materials to be assessed both in terms of pressure range, accuracy of sorption volume and time period.

For the work identifying the effect of microwaves on the onset of hydrogen decrepitation in magnetic materials a low data resolution and low accuracy of gas volume changes was acceptable. However to make measurements of the rate of reactions involving hydrogen storage materials in order to assess the impact of microwave processing for more accurate systems are required.

There were a series of developments in this project that reflected the material types being assessed from low temperature low pressure experiments on NdFeB magnets to higher temperature and pressure cycling of magnesium hydride.

2.2.1 Development Iterations in the technology

Although there were significant developments in the use of hybrid heating concepts prior to the start of this work, significant progress was needed in the development of suitable hydrogen control systems that would function effectively in conjunction with microwave field. Previous work had shown that it is possible to use an open muffle through which inert gas could be passed but this was not suitable for the hydrogen atmospheres required for this work.

Two gas measurement methodologies were used in the project; the first used the change in pressure in a fixed volume at a constant temperature to monitor the reaction onset and rate of the absorption of hydrogen by NdFeB. This was suitable for this system due to the low number of variables in the system and relatively simple measurements required for the initial assessment work.

The second methodology involved measuring the gas flow on both the input and output of a system and using the difference in flow to monitor the rate of absorption or desorption reactions. This system also needed to be capable of raising and lowering the pressure in a controlled manner between set pressure values in addition to maintaining a constant pressure during changes in temperature.

The system development started with a small bench top apparatus based on a domestic microwave which progresses to include a sophisticated gas control system and eventually a basic hybrid system temperature control system before development in to a full scale, fully controllable and instrumented system capable of measurements at higher pressure and high temperature.

2.2.2 Development rig based on a domestic microwave

The first attempt at the creation of an integrated gas system with a microwave power source was conducted at The University of Birmingham. This used a commercial microwave oven with a carefully designed choke system to allow a gas system to be inserted through the side of the unit.

The first system developed used an isolated gas system that allowed in-situ monitoring of both the temperature and pressure. The development process started with the building of a basic bench top system utilising an adapted commercial Panasonic NNT573 900W inverter microwave, with an internal cavity volume of 27400cm³.

This multi-mode microwave was chosen as it is one of the few commercially available systems that use an inverter circuit to supply the current to the magnetron, thus allowing variation in the current supply to the magnetron giving a variable output power.

This is an important feature as it allows the control of power and field strength within the cavity without on-off duty cycling used in many systems to reduce the average power input.

The power levels are set to nominal values which have associated electric field strength (Table 2.1). The electric field strength was calculated from the increase in thermal energy of a 500ml water load placed within the cavity[115, 120].

Three power settings were used during the microwave treatment referred to as High and Medium and Low power. The corresponding power densities (P) calculated from the heating of a known volume of de-ionised water is given by[120]:

Equation 21

$$P = MC_p \frac{\Delta T}{t}$$

where: P= power converted to heat (Watts) M= Mass of the load(kg) Cp= Heat capacity J/°Cg ΔT= Change in temperature (K) t= Time (seconds)

The power density can then be used to calculate the maximum electrical field strength, E.

Equation 22

$$E_{\max}^2 = \frac{4P}{(2\pi f)\epsilon_0\epsilon_{\text{eff}}''}$$

where: E_{\max}^2 = maximum electrical field strength (V) P= power converted to heat (W) f=Frequency (hertz) ϵ_0 = Permittivity of free space ϵ_{eff}'' = the effective loss factor

Table 2.1: power settings and electric field strength of the multimode microwave

| Power Setting | Power Output (W) | Max Electric field strength (kVm ⁻¹) |
|---------------|------------------|--|
| High | 900 | 42.05 |
| Medium | 600 | 35.06 |
| Low | 250 | 24.66 |

Due to the variation in field strength that can exist in multimode cavities it was essential to locate the sample at the centre of the cavity, ensuring the sample was in the same position within the cavity for each test. In larger cavities it is usual to have a mode stirrer which helps to distribute the field more evenly, in a domestic system the rotating plate serves the same purpose but it was

unfeasible to introduce either a mode stirrer or rotating gas system in a small cavity.

2.2.3 The development of a volumetric gas control system

The system to expose the sample to hydrogen is shown in figure 2.4. The valves to control the inlet of hydrogen (H_2) and vacuum level were controlled manually. The volume of the closed gas system was fixed at $\approx 965\text{ml}$, including all pipe work and flexible hose, with the quartz vessel having an internal volume of 415ml . In operation the system is evacuated to remove oxygen before the hydrogen is introduced, thus preventing the formation of a potentially explosive atmosphere.

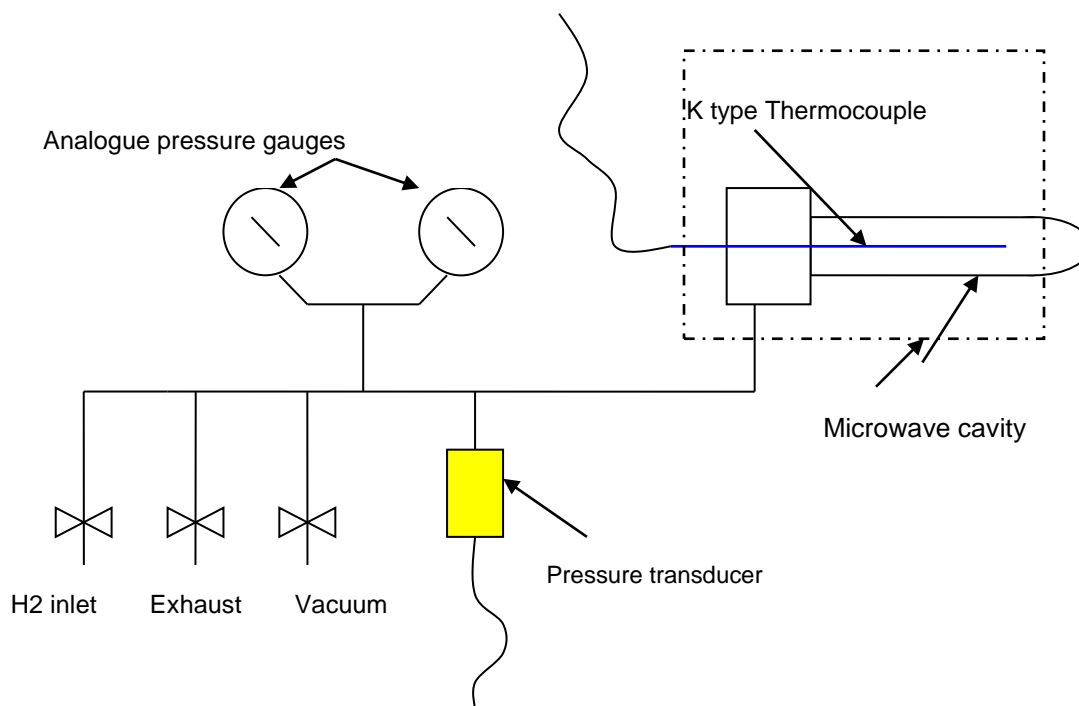


Figure 2.4: schematic representation of the fixed volume gas system.

2.2.3.1 Temperature measurement and data recording

Temperature monitoring was through the insertion of a K type thermocouple through the gas inlet with the tip in contact with the sample material. For this system temperature control was not possible due to the lack of access into the microwave power control circuits. The temperature data from the thermocouple

was recorded using a Fluke digital potentiometer linked to a pc and then the voltage data converted to the temperature increase reading ΔT using the following equation from the TC thermocouple standard guide,

Equation 23

$$\Delta T = a + bX - cX^2 + dX^3 - eX^4 + fX^5 - gX^6 + hX^7 - iX^8 + jX^9$$

$$X = (V + Y) * 1000$$

where: V= voltage recorded, T=Temperature, a, b, c, d, e, f, g, h, i, j= constants

The addition of the ambient temperature to the recorded temperature is required as the potentiometer is not “cold junction compensated”. The recorded potential difference is only a measure of the change in temperature between the thermocouple and the potentiometer

2.2.3.2 Pressure measurement and data recording

The pressure transducer used gives a linear output voltage with pressure and this data was also recorded via a fluke digital potentiometer linked to a pc. The voltage data was then converted to a pressure reading using a linear equation calibrated against the additional analogue pressure gauge. The manual gas control system enabled the monitoring of the gas pressure throughout an experiment, although with little ability to control conditions.

For the experiments the pressure in the system was set at the desired level and then the system was sealed off and the pressure change monitored throughout the reaction. A pressure relief valve was used to limit any significant over pressure generated by the heating of the system.

The most challenging aspect was finding a suitable reactor muffle that would be able to hold a pressure of hydrogen. Most systems used for the measurement of hydrogen reactions use stainless steel as the construction material due to the ease of fabrication and resistance to chemical or thermal treatments. For the

microwave system the material chosen for the pressure muffle must additionally be microwave transparent. Several options were initially investigated including polymers such as PTFE, PEEK, polypropylene and polyethylene, and ceramics such as soda glass, fused alumina and silica. The polymer materials have been used for low temperature/ low pressure commercial systems and had sufficient transparency to the microwave field, but would not be suitable due to the possibility of localised heating in the sample causing softening of the materials. For the ceramic materials alumina is very difficult to fabricate and soda glass was found to be unsuitable due to the high dielectric loss factor at increased temperature. Therefore silica glass was selected as the best option for the gas system. The design of a system that could hold pressure was also difficult due to the challenge of connecting the metal pipe work to the silica muffle. Glass-to-metal sealing is a difficult task and for this work a pre joined Jennings $\frac{3}{4}$ " vacuum tube was used which was braised into a bespoke stainless steel fitting which could be mounted through the side wall of the microwave (Figure 2.5). Integrating a glass-metal seal into pressure system was made easier by limiting the hydrogen pressure to 0.5 bar above atmospheric pressure which was 50% of the design pressure of the seal.



Figure 2.5: Silica sample tube positioned in the multimode domestic microwave cavity

Throughout the research and development of the microwave systems for this project, leak prevention and detection principles have been rigorously observed in line with the risk assessments required for all work. These precautions included the elimination of microwave leakage points by ensuring all metallic joints are used, and that any holes were positioned with choke devices to prevent field leakage. Additionally prior to each use the system is leak checked using hand held detection equipment and a zero tolerance limit is set prior to use.

To ensure that there was no microwave leakage from the cavity the diameter of the hole in the cavity is kept as small as possible but is dictated by the restraints of sample size and experimental apparatus to be used within the cavity. The external diameter of the hole is 40mm which is the same in both the internal cavity and the external cover with a gap between the cover and the internal cavity of 18mm.

The sleeve (figure 2.6) is a hollow tube that passes both through the internal cavity and the exterior cover allowing the apparatus to be held in place and reducing the number of joints required. The aluminium construction reduced any heating effect of the material inside the cavity due to the high conductivity of the material. Additionally the length of the sleeve (greater than 1.5 wavelengths) and the small diameter (less than $\frac{1}{2}$ wavelength) prevented any propagation of the microwave field out of the cavity acting as a choke[117].

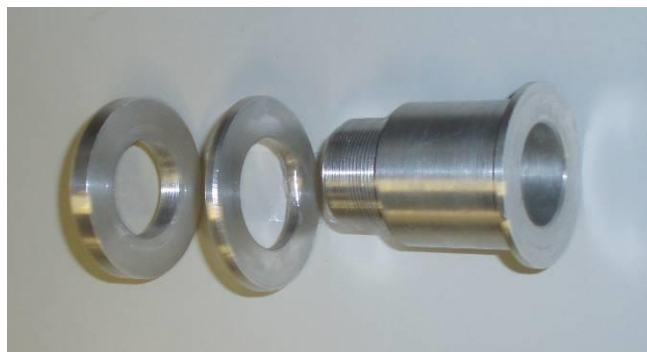


Figure 2.6: Choke sleeve assembly, showing the retaining nut spaces and sleeve

This sleeve is held in place by a threaded flange on the internal side and an aluminium nut which compressed a spacer between the two metal sheets approximately 18mm in thickness, to prevent the cavity and external wall from being deformed (Figure 2.7). The external joint connecting to the experimental apparatus is a compression fitting between two flat surfaces limiting the gap through which any microwave radiation can pass.

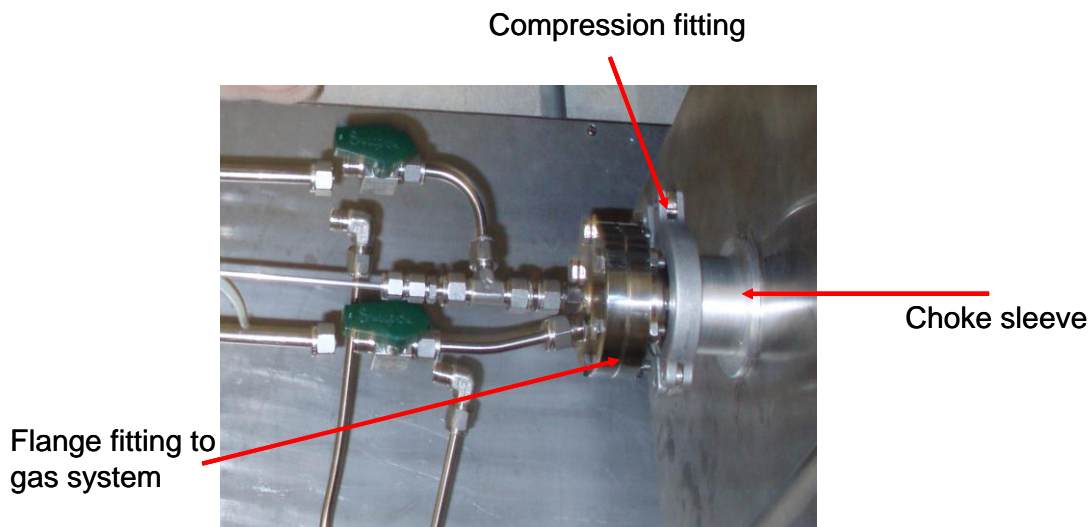


Figure 2.7: Gas fittings and holder in position through the cavity wall of the microwave.

2.3 Development of the Mixed Gas Control System

In order to control pressure during isobaric or variable temperature experiments it was essential to develop a system capable of controlling the pressure to an accuracy of just a few mbar, to allow accurate determination of the rate of reaction.

On the Hidden gravimetric analysis systems developed externally, there are two systems that can be used to accurately control the pressure; the first uses a series of valves controlled by stepper motors and the second uses a mass flow controller system. It was decided that the use of mass flow controllers would provide a more stable and easier to set up system due to the constant feedback that could be used to control the system.

Figure 2.8 shows a schematic of the system developed for the control of the gas pressure within the system the reactor at the University of Birmingham.

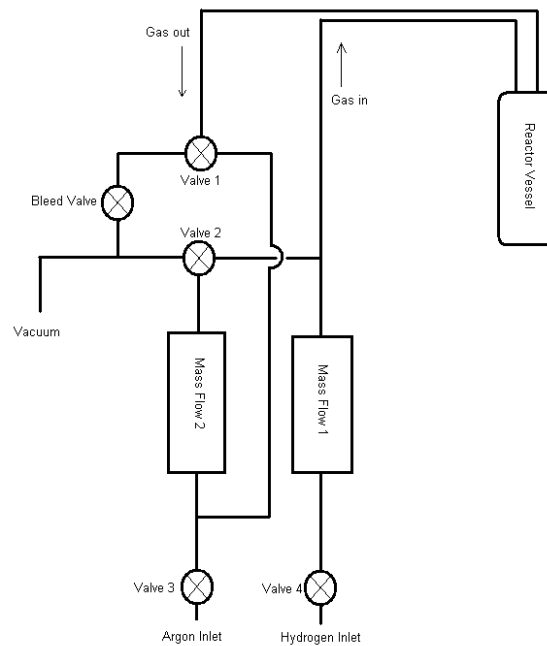


Figure 2.8: Schematic diagram of the gas control system

The system developed uses two Brooks Smart flow 5850S mass flow controllers with an orifice size of 0.004" giving full scale control between 0 and 600ml/min, with a stated error of $\pm 0.25\%$ of flow + 0.5 ml/min[121].

Figure 2.9 shows an image of the operational control unit fixed onto a base plate to allow easy repositioning with various reactors.

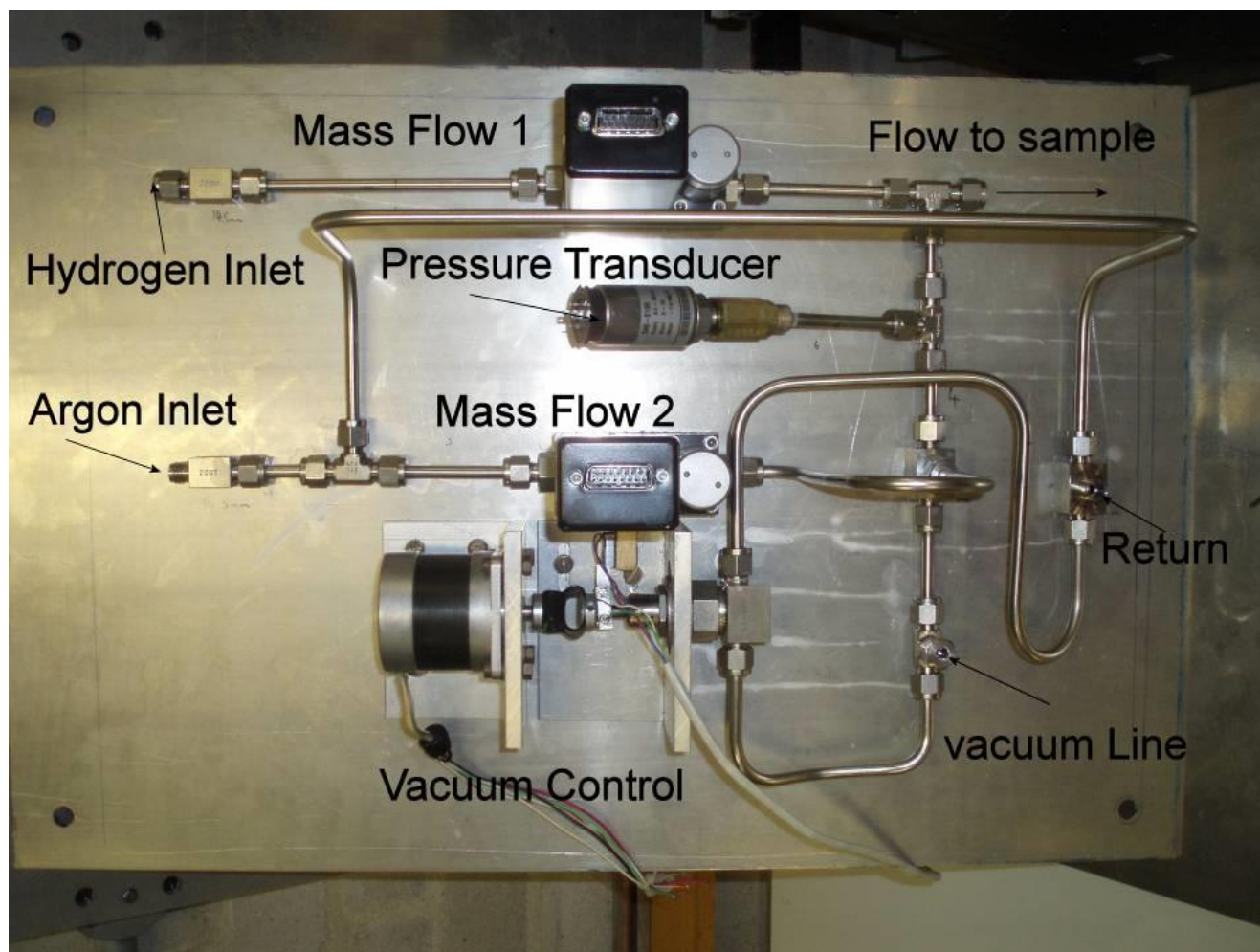


Figure 2.9: Image of the gas control system in position

The valves shown in the diagram allowed each mass flow controller to be isolated to assist leak checking but also allow the system to operate in two modes. The schematic diagram in figure 2.10 shows the basic operating principle of the system where gas flow is measured and controlled on the inlet to the reactor vessel (Mass Flow 1), and measured and controlled on the exit through Mass flow 2 this process was called differential gas sorption.

Differential Gas Sorption

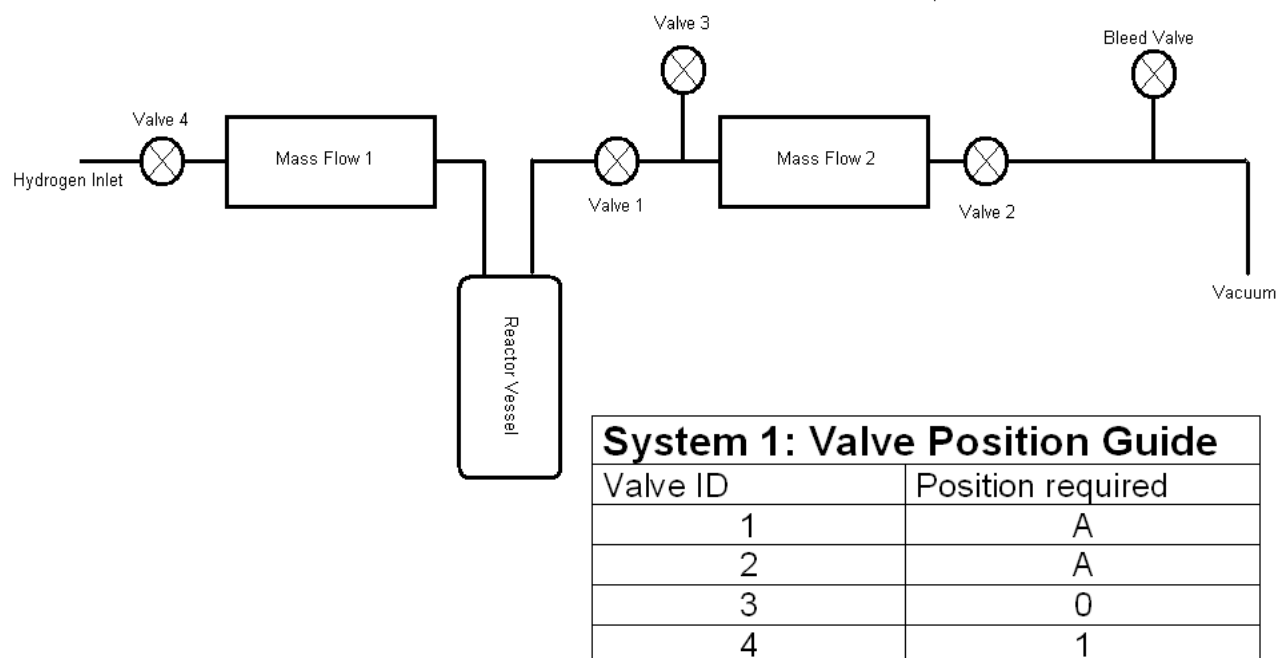


Figure 2.10: Mode 1 operation with mass flow controllers in series

The second mode (Figure 2.11), mixed gas control, used the two mass flow controllers in parallel controlling two gas streams to allow the control of mixed atmospheres, with the pressure control operated by a stepper motor controlled bleed valve. The mixed gas system can produce controlled atmospheres with a mix of two gas stream in flexible ratios and can also constantly vary the gas ratio in the system. This dual system approach was necessitated by the high capital cost of the mass flow controllers and the need to make the system as flexible as possible.

Mixed gas/partial pressures

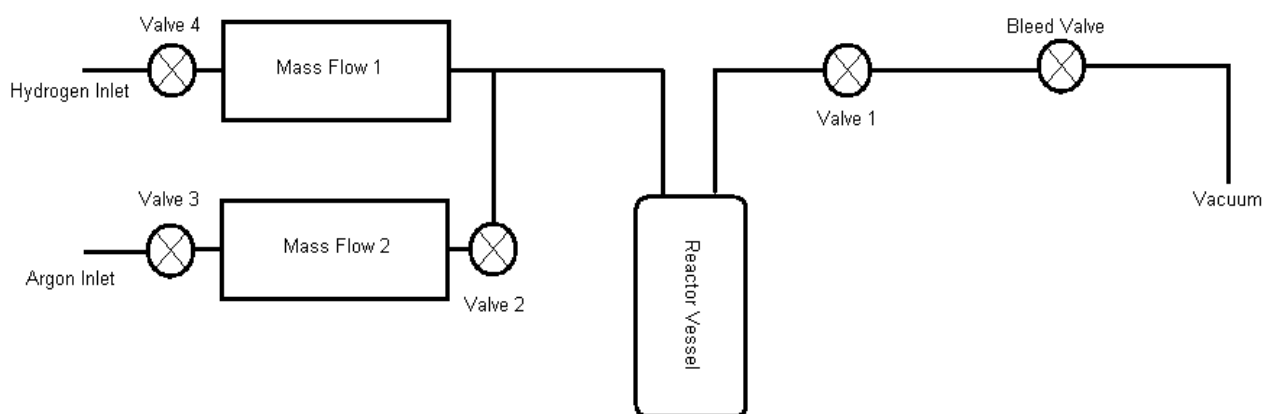


Figure 2.11: Mode 2 operation of the system with mass flow controllers used in parallel to provide mixed atmospheres

Control of the mass flow controllers was undertaken using a RS485 control circuit which allows multi drop communication links and control over several digital devices. This circuit was linked through a RS 232-485 converter to give a suitable interface for a PC with the addition of a 24V DC supply to drive the actuators and sensors in the mass flow controllers. The circuit diagram is shown in Figure 2.12 with the final installed control unit shown in figure 2.13.

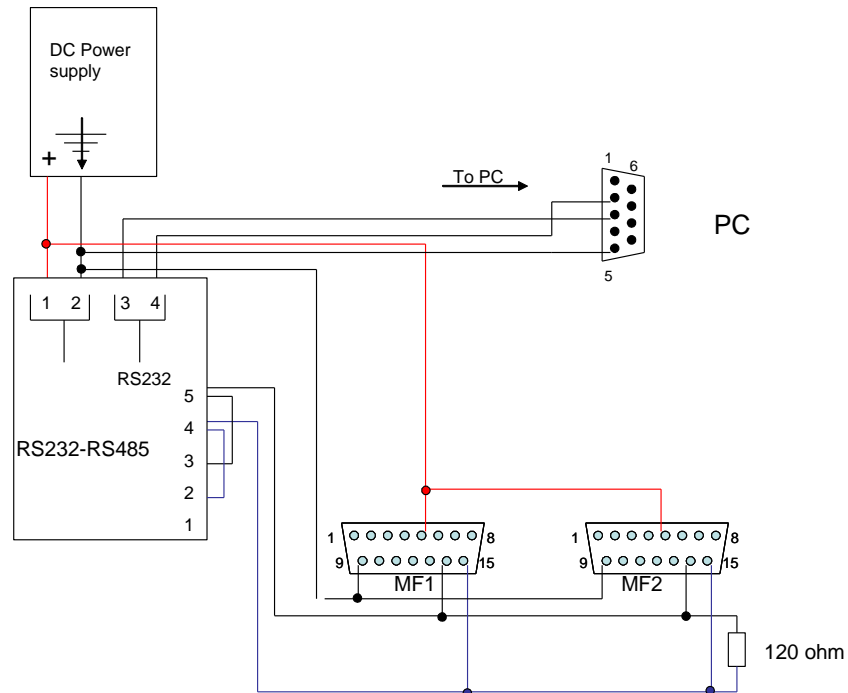


Figure 2.12: Wiring diagram for the mass flow control system using an RS 485 control system

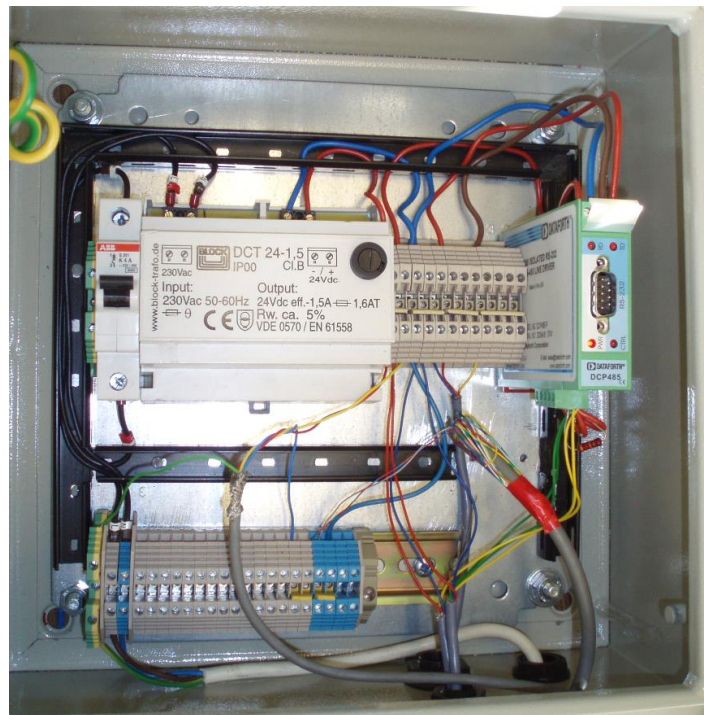


Figure 2.13: Rack mounted control and power supply unit for the mass flow control system

The control system integrated the Brooks Smart Flow control software, provided with the units, into a Microsoft Visual Basic program that gave a user friendly interface for setting pressure levels and ramp rates and recording data. Figure 2.14 shows a screen grab of the software developed specifically for this project and including several key functions:

- Pressure control
- Program setting of up to 6 pressure steps
- Temperature recording and offsetting
- Data file storage
- Direct control of the mass flow controllers

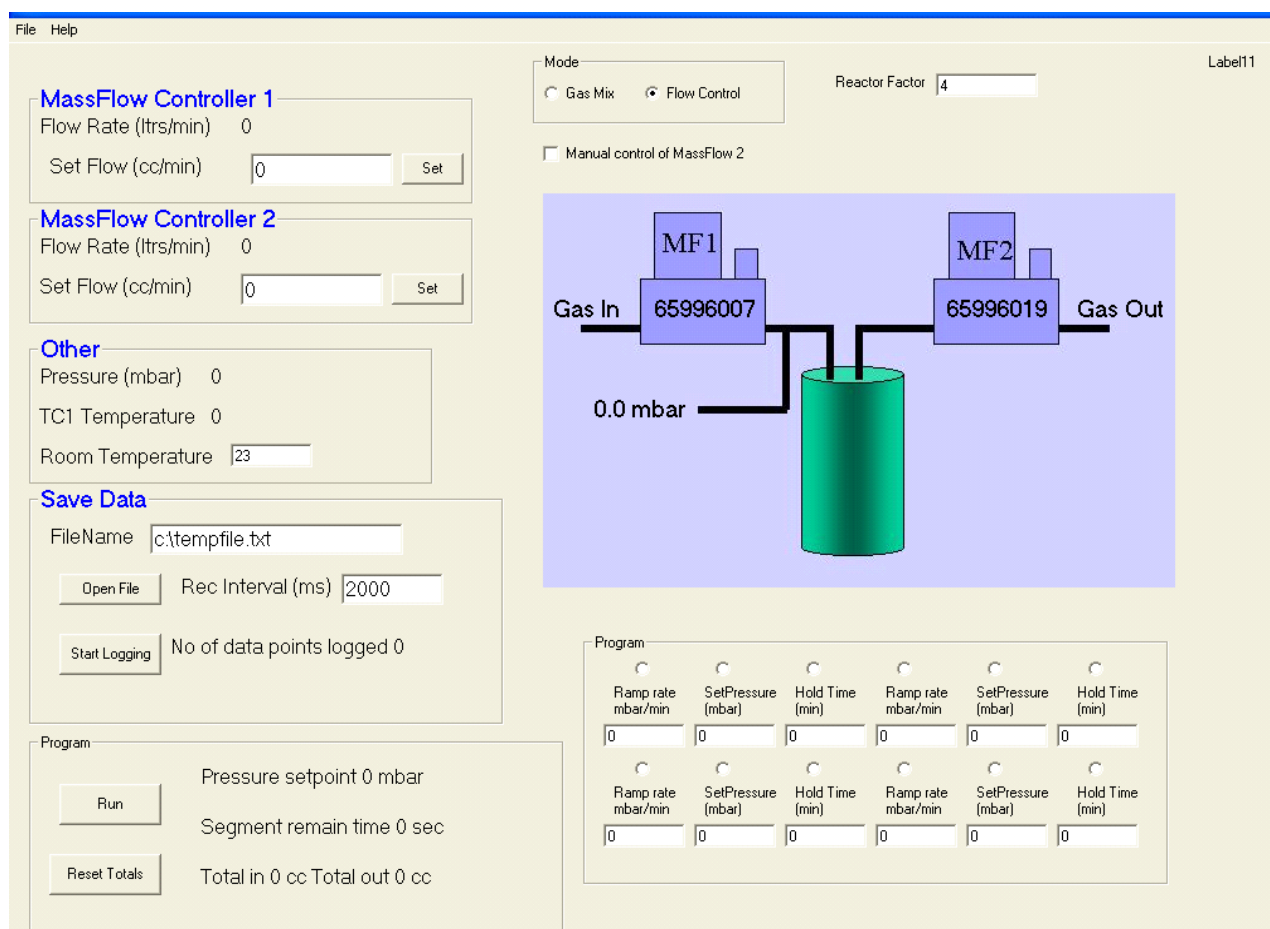


Figure 2.14: The control interface for the MGCS built in Microsoft visual basic

The pressure control function used a fuzzy logic approach to control the pressure to a set point. This involved subtracting the measured pressure reading from the set point value; if this value was negative the pressure in the reactor was too high and the exit mass flow controller would open and vice versa for lower pressure. The degree to which the valve opens is controlled by multiplying the difference between the set point and the measured value by a factor which is tuned to the size of the gas system, in the software this is termed the “reactor factor”.

If the measured pressure is 50 mbar below the set point and the reactor factor is set to 5, the inlet mass flow controller would allow a flow of 250ml/min. By adjusting the size of the multiplying factor it is possible to reduce the risk of overshooting the pressure set point but still maintaining the ability to follow ramp rates accurately.

The system was set to assess the pressure and react at a rate of 10 adjustments per second (10Hz). In practice the accuracy of the system was limited by the pressure transducer which had a wide scale range of 0-15 bar, but had a maximum error of around 2 mbar at 10 bar[122].

This error caused fluctuations in the measured pressure which triggered the mass flow controller to open and close giving some noise to the gas flow data when the pressure was static.

The limitation in the performance of the system was operating at substantially below atmospheric pressure. The mass flow controllers worked optimally when the pressure difference across the device was greater than 1 bar. With the system under partial vacuum the pressure differential between the vacuum line and the system dropped, causing the maximum achievable flow through the device to drop in an asymptotic manner. The lowest controllable pressure achieved in the system was around 100mbar. To completely evacuate the system it was necessary to open a separate vacuum line bypassing the mass flow controller.

There was a range of possible materials that were initially considered to be of interest including magnesium and several complex hydride materials. The desorption temperature of all these materials lies below 800°C, so this was set as our target temperature for continuous operation. The high pressures required for recombination of many of the complex hydrides was considered outside the scope of this project so magnesium was taken as a good basis, the conditions required for cycling the material under hydrogen being 200°C – 400°C and up to 10 bar hydrogen pressure.

The challenges in the development were to find a method of controlling the temperature experienced by the sample temperature measurement that would give a reliable value whilst not being affected by the applied field.

2.3.1 Variable power microwave with temperature control and MGCS

Due to the low dielectric loss of the magnesium it proved difficult to control the temperature effectively using the microwave alone. This led to the adaption of a second Panasonic NNT573C combination microwave, which had additional 200W convection heating function. The adaptation involved the replacing the internal thermal control system with an external system to control the heating elements. By changing the control system it was possible to keep the heating elements at 100% and increase the maximum operating temperature from 220°C to 330°C. This also required additional insulation around the cavity to maintain the temperature by reducing thermal losses. The system was effective in increasing the temperature but due to high temperature in the microwave power supply and insufficient cooling the electronics failed after 4 trials.

Additionally as figure 2.15 illustrates the control of the system was insufficient to allow accurate measurement of the reaction kinetics under microwave fields.



Figure 2.15: Microwave system with gas control board at the University of Birmingham, with vacuum system control and logging computer and the adapted multimode microwave system.

The temperature from the experiment shown increased in a controlled manner up to 220°C; however, once the electromagnetic field started to couple in to the sample the temperature increased rapidly with 250W of microwave power concentrated in a 2g sample. Without a method to significantly reduce the microwave power or control the energy input into the sample it was not possible to effectively assess the effect of microwave fields on the material.

The development of a pressure control philosophy had been successful with the unit based on a domestic microwave, however, the control of temperature was very difficult achieve. It had been hoped that by reducing the power of the microwave we would be able to moderate the heating and obtain stable temperatures, however, the changes in the temperature around key points were far too fast to allow manual control. Figure 2.16 illustrates this effect as the sample is pre-heated to 220°C using the incorporated heating elements before the microwave is started. This causes a linear heating rate up to 250°C, when a thermal runaway occurs and increases the sample temperature to 780°C in

around 3 seconds. This effect is common in uncontrolled microwave systems and is one of the key reasons C-Tech have concentrated on using a radiant controlled heating system with a relatively small proportion of microwave energy.

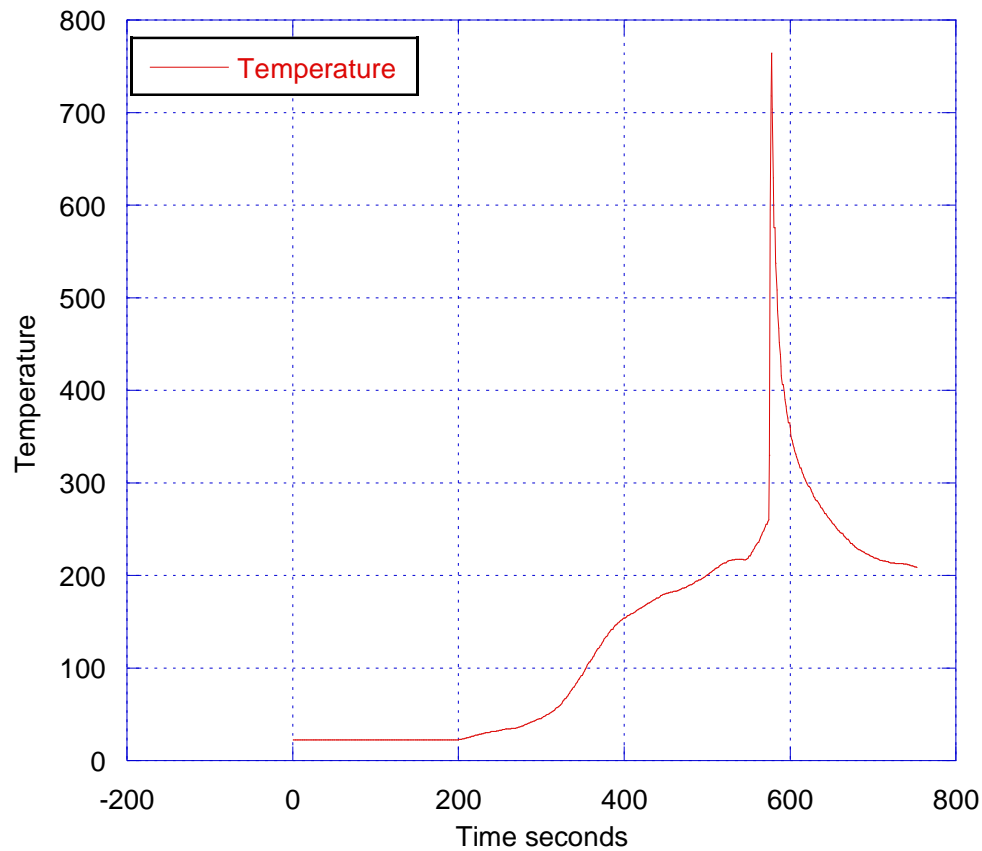


Figure 2.16: Sample temperature increase during heating and microwave irradiation at low power, showing the uncontrolled heating of a magnesium hydride.

2.3.2 C-tech rig development with high pressure gas control system

The next stage of the technical development required the additional control and accuracy of the hybrid research furnace developed at C-Tech Innovation. This system used a 1.2 kW 2.45 GHz microwave power supply unit, manufactured by Sairem, fitted to a specifically designed furnace capable of accurate control up to 1600°C.

The advantage of the Sairem system as a research unit is that the power is variable and stable from 0-100% output. This enables a wide range of processing

conditions from very low field strengths up to full power. The internal view of the system in figure 2.17b shows the silica muffle and internal structure of the furnace including the MoSi₂ heating elements and the thermocouples. Figure 2.17a shows the sample transfer glove box situated below the furnace to allow inert sample handling.

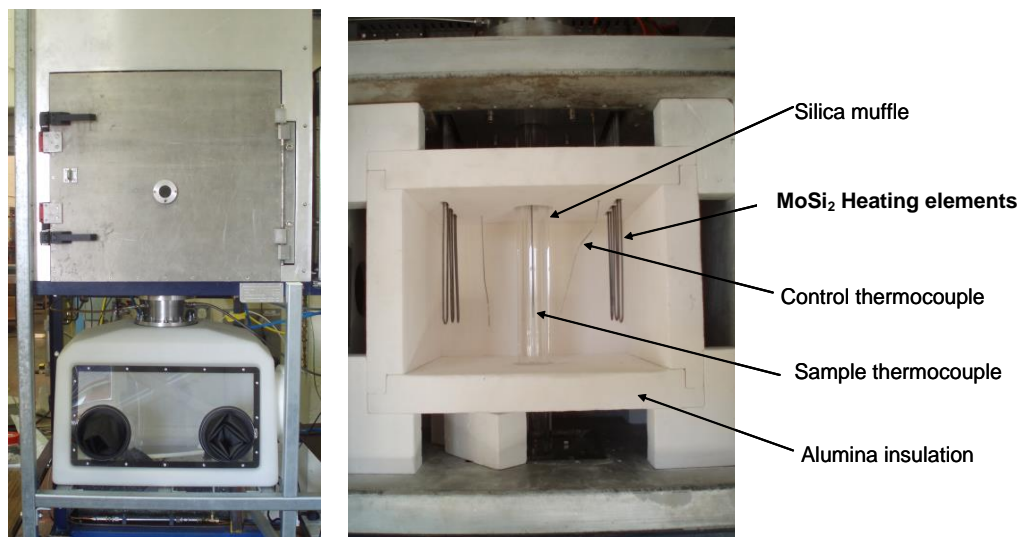


Figure 2.17a) External view of the hybrid furnace at C-Tech Innovation showing the glove box, 2.17b) internal view of the system showing the insulation silica muffle heating elements and control thermocouples

The control system uses Eurotherm 900 series dual loop temperature control that allows both the radiant and microwave elements to be controlled independently, which can be used to limit thermal runaway by automatically reducing the microwave input if the temperature rises rapidly.

During most of the experiments in this project the manual control of the microwaves was used to increase the reproducibility of the reaction conditions.

In addition to the microwave system there was additional 27 MHz radio frequency (RF) unit fitted to the system which allowed up to 5kW of RF power to be passed into the cavity, with the much lower frequency giving far higher electric field strength than the microwave unit. This system is run independently from the other thermal controls and requires an additional tuning circuit to match the capacitance of the sample placed in the furnace.

The radiant elements used in the system are Super Kantal MoSi_2 , which are stable up to 1800°C and provide a stable thermal power input of up to 1800W . The insulation used in the system is critical as any dielectric losses in the insulation will directly affect the distribution of the microwave or RF fields. Therefore Rath 100% alumina insulation material was chosen due to its extremely low dielectric loss up to 1200°C .

The processing of the alumina insulation can also dramatically affect the losses in the system for example small traces of metals in the tap water used to produce the material can increase the dielectric loss significantly and variations in the material have been responsible for significant errors in previous work.

There was an existing gas system fitted to the hybrid furnace consisting of an open muffle that had been used for atmospheric pressure under inert atmospheres. The previous work in the field has concentrated on sintering materials in air or under flowing inert gases and these systems were almost exclusively operating in the temperature regime between 800°C and 1600°C [101,102,115].

To allow the higher pressure required for the cycling of magnesium hydride a system was designed with a cylindrical muffle running vertically through the centre of the microwave cavity. This design allowed a system with no glass to metal seals as these were replaced by O-ring seals at the ends of the muffle which with water cooling allowed the maximum operating temperature to be 800°C . The O-ring seals also allowed the thermal expansion of the glass tube during heating without placing any strain on the joints. Figure 2.17 shows a schematic diagram of the muffle running through the furnace with the aluminium housings at each end containing the gas connections.

In order to accommodate the maximum design pressure of 20 bar the furnace system had to be reinforced using a steel frame which supported the aluminium end caps as calculation of the force exerted could deform the furnace structure by more than 10mm .

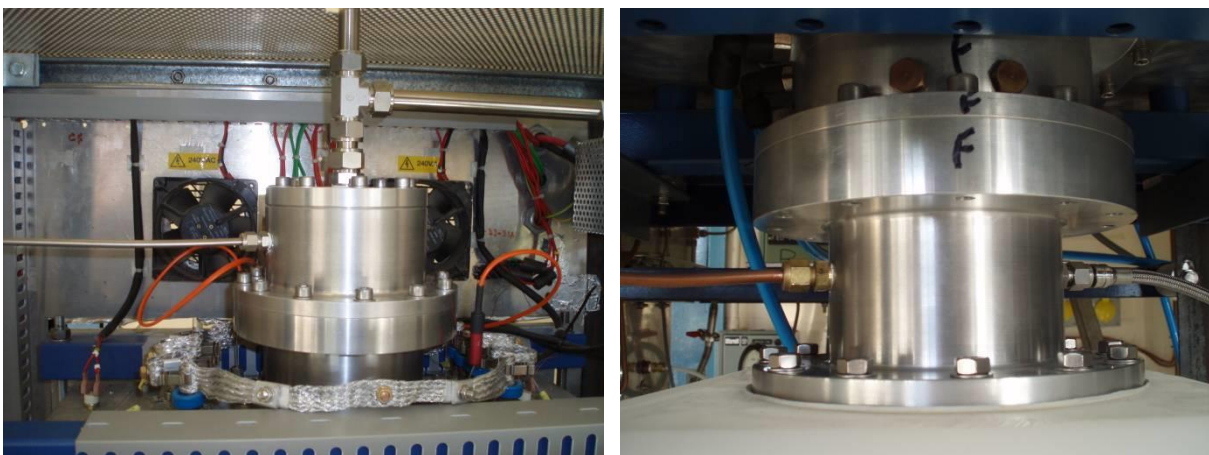


Figure 2.18 a) Top housing for the silica muffle incorporating pressure relief, gas exit, and water cooling channels to aid sealing. b) bottom muffle housing incorporating gas inlet, exhaust, and glove box coupling.

The addition of a glove box below the furnace allowed sample transfer from the sealed containers into the sample holder under inert conditions. Prior to use the glove box was purged with argon for 1 hour to reduce the oxygen content to below 10 ppm as measured by oxygen sensors.

Initially it was expected that the error on the mass flow controllers would be too high to give accurate measurements of the reaction of the materials and would only be suitable for maintaining a set pressure. Therefore initial designs for the systems to measure the uptake of hydrogen in hydrogen storage materials included adaptations to allow the use of a gravimetric balance. This would involve the replacement of the top end cap with a fitting connecting it to a high pressure Sartorius type balance head. However, the repeatability of the data showed that the measured error in the system was much lower than expected. The significant errors from the calculation of buoyancy effects and convection currents in gravimetric systems are difficult to accurately calculate without significant calibration and system development to produce a highly accurate capable of measuring mass changes in the order of 10^{-6} grams. Systems such as the Hidden's Intelligent Gravimetric Analyser equipment, used at the University of Birmingham, have been developed over many years but due to the cost and

uncertainty of the performance with microwave fields travelling into the sensitive electronic measurement systems gravimetric systems were discounted.

The key system design parameters:

- Gas system, muffle pressure rating designed to operate at up to 8 bar with a safety test pressure of 20bar
- Sealing the silica tube into the system required allowance of thermal expansion of 4 mm along the length and seal hydrogen up to 20bar from vacuum
- Water cooling for all seals to allow continuous operation above the design temperature for the elastomer seals
- Incorporation of a glove box and loading method to allow inert sample transfer from transport containers to the measurement equipment

2.3.3 The development of fibre optic temperature control system

It was understood from early in the project that the measurement of temperature would be an important consideration. This importance was both from a process control standpoint and also to ensure that the data generated was real and not a function of poor measurement.

The temperature measurement in dielectric fields is known to be challenging topic due to the interaction of many measuring systems with the electric and magnetic fields that can lead to anomalous results. There had previously been significant effort by the staff at C-Tech Innovation to develop shielding filtering methods that allowed accurate measurements using thermocouples, but the risk of localised heating of the tip or interference with the mV signal generated was still a possibility.

To find a suitable alternative system several options were considered including pyrometers and fibre optic systems.

Pyrometers are dependent on the emissivity of the object which is related to the surface condition of the sample. The emissivity was found to change, often drastically, with surface roughness, bulk and surface composition, and even the

temperature itself. At 300°C the low emissivity of the surface can give errors due to other emissive objects in the cavity.

Two fibre optic technologies were investigated for the application. The first was a Luxtron system based on luminance and the second was an OpSens system based on band gap changes in a semiconductor. The system is based on the interference patterns in a GaAs crystal bonded to the end of the fibre optic probe. The GaAs changes its band gap with temperature and this can be used as an accurate measure of the temperature at the point of contact. Figure 2.19 shows a schematic of the sensor tip of the white light interferometer of the type used.

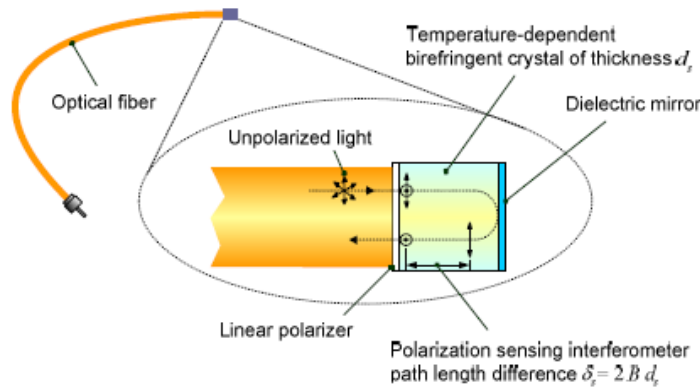


Figure 2.19: Schematic representation of an OpSens white light interferometer fibre optic tip [145]

Due to the performance of an existing 250°C OpSens system a development program was initiated with the company to develop specific sensors that would be suitable for operation at 300-350°C.

This was significantly beyond the material limits of the polymer protective coatings and adhesives used to assemble the fibres. A materials selection program lasted several months to identify and test suitable materials that could operate for long periods at high temperature in a hydrogen atmosphere. This process delivered a range of materials that were suitable for the temperatures but the hydrogen atmosphere caused continued difficulties.

Figure 2.20 shows one of the development probes before and after treatment at 350°C under a hydrogen atmosphere. The hydrogen caused significant discoloration of the adhesives and the coatings on the fibre shortening the life to a few hours from 200 hours operation under inert atmospheres. Following this it was decided to use the fibre optic inside a thin walled 3mm silica tube with a sealed end. This silica tube prevented the hydrogen from discolouring and damaging the fibre but allowed relatively quick response to the temperature.



Figure 2.20: OpSens fibre optic probe before and after 2 hours at 350°C under 7 bar hydrogen atmosphere

To control the system the 0-10V output from the signal conditioner was used in place of a thermocouple input to control the furnace temperature on the Eurotherm system.

2.3.4 RF variations collar/ sample holder changes power input tuning

One of the avenues explored in the project was the development of an applicator suitable for allowing an RF field to be used in addition to the microwave and radiant heating elements. There was prior development of systems at C-Tech Innovation using a systems that incorporated both microwave and RF systems with some success and results that exceeded the performance of either technology used in isolation. The design of the cavity and the sample position made the design of the applicator difficult. Unlike microwave fields which can be launched into a cavity via a waveguide, an RF system applies a field between a high voltage electrode and an earth plane usually in the form of a capacitor. In

the usual circumstance the dielectric material to be heated is placed between the two electrodes and is then subject to the high frequency field.

In the equipment developed at C-Tech the sample was located at the centre of the cavity to maximise the consistency of the microwave field which made it difficult to engineer a solution that could adequately apply the RF without significantly affecting the microwave field. The solution developed used a separate floating electrode which uses the capacitive interaction between the high voltage electrode to couple the field to a position closer to the sample.

Unfortunately the first iteration of the system caused too much interaction with the microwave field, shielding the material. The structure was then altered to reduce the effect on the microwave field, however, in order for this structure to have an influence on the sample the field strength would have to be increased significantly. The increased field strength initiated a plasma in the base of the cavity and silica muffle which caused a significant amount of damage to the sample holder. Following this it was decided to concentrate on the microwave only operation mode for these samples.

2.3.5 The measurement of dielectric properties of magnesium and magnesium hydride

The measurement of low loss material is a difficult objective. There are several possible methods for determining the dielectric properties which are based on either transmission or the use of a resonant cavity. Resonant cavity methods such as Tm010 cavities are used for the measurement at single frequencies and ideal for solid materials with a low dielectric loss.

As the material is a powder it was decided to use a transmission type system where the material is compressed into a holder and then a flat faced concentric probe is placed on the surface. Using an S parameter test kit with a network analyser it is then possible to measure the response of the material to an applied field. The network analyser is capable of operating over a frequency range from 1MHz to 3GHz, however, the combination of probe and calibration standards

used in this work limited the accuracy of the measurement to a range of 500MHz either side of the 2.45GHz target frequency.

In order to accurately measure the materials in a more indicative environment the equipment was set up in a glove box flushed with an inert argon atmosphere. This measurement involved passing and reconnecting the 50 ohm calibrated cable and sensor through the side of the glove box before recalibrating the system under the inert atmosphere and conducting the measurement.

After conduction the room temperature measurements options were explored for high temperature measurement techniques that would allow the dielectric properties of the materials to be measured at the operating temperatures. There are not many options for this measurement and very few standards are available for the calibration of equipment. It was therefore decided to set up a basic system using a ceramic sample holder positioned on a hot plate in an inert atmosphere. The methodology was however unsuccessful as the temperature increase in the probe changed the calibration and probe response significantly. Following this further investigation led to work on a Tm₀₁₀ resonant cavity method for dielectric measurements at high temperature and in various atmospheres, however, this was not completed during the project.

3. Results of the reaction kinetics of metal hydrides under microwave fields

3.1 Material Characterisation of Magnesium Hydride

The novel processing of materials in this project was the key area of innovation and development, however, to understand the results in this work it is essential to understand the properties of material prior to any treatment. The analysis of starting materials in terms of structure, composition and sorption properties both in terms of kinetic and thermodynamic properties was an important step.

The material preparation for the work was all undertaken at the University of Birmingham where the analysis equipment allowed standardisation of samples prior to transport to C-Tech Innovation where the equipment was built, commissioned and used.

All of the magnesium samples were prepared from MgH_2 supplied by Goldschmidt. The material was milled under an argon atmosphere in a Restch planetary mill with a 10:1 ball to powder ratio using stainless steel balls and a stainless milling pot.

The same sample preparation was used for all samples with milling for 5 hours at 160 rpm in 15 minute segments with a 15 minute cool down period between run periods to allow heat to dissipate and prevent unwanted thermal processes. This reduced the effect of frictional heating in the materials in an attempt to reduce desorption and maintain the milled structure. The milling methodology was one developed in a previous European project at the university and found to deliver the most reproducible results for magnesium hydride preparation in terms of crystallite size and structure.

If additions of catalyst materials were required then at the end of 4½ hours of milling time the additions would be added for the last half hour. This time was

chosen to allow sufficient mixing to give even material properties and reduce variation in the milled structures formed that could be developed with the addition of a material that may alloy with the magnesium in longer times. Each sample preparation process produced 20 g of MgH_2 materials which was stored under argon atmosphere in the University of Birmingham Glove box prior to use.

The 5 hour milling process for the magnesium hydride aimed to reduce the crystallite size and generate fresh, clean surfaces that will give improved kinetics in the temperature range to be investigated. After milling, scanning electron microscopy was undertaken to examine the changes in morphology. Figure 3.1 shows the change from the rounded as received particles into 100-150 μm range with smooth surfaces; as expected, milling for five hours under argon has dramatically reduced the particle size although the agglomeration of multiple particles gives the impression of a large variation of particulate sizes.

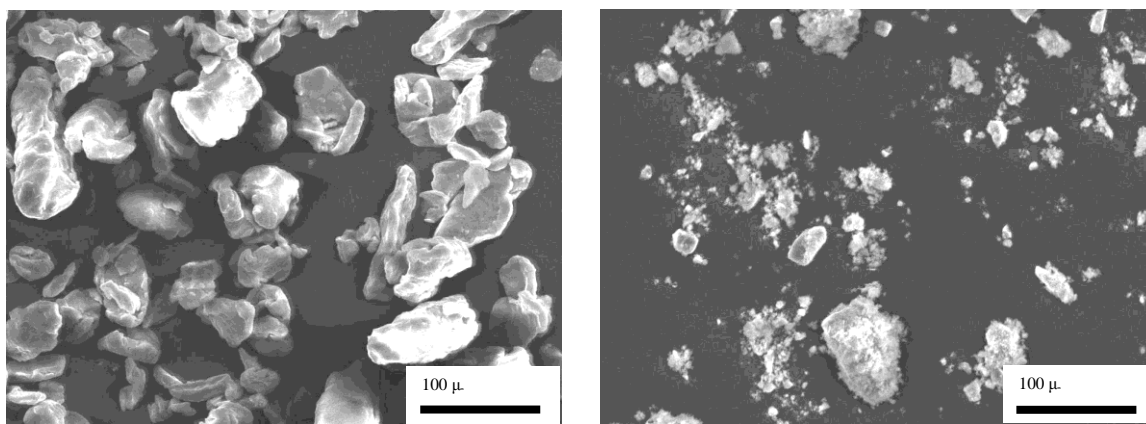


Figure 3.1: SEM micrograph of the as received Goldschmidt magnesium hydride and the material after 5 hour of ball milling, showing the reduction in the particle size and the increased surface roughness of the particles.

Further analysis of the distribution of particle size was obtained from laser particle size analysis. This method suspends the particles in cyclohexane, and uses ultrasonic agitation to reduce the agglomeration of the hydride particles. The distribution of particle sizes shows the peak of the distribution at 9 μm and a standard deviation of 6.1 μm . However this is only a measure of the particle size and gives no real indication of the crystallite size of the material, which can be

obtained through the analysis of the peak broadening of XRD using the Sherrer equation.

Powder X-ray diffraction patterns for the MgH_2 samples were collected using a Bruker D8 diffractometer with $\text{Cu K}\alpha$ X-ray source operating at 40 kV and 40 mA. Diffraction patterns were collected over the range of 20° to 80° , with a step size of 0.02° and a time of 1 second per step. Data was analysed using Bruker's Eva software. MgH_2 samples were prepared for XRD by mounting samples into a Perspex sample holder in an Ar glove box, and an amorphous tape was applied to seal the samples from the atmosphere during the analysis.

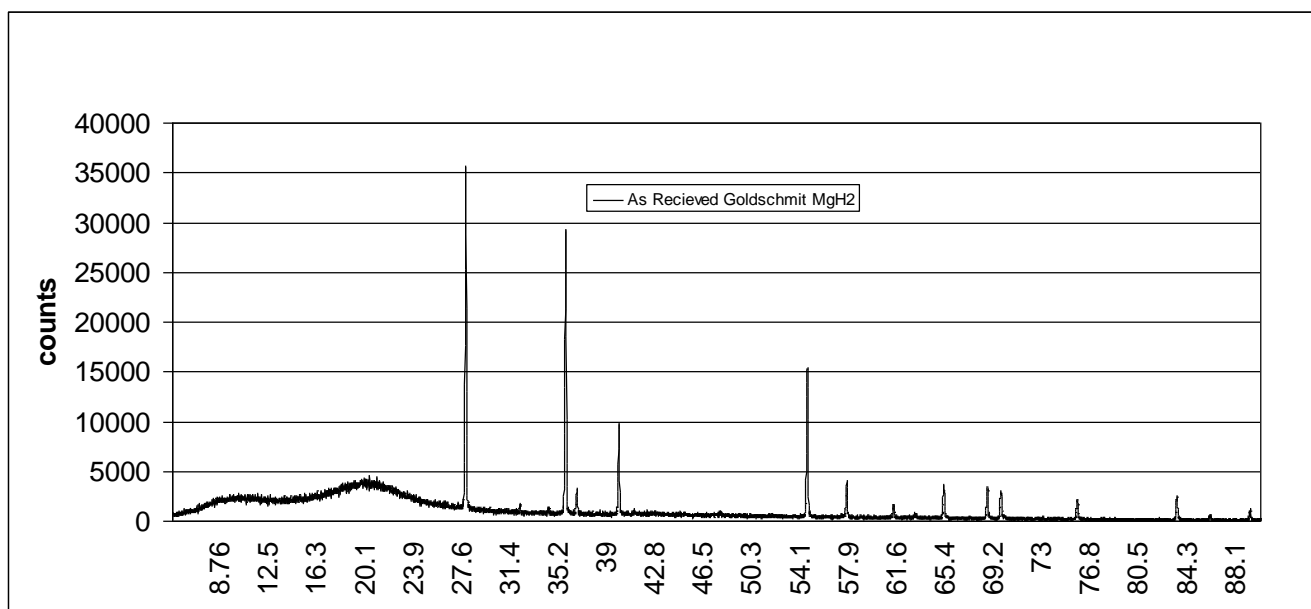


Figure 3.2: X-ray powder diffraction pattern for Goldschmidt magnesium hydride as received.

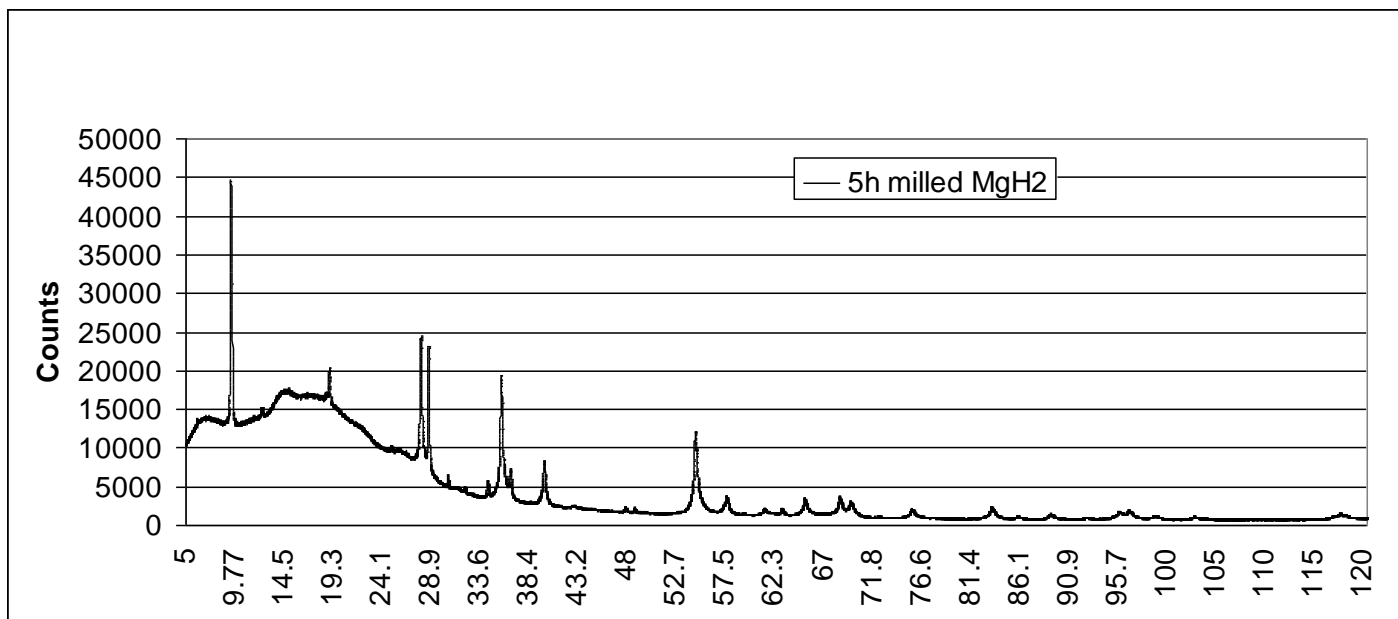


Figure 3.3: X-ray powder diffraction pattern for Goldschmidt magnesium hydride after 5 hours milling

Average crystallite sizes and internal strain measurements were calculated from the collected diffraction patterns using the Williamson-Hall method, which accounts for the line broadening in a diffraction pattern caused by small crystallite size and the presence of internal strain.

In a crystalline sample, X-ray diffraction results from constructive and destructive interference caused by scattering of X-rays from atoms in a regular array, with diffraction lines appearing at angles that satisfy Bragg's law.

When crystallites are small enough that they do not contain enough atomic planes within them to fully cancel out scattering at angles close to a given Bragg angle, line broadening occurs.

The Scherrer formula relates the line broadening (b) to the size of the crystallites (t), where b is the total line broadening (full width half maximum, FWHM) with the instrument line broadening β subtracted.

Usually line broadening β_T is assumed to be due to finite grain size, and is described by the Sherrer equation:

Equation 24

$$\beta_{\tau} = \frac{\lambda}{\tau \cos \theta}$$

Where λ is the x-ray wavelength, θ is the Bragg angle, and τ is the mean effective particle size.

Based on this the Sherrer equation the calculated crystal sizes are given in table below. The error in the measurements is calculated as standard deviation in the measured broadening with the addition of the measurement error based on a standard Al_2O_3 calibration standard.

As the materials is mechanically processed there is also a possible component of the line broadening which can be attributed to the dislocations within the crystal structure. This is called strain induced broadening which will induce a change in the peak broadening linked to the diffraction angle. If crystal size is the only reason for broadening then the value of $\beta_{\tau} \cos \theta$ will be independent of the diffraction angle. The presence of strain-induced broadening β_{ε} which is given by the Wilson formula:

Equation 25

$$\beta_{\varepsilon} = 4\varepsilon \tan \theta$$

Here, ε is the dimensionless value for ‘microstrain’ which is assumed to be proportional to the square root of the density of dislocations. Assuming that the contributions to peak broadening are equal, then Williamson-Hall[123] showed that total the reflection broadening β_{hkl} can be expressed as:

Equation 26

$$\begin{aligned}\beta_{hkl} &= \beta_{\tau} + \beta_{\varepsilon} = \frac{\lambda}{\tau \cos \theta} + 4\varepsilon \tan \theta \\ \therefore \beta \cos \theta &= \frac{\lambda}{\tau} + 4\varepsilon \sin \theta\end{aligned}$$

Now plotting $\beta\cos\theta$ against $4\sin\theta$ should produce a linear regression line, where the gradient is the micro strain and the intercept is $\frac{\lambda}{\tau}$. This allows the micro strain and average crystal size to be determined independently from the data.

Figure 3.4 below shows a plot of $\beta\cos\theta$ against $4\sin\theta$ and as can be seen the variation with respect to Bragg angle is minimal, with the gradient of all conditions is ± 0.0002 , determining that the peak broadening is predominantly the result of the crystal size effects.

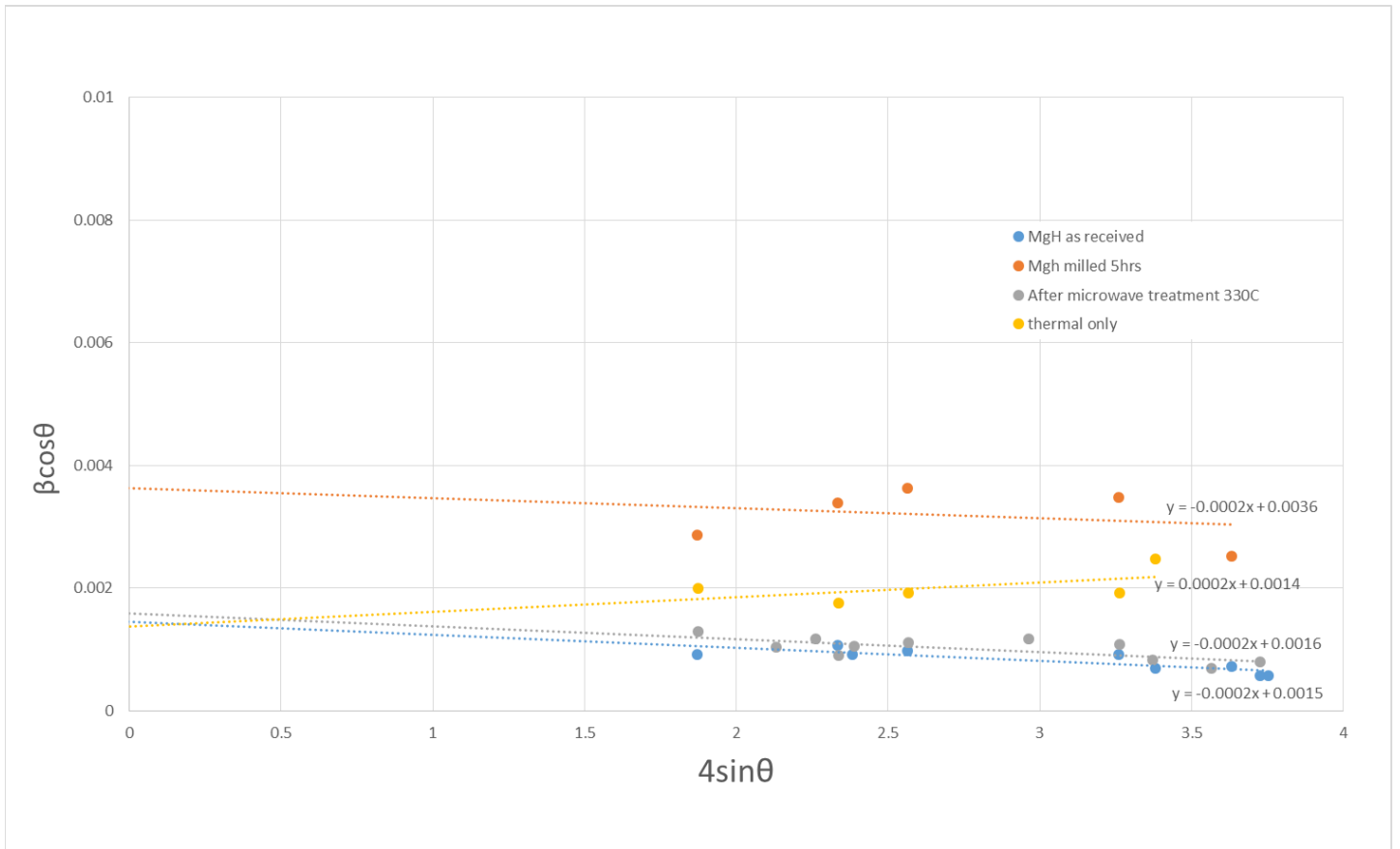


Figure 3.4: showing the flat gradient of the Williamson-Hall plot which indicates the relatively insignificant contribution of microstrain to the line broadening.

The analysis of XRD patterns gives the crystallite size for the as received magnesium hydride of $1.2 \mu\text{m}$ which is reduced after 5 hours of milling to a value

of 350 nm. Table 3.1 shows the full width half maximum values for the milled and as received material along with the individual and mean grain sizes.

Table 3.1: Calculated grain size from XRD patterns using the Sherrer equation and full width half maximum values for as received and ball milled material and error calculated as standard error + variation

| Peak Angle | As received FWHM | As received grain size Å | 5 hour milled FWHM | 5 hour milled grain size Å |
|------------------|------------------|--------------------------|----------------------|----------------------------|
| 27.88 | 0.094 | 1137 | 0.2 | 439.4 |
| 35.69 | 0.107 | 1098 | 0.251 | 348.6 |
| 39.85 | 0.106 | 1278 | 0.282 | 311.4 |
| 54.57 | 0.122 | 1154 | 0.353 | 260.2 |
| 65.25 | 0.131 | 955.48 | 0.356 | 273.1 |
| Mean grain size | As received | 1153.7 Å | 5 hours milling time | 315.2 Å |
| Calculated error | | 134.23 Å | | 64.73 Å |

The desorption properties of the material are improved considerably with the milling process, as shown in figure 3.5. For the as received material the onset of desorption occurs at above 380°C, nearly 100°C higher than the milled material. This could be due to oxidation of the surface affecting the desorption and recombination reaction, as once the reaction has initiated for the as received material the rate of desorption is high.

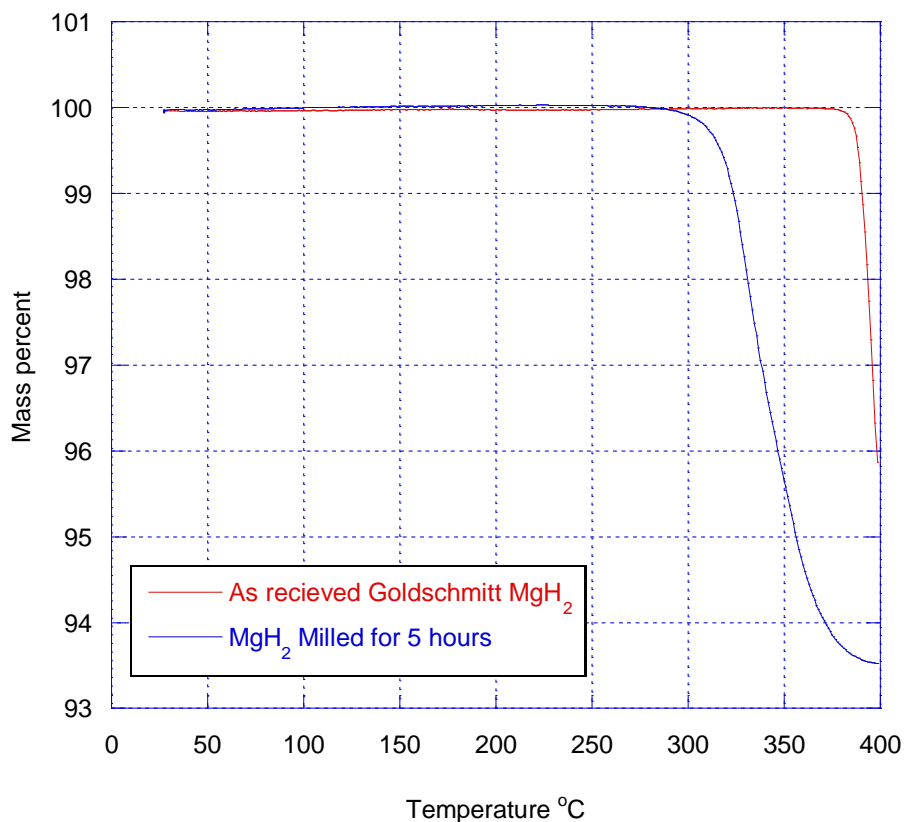


Figure 3.5: TGA trace of desorption behaviour of as received and ball milled magnesium hydride. Heated at 2°C/min to 400°C under flowing argon atmosphere

The repeatability of the production of samples was a key aspect and TGA analysis was used in order to ensure consistency. Samples were taken from each batch of milled powder and the repeatability both of the production process materials handling and experimental technique are evident in figure 3.6. The 3 batches shown have an onset of desorption within 5°C and the total mass loss repeatable to 0.3% of sample mass.

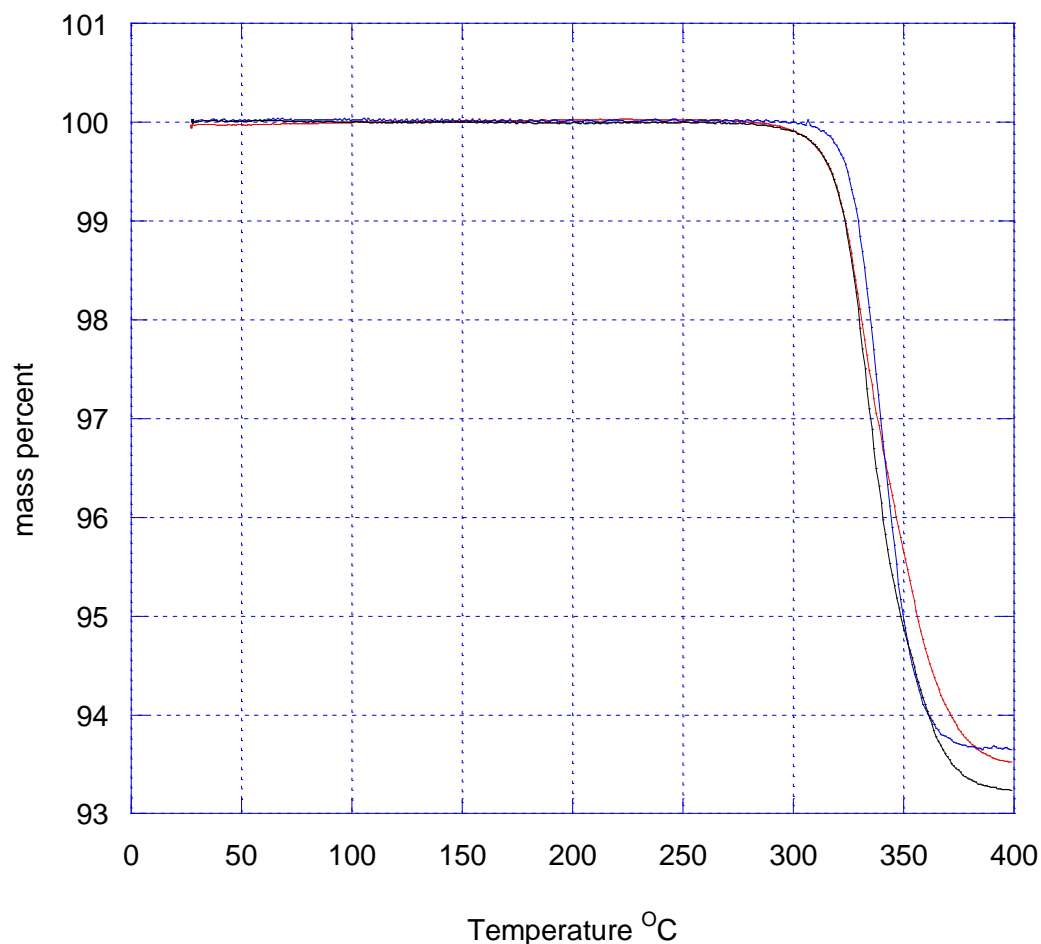


Figure 3.6: TGA traces showing the consistency of ball milled magnesium hydride produced over a period of two years.

The thermodynamics of the system were also checked using Sieverts type apparatus to ensure that the material followed the expected pressure composition isotherms. Figure 3.7 shows the experimental results obtained from HTP measurements plotted against the published work from the Hydropark database. The data from the published work is plotted over a much greater pressure and temperature range, but the values agree well with the experimental data, giving an enthalpy of formation of 76.2kJ/mol, slightly higher than the published value of 74.5 kJ/mol. This could be due to small impurities in the material or discrepancies in the sample temperature measurement.

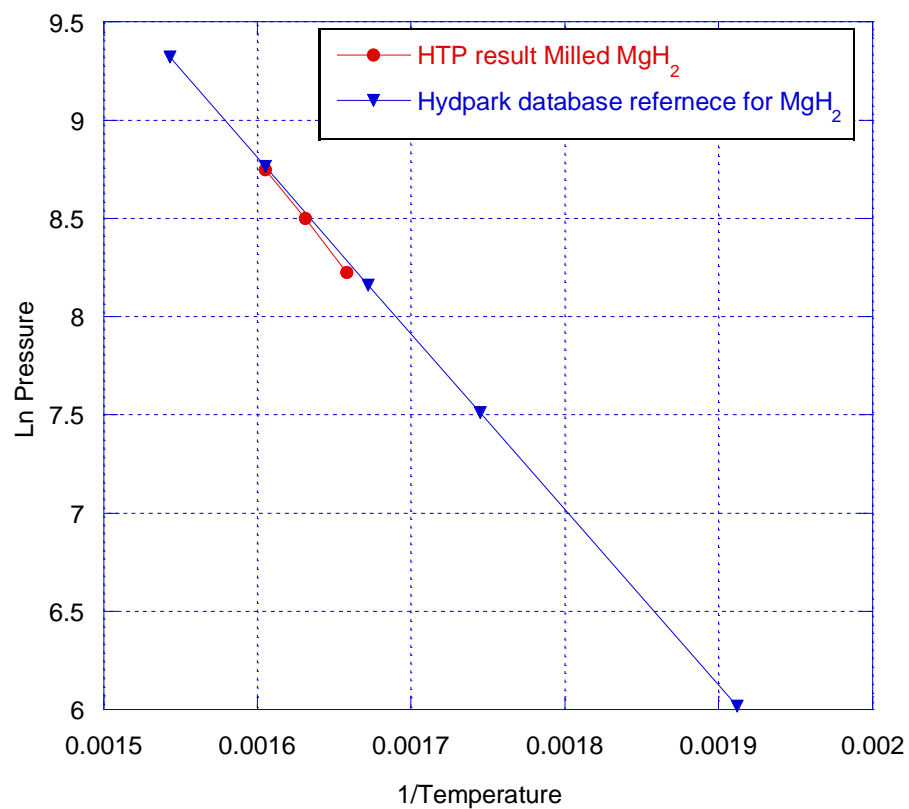


Figure 3.7: Van't hoff plot of log of the plateau pressure plotted against the reciprocal of temperature (K), with data from the Hydпарк database plotted for reference.

3.2 Calibration and development of the flowing gas measurement system

The development of a measurement system capable of operating with the required accuracy and that was compatible with the microwave field has been described previously. In order to validate the system, samples measured in the University of Birmingham's dedicated hydrogen materials characterisation labs were re measured on the C-Tech Innovation microwave system.

The validation involved cycling the materials under hydrogen atmospheres and assessing the measured volume of gas desorped and absorbed as a measure of the mass change, the rate of desorption / absorption to ensure the kinetics were similar and the temperature stability of the far larger volume furnace and muffle assembly.

- 4g samples pre weighed and loaded under argon atmosphere
- System is purged and pressurised to 7 bar to prevent desorption during the heating process.
- Sample heated using radiant control of the furnace with no microwave field applied, this enabled controlled and accurate heating at specified ramp rates to ensure stability of the materials in the furnace system.

Isothermal Desorption Experiments

- 7000 mbar starting pressure
- Microwave field applied (if required)
- Reduce pressure to 500 mbar
- Maintain the pressure by controlling the outlet MFC to vacuum

Isothermal Absorption Experiments

- 500mbar starting pressure
- Microwave field applied (if required)
- Increase pressure to 7000 mbar
- Maintain the pressure by controlling the MFC as gas is absorbed

A question that needed to be resolved was the effect of the cumulative error in the measurement of materials. As the mass flow controllers used for the measurements had both a fixed error and a flow related element a concern was that over a full cycle there could be significant measurement error in the volume of gas passed through the units, with a fixed error of 0.1 ml/min plus 0.25% of flow set point.

To test this, a series of experiments running the units at a fixed pressure and fixed input flow rate were carried out. This was followed by repeated cycling from 500 mbar – 7000 mbar at rate from 50 ml/min to a maximum of 600 ml/min. The error calculated from the accuracy figures was far in excess of the measured variation in the values with the average variation less than 0.1 ml/min for the fixed flow experiments and below 10 ml in total volume for all of the ramp trials.

3.2 The development of the measurement system

The first task was to validate the system for the measurement of hydrogen absorption and desorption from the magnesium. Initial problems with the system included variations in the kinetic properties between cycles. This reduced the desorption rate dramatically over a number of cycles.

The cause of the changes was speculated to occur from leaks in the system allowing the ingress of small amounts of oxygen or surface contamination of the samples with materials in the system. In order to resolve these problems the system was stripped and systematically cleaned, degreased and rebuilt with the

addition of zeolite and activated carbon filters on both the gas inlets and the vacuum lines to remove any moisture in the gas lines.

Following the work to demonstrate the practicality of the system, a series of samples of samples were tested to assess the reproducibility of results both due to the system and between samples. Figure 3.6 shows the 1st desorption of 3 samples from the same batch of material recorded over a 2 week period. This clearly shows the storage and transportation methods used were acceptable and the variation between the measured values was small. Given the error in the measurement values for a given ramp, the 15cm³ variation in the volume of desorbed gas over 5000 seconds indicated that the materials and measurement techniques are able to produce valid data for the further experiments.

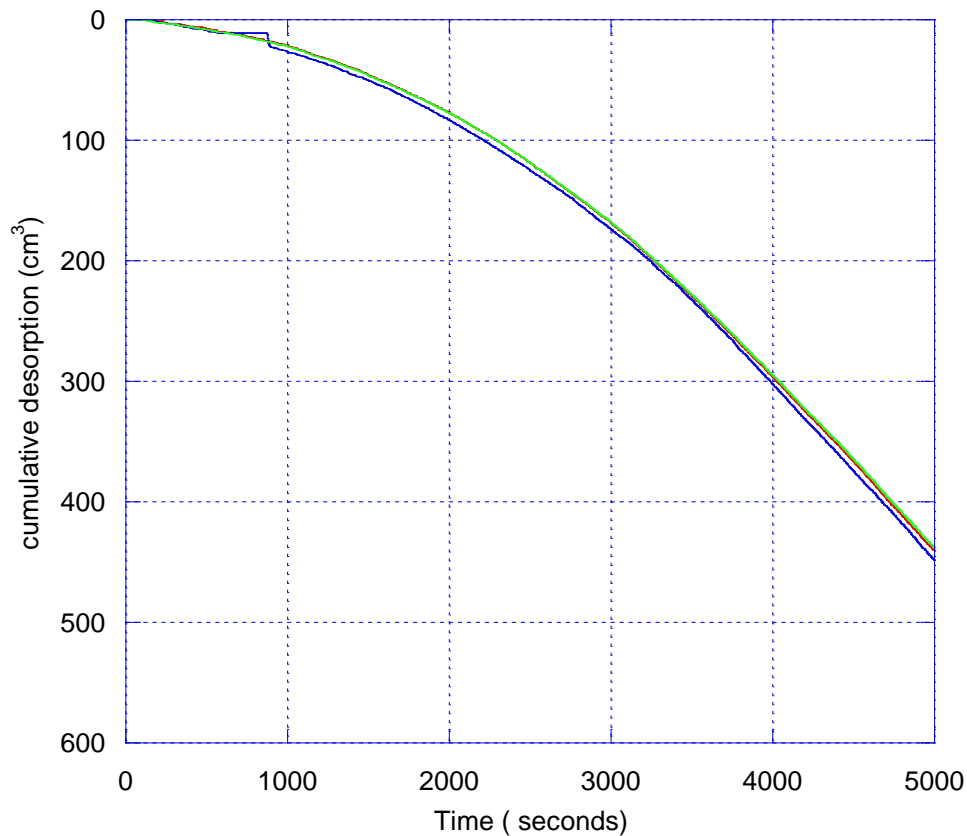


Figure 3.6: Cumulative desorption from the 1st desorption cycle of 3 separate magnesium hydride samples at 330°C. (Samples taken from a single batch and measured over a 2 week period)

3.3 The measured dielectric properties of magnesium and magnesium hydride

In addition to the chemical and structural properties of the materials used in the project the dielectric properties could also have an impact on the performance of the materials under a microwave field.

A network analyser and concentric probe were used to measure the S parameters of the materials which can be converted to a measure of the real and imaginary parts of the dielectric constant. Figure 3.7 shows the measured value for the dielectric loss factor (imaginary) of the milled materials in both the metal and hydride form. These values were measured at room temperature and across a frequency band from 1×10^8 to 2.55×10^9 ; the data was collected either side of this band but due to the applicator there is significant uncertainty in this data.

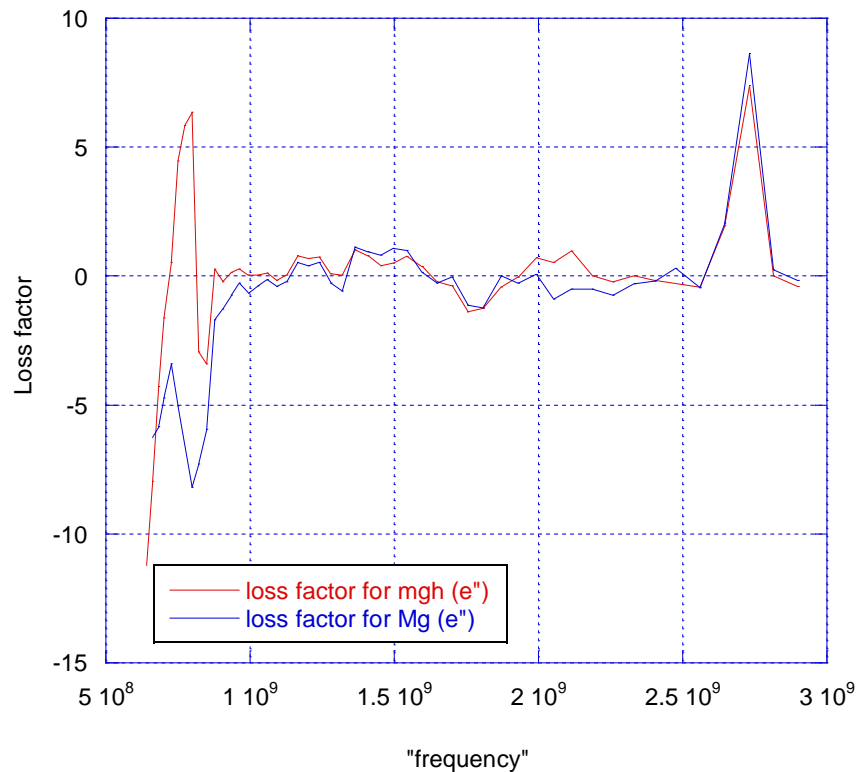


Figure 3.7: Figure showing frequency dependence of dielectric loss factor of Mg and MgH₂ measured under Argon using a concentric surface probe applicator at 298K.

The conclusion is that there is very little dielectric loss from the materials either in the metallic or hydride state, in the powdered form at 2.45 GHz. Unfortunately this data only gives an indication of the value expected at 300-350°C as the probe systems were unsuitable for temperature measurements at above 50°C.

In order to get a rough understanding of the energy absorption of the materials due to the dielectric field a series of experiments were conducted to analyse the heating rate of the materials from a starting temperature of 330°C (Figure 3.8). The experiment was conducted by holding the sample in steady state at 330°C for a period of time to allow stability. The radiant power was then manually fixed to a specific output current and the microwave field applied. The temperature of the sample was measured and the time taken to increase by 10°C to 340°C recorded. The errors in this method are numerous and only give indicative measure of the relative dielectric losses of the material in the two states, for example the microwave field is assumed to be consistent, which is probably not valid on a small scale as the effect of changes in the microwave field due to the presence of the hydrogen in the microwave cavity are not taken into account.

The energy lost through the conduction and convection to the gas is relatively small due to the low thermal gradient between the surfaces of the particles and the surrounding gas evidenced by the linear increase in temperature. If the thermal loss to the surrounding gas was significant it would be expected that the increase in sample temperature for the hydride phase, with 7 bar of hydrogen surrounding the sample, would slow as the ΔT between the sample and the gas increased during the heating.

This effect is not observed but could provide a further error into the measurement. The results show that the effective energy absorption for the metallic magnesium was around 4 times higher than the hydride phase allowing for the variations in specific heat capacity.

The energy transferred was

- 0.01 W/g absorption for Hydride

- 0.04 W/g absorption for Magnesium

An interesting and possibly significant side note is that with the microwave forward power set to 300 W the 4 g sample in the metallic phase was still absorbing less than 0.2 W. This shows the inherent inefficiency of a large multi-mode cavity being used to treat a very small sample. If scaled up with an optimised applicator, this would equate to around 1 kW supply being able to treat 25 kg of material with the same conditions providing a relatively effective treatment for a large volume of material.

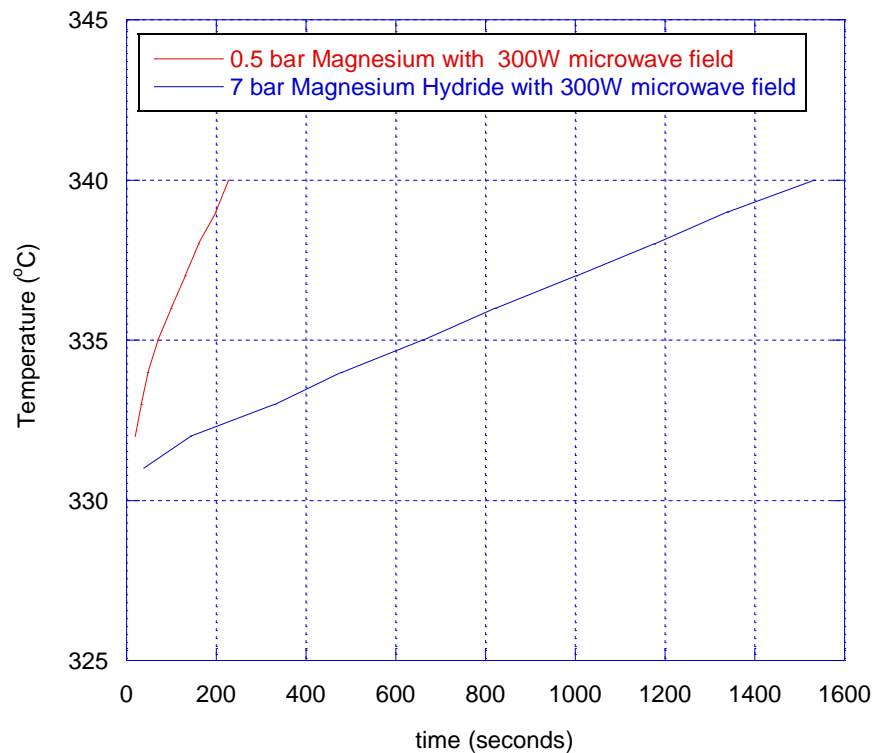


Figure 3.8: Sample temperature change under microwave heating at a field strength of 300W

3.4 The desorption of hydrogen under microwave fields

3.4.1 The effect 300W microwave field on the desorption of H from MgH₂

Figure 3.9 shows the effect of the microwave field on the desorption behaviour of the magnesium hydride at 310°C with a pressure of hydrogen at 500mbar. It is clear from the work that there is a significant increase in the desorption rate when compared to a non-microwave assisted standard thermal decomposition. The data shown is for the 1st 2nd and 3rd desorption cycles of a batch of material with the microwave field being applied throughout the 1st and 3rd cycles. The faster 1st cycle could be attributed to the effect of milling and very clean surfaces on the material but the increase between the 2nd and 3rd runs show a clear effect of the microwave field.

There are some key features of the desorption curves which are affected by the microwave field. The initial decomposition rate is broadly similar in all 3 samples but after approximately 5% of the desorption the microwave field begins to accelerate the desorption and this rate increase continues reaching a maximum value at around 55-60% of the desorption total without any heating observed. This initial slow period could be associated with the formation of Mg islands on the surface from which desorption is easier.

This is in contrast to the standard curve which shows a much more gradual increase in rate and follows a standard kinetic function. The total volumes of gas desorbed in both microwave assisted experiments were very similar and show that although the kinetics are affected by the initial conditions the reactions volumes and total time for the reaction are repeatable.

The other interesting point about the effect of the microwave field is the increased rate is prolonged further through the desorption reaction with a pronounced finish to the curve and shorter tail.

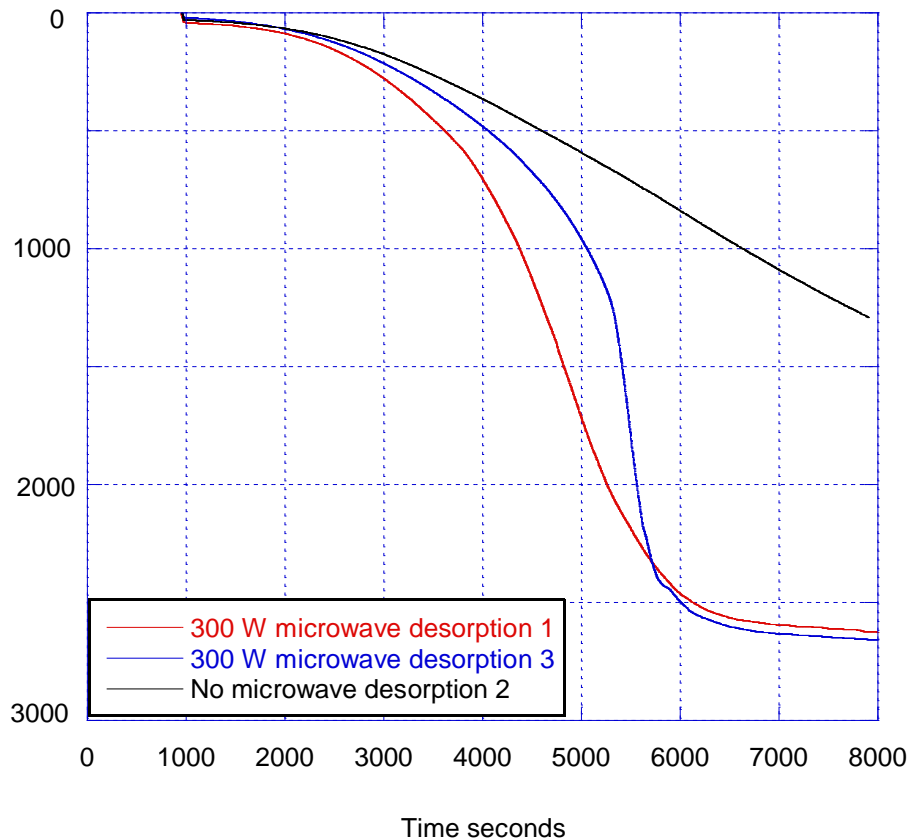


Figure 3.9: 3 consecutive cycles showing the cumulative desorption traces of magnesium exposed to a microwave field of 300W, no microwave and then 300W microwave. (Temperature 330°C pressure of hydrogen 500mbar.)

When the rates of the desorption are compared during the time taken as can be seen in Figure 3.10 there are 3 clear parts of the curve that differ significantly from the non microwave assisted result, before 3800 seconds there is a linear increase in the rate of desorption after the inflection point the rate of desorption increases to a peak in the rate at around 4800 seconds. The peak desorption rate is at around 1.2ml/S which is a significant increase on the maximum desorption rate of the non microwave assisted cycle. The peak in the desorption rate is followed by exponential decay in the rate as the decomposition completes and the MgH_2 phase becomes exhausted.

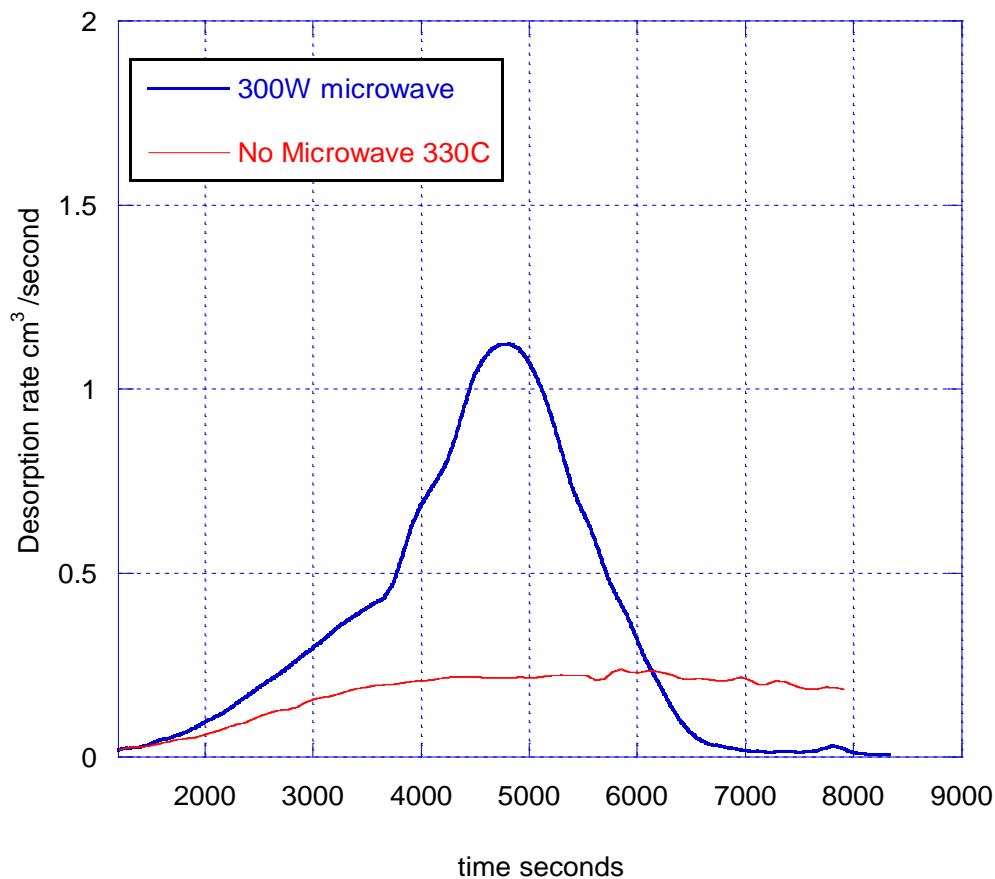


Figure 3.10: Plot of desorption rate measured in cm³/second for 2 cycles at 330 °C with a pressure of 500mbar. This shows a 400% increase in the peak rate of desorption with 300W microwave field present.

The increase in the maximum rate of desorption is around 400% which could be explained by several reasons. The most obvious of these would be an increase in temperature of the sample caused by excess heating from the microwave field. Figure 3.11 shows the temperature profile during the desorption of the MgH₂ at 330°C with a 300W microwave field. The temperature of the material stays constant within 2 degrees of the set point. As with all of the experiments the temperature of the cavity is controlled to ensure the sample temperature remains controlled. As such the changes in the material's dielectric properties affect the absorption of energy from the microwave field, which reduces the radiant heating required in order to maintain the sample temperature.

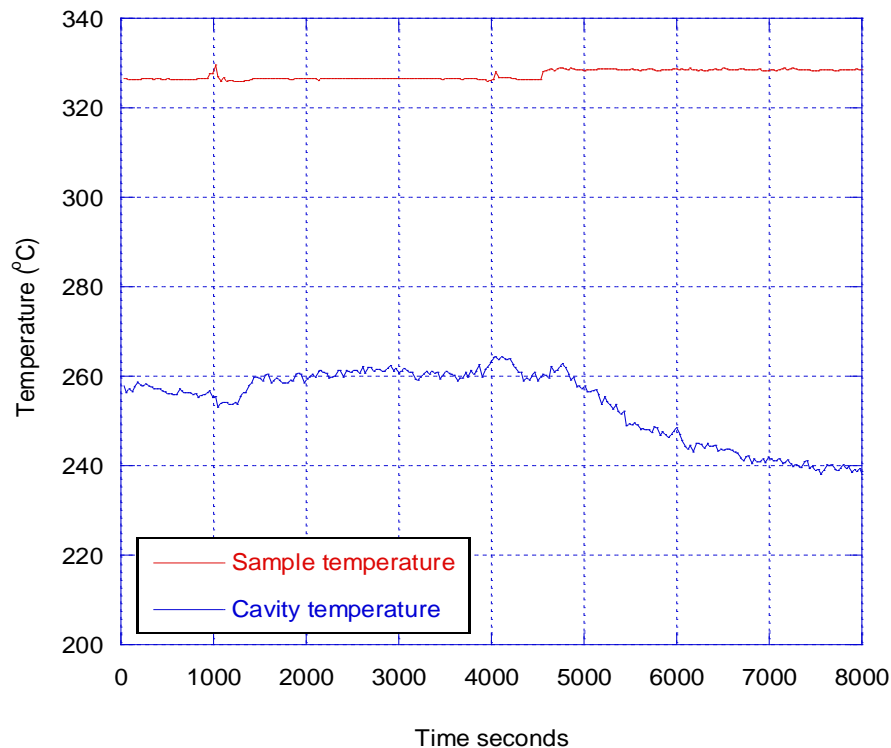


Figure 3.11: Plot of measured sample temperature and cavity temperature during the desorption at 330°C

It should also be noted that the temperature of the cavity was significantly lower than the temperature inside the glass muffle running through the centre of the furnace.

This was consistent across all of the experiments in this work whether the microwave field was applied or not. The reason for this was not immediately clear as the thermocouples used were calibrated against each other regularly and found to be accurate within 1.5°C, however the most likely explanation is the absorption of the long wavelength infra-red heating from the radiant elements heating the muffle while the external environment is constantly evacuated to reduce the risk of hydrogen atmospheres building up.

A further investigation was undertaken with the microwave power cycled on and off for 600 second intervals during the desorption process and the total volume of gas desorbed during each of these periods totalled. This data is shown as a bar chart in figure 3.12. As can be seen the volume of gas desorbed in each of the

periods where the microwave field was applied was significantly higher than the other times, with the greatest changes occurring during the second half of the desorption.

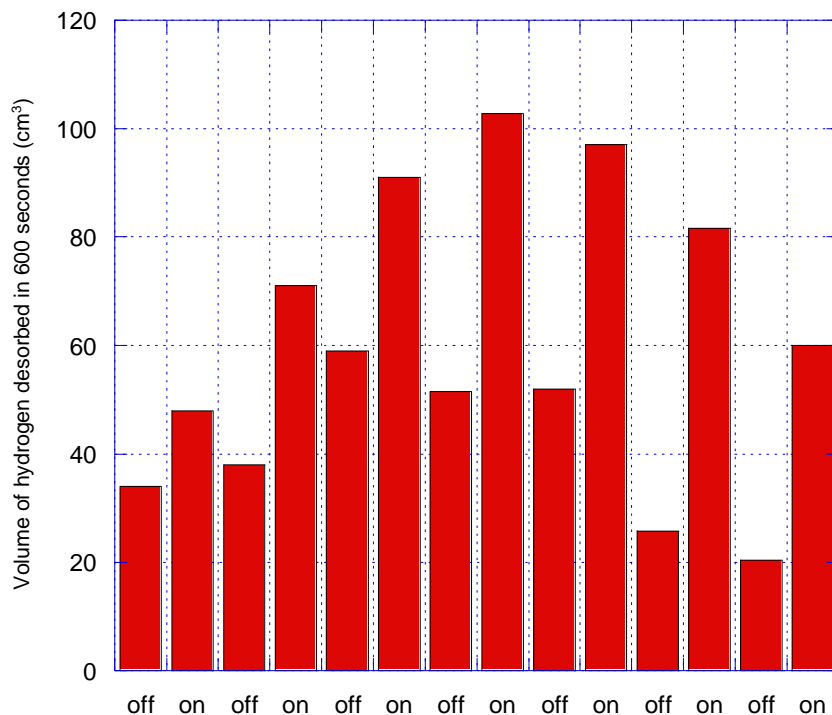


Figure 3.12: variation in desorption rate throughout the reaction with the microwave field cycled on and off for 600 second intervals and the total desorption in the period.

This shows a significant increase in the kinetic rate of the reaction with volume of gas released increasing from 200ml to 600 ml in the last stage of the experiment. This effect was very interesting and could have significant advantages for the use of magnesium as a hydrogen storage material.

3.4.2 Material Properties after cycling under microwave and radiant conditions

One possible cause of the effect of the microwave field on the desorption reaction would be excessive heating or a change in the structure of the material. Table 3.2 shows the crystallite size calculated using the Sheerer equation from XRD analysis taken after 6 cycles both with and without the microwave field at

330°C. There is little difference in the size of the crystallites indicating that over the cycles there have not been significantly higher temperatures seen by the microwave sample that could initiate excess grain growth.

Table 3.2 Crystallite change after desorption cycles under microwave and radiant only cycles calculated using the Sherrer equation from X-ray diffraction.

| Sample | Crystallite size (Å) |
|---|----------------------|
| As Received Goldschmidt Magnesium Hydride | 1100-1200 |
| Milled Magnesium Hydride 5 hours | 300-400 |
| After 6 cycles radiant only (330°C) | 850-1000 |
| After 6 cycles with microwave (330°C) | 900-1000 |

3.4.3 The influence of increasing the microwave field strength

The next obvious point to raise is the effect of reducing the field strength to observe the drop off in activity with field strength. Figure 3.13 shows comparable desorption curves for the desorption of hydrogen with the field strength reduced to 200W and 100W, these again show an increase in rate over the non microwave experiments but still show a clear correlation between the field strength and the desorption rate.

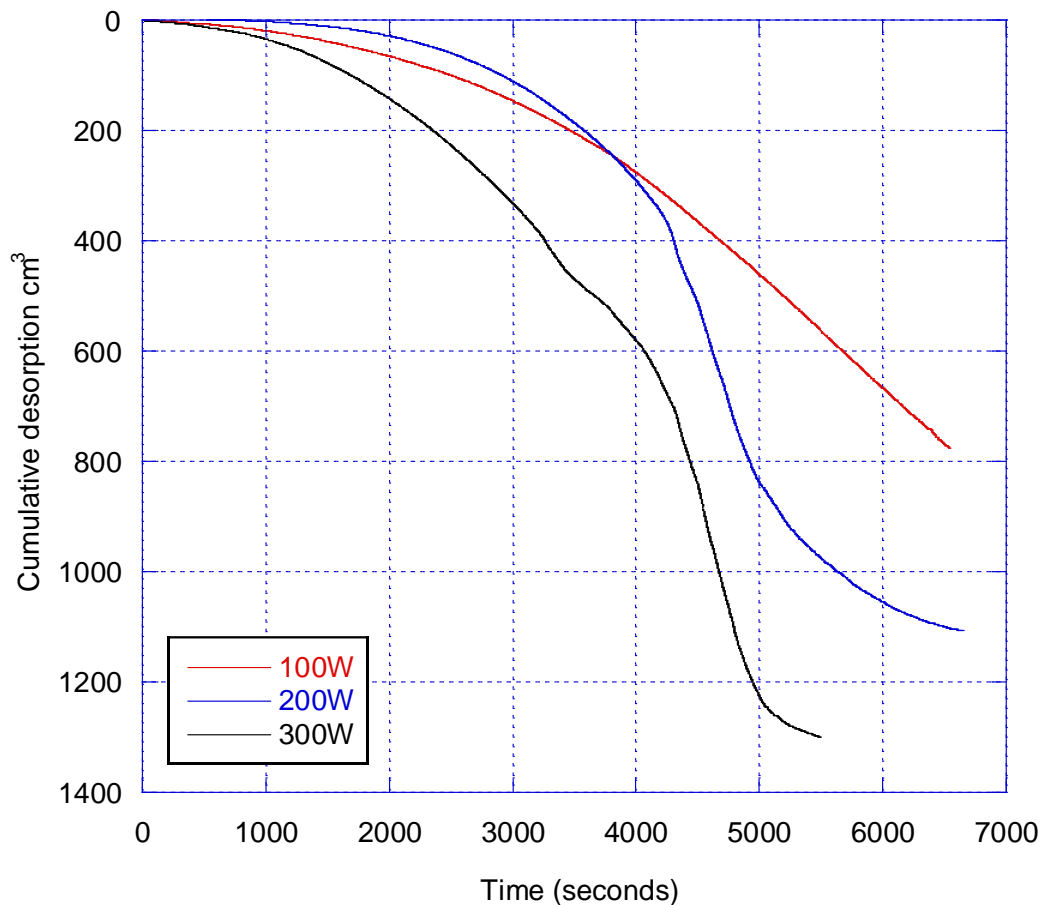


Figure 3.13: Desorption of hydrogen from MgH_2 with varying microwave field strengths from 300W to 100W at 310°C

In conclusion this work has demonstrated that the addition of a microwave field can accelerate the decomposition of MgH_2 significantly with measured desorption rates peaking at 400% of the non microwave samples. The effect is most pronounced in the second half of the desorption where the magnesium phase starts to become the dominant volume in the sample and the amount of metallic surface is increased. This would suggest that the microwave interaction with the alpha phase is a significant controller of the decomposition process and this assumption would help to explain the increasing influence of the field as the reaction progresses. The heating effect of the microwave field should not be overlooked as a possible cause of the acceleration. The measured bulk temperature of the sample is controlled and the increase in temperature is small,

and would not account for the change in reaction rate, however the localised heating phenomena often associated with microwave systems can still effect active chemical sites on surfaces and increase reaction rates. As the desorption is an endothermic process the energy transfer from the microwave field to the localised surface sites could be very quick and may even be associated with the structures formed in the first few layers of the alpha phase where the interstitial hydrogen moves to the surface to reform the hydrogen molecule. In many ways from an engineering view it is the bulk temperature that is the significant value as this determines the amount of energy required for a hydrogen store to operate. From an energy perspective the total amount of energy required for the store to operate is the key value and any reduction in the total by the use of microwave power would be significant.

3.5 The absorption of Hydrogen by Magnesium under microwave fields

The chemisorption of hydrogen to form MgH_2 is a process involving several steps as outlined in the introduction. The initial adsorption interaction with the surface is followed by the splitting of the molecule and penetration of the hydrogen species into the metallic structure. Once the concentration of the hydrogen reaches a critical concentration, coalescence of the particles triggers the formation of a second phase.

In the equipment developed at C-Tech the absorption of hydrogen was studied up to 350°C and up to 7 bar of hydrogen pressure.

Figure 3.14 shows the absorption curves of the magnesium at 330°C with the initial absorption rate always showing the highest level. It was found that at above 6 bar pressure, 600ml/min maximum flow rate on the mass flow controller was insufficient to maintain a constant pressure of the systems due to rapid absorption of the material. This effect yields the linear section of the absorption at the start of the curve as the flow controllers are at the maximum flow.

After this period the pressure stabilises and the rate of absorption drops as the reaction moves to completion. The absorption reaction kinetics were found to be significantly faster than the desorption rates and this effect was associated with the significant over pressure of the hydrogen. The absorption rate is highest initially before dropping as more material is transformed and diffusion through the hydride limits the rate of reaction during absorption.

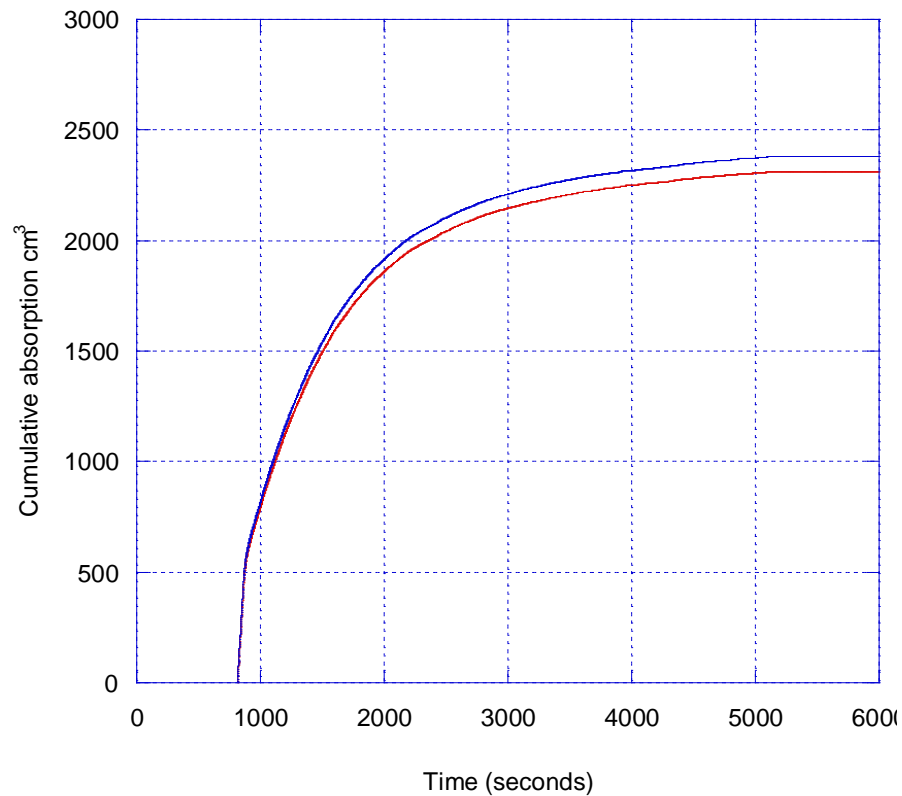


Figure 3.14: The absorption of hydrogen by magnesium at 7000mbar and 330°C absorption cycle 1 and 2

3.5.1 The effect of Microwave fields on the Absorption behaviour of magnesium

The effect of the microwave field on the absorption reaction was highly unexpected. Following the desorption experiments where a significant

acceleration of the reaction was observed it was hypothesised that a similar effect would be observed for the absorption assuming that the increased desorption rate was related to increased diffusion. It was quickly noted that when a microwave field of 300W was applied to the sample the absorption reaction was immediately halted.

Figure 3.15 shows the comparison of a non-microwave and 300W microwave consecutive runs at 330°C with a pressure of 7 bar. As can be seen the non-microwave sample plateaux occurred after around 5000 seconds when the reaction was deemed to be complete; however, for the sample in the microwave field after 4900 seconds the amount of hydrogen absorbed was almost nil. Once the microwave field is removed at this point the reaction starts almost instantaneously and completes at a rate similar to the non-microwave sample.

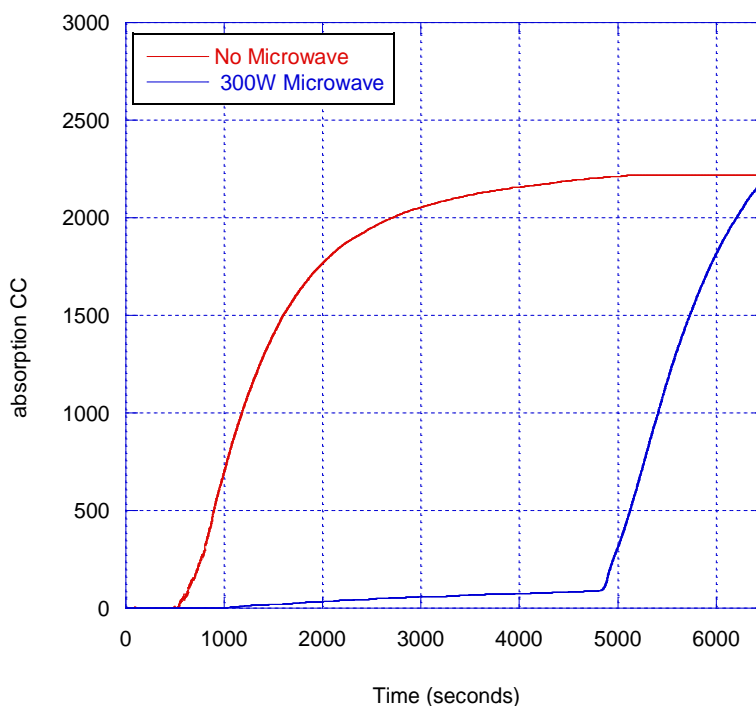


Figure 3.15: Absorption behaviour of Mg at 330°C and 7 bar hydrogen pressure with and without a 300W microwave field

Throughout these experiments the temperature of the sample was measured and remained constant for most of the run with the exception of the initial period when the microwave was started. Figure 3.16 shows this data and the effect of the microwave being switched off at around 5000 seconds where the temperature drops briefly before restabilising.

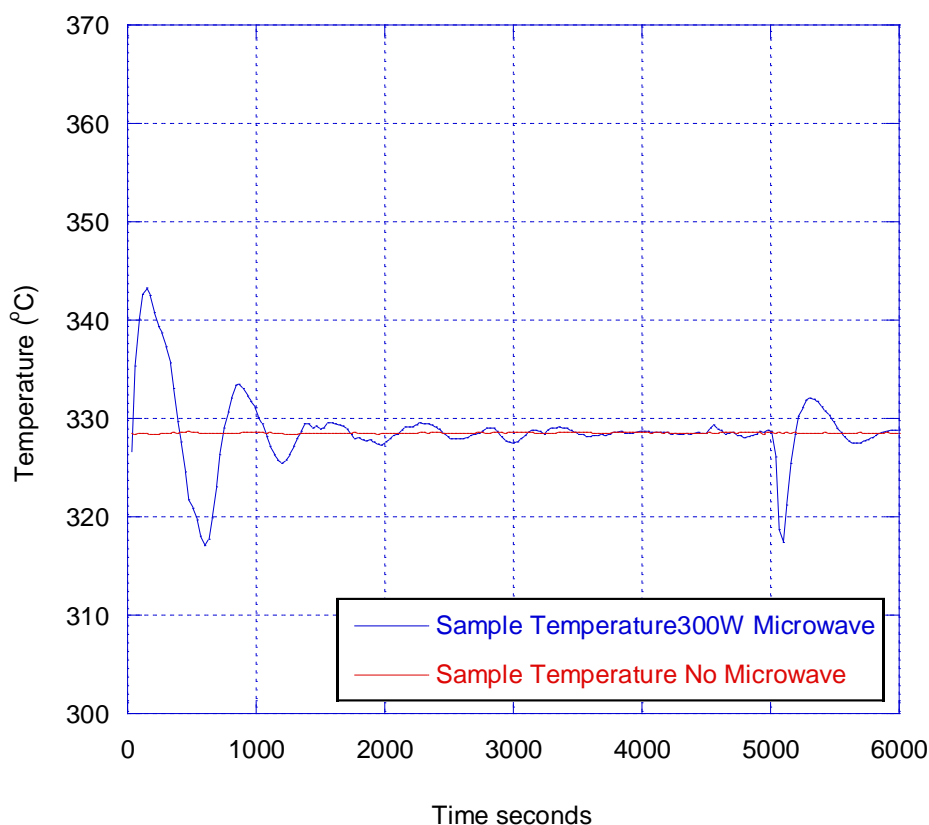


Figure 3.16: Sample temperature of Magnesium samples during absorption with and without 300W microwave field

The effect is extremely strong but does not affect the rate of reaction after the microwave field has been removed. Throughout a series of experiments the rate of absorption remained broadly similar with no clear trend to suggest physical alteration of the material. Figure 3.17 shows the absorption rate of samples with and without the microwave field applied; the variation between samples was similar to that observed in all experiments.

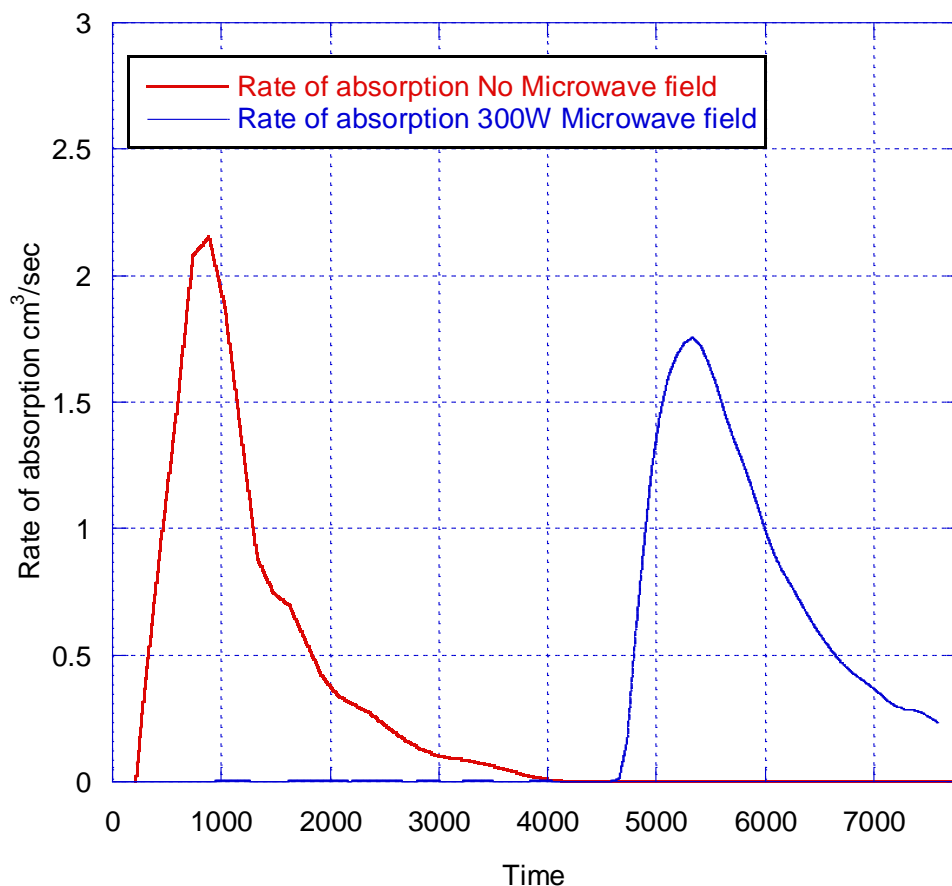


Figure 3.17: Absorption rate of magnesium hydride at 330°C and 7000mbar, showing the displacement of the reaction under the 300W microwave field until the electromagnetic field is removed

Once this effect was observed at the start of the absorption reaction it was important to understand if the effect was diminished as the alpha phase contracted in a similar way to the increasing effect in the desorption as the alpha phase expanded. Figure 3.18, shows the effect is still microwave field at 300W is still strong at 50% completion of the reaction. Further to this the re-application of the field stops the reaction after rapidly acting as a switch to start and stop the reaction at any point.

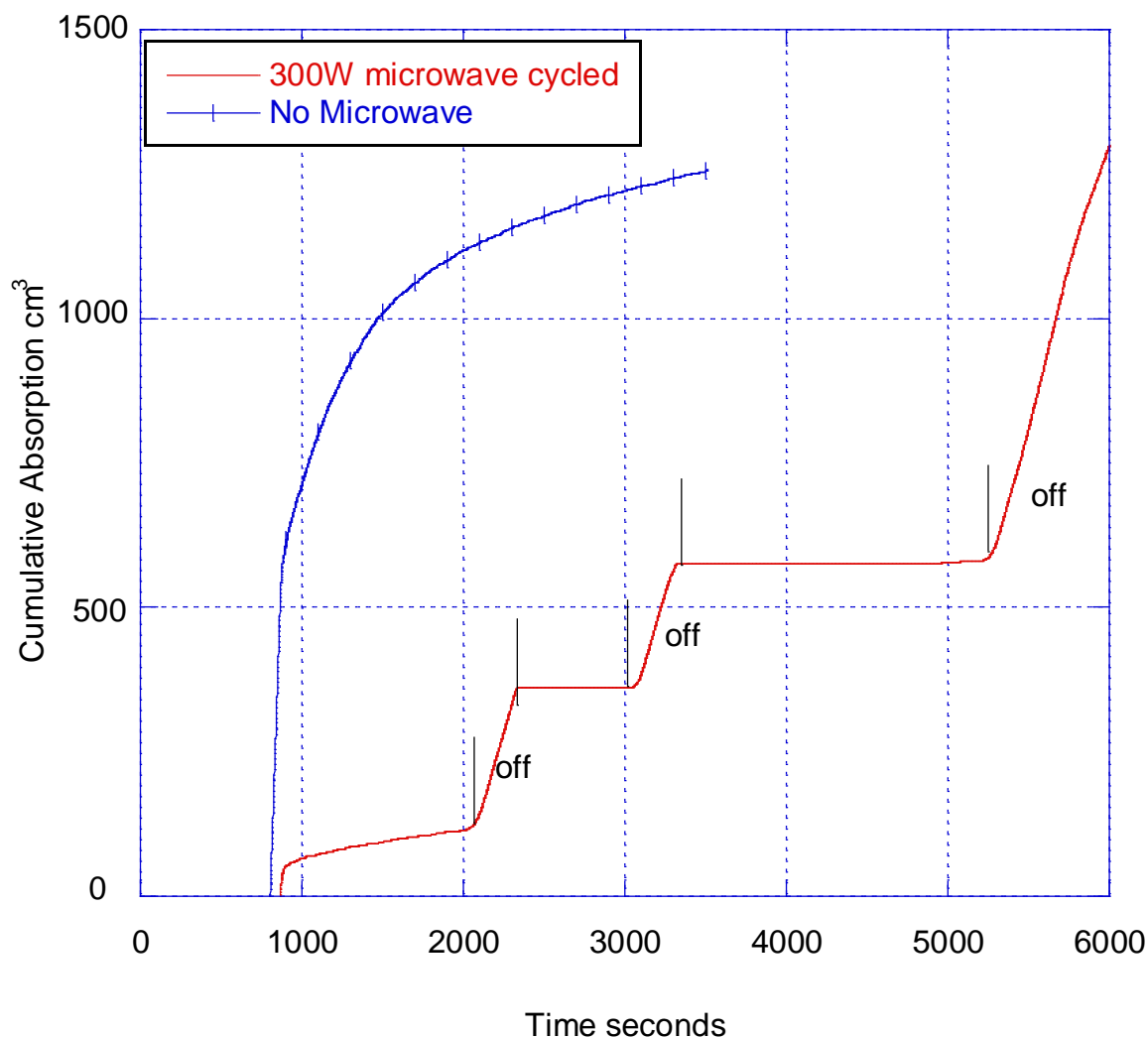


Figure 3.18: The effect of alternating the microwave field on and off during the absorption process at 7000mbar and 330°C with a non-microwave absorption curve for comparison

3.5.2 The effect of reducing the microwave field strength on absorption behaviour

Reducing the applied field strength also has a significant effect on the rate of absorption. With a 300W microwave field the absorption is almost prevented, however, reducing the strength of the field to 200W and then 100W also impacts on the absorption rate when compared to the non-microwave sample. Figure 3.19 shows this effect and it can clearly be observed that there is a strong correlation between microwave power and the reduction in the reaction rate.

It should also be observed that there is a much larger difference in rates between the 200W and 100W samples than the 300W sample. This effect could be due to a saturation phenomenon around 200W or that the effect does not scale in a linear fashion.

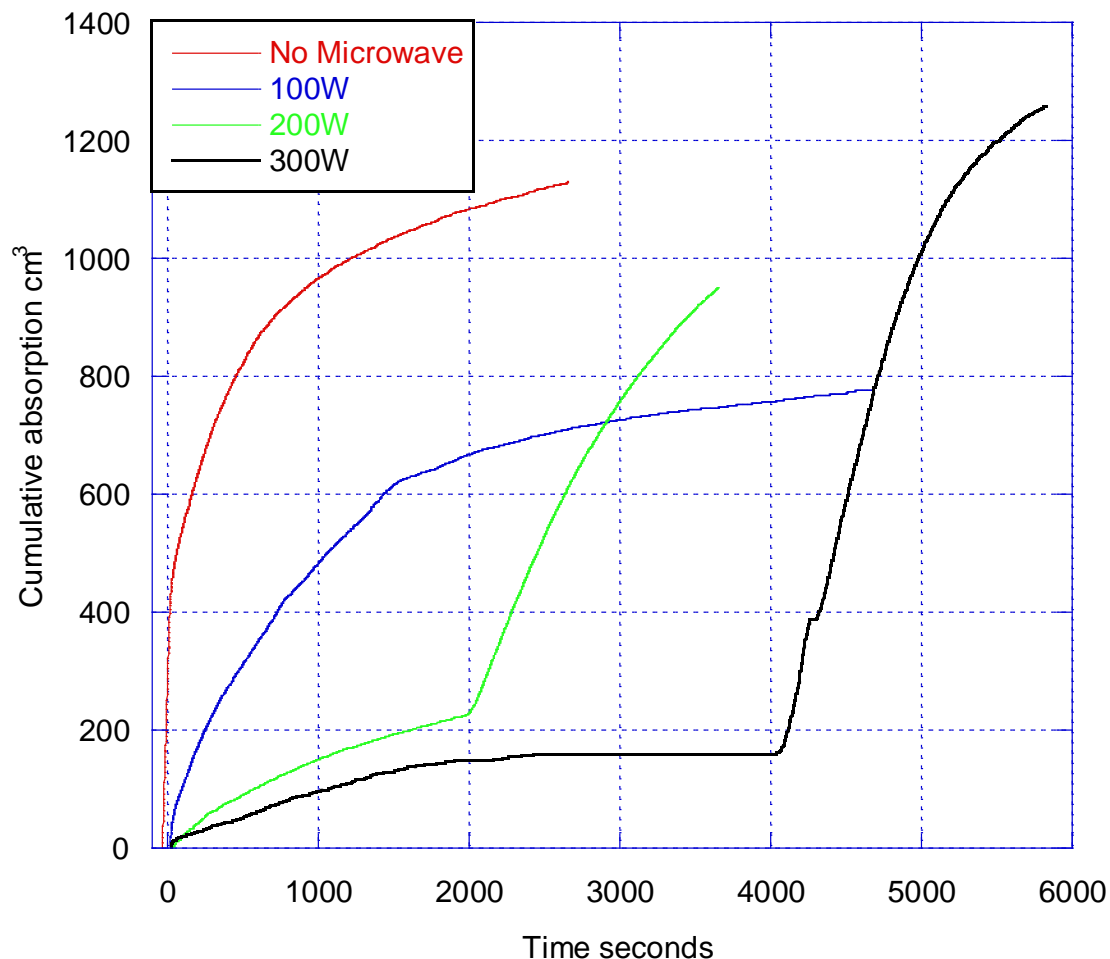


Figure 3.19: Absorption rate for magnesium at 330°C at 7 bar with a range of applied microwave field strengths (300W, 200W 100W, and non-microwave for comparison).

In order to further understand the interaction of the field strength with the reaction rate the power of the microwave field was incrementally dropped from 300W to 50W over 12000 seconds. Figure 3.20 shows the increasing absorption rate with reducing fields and as with the data in figure 3.19 above there is a clear change

in the relationship below a field strength of 200W. Below this level the rate of absorption continuously increases showing the strong correlation between field strength and reaction rate. This also suggests that the effect is not linked to a field strength threshold which may explain the results if there was no effect below a fixed field strength value.

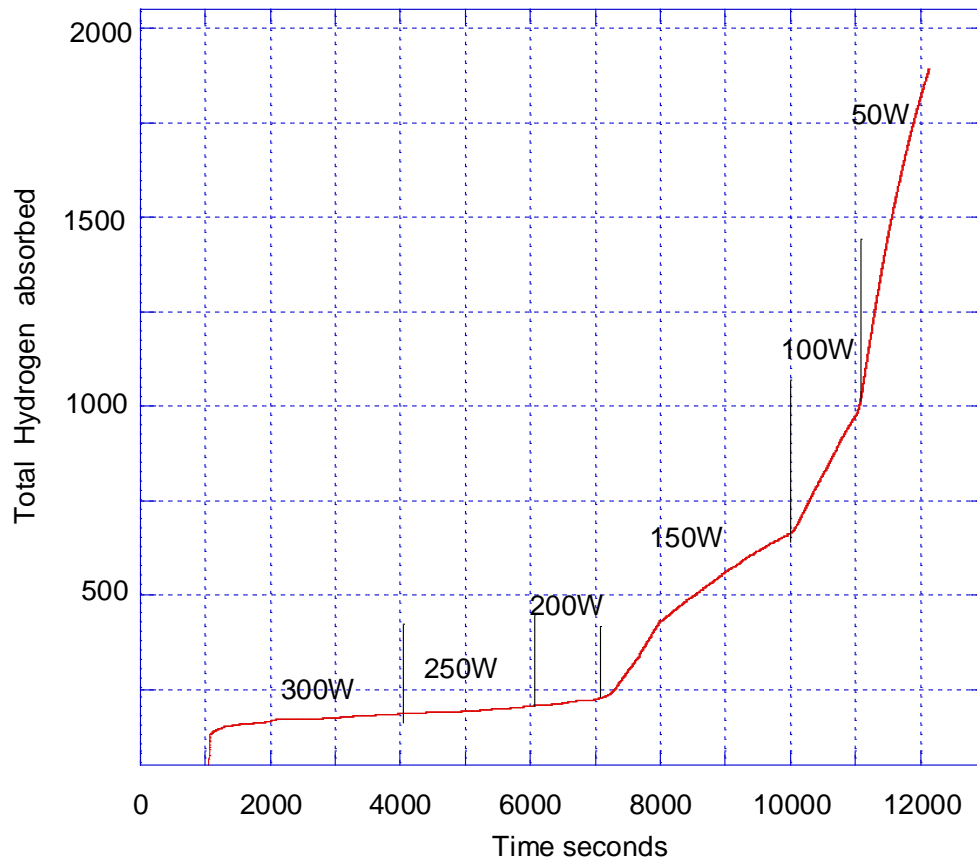


Figure 3.20: Absorption of hydrogen by magnesium at 330°C and 7000 mbar with reducing microwave field strength from 300W to 50W showing an increasing absorption rate with power reduction.

3.6 Catalysed magnesium hydride

The impact of the microwave field on the pure magnesium showed significant promise as a method for altering the reaction rates under a range of conditions. It was observed that some of the characteristics of the desorption reactions show that there is a clear influence of the hydride phase change on the reaction kinetics.

It was therefore reasonable to expect that there could be an influence of the quantity of metal surface exposed during the reaction. This would fit with models of desorption requiring an exposed metal surface in order for the desorption reaction to take place.

Work on the effects of the addition of two metal catalysts is shown in the following section.

The two additives selected were nickel and iron, which due to the known performance variation in classical thermal studies of the sorption kinetics were hoped to give some further insight in to the nature of the influence of the high frequency electromagnetic fields.

Materials were prepared in the same way as the pure milled magnesium samples from MgH_2 supplied by Goldschmidt. The material was milled under an argon atmosphere in a Restch planetary mill with a 10:1 ball to powder ratio using stainless steel balls and a stainless milling pot.

All the samples were milled for 5 hours at 160 rpm in 15 minute segments with a 15 minute cool down period between run periods to allow heat to dissipate and prevent unwanted thermal processes.

Catalyst materials were added after 4½ hours of milling time the additions would be added for the last half hour. This time was chosen to allow sufficient and even size reduction and mixing to give even material properties and reduce variation in

the milled structures formed that could be developed with the addition of a material that may alloy with the magnesium in longer times.

The nickel used was supplied by Sigma Aldrich as 99.98% purity metal basis, 325 mesh powder with a particle size between 5 and 15 microns.

The iron powder was also 325 mesh powder with a particle size between 5 and 15 microns and supplied by Alfa Aesar with a metal purity of 99.95%.

Each sample preparation process produced 20g of MgH_2 materials which was stored under argon atmosphere in the University of Birmingham Glove box prior to use.

3.6.1 The effect of nickel addition on the desorption kinetics.

From the literature it is well established that the addition of Ni will significantly increase the reaction kinetics of both the absorption and desorption kinetics. Initial studies examined the effect of a 2 molar percent addition of Ni powder in the C-Tech hybrid system. The change in the desorption rate is clear as shown in figure 3.21 where at 310°C and a hydrogen pressure of 500mbar, the initial rate of the desorption is significantly higher than the untreated sample also shown for comparison.

It was found that the addition of Ni reduced some of the variation that had been present with the un-catalysed materials which although reduced by improved methodologies still had some impact on the sample cycle times over the course of a test program. This effect was attributed to the changes at the surface which made the material less susceptible to small changes in surface oxidation.

From the shape of the curve it is clear that the rate limiting step has been affected in the initial stages of the reaction with the desorption behaviour most significantly altered in the initial stages of the reaction. Once the Ni catalysed material has desorbed more than 1500ml the rate of desorption starts to slow

which could be indicative of a change in the rate limiting step as the proportion of MgH_2 phase is reduced and the diffusion rate may play a more significant role.

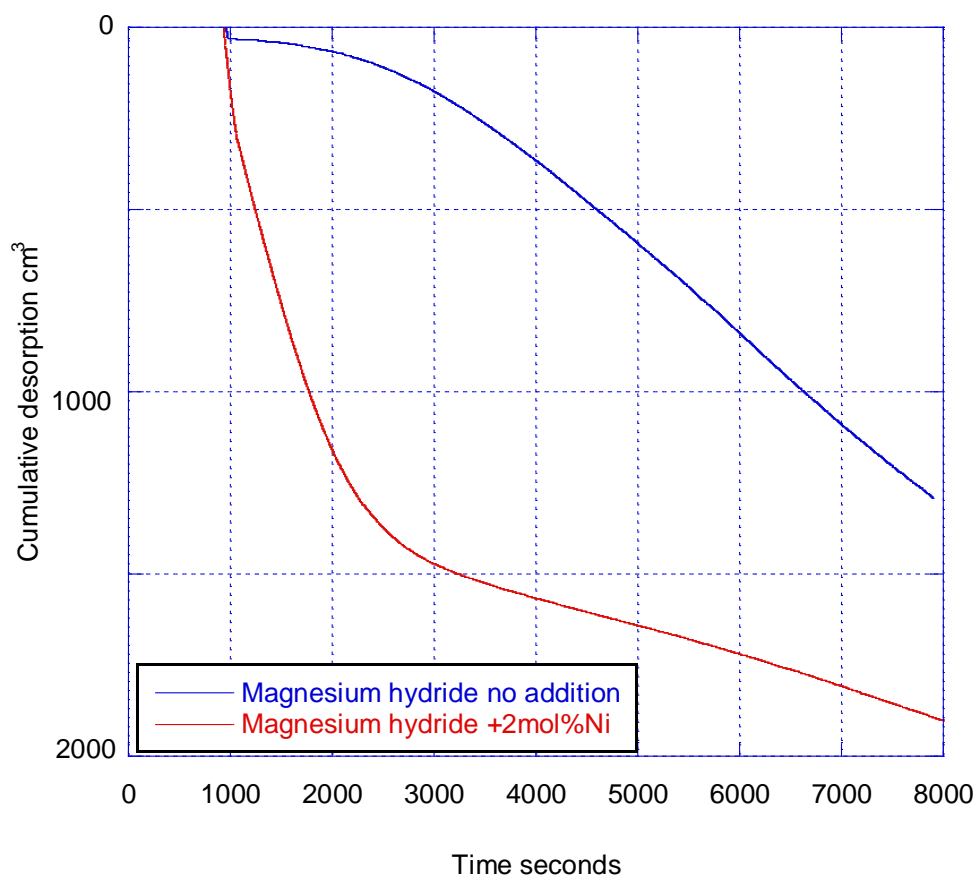


Figure 3.21: Desorption from MgH_2 catalysed with 2mol% Ni at 310°C 500mbar with non-catalysed MgH_2 as a comparison

Given the increase in rate observed in the un-catalysed magnesium hydride a 300W microwave field was applied to the material to assess the impact of the electromagnetic field on a sample where there is clearly a different surface reaction occurring during the recombination step of the desorption. Figure 3.22 shows the effect of the microwave field which increases the desorption rate further leading to extremely quick decomposition with the reactions reaching completion in less than 30% of the time of the uncatalysed materials that were exposed to the same electromagnetic field.

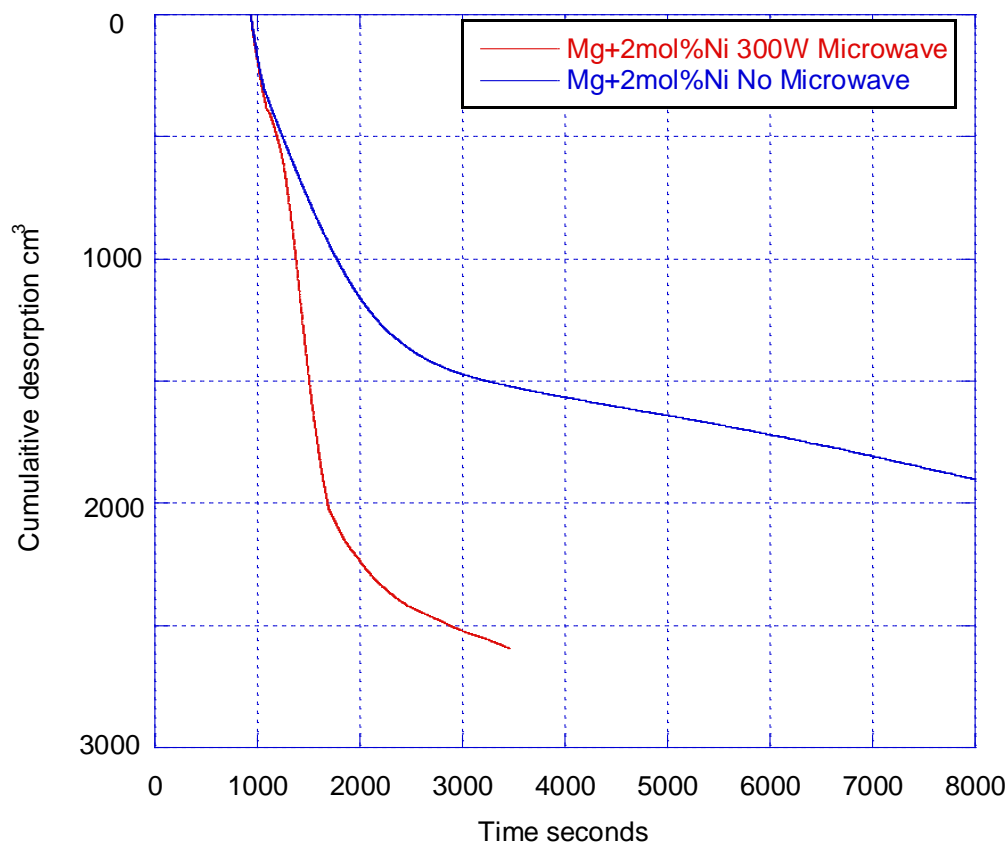


Figure 3.22: Desorption from MgH_2 catalysed with 2 mol% Ni with and without a 300W microwave field at 310°C and 500mbar.

This effect is highlighted in Figure 3.23 where the rate of gas production is plotted against time for the Ni catalysed materials with and without the microwave field. Here there acceleration in desorption occurs as soon as the microwaves are initiated at 1000 seconds, which is contrast to the un catalysed materials where there is a period of time with little initial desorption followed by a more gradual increase. The peak desorption rate achieved with the microwave field is over four times higher than the non microwave samples and shows the significant effect that the microwave field has on the reaction even when there is a good catalyst on the surface.

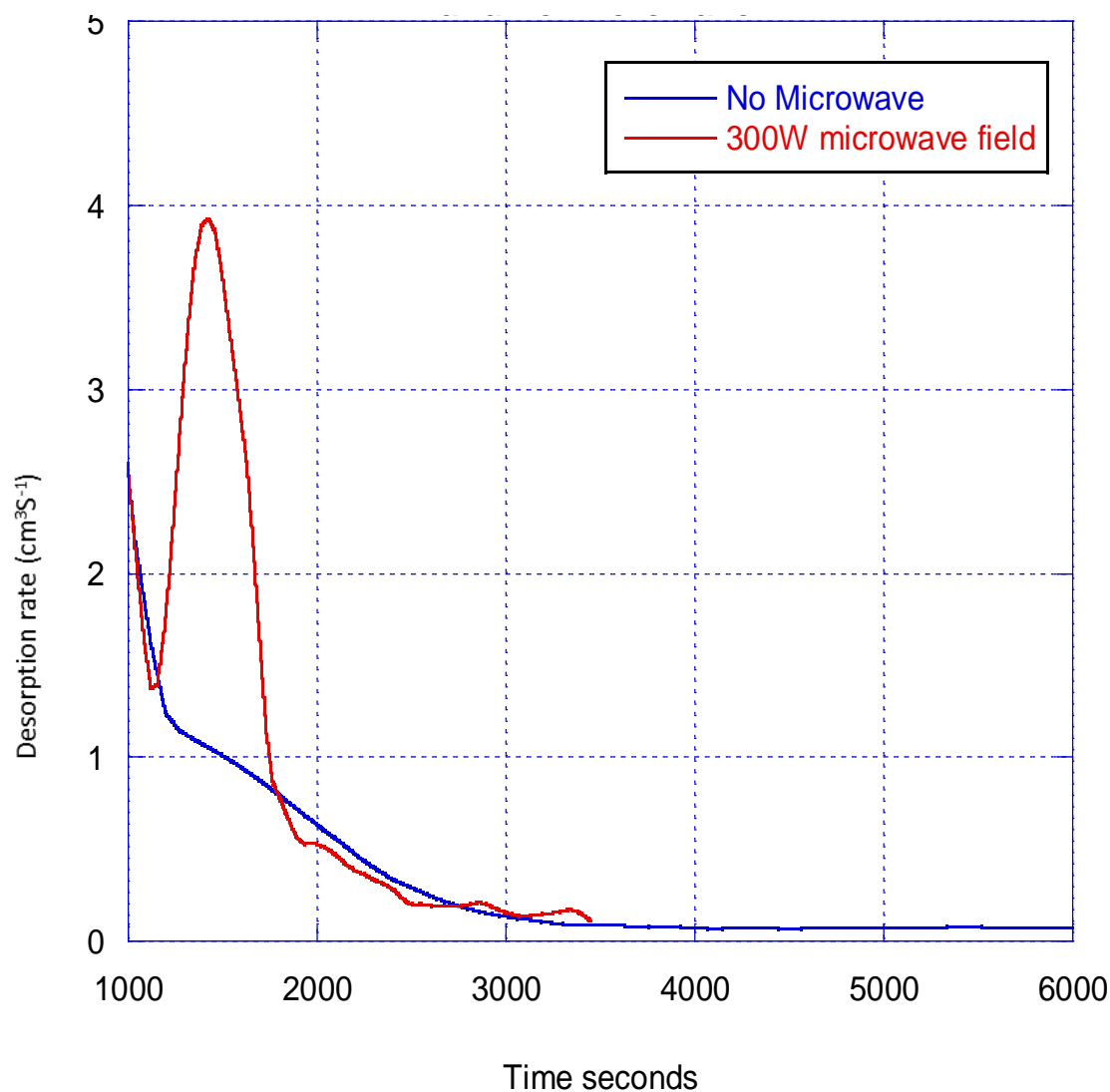


Figure 3.23: Desorption rate (cm^3S^{-1}) profile from MgH_2 catalysed with 2 mol% Ni with and without a 300W microwave field at 310°C and 500mbar

The change in the behaviour of the material with the Ni catalyst is clearly observable in Figure 3.24 when compared to the un-catalysed material. Here the difference in the effect of the microwave field in the early stages of the desorption process can be attributed to the Ni catalyst on the surface. This may be due to the increased activity of the surface allowing an easier recombination and desorption on the surface in the initial stages or that the metal particles allow localised heating around the active Ni sights. This compares to the magnesium

surface where the metal only starts to allow increased activity once a small percentage of the material has decomposed and allowed the influence of the metallised surface to have an effect.

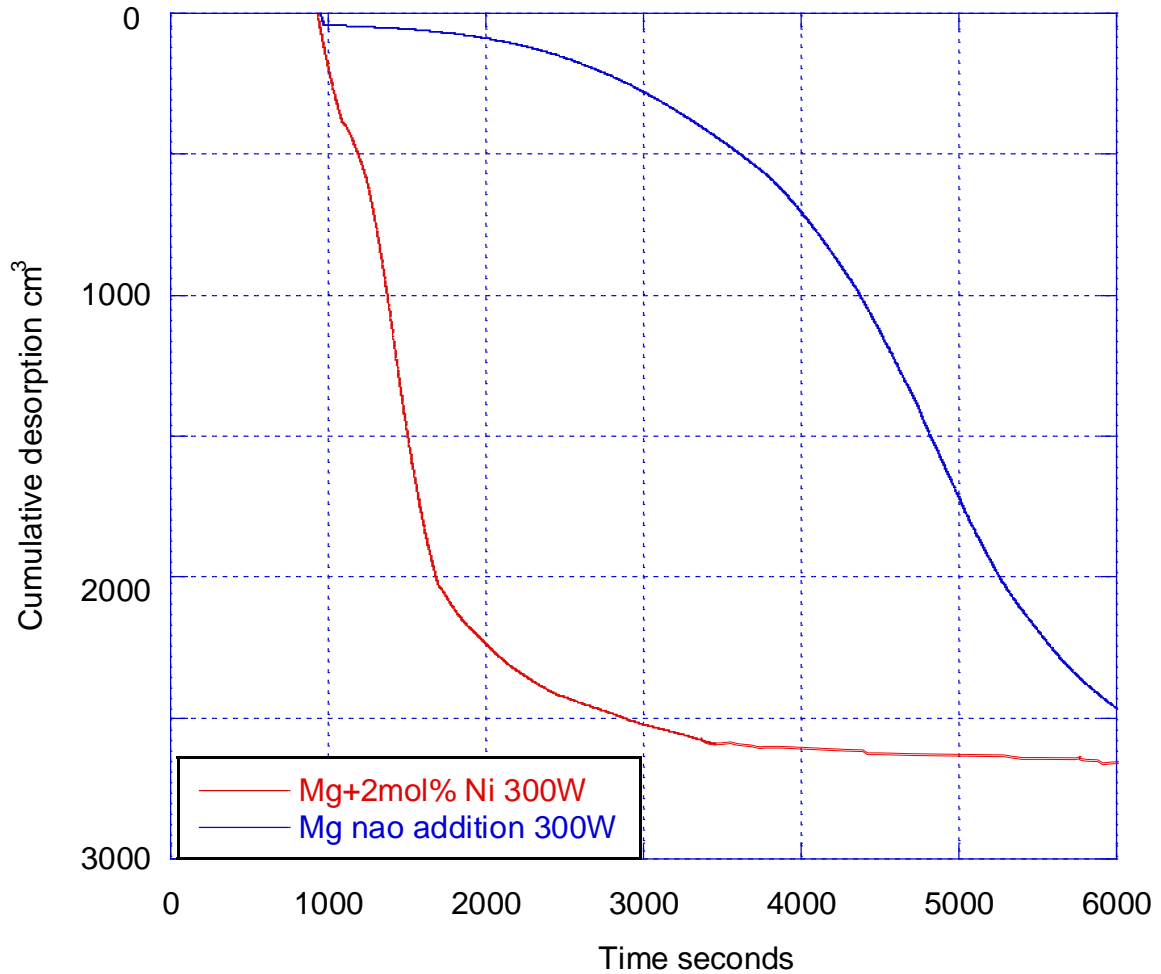


Figure 3.24: Desorption from MgH₂ Catalysed with 2 mol% Ni with 300W microwave field at 310°C and 500mbar with un-catalysed MgH₂ as a comparison

3.6.2 Lower temperature desorption under microwave field

Following a series of experiments looking at progressively lower temperatures for the desorption it was found that the microwave field was, in combination with the nickel addition, able to give strong desorption rates under conditions where without the electromagnetic field desorption was not observed Figure 3.25.

At the temperatures where desorption without the electromagnetic field was not observed it became increasingly important to have a second method of temperature measurement to increase the confidence in the results. The development of the fibre optic sensor capable of working in this temperature range gave increased confidence that these observed effects were real and not the result of measurement errors. The solution developed for the protection of the fibre optic was found to cause a slightly slower reaction to the temperature of the system and induced a lag in the compensation of the radiant heating elements. This is highlighted in figure 3.26, however, the data shows that the maximum temperature reached was only plus or minus 5°C of the set point.

Figure 3.25 shows the desorption rates for the sample with and without the microwave field with a bulk temperature of 270°C. This clearly shows that with no field present at the set temperature there is no decomposition of the magnesium hydride; however, with the microwave field there is a reaction that is only marginally slower than at temperatures above 300°C.

This temperature is low in comparison to many of the desorption studies of magnesium catalysed with a range of materials including V and Ni, showing that there is a strong effect of the microwave field that compares well to state of the art materials developments in the magnesium system.

It should also be noted that as with all the experiments this desorption was into a pressure of 500mbars of hydrogen rather than a zero partial pressure of hydrogen used in many experimental methods.

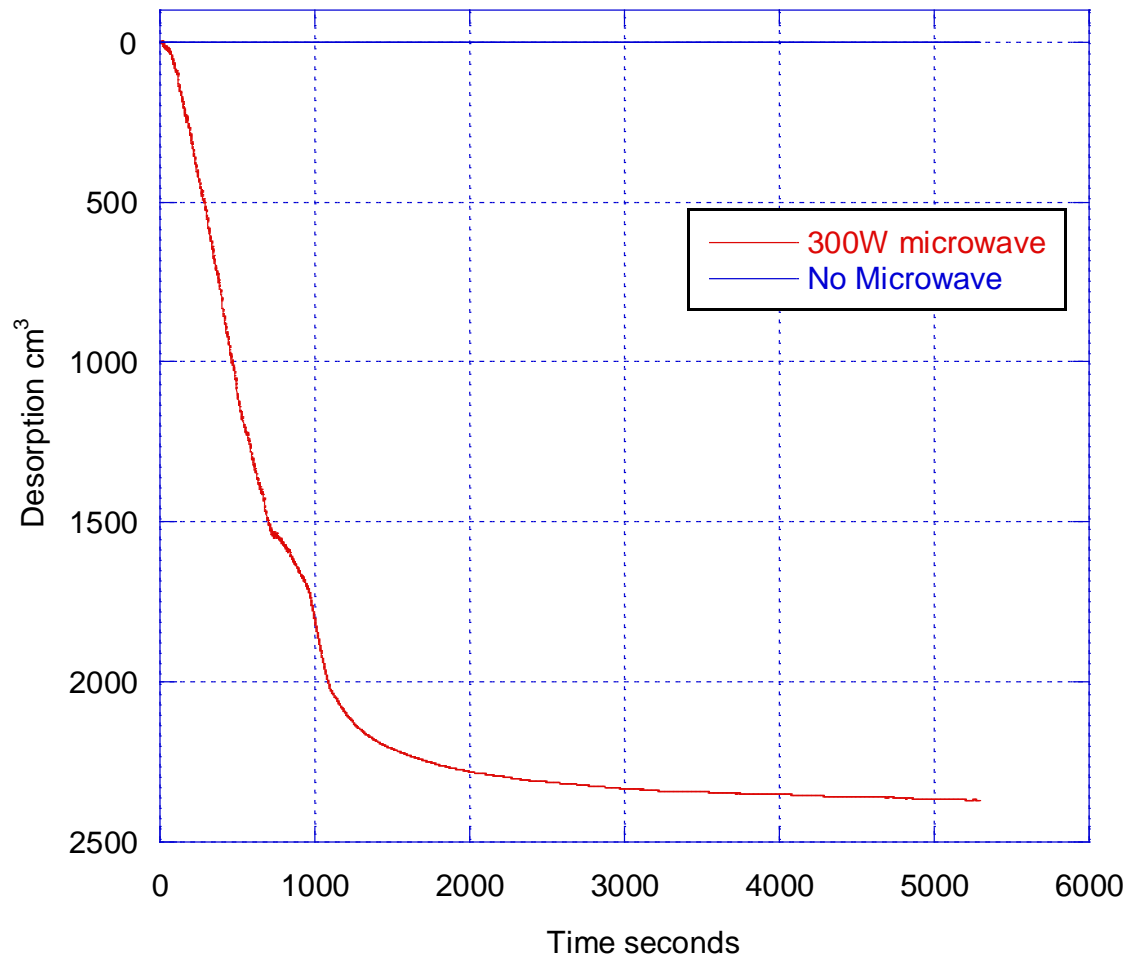


Figure 3.25: Desorption from magnesium hydride with 2mol% Ni, at 270°C with and without a 300W microwave field. Desorption only occurs with the microwave field present.

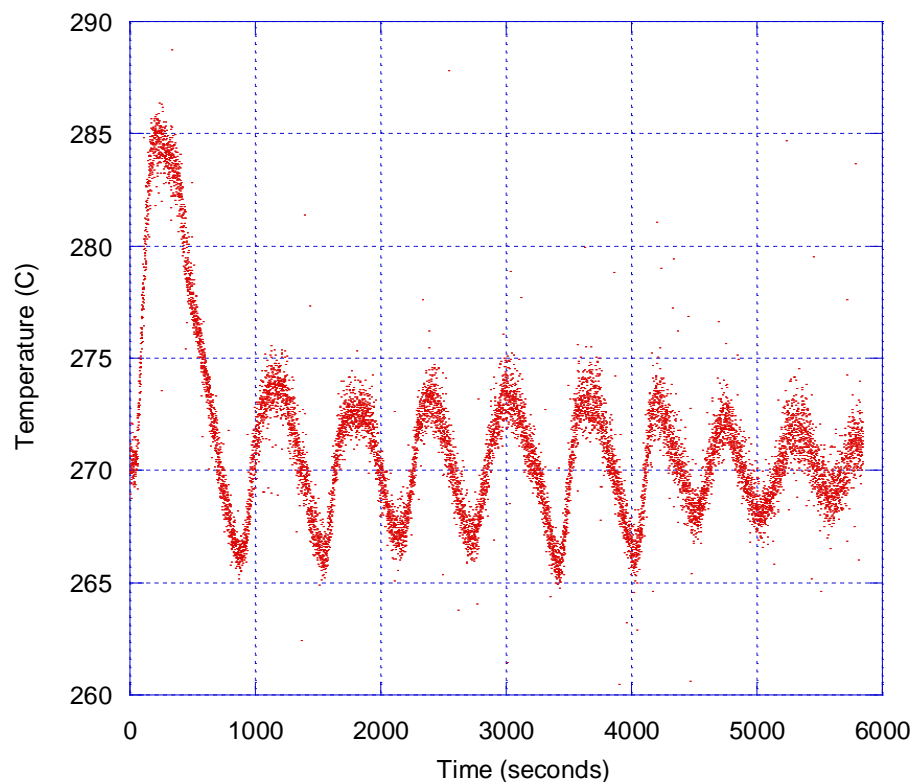


Figure 3.26: Temperature plot during the desorption in Figure 3.25 with a 300W microwave field.

3.6.3 The absorption of hydrogen at lower temperature using Ni catalysed Mg

As expressed previously, one of the underlying uncertainties expressed in microwave assisted chemistry is the measurement of temperature and the conclusions this can lead to when discussing mechanisms for the changes in behaviour observed. To help to clarify the previous experiments indicating that the microwave field prevents the absorption of hydrogen it was important to show that this effect was not due to a small errors in the measurement of the bulk temperature under the microwave field. Figure 3.27 Shows the absorption of a Ni catalysed sample held at 270°C and 7bar pressure of hydrogen under a 300W microwave field. At this temperature the sample is 100°C below the thermodynamic equilibrium pressure and therefore the temperature measurement would need to be significantly flawed if the observed effect the result of microwave heating of the sample surface. The temperature of the

sample was maintained over a period of 86 minutes, to ensure that any thermal gradient in the sample would be able to equalise. If excess surface heating was a major influence in the experiment it would be expected that over time this would start to conduct heat to the centre of the particles and raise the bulk temperature of the sample. As the temperature did not increase over the period of the experiment it is difficult to conclude that the microwave field is causing significant surface heating that would prevent the absorption.

As with all of the previous absorption experiments the removal of the microwave field after 5200 seconds marks a significant change in the reaction with a sudden increase in the absorption rate back to rate observed at the initial stages of non microwave treated samples.

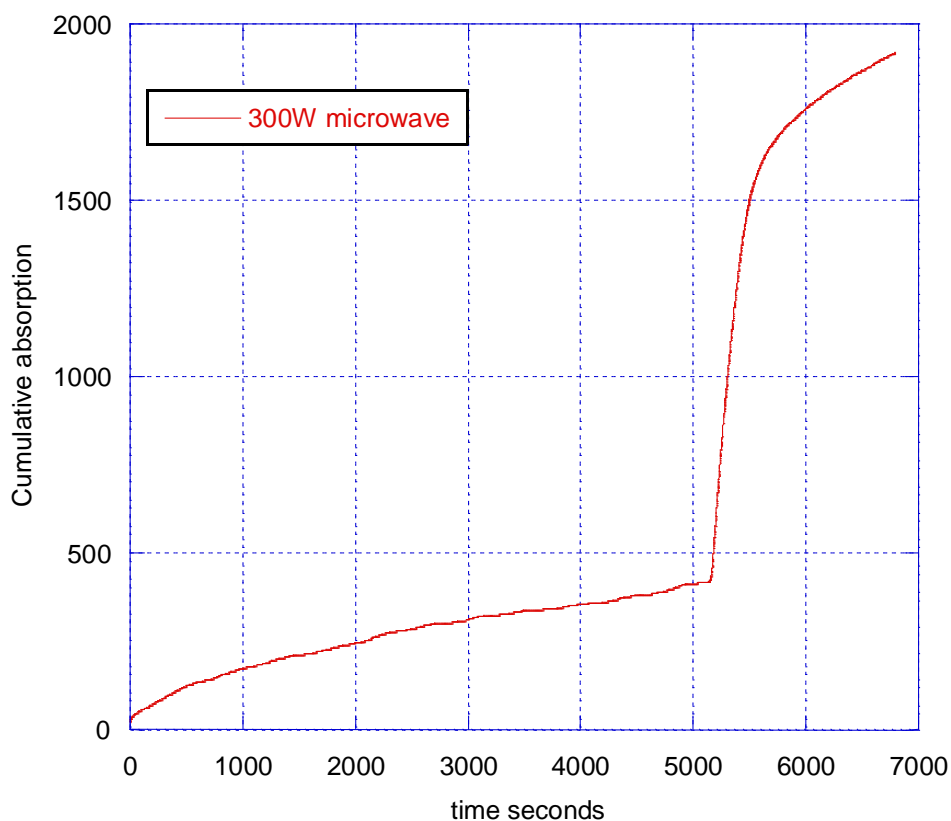


Figure 3.27 Shows the absorption of a Ni catalysed sample held at 270°C and 7bar pressure of hydrogen under a 300W microwave field. The microwave is removed at 5100 seconds.

3.6.4 The sorption Kinetics of Mg catalysed with Fe

Following the observed effects with the addition of Ni, which is a well known catalyst for improving the sorption properties of magnesium, iron was added to look at changing the nature of the metal particle on the surface. The addition of a metal that is known to have a relatively poor catalytic surface for the hydrogen dissociation and recombination reaction would help to distinguish heating effects on the surface caused by metal decoration from any changes in the reaction process caused by the microwave field. If the primary effect of the microwave field is the heating of the surface, which could be one explanation for the increasing reaction rate in the pure magnesium samples as a metal surface is created by initial desorption, or the rapid desorption from nickel doped samples, then the addition of a similarly conductive material of the surface would be expected to produce a similar result to the Ni doped samples.

Milled samples were prepared with the 5 mol% addition of Fe in the last portion of the milling process to ensure good mixing. Figure 3.28 shows a slight improvement in the desorption kinetics at 330°C due to the addition of the iron when compared to the pure milled magnesium with no microwave field applied. This is of the order expected from the literature published in the area which shows a weak improvement from the addition of iron.

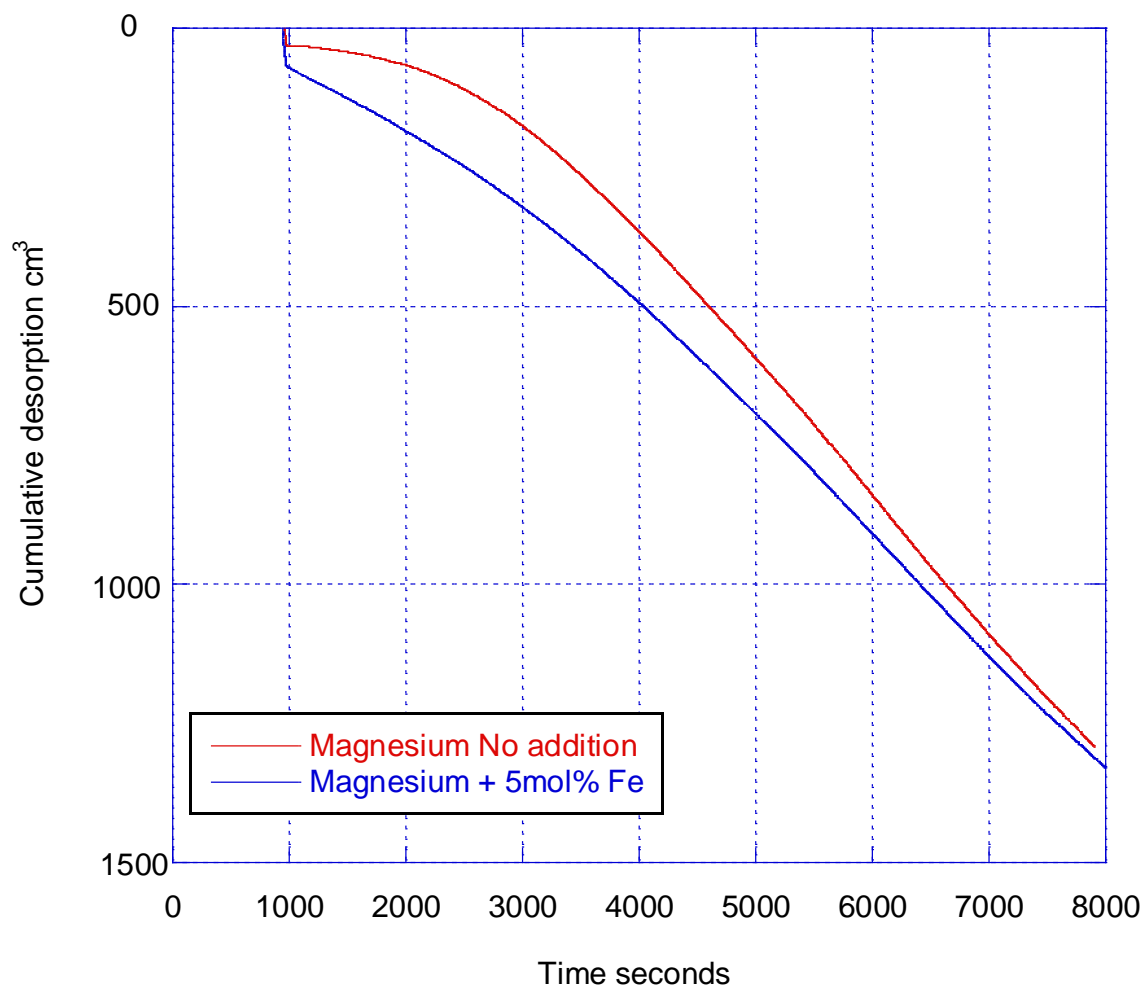


Figure 3.28: Desorption at 330°C and 500mbar showing the addition of 5mol% iron when compared to the pure milled magnesium with no microwave field applied

The effect of the microwave field is again clear in Figure 3.29, where there is a significant increase in desorption rate when compared with a non-microwave desorption. As with both the pure milled magnesium and the Ni catalysed samples the temperature remained steady throughout the desorption process under the microwave field. The shape of the curve is similar to that of the pure magnesium sample with a slow start and an increasing rate reaching a peak at around 50% of the complete desorption. This shape is interesting as it differs from the rapid initial desorption from the Ni doped sample suggesting that the presence of the iron in the microwave field does not initiate the same surface mechanisms. The shape, being similar to that of the pure milled magnesium

suggests that the presence of metal islands on the surface is not the primary cause of the changes under the microwave field.

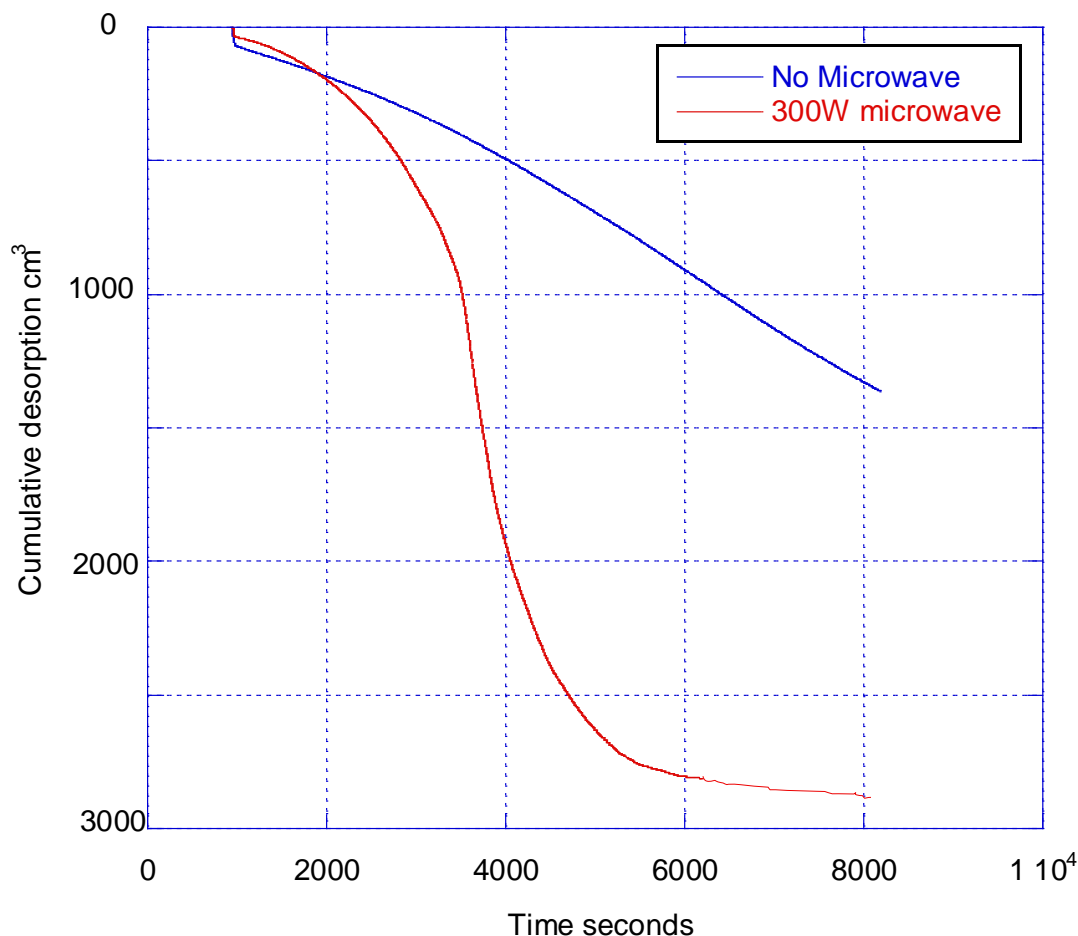


Figure 3.29: Desorption from MgH_2 with 5mol% Fe at 330°C and 500mbar hydrogen pressure showing the improvement in desorption rate with the microwave field

The similarities of the reaction catalysed with iron to the pure milled magnesium are evident in figure 3.30. At 330°C and 500mbar pressure of hydrogen the rates of the reactions follow a similar path with the iron catalysed sample showing a higher initial desorption rate but with the maximum rate of the pure magnesium exceeding the maximum rate of the iron catalysed sample although at a slightly later point in the desorption process.

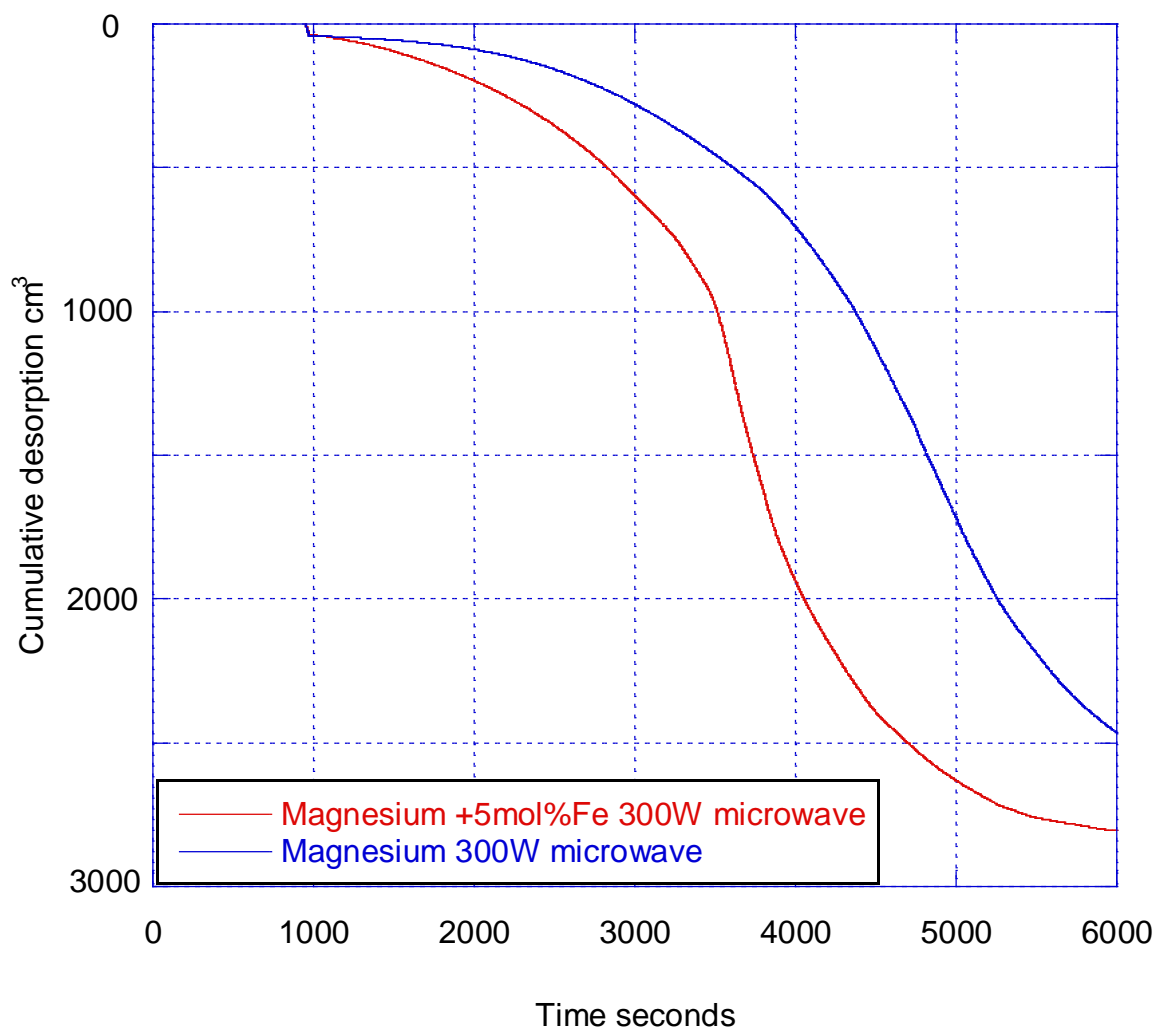


Figure 3.30: comparison of Microwave assisted desorption of milled Mg and Mg with 5mol% Fe

3.6.5 Comparison of rates of desorption under microwave fields

In general terms, although the mechanism is not consistent between the pure magnesium and the iron and nickel catalysed samples, it is clear that the microwave has a very strong effect on the desorption processes. This feature that was consistent throughout all of the samples exposed to the microwave field, independent of surface condition, catalysis, stage of desorption or temperature the effect was significant for every sample.

Figure 3.31 shows a comparison of the rate of desorption throughout the decomposition from 100% MgH_2 to the metallic Mg at 330°C with 300W of microwave field. It is clear that the effect of both the Ni and Fe catalysts is to shift the peak desorption to earlier in the decomposition, this would fit well with the hypothesis that in the desorption process the recombination of hydrogen on the magnesium surface is a rate limiting step.

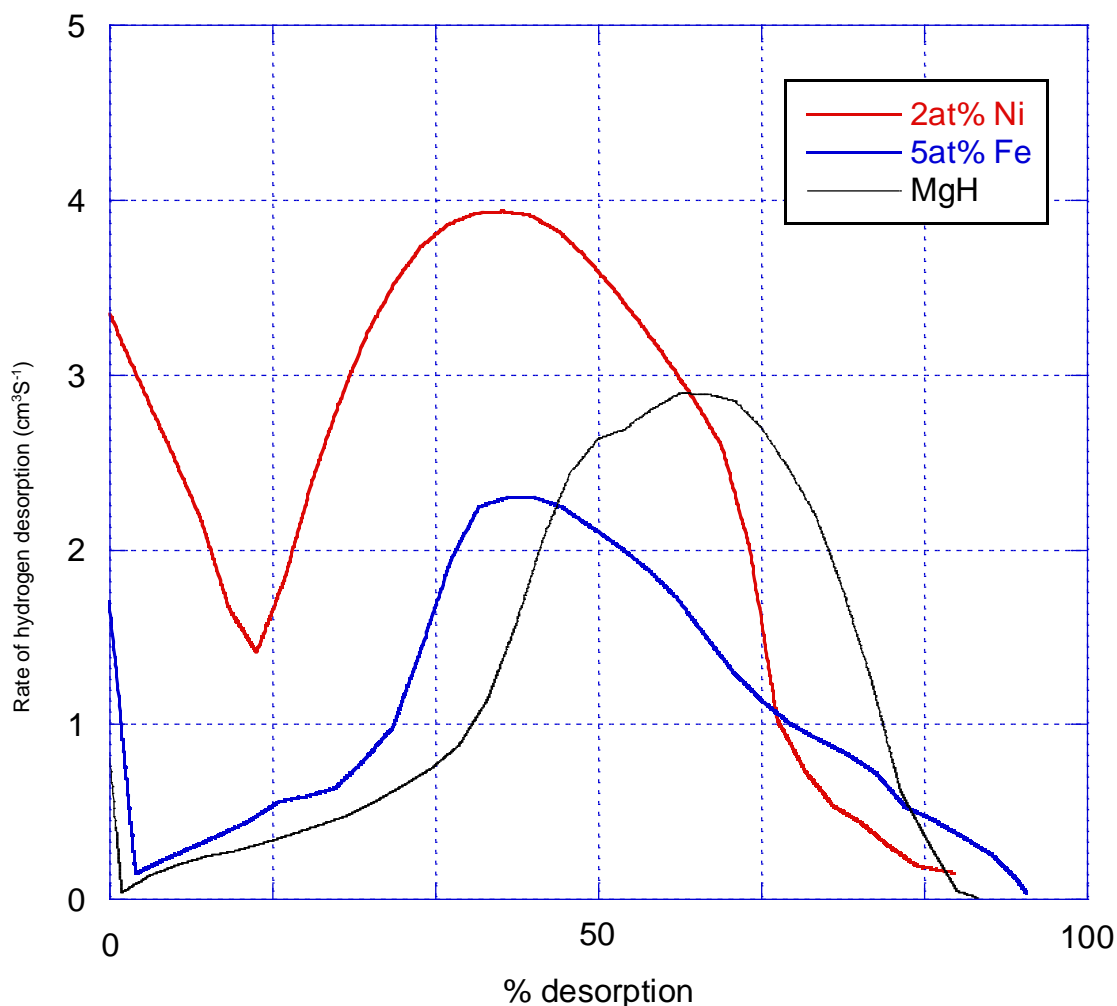


Figure 3.31 shows a comparison of the rate of desorption from Pure MgH_2 and material Catalysed with 5mol% Fe and 2mol% Ni throughout the decomposition from 100% MgH_2 to the metallic Mg at 330°C with 300W of microwave field

The microwave effect is clear in table 3.2 which highlights the dramatic increases in desorption rates of up to 1000% that were seen under a relatively weak

microwave field of 300W. Although the highest increase in the peak desorption rate is for the undoped magnesium sample the material that would be of most practical interest is the Ni catalysed sample. This is due to the high peak and short time to this peak of only 416 seconds from the start of the desorption, 10 times faster than the pure material.

Table 3.2: Peak rates of desorption at 330°C with and without 300W microwave field

| Material | Peak Rate NM ml/sec | Peak rate 300W microwave ml/sec | Rate increase MI/sec | Time for peak rate (Sec) | % increase in peak desorption rate |
|--------------------------------|---------------------------|--|----------------------------|--------------------------------|--|
| MgH ₂ | 0.23 | 2.59 | 2.36 | 4491 | 1026.1% |
| MgH ₂ + 2mol% Ni | 1.1 | 3.91 | 2.8 | 416 | 254.5% |
| MgH ₂ +5mol% Fe | 0.21 | 2.23 | 2.02 | 2652 | 961.9% |

3.6.6 The appearance of activation energy change

Figure 3.32 shows the Arrhenius plot of ln K vs 1/T for measured values of Mg obtained and for Ni catalysed material under a microwave field.

Activation energies for the dehydrogenation of each sample were determined by constructing Kissinger plots using different heating rates. In the Kissinger equation, b is the heating rate, t is the temperature at the desorption maximum, and E_a is the activation energy.

Equation 27

$$b(t) = b_o \exp\left(-\frac{E_a}{RT(t)}\right)$$

By plotting ln(b/Tp²) against 1/T, the activation energy, E_a, can be calculated from the slope of the straight line obtained.

This data was compared to published work from Fernandez to allow comparison with published literature values for the activation energy required for desorption. This is again clear evidence that there is a strong effect on the only the rates of reaction but also the bulk temperature at which these occur.

It is probably the most significant summation of the microwave effect showing that the energy required for the process could be significantly altered. It is, however, unlikely that the magnesium hydride is significantly destabilised by the microwave field and that the effects are largely due to a range of field surface interactions that combine to give the impression of a change in the thermodynamic nature of the reaction.

The activation energy calculated from the gradient of the best fit of the microwave treated sample indicates a value of 48.3kJ/mol in comparison with the literature values for magnesium desorption 120 kJ/mol[51] and significantly lower than the results obtained by Hanada et al at 71.3kJ/mol, who achieved desorption at 160°C using Nb₂O₅ catalysed magnesium hydride [74].

This is significantly below the 74kJ/mol associated with the decomposition of the MgH₂ phase and so is therefore probably an unreliable figure based on this methodology. The methodology relies on a single factor being the rate determining step and if the rate determining step is a balance between

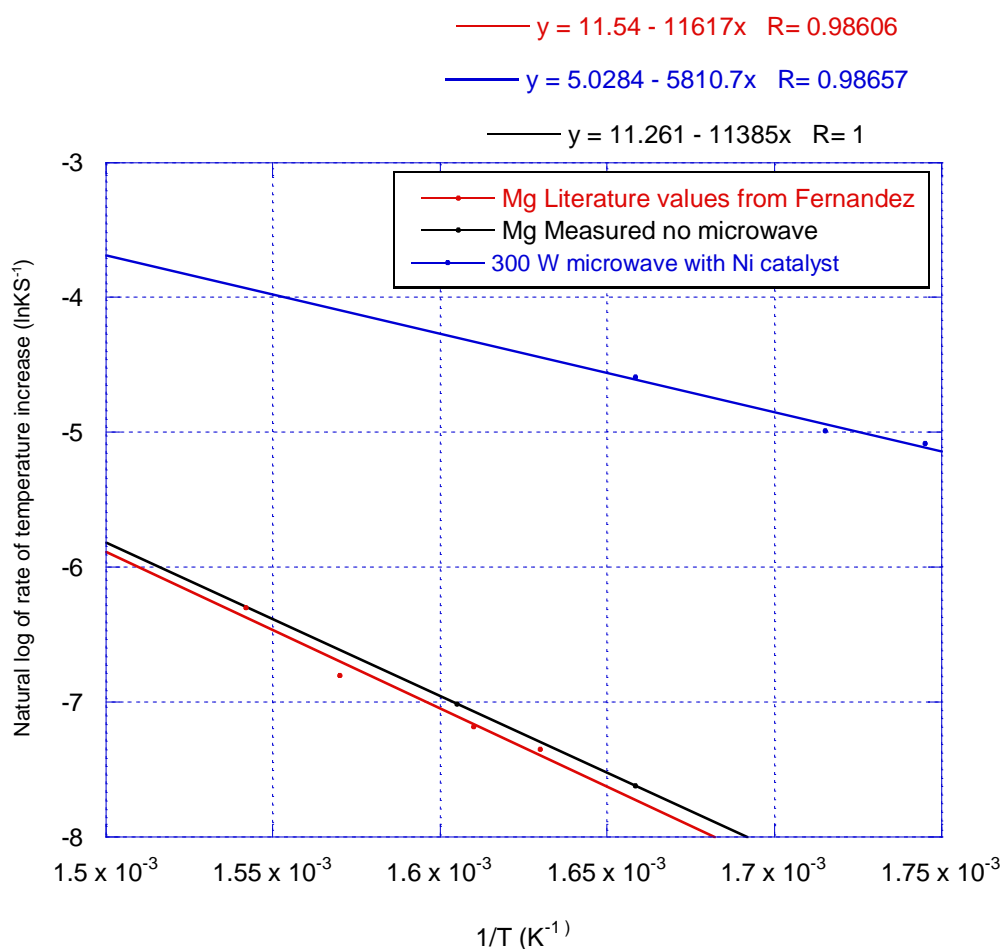


Figure 3.32: Comparison of $\ln K$ values for the calculation of activation energy from the onset temperature of desorption in at a range of ramp rates.

3.6.7 The effect of microwaves on other hydride systems

The effects of the microwave field on both the absorption and desorption of hydrogen from magnesium are clear and repeatable, with effects that are unusual in the published literature. In order to extend the work it was interesting to see if these effects transferred to other materials that react cyclically with hydrogen.

A LaNi_5 sample was selected as an interesting next step but temperature control was found to be difficult at temperatures below 150°C due to the design of the

furnace and the plateau pressures required at elevated temperatures were significantly beyond the limits of the equipment.

A second candidate material was palladium. Although this material is not a candidate for hydrogen storage materials there are several applications where the sorption characteristics of the material are important. Palladium has some similarities with magnesium in the way in which it forms a hydride although with a far more active surface for the dissociation and recombination of hydrogen.

To test the influence of the electromagnetic field it would not be feasible to look at the desorption rate at a fixed temperature and pressure due to the rapid kinetics associated with the reactions in palladium. The system was re-configured for the monitoring of a pressure ramp at a controlled rate, changing the control factors to tune the system to give greater accuracy across a broader range of temperatures.

To run the experiment the sample was loaded into the furnace and the temperature stabilised at the set temperature with the microwave field switched on if required. The pressure was ramped up through the thermodynamic plateau pressure to assess if the reaction is affected by the microwave field in a similar way to the magnesium samples. Figure 3.33 shows this data as a plot of absorption rate in litres per minute against the pressure from 1000 mbar up to 8000mbar at 200°C. The total volume of gas absorbed by the 8g sample was relatively small in comparison to the volume of the system and this leads to some scatter in the results as the mass flow controllers increase the pressure.

The trace in Figure 3.31 shows that the non microwave sample starts to absorb the hydrogen at around 3000 mbar as the rate of the gas input changes. This is followed by an increasing rate of absorption up to 4050mbar where there is a slight shoulder in the absorption followed by a further increase in the rate up to a peak of 0.179 at a pressure of 5000mbar. After this point the absorption rate drops significantly as the material reaches saturation with the hydride phase.

The sample exposed to the microwave field was treated in the same conditions but with a 300W microwave field, again the temperature was allowed to stabilise prior to increasing the pressure. In this circumstance the sample started to absorb hydrogen at 3520mbar, around 500mbar higher than the non microwave sample, with the rate peaking at almost the same flow rate and at around 5350mbar. The upward shift in the curves was again repeatable and the fibre optic temperature measurement used for these experiments indicated no significant shift in temperature during the exposure to the microwave field. However, the observed effect could still be the result of a temperature measurement error as the required increase in temperature for the discrepancy is less than 10°C.

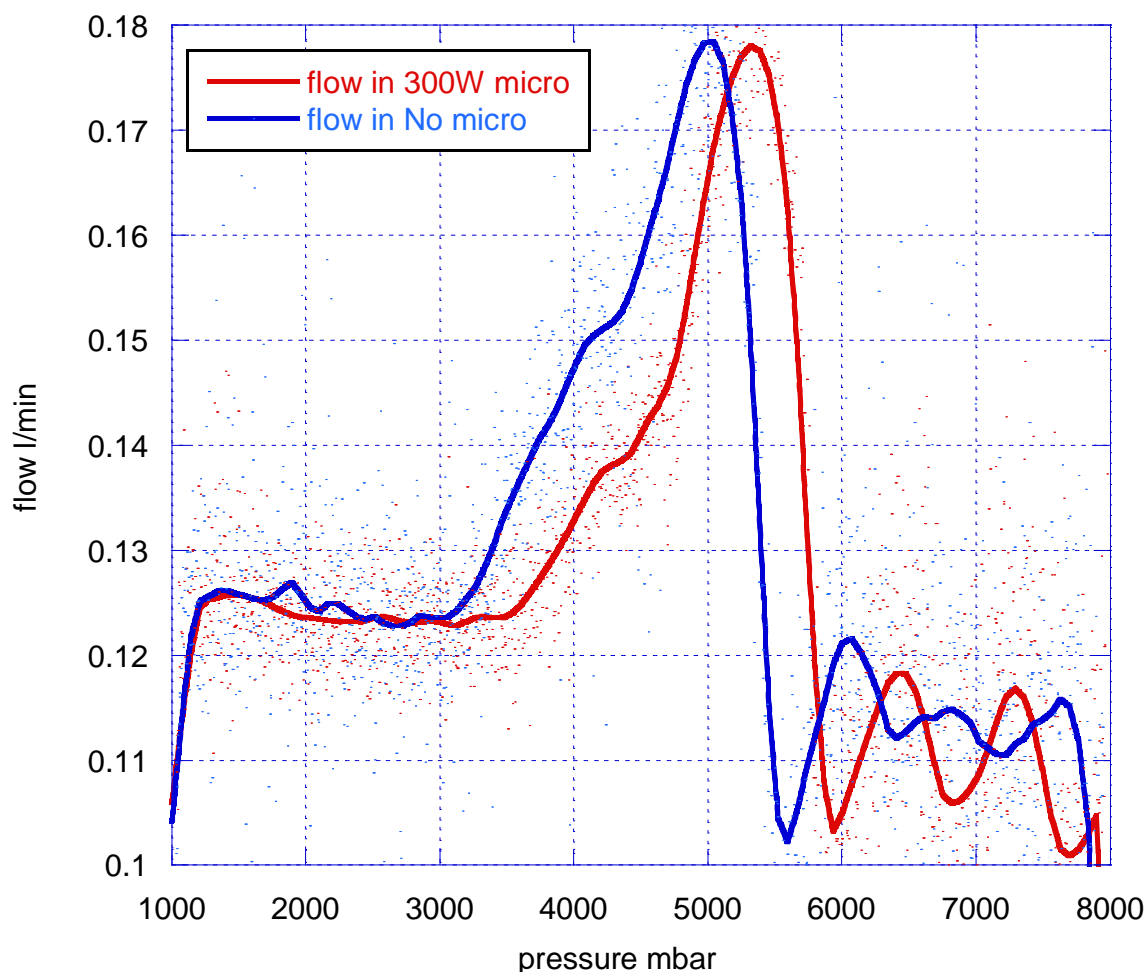


Figure 3.33: Hydrogen absorption rate of palladium at 200°C with increasing pressure with and without 300W microwave field.

The desorption behaviour of the palladium also show a variation in the rates of gas evolution with the presence of hydrogen as the pressure is lowered with a microwave field in place (from 8000mbar to 1000mbar at 100mbar/min).

Without a microwave field present there are two peaks in the desorption trace, which are believed to correspond to the initial desorption corresponding to the decomposition of the hydride phase and the second to interstitial hydrogen in the crystal. The first peak is around 3400mbar and the second at around 2400mbar.

Unlike the absorption data the addition of the microwave field does not shift the pressure at which the peaks in the desorption occurs but changes the relative

height of the peaks suggesting either a change in the structure of the material or a subtle change in the mechanism of desorption. As Figure 3.34 also shows, the temperature variation throughout the experiment was small with no significant changes around the desorption that could indicate significant thermal cause for the observed effects. There is a small variation in the observed temperature but even at extremes the temperature remains within $\pm 2^{\circ}\text{C}$ of the set temperature.

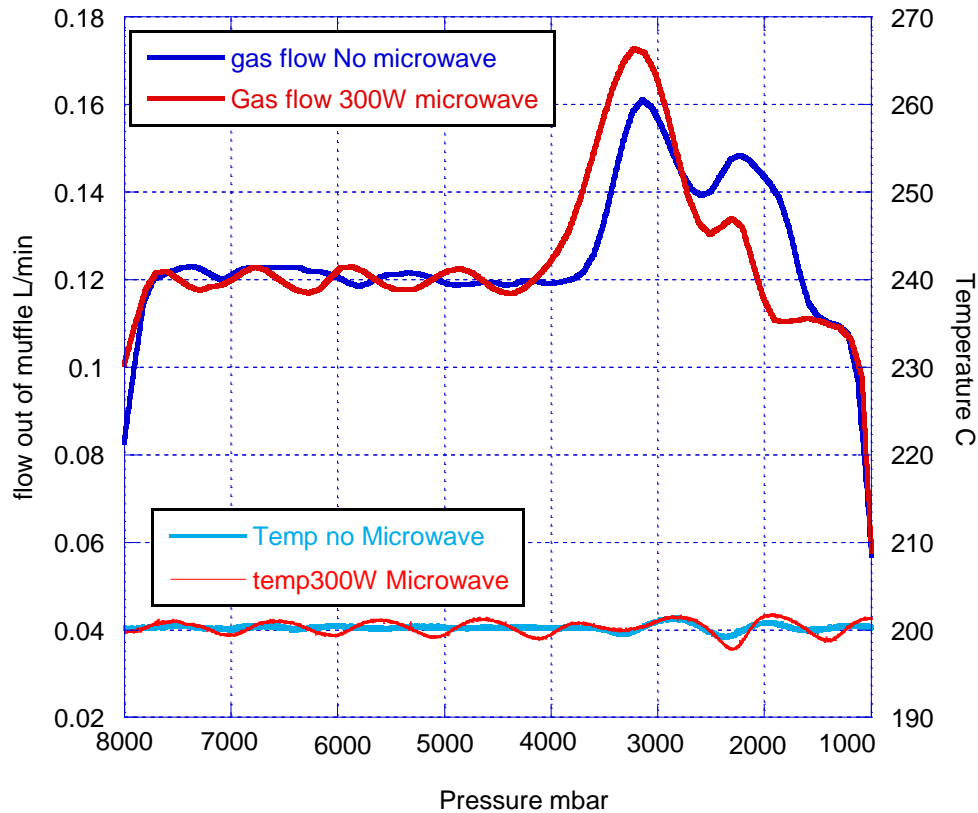


Figure 3.34: Desorption of Pd at 200°C with pressure reducing from 8bar to 1bar at 100mbar/min

In order to assess the impact of the pressure reduction rate, the rate was increased from 100millibar per min to 300millibar per min. This has had the impact of removing the definition of the two peaks and formed just one that starts and stops around the same pressures as the start of the 1st peak and the finish of the 2nd peak (Figure 3.35).

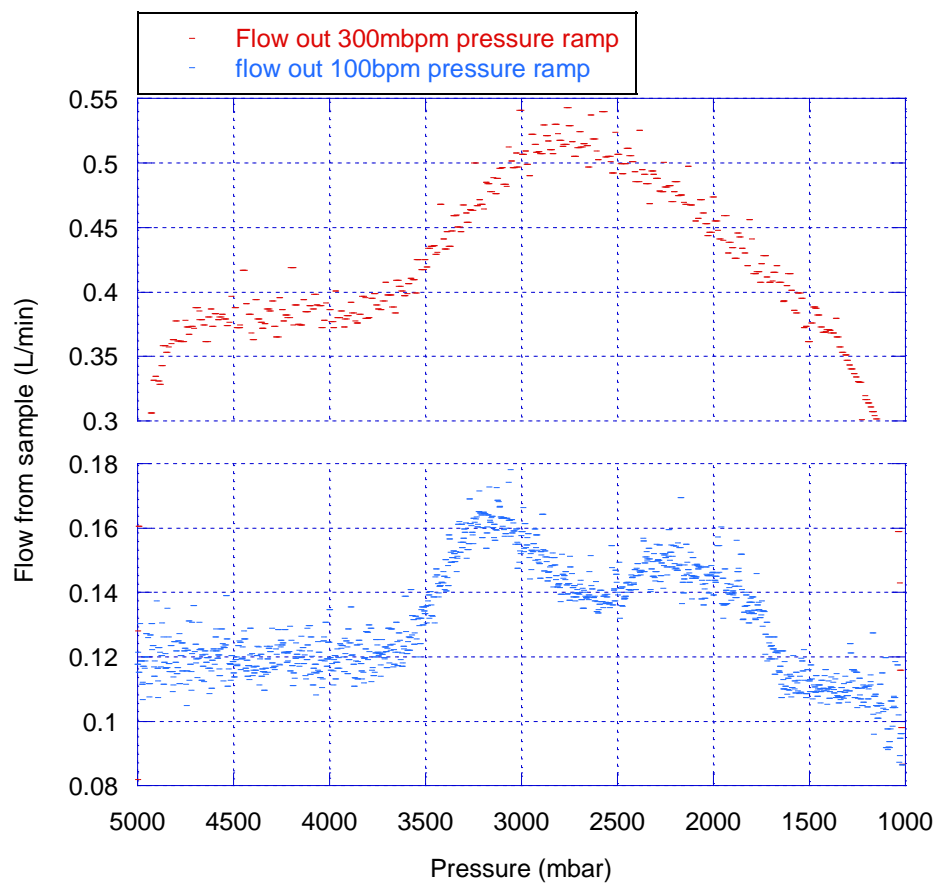


Figure 3.35: Desorption of Pd at 200°C with pressure reducing from 8bar to 1bar at 300mbar/min compared to a pressure reduction rate of 100mbar/min

4 Discussion of results,

The results of the experiments looking at the effect of microwave fields on the absorption and desorption of hydrogen offer some interesting and unexpected results.

The equipment developed in this work has allowed the first studies of these effects for the full absorption and desorption cycle under a microwave field. The published literature both academic and patent studies have briefly mentioned increased rates of desorption reactions under microwave field but there is no published work that has successfully been able to show the effects observed in this work.

It is also believed that the microwave system used in this work was the first controllable system for temperature and pressure with a fixed microwave power which has also allowed the study of the absorption reactions under a hydrogen atmosphere.

Prior to the start of this work it was expected that like many of the applications of microwave fields there would be an increase in reaction rate for the materials under a microwave field. There are previous studies that have identified advantages in using microwaves which include increase in reaction rate that can be aligned to either an increase in localised surface temperature[81] or increased diffusion rates[100] that would directly relate to improved use of hydrogen storage materials in commercial applications. If the dual aims had been achieved then the commercial interest in the technology would be high as the reduced operation and associated energy costs would be a significant advantage.

The choice of magnesium as the main material chosen for the study links to these hopes due to the low material costs and possibilities for widespread applications if the kinetic hurdles could be overcome. However the interplay of diffusion, vacancy distribution, phase changes, surface reactivity, and surface

contamination effects that all affect the reaction rate lead to some interesting areas of discussion with regard to the effects observed in this work.

The two effects to be discussed further are the increase in desorption rate and the significant reduction in the rate of the absorption reaction under a range of conditions.

In all of the desorption reactions whether the material was just milled magnesium hydride or catalysed with either nickel or iron there was a significant increase in the peak desorption rate and a reduction in the time for the reaction to reach completion. The effect was substantial and allowed reaction rates increases of over 1000% for the milled magnesium samples.

The effect of the microwave field on the absorption was also significant with the field causing a reduction in the reaction of the magnesium with hydrogen to practically nil even with significant over pressures of hydrogen and at temperatures 100°C below the thermodynamic equilibrium. This effect is not easy to explain as the measured temperature of the samples remained constant for prolonged periods without the material chemisorbing hydrogen.

It is possible that the changes in the reaction kinetics for both the absorption and desorption reactions are related to the same physical phenomenon, as the reaction is reversible in nature and follows very similar reaction paths.

Possible causes of the changes in reactions could be linked to;

1. Increasing the temperature of the sample
2. Changes in diffusion rate
3. Promotion of one reaction direction beyond parity
4. Changes in the physical structure of the material

4.1 *Temperature measurement*

The first issue to consider is the temperature of the material. This is important as without a good understanding of temperature it is very difficult to determine the causation of any observed effects. In all of the experiments this was the first consideration and extreme care was taken in ensuring that the possibility of inaccurate temperature measurement was accounted for. With a microwave field it is often found that the sample will heat faster than the surrounding atmosphere or the device measuring the temperature will heat preferentially. To counter these effects 2 methods were used; firstly the temperature of the sample was measured with a probe in contact with the material ensuring that the heating of the sample was taken into account, secondly during the experiments the field was momentarily removed and if the device is heating preferentially the low thermal mass of the thermocouple or fibre optic probe will cause the measured temperature to rapidly drop. During this work we found no evidence that the thermocouple was heating and the switch to the fibre optic system developed in the project with OPSENS only increased our confidence in the results.

However the nature of the heating effect within the material does suggest that there could be a thermal influence on the reaction, as was noted the dielectric losses of the materials at temperature varied according to the phase of the material with the metallic phase showing a greater overall loss than the hydride phase.

This can have an influence on the reaction if parts of the sample are heated preferentially generating localised hot spots that can give the appearance of reactions occurring at lower temperatures than would usually be expected. This is a common problem with microwave chemistry as it is difficult to accurately map thermal variations over the scale of microns between one point on a particle and another. This effect can lead to erroneous claims of non-thermal microwave effects which are very hard to disprove but suggest that the microwave changes the thermodynamics of the system can often be ruled out as infeasible. This effect is also one of the key aspects in heterogeneous catalysis where greater

selectivity of catalyst structures can be associated with local hot spots on the surface (ref catalyst).

The observed effects on the desorption could be regarded as a temperature effect with the increasing metallisation of the particles as the Beta phase transforms causing increased localised heating. This could explanation could fit for the un-milled material where there is a time of very low desorption at the start of the reaction before a metal surface is generated. Interestingly this would seem to fit with the mechanism proposed by Evard et al that the rate limiting step is the recombination of the hydrogen molecule on the magnesium hydride surface and that once a metal surface forms the activation energy for the recombination step is reduced[24].

This does not however, explain the observed effect satisfactorily as the measured temperature remains constant. Further, the addition of metal catalysts on the surface should remove some of the surface effects and yet with nickel it a significant increase in desorption rate with the microwave field was still observed.

The absorption reaction is also affected by temperature with an increasing temperature increasing the plateau pressure of the hydride and therefore changing the balance of the system. The observed effect on the absorption whereby the reaction was completely stopped by the application of the microwave field does not fit with the hypothesis of localised heating. The experiment that best illustrates this effect is the where the sample is held at 270°C for 50 minutes under a 300W microwave field without the absorption reaction occurring. This temperature is 100°C below the thermodynamic equilibrium of the material and yet there was no observable increase in temperature during the experiment. If the microwave field was heating the sample locally to above the plateau pressure, the heating effect would have to be stable over the entire surface to prevent the absorption. This thermal gradient of 100°C would then be sufficient to rapidly heat the bulk of the material. The rapid heating of the material was not observed and it is therefore unlikely that the

cause of the absorption behaviour under microwave fields is wholly related to thermal effects.

4.2 The effects of the microwave field on the desorption of hydrogen

Once the thermal effect has been ruled out as a significant cause of the increased desorption rate observed in all of the samples, when exposed to microwave fields, then it is the potential influence of the electromagnetic field on the physical interactions associated with the desorption process.

The desorption in magnesium is a process that has been associated with several theories of rate determining step and the kinetic model that best describes the process.

As discussed in the introduction the overwhelming majority of researchers use the Avrami equation to estimate of the kinetic parameters of the reaction, however this simplified approach is only justified if a single rate limiting step is the dominant factor throughout the reaction.

The variation of opinion on the rate determining step for samples produced in various ways and with different catalytic additives suggests that several steps in the desorption process in magnesium can be rate limiting depending on the specific conditions of the experiment. Desorption could be diffusion limited if the particle size is large or surface recombination limited if the material is milled to induce a fine particle size with significant crystallographic disorder.

In the case of un-catalysed magnesium hydride, that one mechanism for example the diffusion rate was the limiting factor, we would expect a monotonic curve with the maximum rate at the start followed by a decreasing rate throughout the process.

If the rate limiting step was the surface desorption then as a greater proportion of the surface becomes the more active metallic surface, the rate would be expected to increase throughout the desorption. As this effect is not observed with either the pure milled magnesium or with either of the catalysed materials it would be reasonable to conclude that the rate limiting step is not a single process throughout the desorption.

It is possible that the JMA model of nucleation and growth could fit the observed results with the rate of reaction reaching a peak around halfway through the desorption. The work by Fernandez et al[23], analysing the desorption curves, and in situ X ray diffraction by Jenson et al[25], However in these studies it was not possible to distinguish between the possible mechanistic factors and results of could equally be consistent with constant nucleation and a growth control by diffusion rates or fast initial nucleation with a process that is dominated by the two dimensional interface growth. Figure 3.35 shows the theoretical model of a monotonic and JMA based reaction kinetics alongside the equivalent plot for the desorption of magnesium under a microwave field. Although the plots share some similarities it is clear that the real data does not clearly match either of the two more straight forward models of the kinetic reaction. In the data collected under the microwave field the initial rate increase is slow but followed by a change in the nature of the rate increase that accelerates and could indicate the change in the rate limiting step for the material.

.

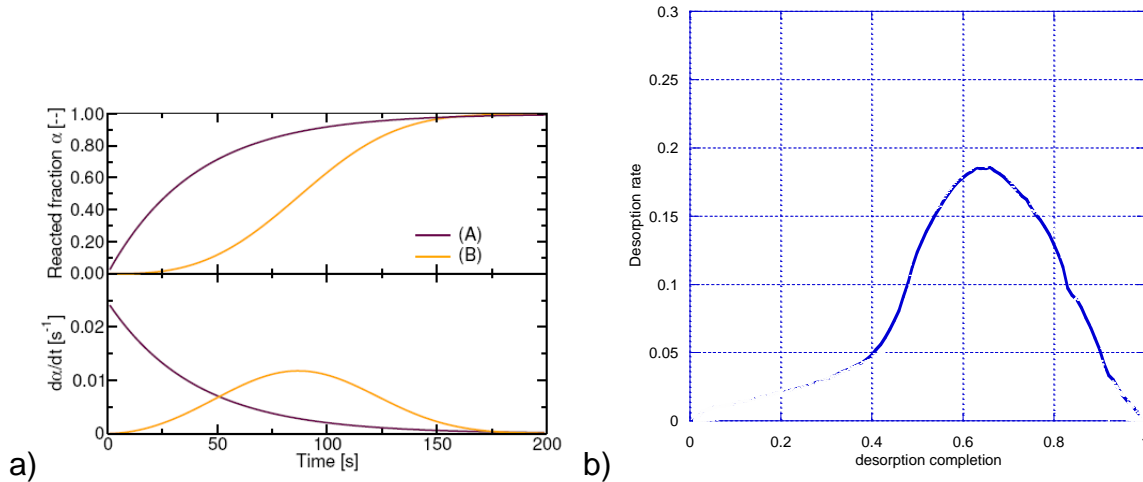


Figure 3.36: a) Graphical illustration of the hydrogen uptake kinetics (above) and hydrogenation rate (below) for the a diffusion limited and b nucleation and growth limited hydrogenation and dehydrogenation curves[25] b) shows the measured desorption rate under a microwave field for milled magnesium at 330°C

The change in the rate limiting step under a microwave field could be consistent with the models developed on the premise that the reacted fraction of the hydride was a key variable, suggested that the rate-controlling step for the desorption of magnesium hydride is the interface chemical reaction at the β to α phase boundary[47, 124]. Evard et al[24] have subsequently extended the work Han and looked at the formation of magnesium islands on the surface of the particles and the relationship with the rate of desorption. They found that the desorption kinetics can be explained by the fact that not completely hydrogenated magnesium has metallic islands reaching the surface of each powder particle.

These serve as an easier channel of desorption than the surface of the hydride phase. This hypothesis could be added to surface modelling of the recombination of the hydrogen molecule on a magnesium hydride surface by Vegge [41]; which shows that the desorption from the surface of the hydride can be a slow process due to the high activation energy.

4.2.2 Changes in diffusion rates

It is possible to theorise that the change in the rate limiting step could be the point at which the surface become sufficiently active for the diffusion processes

to limit the reaction, at which point the microwave field may have an effect on increasing this rate. The evidence for this can be found in the nickel catalysed samples which do not display the slow initial start to the desorption reaction, due to an improved surface, and so therefore are limited by the diffusion and phase boundary movement.

The desorption rate in the Ni samples in both the non-microwave treated samples and the microwave treated samples show similar curve shapes with the increase in the peak desorption rate between the two conditions smaller than in the non-catalysed samples.

The reduction in the calculated activation energy for the material under the microwave field would suggest that under the microwave field the nickel catalysed sample has an activation energy similar to that calculated for the recombination of hydrogen. This suggests that at this point the diffusion has increased under the microwave field to such an extent that it is no longer rate limiting for the reaction. Further evidence that the surface is the key factor is that the ranking of the three sample types (pure Mg, Fe and Ni catalysed) in terms of peak desorption rate with and without the microwave field remains the same, with nickel the highest followed by iron and then pure magnesium.

The close performance of Fe and pure Mg indicates that the poor catalytic surface of the iron behaves as expected increasing the reaction rate only slightly. The movement of the peak of the desorption to slightly earlier in the reaction for Fe catalysed material suggests that the mechanism of preferential pathways as described by Evard et al may be correct and that the delay for the un-catalysed magnesium sample could be a result of this effect[24].

The peak rate of desorption from the samples corresponds to a mass change rate of around 0.01wt%/second, this can be compared to the results on the maximum desorption rates obtained for transition metal oxide catalysts including Nb_2O_5 which has been repeatedly shown to have the best kinetics of magnesium materials[30].

In these cases the samples were produced and tested under widely different conditions being milled using high energy milling for 100 hours to increase the crystalline defects and reduce crystallite size and tested under either high vacuum or into pure helium with a zero partial pressure of hydrogen.

Taken directly the results from this work would rank alongside the scandium oxide in the graph below (Figure 3.37), however the desorption into a zero partial pressure of hydrogen should increase the kinetics of the surface reaction and if the diffusion is not limiting under the microwave fields could lead to a significant improvement.

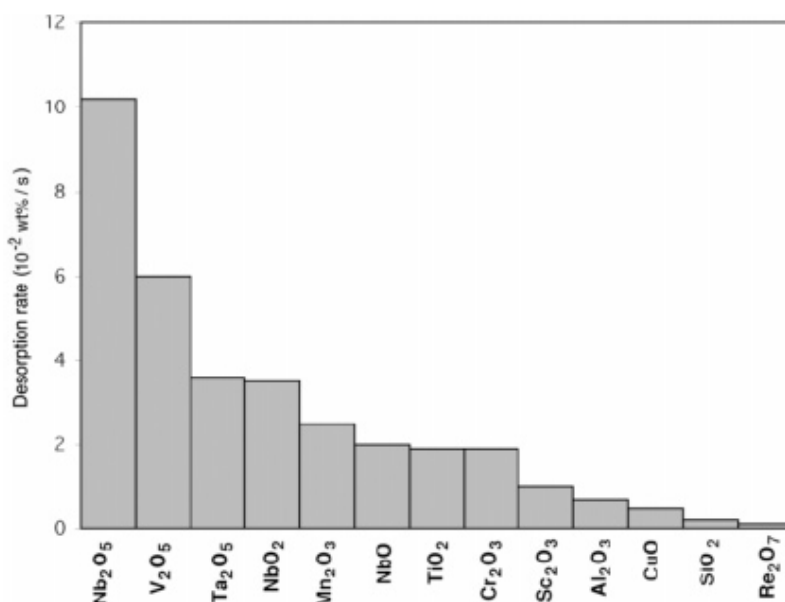


Figure 3.37. Comparison of transition-metal oxides and their catalytic effect on the hydrogen desorption reaction rate of magnesium hydride at 300°C. (calculated between 20% and 80% of the respective maximum capacity.)[72]

Again one of the key costs in commercial production is the high energy milling which is an extremely energy intensive and slow process, if 100 hours of milling is required for every sample then all of the cost advantages associated with using a readily available material such as magnesium would be quickly nullified. If the use of a microwave field can induce a increase in diffusion without the requirement for nano-structured grains and crystallites with significant

deformation there could be a strong economic argument for the application of microwave assisted hydrogen stores.

4.2.3 Changes to the reaction equilibrium

The large change in activation energy observed for the desorption with the use of Ni catalyst and microwaves suggests that although there was no macroscopic variation in the measured temperature from the use of the microwave field it is likely that there were temperature effects occurring in the material.

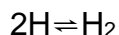
This could be mechanisms such as thermal gradients due to preferential heating of the phase boundary interface, preferential heating of the surface or the metallic phase. All of these options are possible but the determination of the outcome is difficult due to the small scale of these areas and the complexity in trying to understand and model such a complex system.

It would be interesting to model the possible mechanisms that result from the dielectric heating mechanisms but due to the inaccuracies in determining the dielectric properties of the materials, the complexity of modelling a field passing through a powder of varying density, and the constantly changing mixture of the hydride and non-hydride phase as the endothermic reaction takes place it is very difficult to foresee that any theoretical model of the system could approach a realistic simulation.

It is possible to conceive in concept that the equilibrium rates of the reactions are changed by this effect which would manifest in the direction of the reaction progressing more rapidly than would be expected for a set of conditions.

For example the surface recombination of the hydrogen molecule is a balance between H_2 molecules being formed at the surface and others dissociating to $2H$. If the conditions are favourable the chance of a molecule recombining and leaving the surface are higher than the reverse and so the reaction proceeds in a direction favoured by the thermodynamics. The rate of the reaction is therefore

the sum of the reactants moving in one direction minus the reverse reaction happening.



If for example the electromagnetic field interferes with the reverse reaction in this case the dissociation and therefore slows down the reverse reaction it would be expected that the overall effect observed is an increased rate of reaction.

This is given further strength by the change in reaction rates during absorption where the effect could be explained by the reduction in rates of dissociation of the H_2 molecule due to the field effects.

4.2.4 Physical changes in the material structure

The variation in distribution of the electric field and the specific heating of the material at the interface between the alpha and beta phases could result in some of the effects we observe.

The concentration of electric field at interfaces between materials with different dielectric properties is known and interfaces are often associated with excess heating in the design of microwave systems. The ponderomotive effect is one explanation for increased sintering rates achieved with microwave fields and it is argued that the concentration of fields at interfaces has a significant impact on the vacancy distribution[106,107].

Further the interface transition has been highlighted as a possible energy barrier in the process and the direct heating of the interface could induce some of the performance improvement. Further to this the direct heating of the material may account for the drop in the measured activation energy, if a proportion of the energy from the microwaves is being directly or indirectly consumed in the endothermic decomposition of the MgH_2 then this would not be indicated by the measurement of the sample bulk temperature. This leads to the requirement to understand the total amount of energy in the material rather than using the bulk

temperature as a measure of the energy. From the measurement of the energy transfer from the microwave field to the samples with no reaction occurring that there is around 0.01- 0.04 W/g transferred by the dielectric loss mechanisms depending on the phase. At the peak desorption rates observed in this work the decomposition of the MgH_2 requires around 0.14 W/g based on an enthalpy of 74kJ/mol. Therefore the microwave energy transferred to the material could be absorbed by the material and transferred to the endothermic reaction without having an increase in the temperature of the sample.

The only effect would be to reduce the amount of energy required to be transferred from the radiant heating elements and the conduction mechanisms. These effects could align well with the observed data and suggest that the use of microwaves could be an efficient “heating” methodology that through the nature of the reaction provides a significant improvement in overall kinetic activity.

4.3 Absorption kinetics,

The hypothesis that the microwave field would assist the diffusion of hydrogen in the formation of the magnesium hydride was found to be inaccurate. The reaction rate was observed to drop significantly when a microwave field was applied and the effect was observed on the absorption reaction of the magnesium both with and without a catalyst.

4.3.1 Microwave enhanced diffusion

The observed reduction in absorption reaction rate was both strong and effective at relatively low field strengths. This does not fit the hypothesis that a microwave field does not interrupt or change the reaction path but will assist the reaction rate by acting to increase the diffusion rate. This clearly shows that the diffusion is not the rate determining step in the reaction under the microwave field.

4.3.2 Temperature effects

The nature of the absorption reaction is exothermic and therefore it is unlikely that a similar localised heating effect speculated in the desorption results would

be easily identified. The most obvious cause of the effect would be excess heating of the sample which would take the material above the plateau pressure of the surrounding gas and prevent the absorption. However there was no measurable temperature increase in any of the experiments, independent of the measuring technique used.

If the surface heating was affecting the results then logically overtime the thermal gradients would cause the bulk temperature to rise, this would be the case even if a substantial amount of the energy was passed back to the surrounding gas. It is therefore unlikely that errors in the temperature measurements or excess heating are the root cause of the observed effects.

4.3.3 Changes in the surface gas interactions

In materials such as Palladium there have been models developed for the dissociation of the hydrogen molecule on the surface which require the coalescence of vacancies in order to reduce the activation energy for the process. Mitsui et al describe the surface interactions on Pd by using scanning tunnelling microscopy to highlight the changes in the surface. They observed that during reaction, a catalyst surface usually interacts with a constantly fluctuating mix of reactants, products, 'spectators' that do not participate in the reaction, and species that either promote or inhibit the activity of the catalyst.

The creation of active sites for H_2 dissociation will thus involve the formation of individual vacancies and their subsequent diffusion and aggregation with the coupling between these events determining the activity of the catalyst surface. It was found that a minimum of 3 vacancy sites adjacent to each other were required for the dissociation to take place[125].

As vacancies in a lattice can act as charged points it may be feasible that the electric field strength of the microwave field disrupts the coalescence of these sites reducing the activity of the surface. This is one of the theories used in support of increased diffusion in sintering studies, but as the experimental

observation of such effects in more standard processes are extremely difficult it would be challenging to expect these to be undertaken at high temperature under a pressure of hydrogen and with a microwave field present.

There is the possibility that this may be analogous to the effect in the desorption where a possible explanation is the change in the equilibrium rates of the reactions are changed by this effect which would manifest in the reaction not proceeding as expected. This could be the surface interactions as previously discussed or a step in the reaction sequence such as that of the formation of the magnesium hydride phase from the alpha solid solution. As previously mentioned if the electromagnetic field interferes with the reaction and reduces the probability of the dissociation step it would be expected that the overall effect observed is a significantly reduced rate of reaction.

4.3.4 Changes in the structure of the material

Given that the effect of the microwave field on slowing the absorption reaction is strong in both the un-catalysed magnesium hydride and the nickel catalysed magnesium a surface reaction is possible but it is perhaps also relevant to consider the other steps in the absorption process.

Another explanation could be the formation of intermediate phases that have much higher dipole moments than the hydride structure. During the initial penetration of the hydrogen atom into the surface there are structures formed in the sub surface layers where monatomic hydrogen nuclei pass through the surface atomic layers of magnesium.

At this point it is possible that the electric field either imparts a force on the material preventing further diffusion or the dipole moment of the structure is such that there is very rapid localised heating. There is no evidence in the data collected on the dielectric measurements of an effect such as this but as these were taken at under argon at room temperature with no reactions being undertaken this is not unexpected.

Additionally this effect would be localised to an atomically thin section of the surface which would constitute a fraction of the volume of the material, so it is therefore unlikely that even measuring the bulk dielectric properties at realistic conditions would provide much information.

4.4.4 Other possibilities

Due to the difficulty in finding evidence in the literature of this type of effect it has been interesting to look at some more obscure areas that are well outside the scope of the project, these have included looking at spin polarisation which can be changed by photons of a microwave frequency. The hydrogen atom has a higher energy if both are spinning in the same direction, and a lower energy if they spin in opposite direction, but are unlikely to lead to strength of the observed effects as the changes in energy state are very small. This was interesting as it is one of the few quantum changes that can be associated with microwave photons. The energy change in spin polarisation is only 5.9×10^{-6} eV, which is comparable to the energy of a microwave photon at 2.45 GHz which has an energy of 1.624×10^{-24} J or 1.014×10^{-5} eV.

This was an interesting observation but there was little information published to suggest that this effect could change the reactivity of hydrogen or affect the dissociation of the molecule sufficiently to give the observed effects.

4.5 The effect of microwave fields on the reaction of Palladium with hydrogen

The extension of the work to look at other systems hoped to give a further insight on the nature or cause of the effects in magnesium. The reactions of hydrogen with palladium are far faster due to the very active surface for the dissociation and recombination and the fast diffusion through the materials which make palladium ideal for purification membranes. Based on the previous work with magnesium it was thought interesting to look for parallels in the absorption reaction under a microwave field to the limitation of the reaction in magnesium.

The absorption reaction for palladium under a microwave field was found not to be significantly affected, with the onset of the absorption displaced to a slightly higher pressure, although with the reaction kinetics showing a similar rate to the non microwave treated absorption cycle. This would seem to indicate a change in the thermodynamics of the system but taken in isolation the small change in the pressure of the absorption is of little significance as this could be accounted for by a small change in the temperature of the sample of less than 5°C and so would therefore be within the error of the measurement techniques.

More interesting is the behaviour of the palladium during the desorption cycle, where, as the pressure of the atmosphere is lowered, the microwave field affects the relative size of the two desorption peaks. Changes in the size of the peaks have been observed and found to correspond with the hydrogenation conditions used to prepare the sample. The sample preparation and cycling was identical for each of the microwave and non microwave desorption cycles and the effect consistent, indicating that the microwave field may be impacting on the structure of the hydride. However, the effect was not long lasting as hydrogenation and non microwave desorption directly after the microwave cycle failed to show a lasting effect.

4.6 Conclusions

There is a strong and consistent effect on both the absorption and desorption of hydrogen from magnesium whether the material is catalysed or not.

The effect on the desorption is a significant increase in the peak desorption rate which has been increased by over 10 times for pure milled magnesium hydride when compared to the non microwave treated sample. The effect scales with microwave field strength and is controllable to the extent that removing the field slows the reaction rate back to that on a standard non-microwave process. This effect would appear to change the kinetics of the desorption and to change the rate limiting step; however, the nature or cause of this effect has not been clearly determined.

The absorption reaction can be caused to stop entirely under an over pressure of hydrogen of and conditions that would allow readily allow absorption. The effect is controllable as when the microwave field is removed the absorption reaction starts almost instantaneously with no measured change in temperature and reducing the microwave field below a threshold value reduces the effect allowing the reaction rate to increase proportionally.

The maximum microwave energy transfer (300W forward power) was measured at 0.01W/g for the hydride phase material and 0.04w/g for the metallic phase; this suggests that the requirement for a useful hydrogen store for transport applications using around 100kg of magnesium would require a total microwave power of 1-4 kW.

4.7 Future work

The key objective of any future work should be to further understand the nature of the relationship between the magnesium hydride formation and decomposition reactions with the microwave field. Now this effect has been established but not explained the use of in situ monitoring of the formation and decomposition could be useful to highlight how the microwaves effect the desorption reaction. This work should also build upon further understanding of the reaction mechanism for the desorption of hydrogen from magnesium and it may be possible with further study to use the effects under a microwave field to help isolate the key steps in the reaction process. This may involve studies such as in-situ neutron diffraction to monitor nucleation and growth of the phases and if this process is affected by the microwave field.

The absorption effects could be further elucidated by more accurate gravimetric measurements of the uptake at very low rates under a microwave field. This measurement technology may show if the absorption reaction is stopped completely or just below the measurement accuracy of the systems developed in the project.

Further work is under development at C-Tech Innovation to find other uses for the technology in heterogeneous catalysis systems that may have kinetic limitations. This work may start to identify common reaction types or processes between the systems that show which types of process are most susceptible to the microwave field effects observed in the project.

4.8 Future applications

Hydrogen is not seen as a likely storage medium for energy until a suitable reversibility is found in chemical structure over 10 wt% due to system weight and cost of fuel cells. Batteries with range extenders are viable for transport applications at this time. For stationary storage, flow batteries are a cheaper and more extendable option and if there is no weight penalty then other material options for hydrogen storage materials are available. These include LaNi_5 type materials which have larger storage capacities in volume terms, are easy to control, but are heavy. Additionally the cost of hydrogen is still linked to the price of natural gas as the major supply source and without significant increases in the production of electricity it is unlikely that the costs of electrolysed production of hydrogen will come down.

If materials with high weight % but slow desorption kinetics are developed, then microwave assisted processing is a relatively easy thing to test and engineer into a system that offers a viable transport solution, however, the increase in kinetics with a microwave field does not solve the fundamental problems with energy storage in metal hydrides.

For C-Tech Innovation, the technologies and methods developed in the project have been extremely useful for the company on a commercial level and have allowed the development of new products and services. The requirement for dielectric properties under a range of conditions started an investigation into the measurement techniques of dielectric properties at elevated temperature. This work has lead to the development of systems and techniques that could be used for future projects and made commercially successful as a service for customers.

The pressurised muffle system developed in the project for use in the hybrid microwave furnace has been further developed and is now available as a product of C-Tech Innovation's Industrial Products Group. Following this project both the furnace design and dielectric measurement experience has been applied under an EU program looking at reducing the energy required in high temperature processing.

Heterogeneous catalytic reactions are being assessed to look for viable opportunities where the effects observed in this work can build upon experience to find viable applications for the technology. This exploration is looking for analogous situations where surface effects that increases or changes the selectivity of recombination reactions as this may have implications for other chemical processes. One avenue currently being examined is the effect on ammonia reactions and other metal or metal oxide catalysed reactions where selectivity of one form over another could produce a strong positive effect on the production of these materials.

5. The Effect of Microwave Fields on the Hydrogen Decrepitation of NdFeB Type Materials

5.1 Objectives and Business case

This work aims to assess the effect of microwave radiation on the decrepitation rate and hydrogen absorption profile of high energy product magnetic materials, such as Neodymium Iron Boron (NdFeB). The work will look at the effect of microwave power and exposure time to a microwave source in a multimode cavity. In addition this work will attempt to explain the effect of microwave treatment and to understand material-field relationships that are the foundation for this effect.

The price of NdFeB has increased dramatically in recent years due to increased markets in electric motors, wind turbines and hard disk drives. Hydrogen decrepitation is one of the few viable methods for the separation and recovery of the materials prior to recycling. China currently produces 97% of the worlds supply of these materials and there is a strong investor interest in technology or processes that can reduce the dependence of the EU and USA on these politically sensitive supplies.

If microwave processing can assist in the efficient recovery of these materials there would be significant opportunities to exploit this technology globally.

5.2 Introduction to rare earth magnets

Neodymium Iron Boron (NdFeB) type high energy permanent magnetic materials are currently used in a wide variety of applications and offer the highest energy product of any magnetic material. The energy product is in excess of one hundred times greater than that of ferrite magnets based on iron oxide systems. A report by Powdermatrix in 2004[126] listed NdFeB as accounting for around 30% of global permanent magnet sales in an industry estimated at \$4.5B-\$5B

per annum, with projected growth for high energy magnets of 12-15%. The main drivers for growth were listed as:

- Materials development, producing an increase in energy product and reduction in cost of materials.
- Economic drivers, for increased efficiency and new product development.
- Environmental drivers based in legislation concerning carbon dioxide emissions.

High energy magnets are commonly found in many modern applications that include: permanent magnet electric motors, hard disk drives, actuators, alternators, automotive starter motors and microphones. Automotive applications will be of growing importance in the near future with the expected growth of electric and hybrid vehicles due to concerns over current energy costs, pollution and to legislative changes. An example of this trend is the Toyota Prius hybrid electric vehicle, which uses about 2kg of NdFeB magnetic material in every vehicle, in an application that would not have been commercially viable in the past.

Material recycling is an important aspect in the future use of all materials. This is particularly pertinent in the case of automotive applications where “end of life” rules within the EU are already being implemented. The recycling of these materials may be an extra expense for both the manufacturer and the consumer, so industry is looking for materials and processing routes to aid recycling. These measures are justified in terms of the environmental impact (metal contamination of land-fill sites), energy saving (CO₂ reductions) and resource depletion.

In the case of NdFeB the hydrogen decrepitation process (already employed extensively in NdFeB magnet production) may provide a cost effective option for the recovery of magnetic material in the recycling process. The hydrogen decrepitation process causes the break up of magnet from a solid block into a powdered hydride as the hydrogen is absorbed. The hydrogen decrepitation

process allows the possibility to recover the magnetic material from a device (e.g. hard disk drive or electric motor) without disassembly. This would be achieved by simply exposing the complete system to a hydrogen atmosphere in a specially designed chamber. It is likely that the only material in the system to be decrepitated by hydrogen would be the sintered magnet, thus allowing the powder to fall out due to high hydrogen absorption of NdFeB at low pressures; this process would be unlikely to affect any other material in the particular device. This would significantly reduce the cost involved in the recycling and allow the material to be removed from complex geometries without dismantling. Because of the avoidance of additional oxidation powder (extracted) would not require extra processing before being returned to the manufacturing process.

5.3 Literature Review

5.3.1 Magnetic materials

The intrinsic principle behind magnetism is that any moving charge produces both a magnetic field and changes its motion in response to an external magnetic field. Examples include electrons in a television tube or current flowing in a wire. Electrons within atoms also possess a property known as spin; quantum mechanics has shown that spin can behave in two ways, either spin up or spin down. When there is a net spin imbalance of spins up and spins down within an atom, a magnetic dipole exists. Magnetic dipoles give rise to a magnetic exchange energy, which is a measure of retained magnetic moment; at room temperature the magnetic exchange energy is high in elements such as Fe, Co and Ni.

5.3.2 Origins of Magnetism

5.3.2.1 Magnetism within materials

All elements and materials show some degree and form of magnetic behaviour, as shown in the periodic table in figure 5.1. This behaviour can be categorised as one of five types depending on the interaction of the material with an applied field

either: diamagnetism, paramagnetism, ferromagnetism, anti-ferromagnetism or ferrimagnetism. These states are explored below and summarised in figure 5.2.

| <div style="display: flex; justify-content: space-between;"> 1 H 2 He </div> | | | | | | | | | | | | | | | | | |
|---|-------|-------|-------|-------|-------|-------|-------|-------|-------|-------|-------|-------|-------|-------|-------|-----------------------------------|-------|
| 3 Li 4 Be | | | | | | | | | | | | | | | | 5 B 6 C 7 N 8 O 9 F 10 Ne | |
| 11 Na 12 Mg | | | | | | | | | | | | | | | | 13 Al 14 Si 15 P 16 S 17 Cl 18 Ar | |
| 19 K | 20 Ca | 21 Sc | 22 Ti | 23 V | 24 Cr | 25 Mn | 26 Fe | 27 Co | 28 Ni | 29 Cu | 30 Zn | 31 Ga | 32 Ge | 33 As | 34 Se | 35 Br | 36 Kr |
| 37 Rb | 38 Sr | 39 Y | 40 Zr | 41 Nb | 42 Mo | 43 Tc | 44 Ru | 45 Rh | 46 Pd | 47 Ag | 48 Cd | 49 In | 50 Sn | 51 Sb | 52 Te | 53 I | 54 Xe |
| 55 Cs | 56 Ba | 57 La | 72 Hf | 73 Ta | 74 W | 75 Re | 76 Os | 77 Ir | 78 Pt | 79 Au | 80 Hg | 81 Tl | 82 Pb | 83 Bi | 84 Po | 85 At | 86 Rn |
| 87 Fr | 88 Ra | 89 Ac | | | | | | | | | | | | | | | |
| <div style="display: flex; justify-content: space-between;"> 58 Ce 59 Pr 60 Nd 61 Pm 62 Sm 63 Eu 64 Gd 65 Tb 66 Dy 67 Ho 68 Er 69 Tm 70 Yb 71 Lu </div> | | | | | | | | | | | | | | | | | |

Figure 5.1, Magnetic classification of elements within the periodic table [19]

5.3.2.2. Diamagnetism

Diamagnetism is a weak non-permanent form of magnetism whereby, under the effect of an applied magnetic field, a torque is created on the atomic magnetic dipole causing it to rotate about the field direction. This creates a magnetic field in the opposite direction, opposing the applied field and as such a material is said to exhibit a negative susceptibility. The magnetic susceptibility is a dimensionless constant that indicates the degree of magnetization of a material in response to an applied magnetic field. The proportionality of the magnetisation and its sign indicates the amount of magnetic field in the material, with perfect susceptibility being 1. Superconductors are considered to be perfect diamagnets with a susceptibility of -1 , while bismuth is the most diamagnetic element with susceptibility at room temperature of -170×10^{-6} .

5.3.2.3 Paramagnetism

In paramagnets the atomic moments align with the external applied magnetic field direction. Except at very high fields the net magnetization of the material depends linearly on the applied field.[19]

5.3.2.4 Ferromagnetism

Ferromagnetic materials exhibit a parallel alignment of atomic moments whereby the material is spontaneously magnetised without the need for an external field. This parallel arrangement can be disturbed by thermal agitation, with the spontaneous magnetism decreasing with increasing temperature. The temperature at which the spontaneous magnetisation is reduced to zero is known as the Curie temperature T_C . Above this point ferromagnetic materials lose their ferromagnetism and behave like paramagnetic materials. The only elements which are ferromagnetic at room temperature are Fe, Co and Ni, while other examples of common ferromagnetic materials include permanent magnets based on NdFeB or AlNiCo. [19]

5.3.2.5 Anti-ferromagnetism

Anti-ferromagnetic materials exhibit a positive susceptibility and the atomic moments are arranged in an anti-parallel arrangement whereby the atomic moments cancel each other out resulting in zero net moment. Examples of anti-ferromagnetic materials include chromium and manganese. [19]

5.3.2.6 Ferrimagnetism

Ferrimagnetism is a form of magnetism which involves complex ordering of moments within the crystal structure. An unequal balance in atomic moments resulting in spontaneous magnetism. This behaviour can also occur in rare earth materials at low temperature when magnetic moments are able to align. [19]

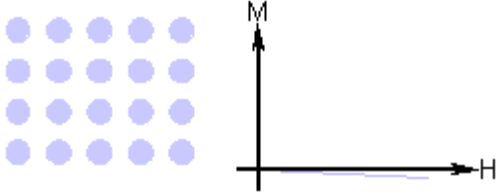
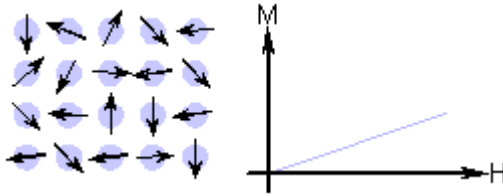
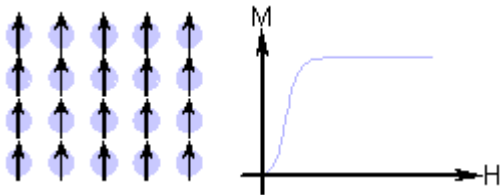
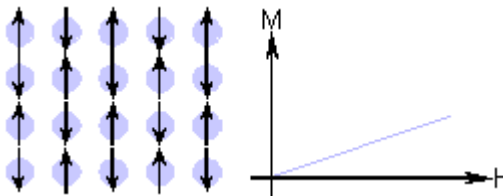
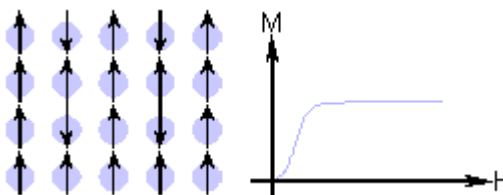
| Type of Magnetism | Susceptibility | Atomic / Magnetic Behaviour | Example / Susceptibility |
|----------------------------|---|--|--|
| <u>Diamagnetism</u> | Small negative. | Atoms have no magnetic moment  | Au -2.74×10^{-6} Cu -0.77×10^{-6} |
| <u>Paramagnetism</u> | Small positive. | Atoms have randomly oriented magnetic moments  | 0.19×10^{-6} β -Sn 21.04×10^{-6} Pt 6 Mn 66.10×10^{-6} |
| <u>Ferromagnetism</u> | Large positive, function of applied field, microstructure dependent. | Atoms have parallel aligned magnetic moments  | Fe $\sim 100,000$ |
| <u>Anti-ferromagnetism</u> | Small positive. | Atoms have mixed parallel and anti-parallel aligned magnetic moments  | Cr 3.6×10^{-6} |
| <u>Ferrimagnetism</u> | Large & positive, function of applied field, microstructure dependent | Atoms have anti-parallel aligned magnetic moments  | Ba ferrite ~ 3 |

Figure 5.2: Summary of magnetic behaviours in materials with respect to magnetic moments and field directions(from A.J Williams [19]).

5.3.1.7 Magnetic domains

Although Ferromagnetic materials are spontaneously magnetised due to exchange interactions, it is possible to find these materials in a demagnetised state. A domain is a region in which all the magnetic moments are orientated in the same direction. A ferromagnetic material exhibits zero external magnetism when these magnetic domains are orientated in a manner such as to cancel each other out, as shown in figure 5.3. When a material with randomly orientated domains is subject to an increasing magnetic field, favourably orientated magnetic domains grow into surrounding domains (depending on the anisotropy), then finally, begin to rotate towards the direction of the applied field. There exists a domain wall between each domain that allows space for the magnetic moment to rotate from the direction of one domain to another and so reduce the overall energy of the system. The width of a domain wall depends on a combination of the anisotropy and the exchange energy; magnetic systems with a high exchange energy and anisotropy will have narrow domain walls compared with systems with a low anisotropy.

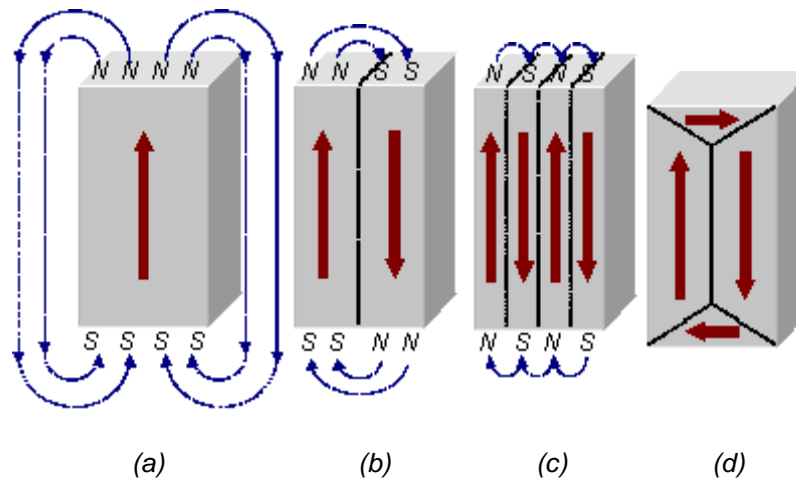


Figure 5.3 Schematic illustration of the break up of magnetisation into domains and the external field pattern for a (a) single domain, (b) two domains, (c) four domains and (d) closure domains[127].

5.3.1.8 Hysteresis

Ferromagnetic materials can be further categorised as either hard or soft magnetic materials, depending on how easy they are to magnetise and demagnetise.

Very different properties are sought for hard and soft magnetic materials; an ideal hard magnetic material will have a high remanence and coercivity, whereas an ideal soft magnetic material is one with little or no remanence or coercivity, but with a high permeability and saturation magnetization. A comparison between the relative coercivity and remanence of several common hard magnetic materials is shown in table 4.1.

The maximum energy product is a useful figure in the comparison of magnetic materials and shows the clear performance advantages that can be gained by the use of rare earth materials over the more conventional magnets.

Table 5.1, Examples of some hard magnetic materials [128]

| Hard magnetic materials | Coercivity (kA/m) | Remanence (Tesla) | Energy Product (kJ/m ³) | Curie Temperature (°C) |
|--|-------------------|-------------------|-------------------------------------|------------------------|
| Sintered Nd ₂ Fe ₁₄ B | 955 | 1.3 | 320 | 330 |
| Sintered samarium cobalt (Sm ₂ Co ₁₇) | 1160 | 1.03 | 183 | 800 |
| Alnico 5 | 45 | 1.26 | 37 | 860 |
| Barium ferrite (BaO.6Fe ₂ O ₃) | 255 | 0.390 | 28 | 450 |

5.4.2 Neodymium Iron Boron compounds (NdFeB)

The microstructure of the alloy comprises three main regions (Phase diagram Figure 5.4), an $\text{Nd}_2\text{Fe}_{14}\text{B}$ matrix phase, a secondary phase of composition $\text{Nd}_{1+\epsilon}\text{Fe}_4\text{B}_4$ and a ternary eutectic at the grain boundaries consisting mainly of an Nd-rich phase.

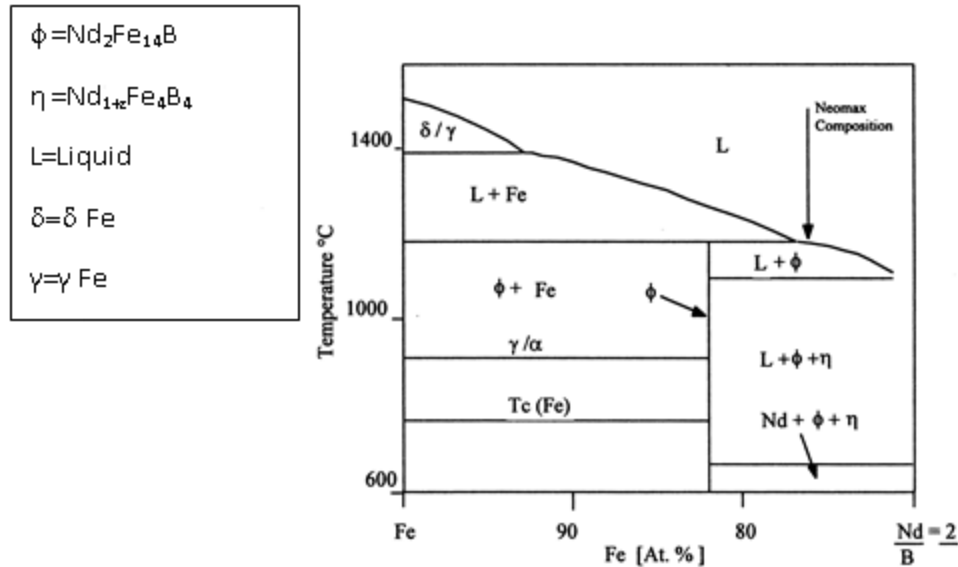


Figure 5.4: Vertical section through the NdFeB phase diagram passing through pure Fe and $\text{Nd}_2\text{Fe}_{14}\text{B}$ [130]

As Fe is a soft magnetic phase this would be highly detrimental to the magnetic properties if Fe phase forms and therefore an excess of B and Nd is required to ensure Fe is not the primary phase to solidify.

$\text{Nd}_2\text{Fe}_{14}\text{B}$ is the useful hard magnetic phase and is responsible for the high saturation magnetisation and remanence of the alloy. The first structural determination of this phase was carried out by Herbst et al [129] using neutron diffraction. Other investigators[130, 131] carried out structural determination by x-ray diffraction and found good agreement with Herbst. These studies revealed that the $\text{Nd}_2\text{Fe}_{14}\text{B}$ phase has a tetragonal structure, illustrated in figure 5.5. The unit cell is very complicated, containing four formula units (68 atoms). Buschow

[132, 133] showed that $\text{Nd}_2\text{Fe}_{14}\text{B}$ is virtually a line compound with a very narrow homogeneity range.

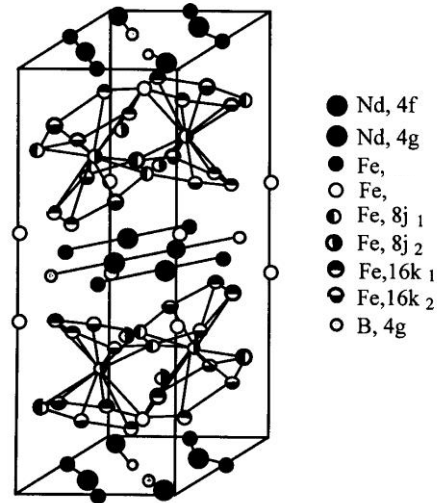


Figure 5.5. Crystal structure of $\text{Nd}_2\text{Fe}_{14}\text{B}$ with hard magnetic c direction vertical after Herbst et al [129].

It is the anisotropy of the crystal with the easy direction of magnetisation in the c axis that gives this NdFeB the high energy product. It is not energetically favourable for a domain to change the direction of magnetisation via intermediate orientations.

The Nd-rich phase is very important to the magnetic properties of the material acting both as an effective magnetic insulator between domains and smoothing the grain boundaries, thus reducing the number and degree of reverse domain nucleation sites. It is also important in the manufacturing process as it allows liquid phase sintering to occur, thus reducing both the sintering time and temperature, resulting in reduced grain growth[134, 135] The phase was reported by Sagawa et al[135] was found to contain 95at% Nd, 3-5at%Fe and a trace amount of boron. Further it was shown that influence of grain boundaries plays

an important role in the hydrogen absorption providing preferential sites and enabling diffusion processes to occur much more rapidly.[127]

5.4.3 Decrepitation of Neodymium Iron Boron Compounds

The study of the decrepitation effect of hydrogen in NdFeB alloys has been investigated by a number of researchers [136-138] and this work has shown that the alloy Nd₁₅Fe₇₇B₈ and related compositions can be powdered readily at room temperature by the hydrogen decrepitation (HD) process. Harris has referred to NdFeB as a material to be the most active with respect to hydrogen absorption and the most favourable candidate with respect to the HD process[139].

The decrepitation process is accompanied by a 5% volume increase in Nd₂Fe₁₄B, resulting in the release of acoustic energy producing a clicking sound the source of which is dependent on the stage that the reaction has reached. During the initial stages of the reaction the sound is caused by the stress field ahead of the hydride which is forming[9]. Calculations from the equilibrium site distances of H-H atoms within the inter-metallic structure show that the expansion of the metal lattice is directly proportional to the number of hydrogen atoms contained within it. Further it was postulated that each hydrogen atom causes a volume increase of 0.29nm³[140]

The increase in volume of the hydride phase is the basis for the decrepitation process. As hydrogen diffuses into the bulk to a particular depth below the surface a critical strain is reached, resulting from the volume difference between the hydrided and non-hydrided material. This causes fracture at the interface and the material breaks into flakes[138]. The extremely reactive nature of the alloy with regard to hydrogen has been attributed to the presence of the neodymium rich phase at the grain boundaries accelerating the decrepitation process and causing extensive cracking to individual crystallites[136].

Decrepitation was described as a two-stage process whereby hydrogen is firstly absorbed into the neodymium-rich phase. The resulting volume change causes a

localised stress concentration triggering inter-granular fracture. Absorption into the $\text{Nd}_2\text{Fe}_{14}\text{B}$ phase in the grains causes a similar volume increase resulting in cracking observable across the surface of the grains. Some of the material is fractured in a trans-granular mode, thus reducing the effective grain size and the remaining grains are heavily cracked and hence extremely friable[136]. Industrial production of NdFeB magnets utilise this fracturing process to produce a powder with a reduced grain size ideal for the jet milling process to reduce the grain size even further.

Studies have shown that the hydrogen absorption process in the $\text{Nd}_{15}\text{Fe}_{77}\text{B}_8$ alloy is a multistage process reflecting the complex nature of the microstructure. The $\text{Nd}_2\text{Fe}_{14}\text{B}$ matrix absorption can only be achieved readily at room temperature in the presence of the Nd-rich grain boundary material. Removal of this material by oxidation (or by a change in composition due to directional solidification) results in the deactivation of the matrix phase. This is confirmed by the fact that the single phase $\text{Nd}_2\text{Fe}_{14}\text{B}$ alloy required an elevated temperature of 150°C in order to achieve hydrogen absorption at reasonable pressures and times. The activation time for the freshly crushed $\text{Nd}_{15}\text{Fe}_{77}\text{B}_8$ alloy at room temperature was very pressure dependent as was the time taken for the absorption process to reach completion.[141]

Figure 5.6 shows a schematic representation of the hydrogen decrepitation process, highlighting the 2 phase starting material, showing the preferential hydrogen absorption at grain boundaries followed by absorption by the grains.

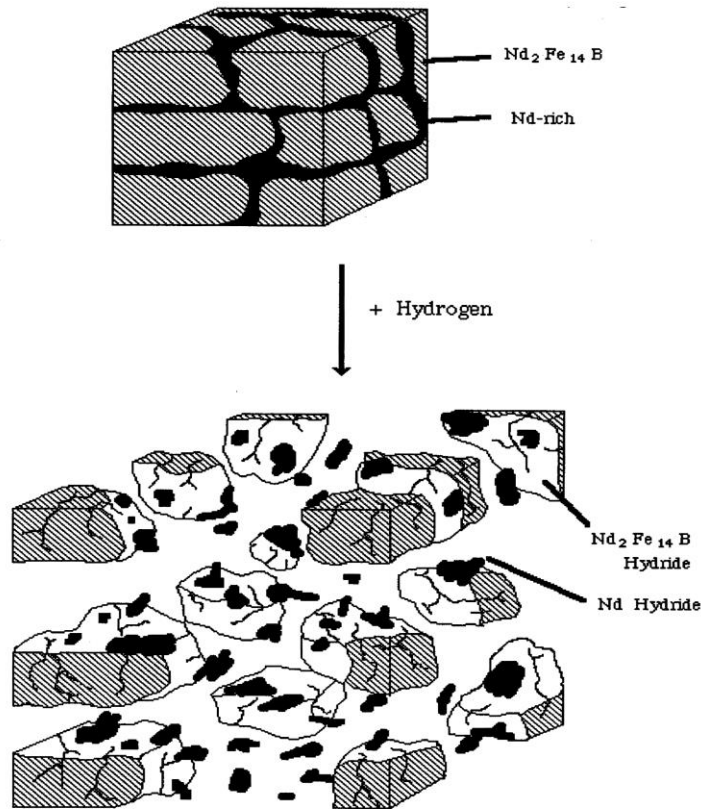


Figure 5.6. Schematic representation of the Hydrogen Decrepitation process in NdFeB alloys[141]

5.4.4 NdFeB Magnet Production

Hydrogen decrepitation is currently a key part of the manufacturing powder metallurgy processing route for NdFeB magnets. Exposure of the cast alloy to hydrogen has several advantages over a more orthodox powder production route. Firstly the hydride formation causes the decrepitation of the ingot. The hydride is brittle in nature and has large internal stresses from the volume expansion due to hydrogen absorption; this increases the efficiency of the jet milling process, thus reducing time and energy expenditure. Jet milling uses a stream of supersonic gas, usually nitrogen, to break up the powder to its final particle size. Grading of the material is undertaken simultaneously by adjusting the height of the internal wall (figure 5.7); only particles small enough to be

carried over the wall exit the chamber resulting in a consistent powder particle size. This process produces a fine and consistent particle size that is required for the production of fully dense sintered magnets.

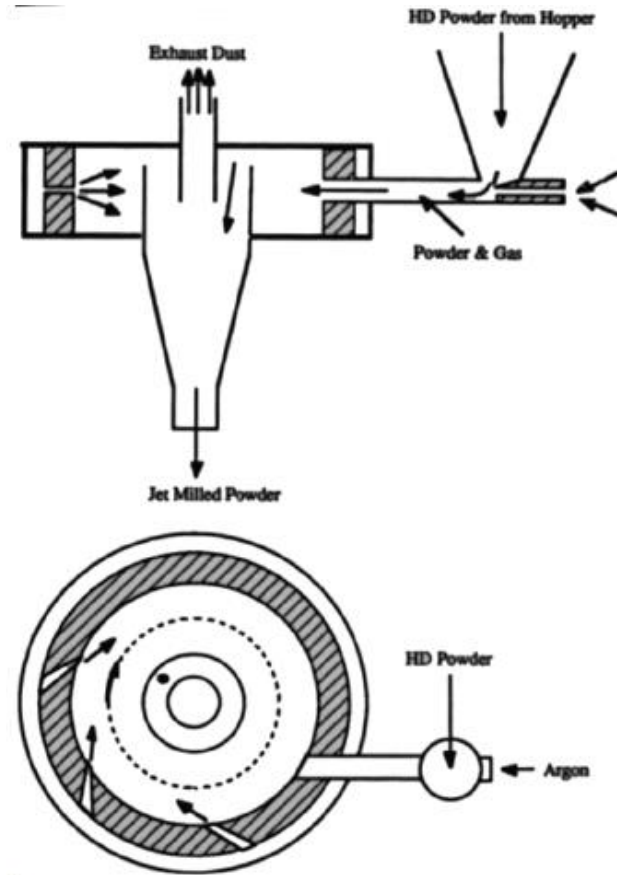


Figure 5.7: Schematic representation of a jet mill used to reduce the particle size with supersonic gas flow[142]

5.4.5 The HDDR process

The hydrogen decrepitation dissociation recombination (HDDR) process is an alternative route to provide powder suitable for bonded magnets or hot pressing. The HDDR process has its initial step in the decrepitation of NdFeB material followed by secondary processing in order to reduce the initial grain sizes for the best magnetic properties. After the decrepitation process has taken place the material is heated to above 700°C under pressure of hydrogen at which point the dissociation reaction occurs. Removal of hydrogen at this stage allows the

recombination of the materials but with the nucleation of the inter-metallic phases based on a high number of nucleation sites. This reduces drastically the average grain size of the starting material so that it can be used in magnet production without the requirement for jet milling.

5.4.6 Compaction and alignment

The compaction and alignment processes are undertaken simultaneously using a uni-axial press with the addition of an electromagnetic coil. The alignment process produces far better magnetic properties as the magnetic easy directions rotate in to line with the field producing the anisotropic material for an ideal permanent magnet.

5.4.7 Finishing

For most applications, such as voice coil motors, magnetic material will be pressed sintered as a large block. This reduces the number of press runs that are needed but dictates that post sintering machining must be undertaken and for this the samples will be cut and machined to final shape. Any excess material could be recycled through the hydrogen decrepitation process.

5.4.8 Coating

Due to the poor corrosion resistance of these materials it is necessary to protect them from moisture in the atmosphere. Therefore magnets are commonly coated with a nickel or polymeric coating in order to prevent corrosion. Nickel coating is undertaken by electro plating the magnets from an electrolytic bath.

5.5 Methodology

5.5.1 Equipment

The equipment used in this work was the same adapted microwave and gas control system as used for the assessment of magnesium hydride samples and detailed in section 2.2.1. The system used the change in pressure in a fixed volume at a constant temperature to monitor the reaction onset and rate of the absorption of hydrogen by NdFeB.

This was suitable for this system due to the low number of variables in the system and relatively simple measurements required for the initial assessment work. The initiation of the absorption of hydrogen into the magnetic phase was monitored by the onset of the pressure drop from the fixed volume. The absorption rate of the hydrogen was plotted from the change in pressure of the system with a fixed volume, using the ideal gas equation to derive the amount of hydrogen absorbed

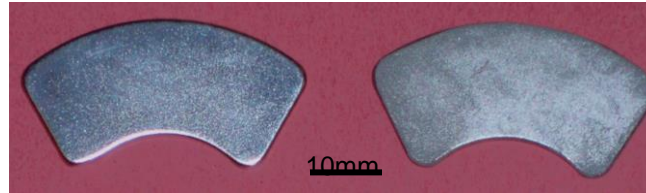
As the absorption in the decrepitation process is of interest primarily as a processing tool for both the production and recycling of magnetic materials the use of fixed volume reactors is suitable representation of production techniques.

Microwave treatments were undertaken in the same adapted domestic microwave system with the changes detailed in section 5.2.2. The system developed used an adapted commercial Panasonic NNT573 900W inverter microwave, with an internal cavity volume of 27400cm³.

This multi-mode microwave was chosen as it is one of the few commercially available systems that use an inverter circuit to supply the current to the magnetron, thus allowing variation in the current supply to the magnetron giving a variable output power without duty cycling. This is an important feature as it allows the control of power and field strength within the cavity without on-off duty cycling used in many systems to reduce the average power input.

5.5.2 Materials

The starting material used in this study was in the form of sintered magnets from the voice coil motors of hard disk drives. Figure 5.8 shows the voice coil magnet samples with the nickel coating (a) and with the coating removed (b) prior to the decrepitation process.



(a)

(b)

Figure 5.8 Photographs of the voice coil motor magnet samples (a) with the nickel coating and (b) with the coating removed.

The cross section of the samples with the coating in place (figure 5.9) shows the 10-15 μ m coating used to reduce the effect of corrosion and oxidation on the magnet.

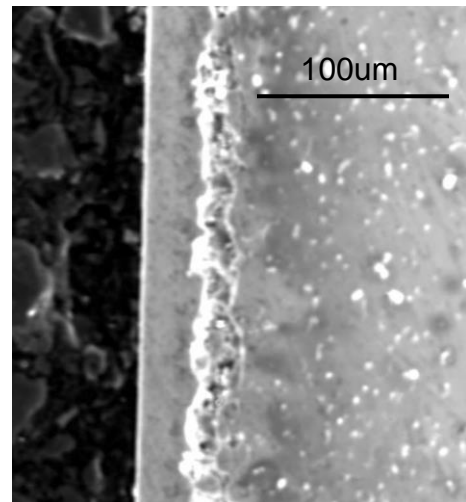
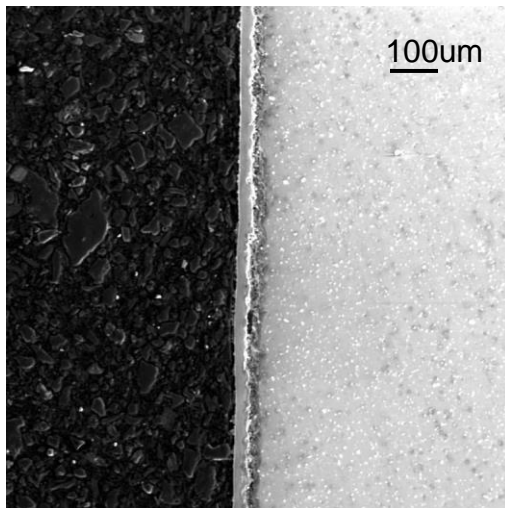


Figure 5.9: SEM micrographs showing cross sections of the nickel coating on the samples that is removed prior to experiments.

The magnets used in this study were the from same manufacturer and a similar batch to those used in a study by Zobotnic et al[143], and their composition was obtained by inductively coupled plasma (ICP) measurements at Less-Common Metals, (Table 5.3)

Table 5.3 ICP measurements of the typical composition of the magnet in atomic percent ($\pm 0.1\text{at\%}$ [143, 144])

| Nd at% | Fe at% | B at% | Pr at% | Dy at% | Nb at% | Al at% |
|--------|--------|-------|--------|--------|--------|--------|
| 14.0 | 77.8 | 6.4 | 0.1 | 0.6 | 0.4 | 0.7 |

Each sample was nickel coated after manufacture to protect the magnets from corrosion in humid atmospheres.

Each sample has a surface area of 12.3 cm^2 and the mean mass calculated from a population of 20 samples was 9.81g with a standard deviation of 0.0768g. Density measurements of the samples was obtained by the weight change when in a dimethylphthalate liquid at 6°C and this gives a mean density of 7.57gcm^{-3} with a standard deviation of 0.17gcm^{-3} , which is in good agreement with expected density for these magnets.

5.5.3 Sample preparation

For the samples used for all the experiments in this study, the preparation was as follows:

The nickel coating was removed from the sintered magnets by grinding the corner of the magnet followed by peeling the rest of the coating away.

The magnet was then exposed to dry laboratory air for a period of 24 hours. The exposure to air would allow an even oxide layer to reform over any scratches produced during the removal of the zinc coating.

The samples were then transferred to the silica reaction vessel using plastic tweezers to prevent scratches or surface contamination.

The size of the samples was determined by the original dimensions of the voice coil motor components, as cutting the sample would introduce inconsistencies in surface roughness and oxide formation on the cut face.

5.5.4 Decrepitation of HDD samples

The decrepitation studies were undertaken in a closed atmosphere of constant volume inside a silica tube. The test sequence involved evacuation of the system for 10 minutes at <0.06 mbar followed by the introduction of hydrogen to a pressure of either 0.5 or 1 bar within a period of 4 seconds. The temperature of the sample and the pressure of the system were recorded via a K type thermocouple in contact with the surface of the magnet and a pressure transducer. The thermocouple was sheathed with stainless steel, which as a good electrical conductor will limit the direct microwave heating. Data recording was linked to a P.C. via a fluke meter converting potential readings from the thermocouple and pressure transducer to a digital readout. Data points were recorded at 2 second intervals from 30 seconds before the hydrogen was introduced. The microwave was turned on within 1 second of the introduction of hydrogen to the sample..

5.6. Results and discussion

From the curve shown in figure 5.10 it is clear that the decrepitation of the material can be split in to two separate stages, namely the activation and the absorption processes. The activation is controlled by the time taken for hydrogen to cause the first rupture in the oxide film exposing the clean surface beneath. The subsequent pressure drop is caused as hydrogen is absorbed by the material to form the hydride and solution of hydrogen within the $\text{Nd}_2\text{Fe}_{14}\text{B}$ matrix

phase. The point at which this reaction causes a drop in the pressure in the system is labelled as the activation point of the reaction. This can be used as a point of comparison to determine the effects of the experimental conditions. The rate of pressure decrease is linked to both the amount of surface available and the hydrogen availability.

Based on the findings of Harris et al[141], calculation of the theoretical hydrogen absorption at 1 bar would be an increase of 0.42wt% and this equates to a volume 983.5ml, which is slightly less than the volume of the gas available to the sample. Because of this limited supply of hydrogen available in the system, the alloy may therefore reach equilibrium with the environment, as the pressure drops, before the equilibrium concentrations are attained and this is dependent on the temperature.

The shape of the graph would suggest that for the part of the absorption after the activation, the rate is determined by the amount of surface that is available for the hydrogenation reaction to occur. This explains the variations in gradient that are observable in both the plots of pressure and temperature of the samples. However as the material is broken down to the coarse powder, fresh surface area becomes available increasing the surface area at which the reaction can take place. This increase in surface should accelerate the reaction kinetics due to the reduced length of diffusion paths, however, this is not the case and the reaction rate drops after the sample has absorbed and so it is probable that the reduction in gas pressure becomes the rate controlling factor. The first fracture in the surface is the point at which the times for the activation of the hydrogen decrepitation are taken.

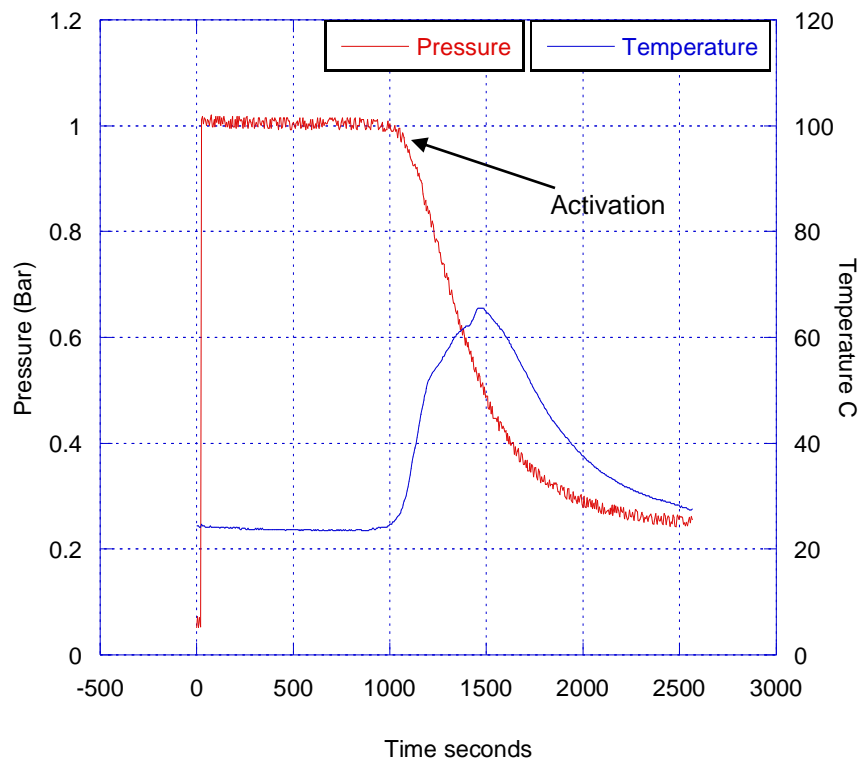


Figure 5.10: Sample in 1 bar hydrogen, no microwave treatment, showing the activation of hydrogen decrepitation reaction and subsequent temperature rise and pressure drop associated with the exothermic reaction

Figure 5.11 shows the decrepitation curves of a number of sintered samples exposed to 1 bar hydrogen pressure with no microwave radiation. The variation in the initiation times is the dominant factor in the process, as the time from initiation to the end of the reaction, at 0.3 bar, is consistent at about 2000 seconds. This would suggest that the improvements in the total time of reaction should be effective at reducing the time for the initiation of the hydrogen decrepitation reaction to occur.

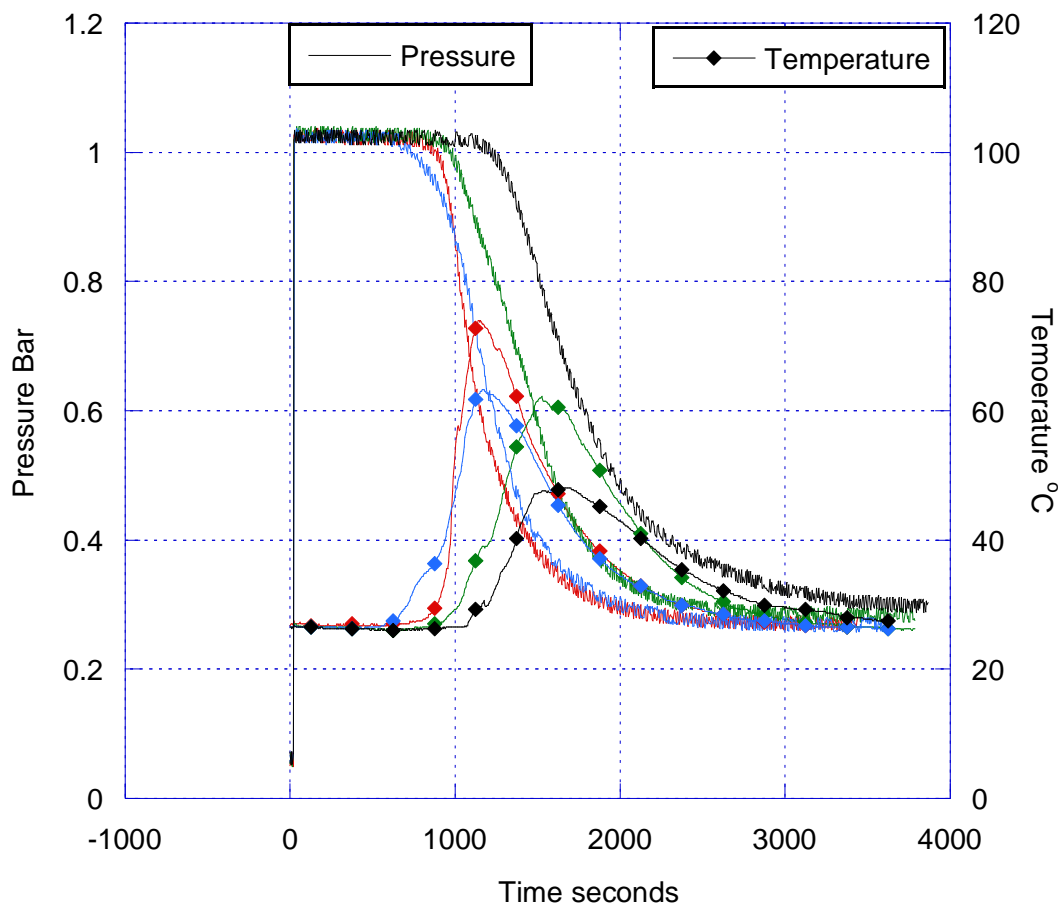


Figure 5.11: Typical pressure change over time from 1 bar hydrogen starting pressure and surface temperature in a closed system at room temperature with no microwave treatment.

The data in table 5.4 shows the variation in the behaviour of the materials when the conditions for the decrepitation are changed and shows the clear effect that temperature has on the reaction. The treatment of microwaves reduces the time to initiation but also has a significant effect on the distribution of initiation times. Whilst there is clear difference between those samples treated with and without microwaves at room temperature the results would suggest that the effect of microwave exposure time is less significant. This effect is also evident in the samples held at a constant temperature above the room temperature throughout the reaction, suggesting that the surface temperature is a key variable in both reducing the activation time and variation.

Table 5.4: showing the data on the time for activation of the reaction, the temperature 20 seconds prior to this point, the peak temperature reached after the activation and the time for the pressure in the system to drop from 1-0.6 bar.

| Sample ID | Sample conditions | Time for activation (Seconds) | Temperature 20 seconds prior to activation | Peak temperature | Time for pressure change 1-0.6 bar |
|-----------|------------------------|-------------------------------|--|------------------|------------------------------------|
| NM 1 | No microwave treatment | 1526 | 23.7 | 34.2 | 3125 |
| NM 2 | No microwave treatment | 2842 | 24.5 | 44.1 | 4192 |
| NM 3 | No microwave treatment | 1002 | 24.5 | 65.3 | 1383 |
| NM 4 | No microwave treatment | 2052 | 23.9 | 42.9 | 2991 |
| NM 5 | No microwave treatment | 973 | 24.1 | 63.0 | 1265 |
| NM 6 | No microwave treatment | 1178 | 23.8 | 58.6 | 1850 |
| NM 7 | No microwave treatment | 752 | 24.1 | 70.5 | 1134 |
| NM 8 | No microwave treatment | 702 | 24.1 | 74.8 | 1233 |
| NM 9 | No microwave treatment | 798 | 23.5 | 74.4 | 1094 |
| NM 10 | No microwave treatment | 1178 | 25.6 | 48.3 | 1650 |
| NM 11 | No microwave treatment | 637 | 27.6 | 63.2 | 1243 |
| NM 12 | No microwave treatment | 929 | 27.5 | 62.2 | 1208 |
| NM 13 | No microwave treatment | 578 | 27.6 | 70.3 | 1095 |
| NM 14 | No microwave treatment | 871 | 26.7 | 58.1 | 1342 |
| NM 15 | No microwave treatment | 856 | 27.2 | 54.8 | 1265 |
| NM 16 | No microwave treatment | 879 | 26.8 | 59.1 | 1312 |
| HM 1 | High power 60 seconds | 500 | 31.8 | 50.1 | 894 |
| HM 2 | High power 60 seconds | 772 | 32.1 | 41.5 | 1388 |
| HM 3 | High power 60 seconds | 916 | 32.9 | 45.2 | 1422 |
| HM 4 | High power 60 seconds | 611 | 33.1 | 56.6 | 1500 |
| HM 5 | High power 60 seconds | 650 | 33.2 | 43.6 | 1000 |
| HM 6 | High power 60 seconds | 637 | 32.1 | 66.7 | 1496 |
| HM 7 | High power 60 seconds | 549 | 41.2 | 62.2 | 1680 |
| HM 8 | High power 60 seconds | 603 | 33.8 | 54.5 | 1408 |
| HM 9 | High power 30 seconds | 655 | 36.700 | 49.4 | 1258 |

| | | | | | |
|-------|-----------------------|-----|--------|------|------|
| HM 10 | High power 30 seconds | 271 | 34.900 | 47.2 | 544 |
| HM 11 | High power 30 seconds | 264 | 31.400 | 60.1 | 626 |
| HM 12 | High power 30 seconds | 655 | 32.4 | 65.4 | 496 |
| HM 13 | High power 30 seconds | 271 | 33.2 | 47.9 | 520 |
| HM 14 | High power 30 seconds | 264 | 32.7 | 45.3 | 470 |
| W40-1 | Constant 40 °C | 557 | 40 | 40 | 900 |
| W40-2 | Constant 40 °C | 716 | 40 | 40 | 1052 |
| W40-3 | Constant 40 °C | 714 | 40 | 40 | 1016 |
| W60-1 | Constant 60 °C | 368 | 60 | 60 | 600 |
| W60-2 | Constant 60 °C | 357 | 60 | 60 | 551 |
| W60-3 | Constant 60 °C | 374 | 60 | 60 | 637 |
| W60-4 | Constant 60 °C | 386 | 60 | 60 | 661 |
| W80-1 | Constant 80 °C | 130 | 80 | 80 | 319 |
| W80-2 | Constant 80 °C | 185 | 80 | 80 | 392 |
| W80-3 | Constant 80 °C | 191 | 80 | 80 | 415 |

From the distribution of the initiation times illustrated in Figure 5.12, it is clear that the microwave exposure plays a significant role in initiating the decrepitation process

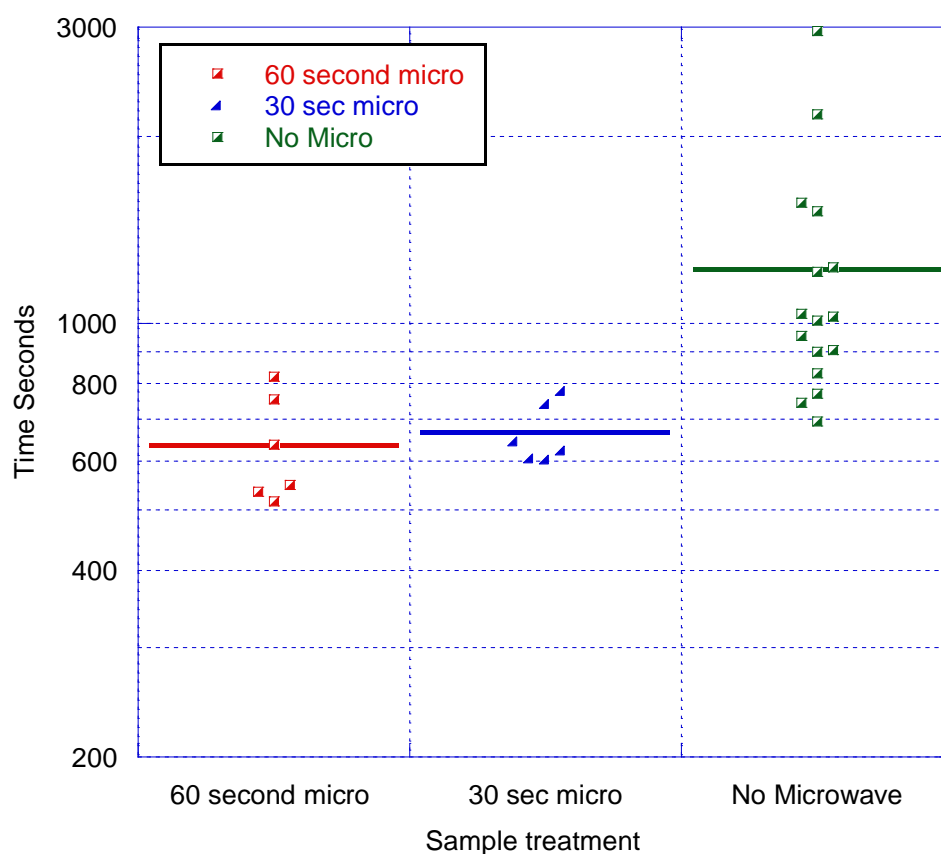


Figure 5.12: Showing the distribution of initiation times for the untreated samples and those exposed to 30 and 60 seconds of microwave power.

The exothermic nature of the hydrogen decrepitation reaction can be shown by the increase in the surface temperature as the reaction is initiated Figure 5.13. It is typical to see a temperature rise of around 30°C associated with this reaction. The temperature peak is associated with the fastest reaction kinetics, followed by the temperature drop as the reaction slows.

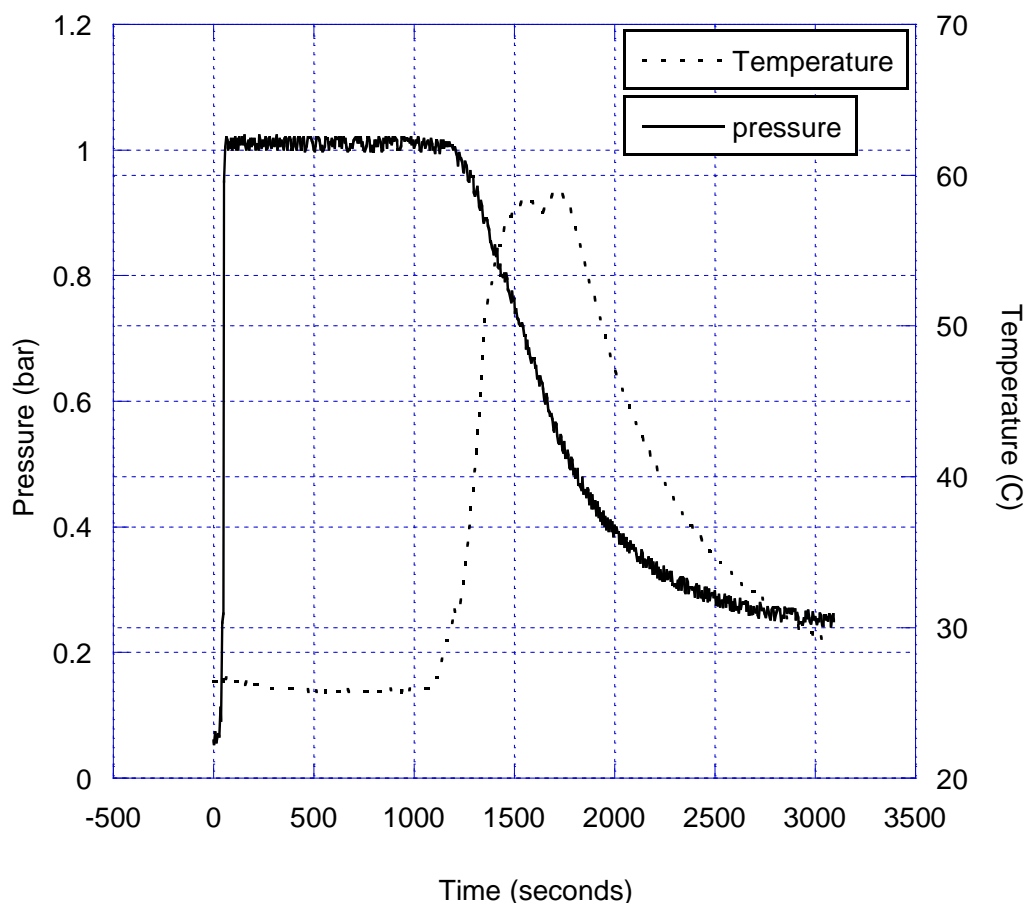


Figure 5.13: Temperature and pressure profile of the decrepitation process with no microwave exposure

When microwave radiation is applied to the sample there is a rapid heating effect associated with the energy input, however, this temperature spike only lasts whilst the microwave radiation is on. The surface temperature then rapidly drops to a point several degrees above room temperature. This may suggest that there is rapid localised heating of the surface of the material without heating the centre, which is then able to act as a heat sink as the energy is dissipated. A greater amount of energy would be needed to heat the sample if the whole magnet was hot. This would take much longer to dissipate and not give the characteristic temperature spike. Figures 5.14 and 5.15 show the temperature and pressure profile of a sample treated with 30 and 60 seconds of microwave radiation, and show the temperature spike followed by rapid cooling to a temperature above the starting room temperature.

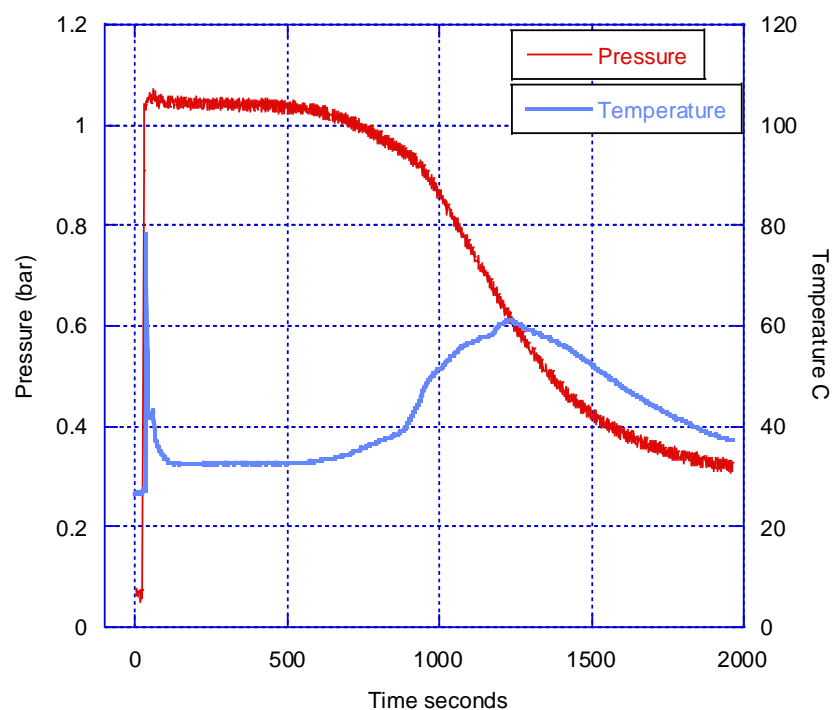


Figure 5.14: Temperature and pressure profile of the decrepitation process of a sample with 30 second microwave treatment.

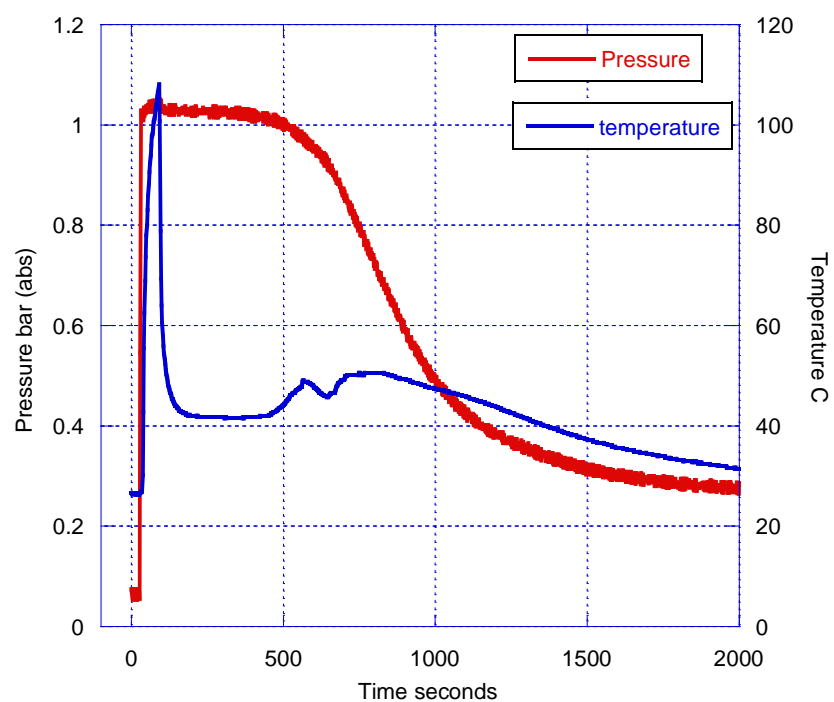


Figure 5.15: Temperature and pressure profile of the decrepitation process of a sample with 60 second microwave treatment.

The temperature of the surface 20 seconds prior to the initiation of decrepitation is shown in figure 5.16. This shows a correlation between increased temperature and reduced initiation times that would be expected for a diffusion controlled process. However, the large increases in temperature experienced by the materials treated for 60 seconds allied to the only slightly reduced incubation times would suggest that the surface temperature is not the only rate controlling parameter. This could suggest either a change in the condition of the surface during microwave treatment or that the diffusion process is accelerated rapidly during the short period when the microwaves are on, either by the higher temperatures or the microwave field.

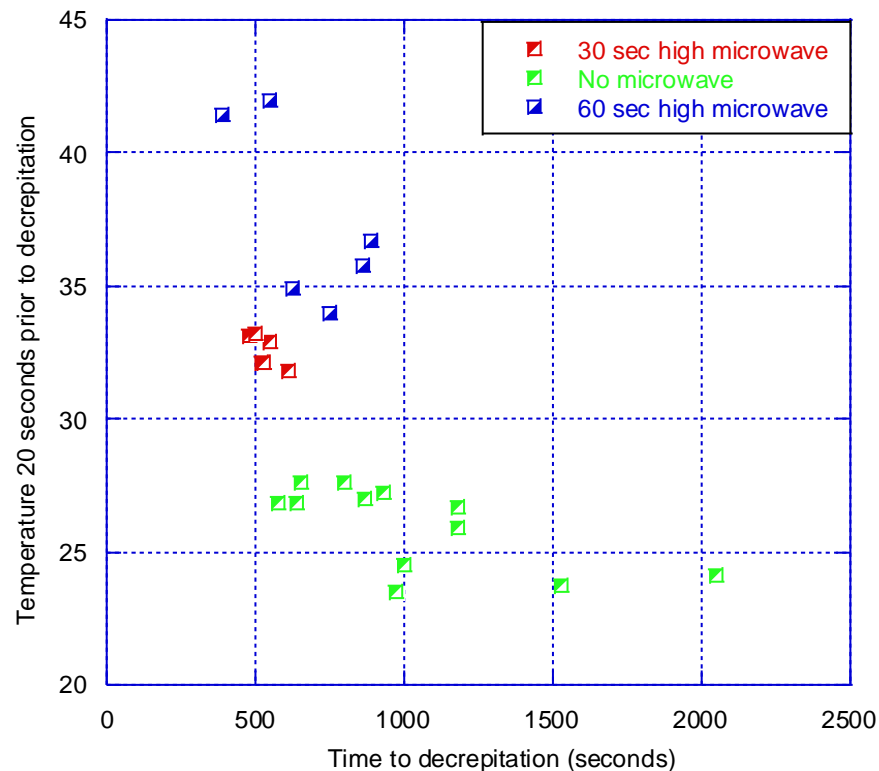


Figure 5.16: Temperature of the surface 20 seconds prior to the initiation of the decrepitation process for samples with 3 levels of microwave exposure.

The return of the surface temperatures back towards room temperature 20 seconds prior to the activation, could suggest that any effect the microwaves are having is related to a short term effect possibly related to surface cracking or interaction with the hydrogen atmosphere. If this effect is related to the weakest

point in the oxide layer then it is likely that this will form the point from which the hydride can nucleate beneath the oxide layer and start the decrepitation process. The SEM images show cross sections of the surface of the samples: prior to hydrogen exposure (figure 5.17), after 400 seconds of hydrogen exposure (figure 5.18) and with 60 seconds microwave treatment and 400 seconds of hydrogen exposure (figure 5.19).

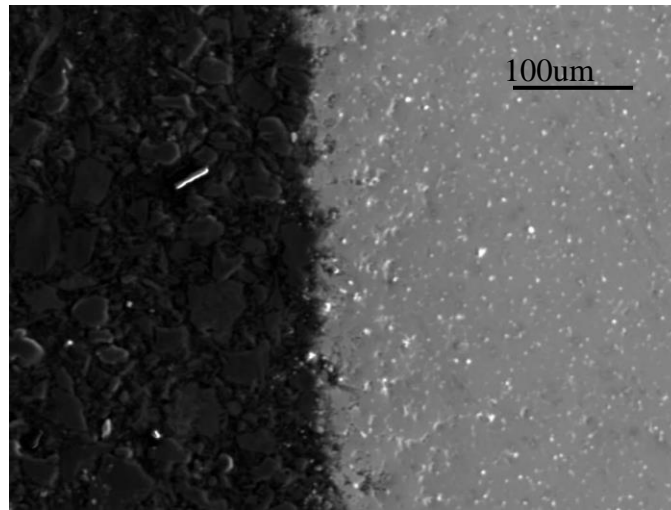


Figure 5.17: Cross section of the surface of the magnet after the removal of the nickel coating after exposure to laboratory air for 24 hours prior to mounting

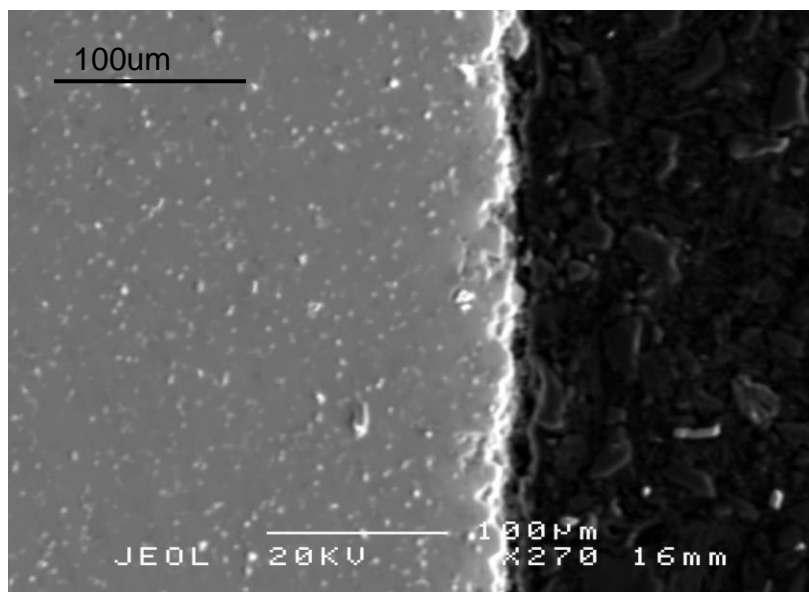


Figure 5.18: Cross section of the surface after exposure to 1 bar hydrogen for 400seconds

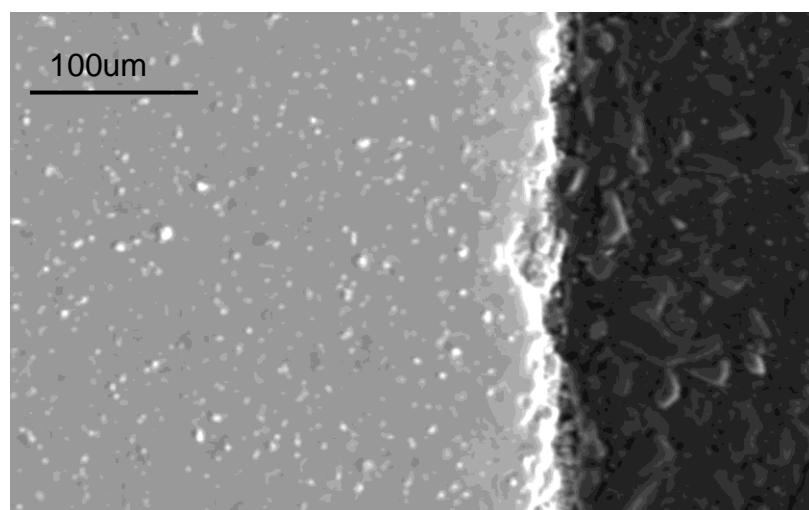


Figure 5.19: Cross section of the surface of a sample exposed to 1 bar hydrogen atmosphere for 400 seconds with 60 seconds microwave treatment

This data showing temperature prior to the initiation can be compared to an effect of maintaining a sample at a steady temperature throughout the duration of the absorption (figure 5.20). The effect of the temperature increase shows a clear acceleration in the time to initiation of the hydrogen decrepitation. The acceleration would be expected if the decrepitation is effected by hydrogen diffusion through an oxide layer that would be accelerated by increased temperature. This would suggest that a similar effect is occurring in the samples using microwave treatment although it is difficult to determine whether there is an increase in hydrogen mobility which is not related directly to an increase in surface temperature.

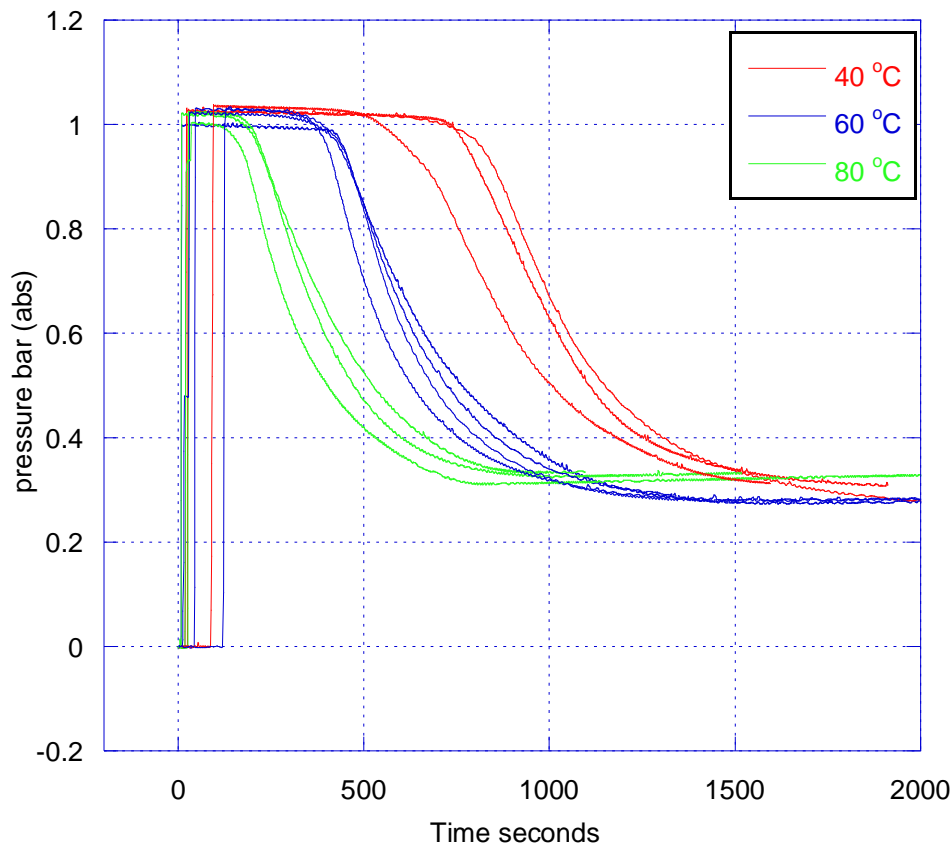


Figure 5.20: Shows the effect of constant temperature exposure, provided by a water bath, throughout the experiment and the reduced activation time with increased temperature

5.7 Conclusion

This work has shown that the time for hydrogen decrepitation to occur within these NdFeB samples can be reduced significantly with the application of the microwave field when compared to samples held at room temperature. However, at this juncture it is not possible to determine the nature of this change, whether it is linked to increase in the mass transport phenomenon due to microwaves or simply to the effect of surface temperature on the diffusion of hydrogen. As the decrepitation is linked to isolated points on the surface of the material it is difficult to show that the measured temperature is even across the surface.

The effect of the higher temperatures created by the water bath or the knowledge that similar effects can be achieved by increasing the pressure of hydrogen, suggests that while the effect is interesting it is unlikely that a commercial advantage can be gained through any increase in diffusion through the use of the microwaves.

Any future work should focus on the mechanism of the reduced activation time of the reaction, by looking at the surface interactions possibly by looking at very low pressures and variations in temperature.

If the conditions can exist whereby activation at 80°C takes a finite amount of time and that this can be reduced through microwave treatments with a lower peak temperature then this may suggest an increase in mass transport that is independent of temperature. However, this would not be conclusive due to the possibility of heterogeneity in the temperature profiles across the surface.

1. OICA, *2009 Production Statistics*. 2010.
2. *2009 Energy Demands Forecast*. 2009, Energy Information Administration, DOE.
3. *International Energy Agency Oil Market Report 2008*. 2008, IEA.
4. Zieger, J. *Automotive design requirements for state of the art pressure and solid state hydrogen stores*. in *Store-Hy Train-IN* 2006. Ingolstadt.
5. Satyapal, S., et al., *The U.S. Department of Energy's National Hydrogen Storage Project: Progress towards meeting hydrogen-powered vehicle requirements*. *Catalysis Today*, 2007. **120**(3-4): p. 246-256.
6. M.Fichtner. *Solid storage technology*. in *Store-Hy Train-IN* 2006. Ingolstadt.
7. Scrosati, B. and J. Garche, *Lithium batteries: Status, prospects and future*. *Journal of Power Sources*, 2010. **195**(9): p. 2419-2430.
8. May, G.J. and S.R. Tan, *Recent Progress in the Development of Beta-Alumina for the Sodium-Sulfur Battery*. *Electrochimica Acta*, 1979. **24**(7): p. 755-763.
9. Pourarian, F., et al., *Magnetic and Crystallographic Characteristics of Cen5-Xfex, Cen5-Xmnx Alloys and Their Hydrides*. *Journal of Solid State Chemistry*, 1986. **65**(1): p. 111-117.
10. Sudworth, J., *The Sodium/Nickel chloride (ZEBRA) battery*. *Journal of Power Sources*, 2001. **100**(1): p. 149-163.
11. Schlapbach, L., *Hydrogen Questions and Answers*. *Nature*, 2009. **460**(13): p. 809-811.
12. Schlapbach, L. and A. Zuttel, *Hydrogen-storage materials for mobile applications*. *Nature*, 2001. **414**(6861): p. 353-358.
13. HyFLEET-Project (2010) *HyFLEET:CUTE hydrogen bus demonstration project*. <http://www.global-hydrogen-bus-platform.com/Home> **Volume**,
14. van den Berg, A.W.C. and C.O. Arian, *Materials for hydrogen storage: current research trends and perspectives*. *Chemical Communications*, 2008(6): p. 668-681.
15. Bartlok, G. *Cryogenic storage options*. in *Store-Hy Train-IN* 2006. Ingolstadt.
16. Zuttel, A., et al., *Hydrogen density in nanostructured carbon, metals and complex materials*. *Materials Science and Engineering B*, 2004. **108**(1-2): p. 9-18.
17. Sandrock, G., *A panoramic overview of hydrogen storage alloys from a gas reaction point of view*. *Journal of Alloys and Compounds*, 1999. **293-295**: p. 877-888.

18. Janot, R., et al., *Influence of crystallinity on the structural and hydrogenation properties of Mg₂X phases (X=Ni, Si, Ge, Sn)*. Intermetallics, 2006. **14**(2): p. 163-169.
19. Callister, W., *Materials Science and Engineering An Introduction*. 5th ed, ed. W. Anderson. 1999. 272-273.
20. Chou, K.-C. and K. Xu, *A new model for hydriding and dehydriding reactions in intermetallics*. Intermetallics, 2007. **15**(5-6): p. 767-777.
21. Chen, X.D., et al., *Hydrogen absorption and release behavior in hydrogen decrepitation process of Nd-Fe-B alloys*. Journal of Rare Earths, 2003. **21**(2): p. 116-119.
22. Bogdanovic, B., et al., *Thermodynamic investigation of the magnesium-hydrogen system*. Journal of Alloys and Compounds, 1999. **282**(1-2): p. 84-92.
23. Fernandez, J.F. and C.R. Sanchez, *Rate determining step in the absorption and desorption of hydrogen by magnesium*. Journal of Alloys and Compounds, 2002. **340**(1-2): p. 189-198.
24. Evard, E.A., I.E. Gabis, and M.A. Murzinova, *Kinetics of hydrogen liberation from stoichiometric and nonstoichiometric magnesium hydride*. Materials Science, 2007. **43**(5): p. 620-633.
25. Jensen, T.R., et al., *Dehydrogenation kinetics of pure and nickel-doped magnesium hydride investigated by in situ time-resolved powder X-ray diffraction*. International Journal of Hydrogen Energy, 2006. **31**(14): p. 2052-2062.
26. Sakintuna, B., F. Lamari-Darkrim, and M. Hirscher, *Metal hydride materials for solid hydrogen storage: A review*. International Journal of Hydrogen Energy, 2007. **32**(9): p. 1121-1140.
27. Stampfer, J.F., C.E. Holley, and J.F. Suttle, *The Magnesium Hydrogen System*. Journal of the American Chemical Society, 1960. **82**(14): p. 3504-3508.
28. Fátay, D., Á. Révész, and T. Spassov, *Particle size and catalytic effect on the dehydriding of MgH₂*. Journal of Alloys and Compounds, 2005. **399**(1-2): p. 237-241.
29. Aguey-Zinsou, K.F., et al., *Effect of Nb₂O₅ on MgH₂ properties during mechanical milling*. International Journal of Hydrogen Energy, 2007. **32**(13): p. 2400-2407.
30. Barkhordarian, G., T. Klassen, and R. Bormann, *Kinetic investigation of the effect of milling time on the hydrogen sorption reaction of magnesium catalyzed with different Nb₂O₅ contents*. Journal of Alloys and Compounds, 2006. **407**(1-2): p. 249-255.

31. Borgschulte, A., et al., *Hydrogen dissociation on oxide covered MgH_2 by catalytically active vacancies*. Applied Surface Science, 2008. **254**(8): p. 2377-2384.
32. Dobrovolsky, V.D., et al., *Influence of TiB_2 addition upon thermal stability and decomposition temperature of the MgH_2 hydride of a Mg-based mechanical alloy*. Journal of Alloys and Compounds, 2008. **465**(1-2): p. 177-182.
33. Gennari, F.C., et al., *Catalytic effect of Ge on hydrogen desorption from MgH_2* . Journal of Alloys and Compounds, 2002. **334**(1-2): p. 277-284.
34. Jeon, K.-J., A. Theodore, and C.-Y. Wu, *Enhanced hydrogen absorption kinetics for hydrogen storage using Mg flakes as compared to conventional spherical powders*. Journal of Power Sources, 2008. **183**(2): p. 693-700.
35. Vajo, J.J., et al., *Altering hydrogen storage properties by hydride destabilization through alloy formation: LiH and MgH_2 destabilized with Si*. Journal of Physical Chemistry B, 2004. **108**(37): p. 13977-13983.
36. Vajeeston, P., et al., *Structural stability and pressure-induced phase transitions in MgH_2* . Physical Review B, 2006. **73**(22).
37. Moysés Araújo, C. and R. Ahuja, *Electronic and optical properties of pressure induced phases of MgH_2* . Journal of Alloys and Compounds, 2005. **404-406**: p. 220-223.
38. Isidorsson, J., et al., *Optical properties of $MgH_{\{2\}}$ measured in situ by ellipsometry and spectrophotometry*. Physical Review B, 2003. **68**(11): p. 115112.
39. Norskov, J.K. and F. Besenbacher, *Theory of Hydrogen Interaction with Metals*. Journal of the Less-Common Metals, 1987. **130**: p. 475-490.
40. Pozzo, M. and D. Alfè, *Hydrogen dissociation and diffusion on transition metal (= Ti, Zr, V, Fe, Ru, Co, Rh, Ni, Pd, Cu, Ag)-doped $Mg(0001)$ surfaces*. International Journal of Hydrogen Energy, 2009. **34**(4): p. 1922-1930.
41. Vegge, T., *Locating the rate-limiting step for the interaction of hydrogen with $Mg(0001)$ using density-functional theory calculations and rate theory*. Physical Review B, 2004. **70**(3).
42. Sprunger, P.T. and E.W. Plummer, *An Experimental-Study of the Interaction of Hydrogen with the $Mg(0001)$ Surface*. Chemical Physics Letters, 1991. **187**(6): p. 559-564.
43. Töpler, J., et al., *Measurements of the diffusion of hydrogen atoms in magnesium and Mg_2Ni by neutron scattering*. Journal of the Less Common Metals, 1982. **88**(2): p. 397-404.

44. Óskarsson, F., W. Stier, and H. Jónsson, *Calculations of the binding energy and diffusion of hydrogen in pure magnesium metal and magnesium hydride*.
45. Jiang, T., L.X. Sun, and W.X. Li, *First-principles study of hydrogen absorption on Mg(0001) and formation of magnesium hydride*. Physical Review B. **81**(3).
46. Borgschulte, A., R. Gremaud, and R. Griessen, *Interplay of diffusion and dissociation mechanisms during hydrogen absorption in metals*. Physical Review B, 2008. **78**(9).
47. Stander, C.M., *Kinetics of Decomposition of Magnesium Hydride*. Journal of Inorganic & Nuclear Chemistry, 1977. **39**(2): p. 221-223.
48. Sun, Y., et al., *Effects of powder flowability on the alignment degree and magnetic properties for NdFeB sintermagnets*. Journal of Magnetism and Magnetic Materials, 2006. **299**(1): p. 82-86.
49. Zaluska, A., L. Zaluski, and J.O. Ström-Olsen, *Nanocrystalline magnesium for hydrogen storage*. Journal of Alloys and Compounds, 1999. **288**(1-2): p. 217-225.
50. Li, H.W., et al., *Effects of ball milling and additives on dehydriding behaviors of well-crystallized Mg(BH₄)(2)*. Scripta Materialia, 2007. **57**(8): p. 679-682.
51. Huot, J., et al., *Structural study and hydrogen sorption kinetics of ball-milled magnesium hydride*. Journal of Alloys and Compounds, 1999. **295**: p. 495-500.
52. Suryanarayana, C., *Mechanical alloying and milling*. Progress in Materials Science, 2001. **46**: p. 184.
53. Ichikawa, T., et al., *Hydrogen storage properties on mechanically milled graphite*. Materials Science and Engineering B-Solid State Materials for Advanced Technology, 2004. **108**(1-2): p. 138-142.
54. Huot, J., et al., *Structural study and hydrogen sorption kinetics of ball-milled magnesium hydride*. Journal of Alloys and Compounds, 1999. **293**: p. 495-500.
55. Dornheim, M., et al., *Tailoring hydrogen storage materials towards application*. Advanced Engineering Materials, 2006. **8**(5): p. 377-385.
56. Walton, A., V. Mann, and I. Harris, *Milling time effects on crystalite size and hydrogen sorption characteristics*. 2003, The University of Birmingham p. 1.
57. Huhn, P.A., et al., *Thermal stability of nanocrystalline magnesium for hydrogen storage*. Journal of Alloys and Compounds, 2005. **404**: p. 499-502.

58. Novakovic, J.G., et al., *Changes of hydrogen storage properties of MgH_2 induced by heavy ion irradiation*. International Journal of Hydrogen Energy, 2008. **33**(7): p. 1876-1879.
59. Danaie, M., et al., *Analysis of deformation twins and the partially dehydrogenated microstructure in nanocrystalline magnesium hydride (MgH_2) powder*. Acta Materialia. **58**(8): p. 3162-3172.
60. Borgschulte, A., et al., *Catalytic activity of noble metals promoting hydrogen uptake*. Journal of Catalysis, 2006. **239**(2): p. 263-271.
61. Kwon, S., et al., *Enhancement of the hydrogen storage characteristics of Mg by reactive mechanical grinding with Ni, Fe and Ti*. International Journal of Hydrogen Energy, 2008. **33**(17): p. 4586-4592.
62. Charbonnier, J., et al., *Hydrogenation of transition element additives (Ti, V) during ball milling of magnesium hydride*. Journal of Alloys and Compounds, 2004. **383**(1-2): p. 205-208.
63. Liang, G., et al., *Hydrogen absorption properties of a mechanically milled Mg-50wt%LaNi₅ composite*. Journal of Alloys and Compounds, 1998. **268**(1-2): p. 302-307.
64. Puzskiel, J.A., P. Arneodo Larochette, and F.C. Gennari, *Hydrogen storage properties of Mg_xFe (x: 2, 3 and 15) compounds produced by reactive ball milling*. Journal of Power Sources, 2009. **186**(1): p. 185-193.
65. Riktor, M.D., et al., *Hydride formation in ball-milled and cryomilled Mg-Fe powder mixtures*. Materials Science and Engineering: B, 2009. **158**(1-3): p. 19-25.
66. Patah, A., A. Takasaki, and J.S. Szmyd, *Influence of multiple oxide (Cr_2O_3/Nb_2O_5) addition on the sorption kinetics of MgH_2* . International Journal of Hydrogen Energy, 2009. **34**(7): p. 3032-3037.
67. Hanada, N., et al., *SEM and TEM characterization of magnesium hydride catalyzed with Ni nano-particle or Nb_2O_5* . Journal of Alloys and Compounds, 2008. **450**(1-2): p. 395-399.
68. Huang, Z.G., et al., *Effects of iron oxide (Fe_2O_3 , Fe_3O_4) on hydrogen storage properties of Mg-based composites*. Journal of Alloys and Compounds, 2006. **422**(1-2): p. 299-304.
69. Klie, R.F., M.M. Disko, and N.D. Browning, *Atomic scale observations of the chemistry at the metal-oxide interface in heterogeneous catalysts*. Journal of Catalysis, 2002. **205**(1): p. 1-6.
70. Schwab, G.M., *Alloy Catalysts in Dehydrogenation*. Discussions of the Faraday Society, 1950(8): p. 166-171.
71. Aguey-Zinsou, K.F., et al., *Using MgO to improve the (de)hydriding properties of magnesium*. Materials Research Bulletin, 2006. **41**(6): p. 1118-1126.

72. Barkhordarian, G., T. Klassen, and R. Bormann, *Catalytic mechanism of transition-metal compounds on Mg hydrogen sorption reaction*. Journal of Physical Chemistry B, 2006. **110**(22): p. 11020-11024.
73. Oelerich, W., T. Klassen, and R. Bormann, *Metal oxides as catalysts for improved hydrogen sorption in nanocrystalline Mg-based materials*. Journal of Alloys and Compounds, 2001. **315**(1-2): p. 237-242.
74. Hanada, N., et al., *Remarkable improvement of hydrogen sorption kinetics in magnesium catalyzed with Nb₂O₅*. Journal of Alloys and Compounds, 2006. **420**(1-2): p. 46-49.
75. Liang, G., et al., *Catalytic effect of transition metals on hydrogen sorption in nanocrystalline ball milled MgH₂-Tm (Tm=Ti, V, Mn, Fe and Ni) systems*. Journal of Alloys and Compounds, 1999. **292**(1-2): p. 247-252.
76. Johnson, S., et al., *Chemical activation of MgH₂; a new route to superior hydrogen storage materials*. Chemical Communications, 2005: p. 2823-2825.
77. Mao, J., et al., *Improved hydrogen storage of LiBH₄ catalyzed Magnesium*. Journal of Physical chemistry 2007. **111**: p. 12495-12498.
78. Prigent, J. and M. Gupta, *Ab initio study of the hydrogenation properties of Mg-based binary and ternary compounds Mg₂X (X = Ni, Si) and YMgNi₄*. Journal of Alloys and Compounds, 2007. **446-447**: p. 90-95.
79. Tsuda, M., et al., *Magnetized/charged MgH₂-based hydrogen storage materials*. Applied Physics Letters, 2005. **86**(21).
80. Borgschulte, A., et al., *Electrohydrogenation of MgH₂-thin films*. Applied Physics Letters, 2007. **90**(7).
81. Will H, Peter S, and B. Ondruschka, *Microwave-Assisted Heterogeneous Gas-Phase Catalysis*. Chemical Engineering & Technology, 2004. **27**(2): p. 113-122.
82. Bykov, Y.V., K.I. Rybakov, and V.E. Semenov, *High-temperature microwave processing of materials*. JOURNAL OF PHYSICS D: APPLIED PHYSICS, 2001. **34**: p. R55-R75.
83. Zaluska, A.M., CA), Zaluski, Leszek (Montreal, CA), Strom-olsen, John (Westmount, CA), Schulz, Robert (Sainte-Julie, CA), *Method for inducing hydrogen desorption from a metal hydride*. 1999, Hydro, Quebec (Montreal, CA),McGill University (Montreal, CA): United States.
84. Zaluska, A.M., CA), Zaluski, Leszek (Montreal, CA), Strom-olsen, John (Westmount, CA), Schulz, Robert (Sainte-Julie, CA), *Method for inducing hydrogen desorption from a metal hydride*. 2000, Hydro, Quebec (Montreal, CA),McGill University (Montreal, CA): United States.
85. Matsuo, M., et al., *Effects of microwave irradiation on the dehydriding reaction of the composites of lithium borohydride and microwave absorber*. Applied Physics Letters, 2007. **90**(23).

86. Nakamori, Y., S. Orimo, and T. Tsutaoka, *Dehydriding reaction of metal hydrides and alkali borohydrides enhanced by microwave irradiation*. Applied Physics Letters, 2006. **88**(11).
87. Nakamori, Y., et al., *Effects of microwave irradiation on metal hydrides and complex hydrides*. Journal of Alloys and Compounds, 2007. **446**: p. 698-702.
88. Matsuo, M., et al., *Complex Hydrides with (BH₄)⁻ and (NH₂)⁻ Anions as New Lithium Fast-Ion Conductors*. Journal of the American Chemical Society, 2009. **131**(45): p. 16389-+.
89. Thostenson, E.T. and C. T.-W., *Microwave processing: fundamentals and applications*. Composites: Part A, 1999. **30**: p. 1055-1071.
90. Frank, A. *Components Of Electromagnetic Wave* [cited; Available from: <http://www.pas.rochester.edu/~afrank/A105/LectureV/LectureV.html>].
91. Saltiel, C., Z. Fathi, and W. Sutton, *Materials Processing with Microwave-Energy*. Mechanical Engineering, 1995. **117**(8): p. 102-105.
92. *cavity magnetron*. Encyclopedia Britannica Online 2004 [cited 2009 17/2/09]; cavity magnetron cut-away diagram]. Available from: <http://media-2.web.britannica.com/eb-media/05/205-004-F27EDE44.jpg>.
93. Bruce, R.W. *Materials Research Society Symposium Proceedings: Microwave Processing of Materials*. in *Microwave processing of Materials*. 1988. Reno, Nevada, USA: Materials Research society.
94. Al-Harashsheh, M. and S.W. Kingman, *Microwave-assisted leaching - a review*. Hydrometallurgy, 2004. **73**(3-4): p. 189-203.
95. Cheng, J.P., R. Roy, and D. Agrawal, *Experimental proof of major role of magnetic field losses in microwave heating of metal and metallic composites*. Journal of Materials Science Letters, 2001. **20**(17): p. 1561-1563.
96. Rybakov, K.I., et al., *Microwave heating of conductive powder materials*. Journal of Applied Physics, 2006. **99**(2).
97. German R, *Sintering theory and practice*. 1996, New York: Wiley Interscience. 94-119.
98. Willert-Porada M, *Microwave Processing of Materials IV*, in *Materials Research Society Symp. Proc. vol 347*, M.F. Iskander, Editor. 1994, Materials Research Society: Pittsburgh, PA. p. 31-43.
99. German R, *Sintering theory and practice*. 1996, New York: Wiley Interscience. 78-91.
100. Janney M and Kimrey H, *Diffusion-controlled processes in microwave-fired oxide ceramics*, in *Microwave processing of materials II, Materials Research Society symposium Proceedings*, 1991, Materials Research Society: Pittsburgh. p. 215-227.

101. Rowley, A.T., et al., *Microwave-assisted oxygenation of melt-processed bulk $\text{YBa}_2\text{Cu}_3\text{O}_{7-\delta}$ ceramics*. Journal of Materials Science, 1997. **32**(17): p. 4541-4547.
102. Wroe, R. and A.T. Rowley, *Evidence for a non-thermal microwave effect in the sintering of partially stabilized zirconia*. Journal of Materials Science, 1996. **31**(8): p. 2019-2026.
103. SAITA H, et al., *Microwave Sintering Study of NiCuZn Ferrite Ceramics and Devices*. Japanese journal of applied physics, 2002. **41**: p. 86-92.
104. JANNEY M. A., et al., *Enhanced diffusion in sapphire during microwave heating*. JOURNAL OF MATERIALS SCIENCE 1997. **32** p. 1347-1355.
105. Whittaker, A.G., *Diffusion in microwave-heated ceramics*. Chemistry of Materials, 2005. **17**(13): p. 3426-3432.
106. Booske, J.H., et al., *Microwave ponderomotive forces in solid-state ionic plasmas*. PHYSICS OF PLASMAS, 1998. **5**(5): p. 1664-1670.
107. Rybakov, K.I. and V.E. Semenov, *Mass transport in ionic crystals induced by the ponderomotive action of a high-frequency electric field*. Physical Review B, 1995. **52**(5): p. 3030.
108. Will. H, *Microwave Assited Hetrogeneous Gas Phase Catalysis*. Chemical Engineering & Technology, 2004. **27**(2): p. 113-122.
109. Xunli Zhang, et al., *Apparent equilibrium shifts and hot-spot formation for catalytic reactions induced by microwave dielectric heating*. Chemical Communications, 1999: p. 975-976.
110. Freeman S, Booske .J, and Cooper .R, *Microwave field enhancement of charge transport in Sodium Chloride*. Physical Review letters, 1995. **74**(11): p. 2042-2045.
111. Rybakov, K.I. and V.E. Semenov, *Possibility of plastic deformation of an ionic crystal due to the nonthermal influence of a high frequency electric field*. Physical Review B, 1994. **49**(1): p. 64-68.
112. Vayenas, C.G., et al., *Electrochemical Promotion in Catalysis - Non-Faradaic Electrochemical Modification of Catalytic Activity*. Electrochimica Acta, 1994. **39**(11-12): p. 1849-1855.
113. Bebelis, S. and C.G. Vayenas, *Non-Faradaic Electrochemical Modification of Catalytic Activity .1. the Case of Ethylene Oxidation on Pt*. Journal of Catalysis, 1989. **118**(1): p. 125-146.
114. Vayenas, C.G. and C.G. Koutsodontis, *Non-Faradaic electrochemical activation of catalysis*. Journal of Chemical Physics, 2008. **128**(18).
115. Wroe, F., *Radio frequency and microwave assisted processing of materials*, U.S.P. Office, Editor. 1999, EA Technology: US.

116. Wroe, F., *Method of Processing ceramic materials and a Microwave furnace Therefore*, U.S.P. Office, Editor. 1994, EA Technology Limited: US.
117. Wroe, F., *Appendix for Ibstock on the microwave processing of Bricks*. 1996, EA technology.
118. Wroe, F. and A.T. Rowley, *Microwave enhanced sintering of ceramics*. 1995, EA Technology Ltd.
119. Van Loock, W., *European regulations, safety issues in RF and microwave* Ghent University. p. 86-95.
120. Rowley, A.T., *Microwave enhanced Sintering of ceramics*. 1994, EA Technology. p. 1-19.
121. Brooks-Instruments, *Brooks Smart Mass Flow Meters and Controllers*, D.S.f.S.f.M.S.a. 5864S, Editor. 2006, Brooks Instruments.
122. Gems-Sensors, *Data Sheet for 2200 serie industrial pressure transducer*. 2006: RS online.
123. Williamson, G.K. and W.H. Hall, *X-RAY LINE BROADENING FROM FILED ALUMINIUM AND WOLFRAM*. Acta Matallurgica, 1953. **1**(1): p. 22-31.
124. Han, J.S., M. Pezat, and J.Y. Lee, *A Study of the Decomposition of Magnesium Hydride by Thermal-Analysis*. Journal of the Less-Common Metals, 1987. **130**: p. 395-402.
125. T. Mitsui, et al., *Dissociative hydrogen adsorption on palladium requires aggregates of three or more vacancies*. Nature, 2003. **VOL 422** p. 703-705.
126. PowdermatriX Faraday Partnership, *MAGNETIC SECTOR TECHNOLOGY ROADMAP*. 2004, PowdermatriX: Stoke-On-Trent. p. 1-18.
127. Harris, I.R. and A.J. Williams, *The character and role of grain boundaries in NdFeB-type alloys and magnets*. Zeitschrift Fur Metallkunde, 2002. **93**(10): p. 983-990.
128. Jiles, D., *Introduction to magnetism and magnetic materials*. 1991: Chapman and Hall. 99.
129. Herbst, J.F., et al., *Relationships between Crystal-Structure and Magnetic-Properties in Nd₂Fe₁₄B*. Physical Review B, 1984. **29**(7): p. 4176-4178.
130. Givord, D., H.S. Li, and J.M. Moreau, *Magnetic-Properties and Crystal-Structure of Nd₂Fe₁₄B*. Solid State Communications, 1984. **50**(6): p. 497-499.
131. Boller, H. and H. Oesterreicher, *On the Structure of Nd₂Fe₁₄B*. Journal of the Less-Common Metals, 1984. **103**(1): p. L5-L7.

132. Buschow, K.H.J., et al., *Magnetic and Crystallographic Properties of Ternary Rare-Earth Compounds of the Type $R_2Co_{14}B$* . Journal of Magnetism and Magnetic Materials, 1985. **51**(1-3): p. 211-217.
133. Buschow, K.H.J., D.B. Demooij, and H.M. Vannoort, *Properties of Metastable Ternary Compounds and Amorphous-Alloys in the Nd-Fe-B System*. Journal of the Less-Common Metals, 1986. **125**: p. 135-146.
134. Sagawa, M., et al., *New Material for Permanent-Magnets on a Base of Nd and Fe*. Journal of Applied Physics, 1984. **55**(6): p. 2083-2087.
135. Sagawa, M., et al., *Permanent-Magnet Materials Based on the Rare Earth-Iron-Boron Tetragonal Compounds*. IEEE Transactions on Magnetics, 1984. **20**(5): p. 1584-1589.
136. Harris, I.R., C. Noble, and T. Bailey, *The Hydrogen Decrepitation of an $Nd_{15}Fe_{77}B_8$ Magnetic Alloy*. Journal of the Less-Common Metals, 1985. **106**(1): p. L1-L4.
137. Harris, R., et al., *The Use of Hydrogen in the Processing and in the Characterization of Nd-Fe-B Magnets and Alloys - an Update*, in *Advanced Materials '93, I - a & B - a: Ceramics, Powders, Corrosion and Advanced Processing; B:1994*. p. 969-974.
138. McGuinness, P.J., et al., *The Hydrogen Decrepitation Behavior of Alloys and Magnets Based on $Nd_{16}Fe_{76}B_8$* . Journal of Applied Physics, 1990. **67**(9): p. 4626-4628.
139. Harris, I.R., et al., *Nd-Fe-B Permanent-Magnets - Hydrogen Absorption Desorption Studies (Hads) on $Nd_{16}Fe_{76}B_8$ and $Nd_2Fe_{14}B$* . Physica Scripta, 1987. **T19B**: p. 435-440.
140. Westlake, D.G., *Site Occupancies and Stoichiometries in Hydrides of Intermetallic Compounds - Geometric Considerations*. Journal of the Less-Common Metals, 1983. **90**(2): p. 251-273.
141. Harris, I.R., et al., *Nd-Fe-B Permanent Magnets: Hydrogen Absorption/Desorption Studies (HADS) on $Nd_{16}Fe_{76}B_8$ and $Nd_2Fe_{14}B$* . Physica Scripta, 1987. **T19**: p. 435-440.
142. Harris, I.R. and P.J. McGuinness, *Hydrogen - Its Use in the Processing of Nd-Fe-Type Magnets*. Journal of the Less-Common Metals, 1991. **172**: p. 1273-1284.
143. Zobotnic, M., *hydrogen decrepitation for recycling of magnets*. 2008, University of Birmingham. p. 1-5.
144. Zobotnic, M., *Unpublished work*, University of Birmingham.
145. Opsens inc, *Opsens white light polarization interferometry technology*, 2014, <http://www.opsens.com/pdf/WLPIREV2.3.pdf>, downloaded 1.4.14